UNIVERSIDAD AUTÓNOMA DE SAN LUIS POTOSÍ

Doctorado Institucional en Ingeniería y Ciencia de Materiales

Application of Mechanochemical Procedure on Aqueous Cr(VI) Removal with Additives of Activated Carbon and Fe^0/Fe_2O_3

TESIS

QUE PARA OBTENER EL GRADO DE

DOCTOR EN INGENIERÍA Y CIENCIA DE MATERIALES

PRESENTA

Yi Fang

ASESOR

Dr. Alejandro López Valdivieso

Dr. Changsheng Peng

PATROCINADO POR CONACyT Beca número 900339

San Luis Potosí , S.L.P. Marzo 2022

UNIVERSIDAD AUTÓNOMA DE SAN LUIS POTOSÍ

Doctorado Institucional en Ingeniería y Ciencia de Materiales

Application of Mechanochemical Procedure on Aqueous Cr(VI) Removal with Additives of Activated Carbon and Fe^0/Fe_2O_3

TESIS

QUE PARA OBTENER EL GRADO DE

DOCTOR EN INGENIERÍA Y CIENCIA DE MATERIALES

PRESENTA

Yi Fang

ASESOR

Dr. Alejandro López Valdivieso

Dr. Changsheng Peng

Dr. Alejandro López Valdivieso ________________

Dr. Changsheng Peng ________________

Dra. Mildred Quitana Ruiz ________________

Dra. Jessica Viridiana García Meza ________________

Dr. Yuri Nahmad Molinari ________________

Dr. Shaoxian Song ________________

San Luis Potosí , S.L.P. Marzo 2022

Acknowledgments

Foremost, I would like to express my sincere gratitude to the National Council of Science and Technology of Mexico (CONACyT) to support my Ph.D. study (Grand No. 900339) and my advisors Prof. Alejandro López Valdivieso and Prof. Changsheng Peng for their patience, motivation, enthusiasm, and immense knowledge. Their guidance helped me in all the time of research and writing of this thesis. I could not have imagined having the better advisors and mentors for my Ph.D. study.

Besides my advisor, I would like to thank the rest of my thesis committee: Dra. Jessica Viridiana Garcia Meza. Dra. Mildred Quintana Ruiz, Dr. Shaoxian Song, and Dr. Yuri Nahmad Molinari, for their encouragement, insightful comments, and hard questions.

My sincere thanks also go to Dra. Aurora Robledo-Cabrera, for offering me huge support on the materials characterization and analysis of SEM, EDX, XRD, Raman spectra, and BET. I thank my fellow labmates in Surface Chemistry Laboratory: Ke Yang, Yipeng Zhang, Selene, Marichuy, Diana, and Naira, for the stimulating discussions, for all the fun we have had in the last four years, and for the gaining insights into Mexican culture and food.

Last but not the least, I would like to thank my family: my parents Aiguo Fang and Yinjiao Qian, and the family of my elder brother: YI Fang, Tao Miao, and their baby girl: Beilei Fang, for supporting me spiritually throughout my Ph.D. period in Mexico and my life.

Abstract

The green technique of mechanical ball milling has been extensively employed in the fabrication of environmentally functional materials. The improved specific surface area and modified surface properties of the resulting materials contribute to the high performance in pollutant removal. In this work, to improve the performance of low-cost activated carbon and sponge iron powder under neutral conditions. Ball milling was used to pretreat activated carbon and treat the mixture of surface oxidized sponge iron powder and contaminant solution, wherein the strong oxidant and toxic Cr(VI) was chosen as the target pollutant. The reduction coupling with precipitation was dominantly attributed to the removal of Cr(VI), wherein the surface enhanced surface functional groups and hydrophilicity within ball milling were the main mechanisms subject to the elimination of Cr(VI) which was substantiated by Boehm's titration. Furthermore, surface precipitated Cr(III) oxides have been shown to impede Cr(VI) removal, and acidic washing experiments can rejuvenate the used activated carbon by dissolving the Cr(III) oxide layer. Moreover, the reduced Cr (III) and adsorbed Cr (VI) can be recovered by acidic and alkaline elution, respectively.

The inherent demerits of zerovalent iron, such as surface passivation in solution and low electron efficiency, could be mitigated perpetually by ball milling. Removal efficiency of Cr(VI) maintained over 60 % over a wide pH of 4-10 in presence of ball milling, while negligible Cr(VI) decrease was noticed in absence of ball milling. XPS spectra analysis supported that reduction of Cr(VI) to Cr(III) followed co-complexed with Fe(III) as $Fe_{0.33}Cr_{0.67}(OH)_3(s)$ was the foremost elimination pathway of Cr(VI). The effect of dissolved oxygen on Cr(VI) removal can be divided into two segments as per the pH; the generated Fe(II) that originated from the Fe^0 oxidation by dissolved oxygen facilitated to the reduction of Cr(VI) at acidic conditions, whereas the produced Fe(II) ions were oxidized at alkaline conditions and the electron efficiency of Fe was alleviated likewise. Uncovered fresh core Fe^0 to the aqueous Cr(VI) by the motion of ball milling which was the main mechanism that diminished the surface passivation layer of Cr(III)/Fe(III) hydro(oxides). Furthermore, the depletion curve of Cr(VI) as function of time under different initial concentration, dosage, and rotational speed was consistent with zero order kinetic model.

Keywords: Mechanochemical Procedure, Ball Milling, Activated Carbon, Zero-Valent Iron, Chromium, Reduction

CONTENT

Index of Figures

Index of Tables

Chapter I. **Introduction**

Mechanochemical procedures (MCPs) as an emerging technology for nanomaterial (nano-zero valent iron, nano activated carbon) preparation, has arouse more and more attentions by researchers[10-15]. MCPs is fast become a key technology in environmental material synthesis with sustainable and low-cost. And physical and chemical characteristics of materials will be enhanced like hydrophilic and adsorption performance on inorganic matters[16, 17]. In general, MCPs defect the material particle through shear and impact force generated from high energy collision between milling balls and medium. The size of medium particles or grain declined rapidly after undergoing repeat flatten, deformation, disintegration, and the size of medium won't further refined even longer milling duration executed due to the cold-welding and agglomeration of particles[19]. In addition to the particle size reduction, when mixed desired medium with functional agents like active metal and organic matters to produced specific characteristic materials. The evidence of target material modification assistant with mechanically milling can be clearly seen in the case of study of Yulin Zheng et al, in which the MgO introduced into milling jar with biochar to prepare dual-functional adsorbent for cationic dye and anionic phosphate removal, the adsorption performance of MgO-biochar improved significantly compared to the pristine biochar[25]. Common equipment for MCPs are planetary ball-milling, tumbler ball-milling, attrition ball-milling and vibration ball-milling, details seen in Fig 1-1, when considering the size limitation for laboratory-scale application; the planetary ball-milling of high rotate speed, compact size and multiple milling jars was an optimum choice for laboratory trial.

Figure. 1-1 Four conventional ball-milling machines and their working principles[26], (a) planetary ball-milling, (b) tumbler ball-milling, (c) attrition ball-milling, (d) vibration ball-milling, copyright 2020, Elsevier.

Chromium is widely used in industry as plating, alloying, textile dyes and pigments. Due to the wide application of chromium in industry, the consequent environment contamination has become a central issue and has arouse the attention of researchers [27-30]. Cr (VI) exists in the forms of chromate (CrO_4^{2-}), dichromate ($Cr_2O_7^{2-}$) and CrO_3 are considered to be the most toxic forms of chromium, chromium poisons the plants in the form of hexavalent chromium for its highly mobile and toxic while trivalent chromium is less mobile and toxic (Deepti S et al., 2018). Cr(III) is an essential micronutrient to human, while Cr(VI) is toxic and can cause severe diseases such as kidney circulation, dermatitis and lung cancer[29]. Therefore, attention should be activated for sequestration or reduction Cr(VI) to Cr(III) from aquatic environments for the protection of environment and public health.

The conventional methods for the removal of Cr(VI) from wastewater are membrane filtration, precipitation, and ion exchange[28]. There are some disadvantages of these methods including high chemical dosage, high capital and operation cost, high energy consumption and potential secondary effluent[27]. The activated carbon (AC) is the most widely used material for its readily available, low cost, high specific surface area which range from 500 to 1500m^2 g^{-1}, developed internal microporous structure and wide spectrum of surface functional groups like carboxylic group[31]. AC derived from biomass like coconut shell, wood coal, hazelnut shell, *Terminalia arjuna* nuts and rubber wood sawdust, the adsorption capacity of synthetic adsorbent from these biomass on Cr(VI) range from 4.4 to 170.0 mg g^{-1} [32-35]. In order to further improve the adsorption performance of AC, modification of the activated carbon by chemical procedure to enhance its surface functional group, AC was prepared from *Longan* seed by chemical modification with sodium hydroxide (NaOH) which possess adsorption capacity on Cr(VI) was 35.02 mg/g and higher than the pristine AC[36]. AC pretreated by heating with sulfuric acid and nitric acid, the maximum adsorption capacity are 7.485 and 10.929 mg/g, respectively[37]. By way of illustration, Kronje,K,J et al activated the sugarcane bagasse by zinc chloride, results indicated that the removal rate was over 87%[38]. Compared to the chemical modification, physical treatment presents several advantages, no secondary effluent after physical treatment and easily operation. Conventional physical treatment are activation with steam, gasification in CO_2 or in a water-nitrogen mixture[39, 40].

Most of the adsorption treatments were pre-adjusted to the acid condition and the pH value were 2-4[29, 41-43]. At the acid condition the surface function group were protonated and facilitated the redox reaction between contaminants and electron on AC. But the adjustment of acid condition required numerous acid solution and subsequently cause the emission problem of acidic effluent. Augment the removal capability of AC at near-neutral pH could be a promising solution for removal of Cr(VI).

On the other hand, improving the adsorption capacity of activated carbon through mechanical grinding rarely seen in the related research literatures[44-49]. Crushing the activated carbon particle into finer particle by ball milling, the activated carbon become smaller particulate in the process of milling, thus more surface functional groups were exposed and higher specific surface area, the adsorption performance could be improved, correspondingly.

Zero-valent iron as another common low-cost material has received much attention on contaminants removal, while the inherent demerits of zero-valent iron like easily-agglomeration, atmospheric oxidation, passivation in solution and the low electron efficiency have inhibited its implication. MCP could remove the surface oxidation layer through the repetitive collision which makes it a promising method on mitigating the drawbacks and improving the lifespan of zero-valent iron.

1.1. The sequestration of aqueous Cr(VI) by zerovalent iron-based materials

1.1.1. Introduction

Chromium (Cr) has a wide range of industrial applications such as plating, alloying, leather tanning, metallurgy, textile dyes, and pigments. Thus, Cr-contaminated sewage has become a big issue and has attracted the attention of experts to eliminate Cr by employing various kinds of materials like activated carbon [27], alkalic modified activated carbon [29], green synthesized zero-valent iron [28, 50, 51] and well-designed nanocarbon spheres [30]. Cr mainly occurs in two different states in nature such as hexavalent chromium (Cr(VI)) and trivalent chromium (Cr(III)). Cr(VI) has mutagenic and carcinogenic effects in humans because of their higher mobility and toxicity behavior. It can cause severe diseases such as kidney circulation, dermatitis, and lung cancer in humans [29]. While, Cr(III) is less mobile, more stable, and less toxic than Cr(VI) [52]. It can be converted into chromium hydroxide ($Cr(OH)_3$), which can be precipitated out at moderately acidic to alkaline pH and can also serve as an essential micronutrient. Therefore, the removal or reduction of Cr(VI) anions to nontoxic and immobile Cr(III) ions is important for protecting the environment and public health.

Moreover, conventional methods such as adsorption, reduction, membrane filtration, precipitation, and ion exchange have been employed to remove heavy metals from sewage [28, 53]. Whereas, the reduction and adsorption procedure of Cr(VI) has attracted more attention because of its cost-effectiveness as compared to membrane filtration [54], ion exchange [55], and electrochemical treatment technologies [35]. Further, iron and modified iron compounds have been extensively applied for Cr(VI) elimination owing to having their higher activity and feasible synthesis protocols such as green technologies [28, 50, 51, 56], mangrove fungus reduction method [57], in-situ growth method [58] and replacement reactions method [59]. Further, the nanoparticles of ZVI have shown a great potential application in the treatment of real tannery wastewater and the removal ratio of 100, 70, 73, and 88% were noticed for Cr(VI), TOC, COD, and phenol, respectively [60]. Since the first exhaustively documented practical application of ZVI on groundwater remediation with the permeable reactive barrier (PRB) in 1996 [61], the development of ZVI-based materials has received considerable attention for environmental remediation. Regarding this, Fig. 1-2 is depicting a comprehensive summary of the advancements in ZVI-based materials for sewage treatment.

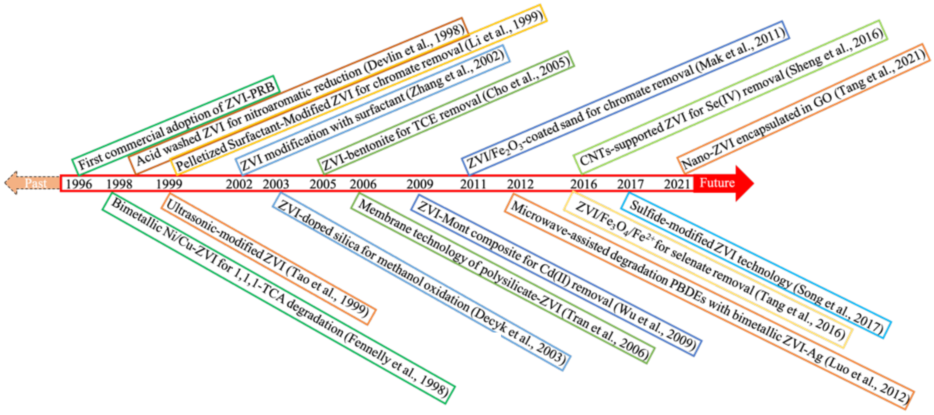

Figure. 1-2 The major events of ZVI-based materials development over the past 25 years (1,1,1 TCA (1,1,1-trichloroethane), TCE (trichloroethylene), Mont (Montmorillonite), CNTs (carbon nanotubes), PBDEs (polybrominated diphenyl ethers), GO (graphite oxide)) [1, 2 3 4 5 6 7, 62 8 9 18 20, 63 21, 22]

Notably, certain factors such as particle size [64], pH value [65, 66], co-existing ions [67, 68], hydrodynamic filed [69] and contaminant concentration were restricted performance of iron [70]. The passivation layer on the surface of the iron particle formed under alkaline conditions could sequester the electron derived from iron, wherein the passivation layer was mainly contained non-conductive hydroxide of iron and Cr [71]. Research efforts have been done on impairing the effect of the passivation layer. For instance, the iron/aluminum bimetallic material presented higher Cr-elimination performance as compared to the elemental iron [72]. In addition to unfavorable impacts induced by the surface oxidized layer, nZVI particles are preferred to clump in the aqueous solution where the activities of iron were limited remarkably [73]. To solve this issue, a stable nZVI containing material was synthesized through embodied nZVI in MCM-41 for the improvement of the performance and longevity of nZVI in solution [74]. The most common measures to promote the capability of iron include composited bimetallic materials (Al-Fe, Zn-Fe, Pb-Fe, Cu-Fe, Ni-Fe, Ag-Fe) [75, 76], loaded iron on carbon template [77], and mixed iron with elemental sulfur or sulfide [78]. The preparation procedures for iron-bearing materials fluctuate by considering the limitations caused by poor solution dispersion and easy air oxidation of iron. To enhance the dispersion of nZVI in solution, carbon nanotube-supported nZVI was synthesized through liquid-phase reduction method and Cr removal efficiency was found to be around 36% higher than bare nZVI [79]. While, the reduction of 10 ppm Cr(VI) solution to ~1ppm was observed in three days by employing activated carbon-supported iron prepared by carbothermal reduction technique [77]. Similarly, the carbon skeleton improved the stability of iron dramatically [80].

Therefore, a comprehensive summary of ZVI-based materials development was essential to design a compatible environmental material with practical contamination sites. Even though some review papers have recapitulated the versatile ZVI technology from the synthesis procedure to different countermeasures against the limitations of pristine ZVI [81, 82]. As well as another review paper has discussed the effect of solution chemistry and operational conditions on ZVI property [83]. Rare review papers systematically considered the co-effect of pH and DO on the performance of ZVI-based materials on targeted pollutant sequestration. For example, the efficiency of ZVI towards Cr(VI) removal was suppressed in the presence of oxygen [84], but another study discovered the opposing results in the presence of oxygen [85]. Briefly, the pH could greatly involve in the corrosion of ZVI and product establishment with DO. Therefore, we delicately evaluated the co-effect of pH (acid or alkaline) and DO (oxic or anoxic) on the capability of ZVI-based materials. Moreover, the literature involved in the preparation methods of ZVI-based materials (liquid-phase reduction and mechanical methods), four common ZVI-based materials (carbon-ZVI, sulfur-ZVI, bimetal of ZVI, and magnetite-ZVI composites), mechanism of Cr(VI) elimination, field application, and market penetration of ZVI-based materials were carefully discussed herein.

1.1.2. Synthesis of ZVI-based Materials for the Removal of Chromium

Various technologies can be classified into chemical and physical methods for the fabrication of ZVI-based materials to remove Cr from the environment. Chemical reductants (such as molecular hydrogen, hydrazine hydrate, $NaBH_4$, CO, etc.) were applied for Cr-reduction. While, the physical methods comprised mechanical crushing and metal electrode precipitation [86]. To the best of our knowledge, most of the researches only focused on the application of chemical reduction methods by using $NaBH_4$ [87] and mechanical milling [88, 89].

1.1.2.1 Liquid-phase Reduction

The liquid-phase reduction or borohydride reduction method is based on ferric and ferrous ions as ZVI precursors and $NaBH_4$ as a reducing agent. The earliest recorded prepared nano-scale ZVI was $FeBr_2$(aq) and $FeBr_3$(aq), which were reduced by $NaBH_4$ in the aqueous solution [90]. Similarly, various other researchers synthesized nano-scale ZVI with narrow size distribution (10-100 nm) [91, 92] and also coated with oxide shells [93]. For its preparation, the desired amount of Fe precursor such as degassed $FeCl_3$ solution was dropped with sodium borohydride solution (1 drop/s), the reduction reaction is presented in Eq (1-1). After the accomplishment of the reaction, the mixed solution was allowed to settle down for 20 min, and then it was centrifuged for collection of ZVI [94]. The synthesis process was conducted under an inert atmosphere as-synthesized ZVI can be easily oxidized in air.

$$4Fe^{3+} + 3BH_4^{-} + 9H_2O \rightarrow 4Fe^{0} + 3H_2BO_3^{-} + 12H^{+} + 6H_2\,(gas) \quad (1\text{-}1)$$

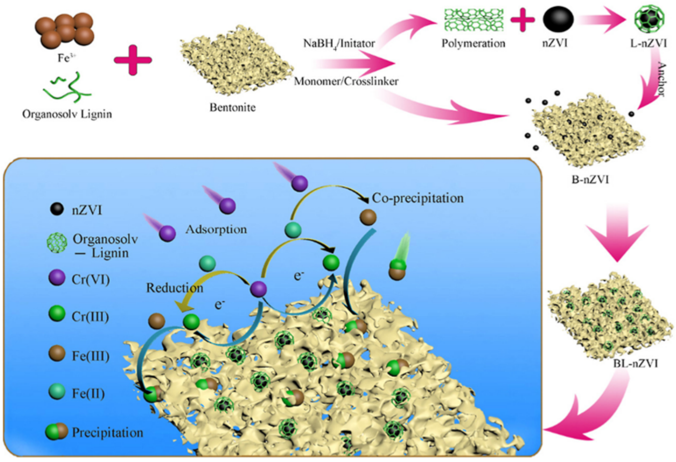

Figure. 1-3 The schematic illustration of the preparation of BL-nZVI by liquid-phase reduction method, and the removal process of Cr(VI). The Cr(VI) was reduced by loaded-ZVI and followed co-precipitation with Fe(III) [95], Copyright 2020, Elsevier.

Although extensive research has been carried out on bare ZVI preparation, the reactivity of nZVI might be lowered due to agglomerate irreversibly in the solution. ZVI doped on the template such as activated carbon [96], biochar [97], graphite [98] and chitosan [99] has demonstrated outstanding dispersion in the solution. Meanwhile, the removal performance of Cr(VI) was improved considerably for ZVI-loaded material concerning their monometallic counterpart. A group of researchers successfully produced biochar-supported nZVI by liquid reduction technique, wherein nZVI was loaded on biochar through carboxyl and silicon mineral within biochar. The removal capacity for Cr(VI) was 40 mg/g under initial pH 4.0 and could serve as a candidate material for groundwater remediation [100]. Further, as compared to non-supported nZVI (62.9%), the attapulgite-supported nZVI exhibited 90.6% removal efficiency for Cr(VI). Moreover, the stability and dispersion of nZVI were improved after doping evenly on a supporter of attapulgite [101]. A team of researchers performed a series of experiments to illustrate that bentonite-supported organosolv lignin stabilized nZVI (BL-nZVI) had a higher removal capacity of Cr(VI) than bare nZVI and bentonite-supported nZVI (B-nZVI) [95]. A comprehensive procedure from synthesis to the application has been demonstrated in Fig. 1-3.

1.1.2.2 Mechanical Method

The ball milling (BM) procedure has been proved to be an effective method for the preparation of nZVI [102]. Briefly, the iron grains undergo deformation, fracture, and welding repeatedly in the presence of vigorous collision between milling medium balls and iron particles. The size of the produced ZVI is a function of grinding duration time [103]. Further, the ZVI fabricated by mechanical milling subjects to the coarse size and unregulated shape, but the BM method can easily be scaled up with reasonable expenditures as compared to other approaches [104]. It was reported that the 2 mm grain of ZVI was milled in high energy planetary ball milling for 10 h, and the resulting 20.9 μm meso-ZVI eradicated Cr(VI) and organic pollutant effectively [105]. Recently, it was reported that different masses of AC were combined with 5.6 g of micron-scale ZVI (mZVI) in stainless steel milling jar and then grounded for 30 minutes at 300 rpm. Thereafter, it was followed by the addition of mZVI-AC in acidic and anaerobic Cr(VI) solution. The removal efficiency of Cr(VI) reached 94.01% within 2 h, it was also found that only 22.1% Cr(VI) was removed by the mixture of ZVI and AC [106]. These results verified the findings of a great deal of the previous work of Wang et al, (2020), and their thorough information has been presented in Fig. 1-4 [107].

Besides, the milling-induced displacement reaction to prepare various sizes of ZVI is a promising technology, as it could enable the recycling of scrap iron. The nanocomposites of ZVI with Al_2O_3 or ZnO were obtained after grinding of a sample of metallic aluminum or zinc with magnetite or hematite [108-110]. As the reaction processes have been presented in Eqs (1-2)-(1-4). Thus, by considering the ease of operation, cost-effectiveness, and readily scaling-up, BM is a promising technology for ZVI preparation.

$3Fe_3O_4 + 8Al = 3Fe + 4Al_2O_3$ (1-2)

$Fe_3O_4 + 4Zn = 3Fe + 4ZnO$ (1-3)

$Fe_2O_3 + 2Al = 2Fe + Al_2O_3$ (1-4)

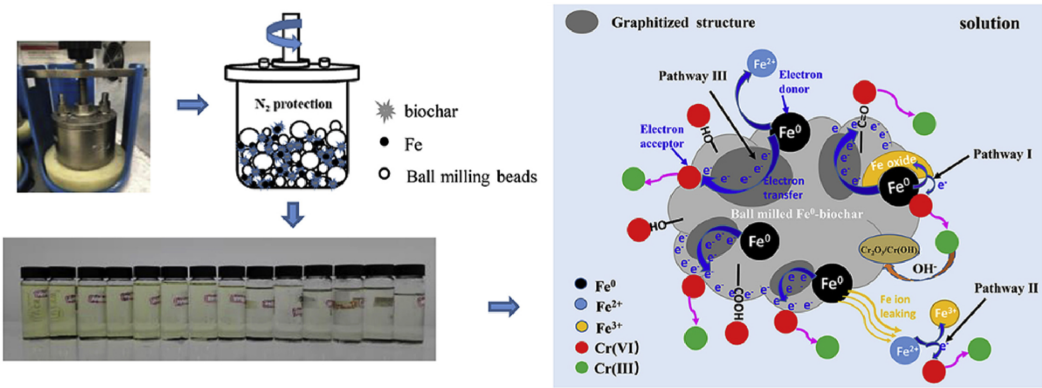

Figure. 1-4 The schematic illustration of the preparation of the biochar-supported ZVI by mechanical ball milling and its application for the Cr(VI) removal. The adsorbed Cr(VI) on pore channel and surface functional groups of biochar was reduced by Fe^0, meanwhile, part of Cr(VI) reduced in solution (Wang et al., 2020c), Copyright 2020, Elsevier.

1.1.2.3. Other synthetic methods

Apart from the numerous studies about chemical reduction and mechanical milling, there are also other non-widely discussed approaches for ZVI fabrication. For instance, the coal and iron oxide (FeO, Fe_2O_3, Fe_3O_4) were introduced into a silica glass tube equipped with a graphite cylinder radiation heater, the coal reacted with H_2O and CO_2 to produce reductant gas CO and H_2 over 800°C, and then CO and H_2 reduced iron oxides to ZVI via the thermal reduction method [111]. Similarly, the goethite was reduced to ZVI by H_2 with heat, nevertheless, the reducing reactant not only included ZVI but also magnetite [91]. Further, the chemical vapor condensation (CVC) process could decompose iron pentacarbonyl ($Fe(CO)_5$) under Ar or He atmosphere to prepare nZVI. Thus, the spherical nZVI (6-25 nm in diameter) was successfully prepared by CVC at

150℃ [112]. Moreover, pulsed electrodeposition (PED) was adopted to reduce aqueous iron salt to ZVI by desired current and voltage. In short, sacrificial iron anode and inert Ti cathode were immersed in $(NH_4)_2Fe(SO_4)_2$-contained electrolyte and were pulsed continuously. Thus, Fe^{2+} ions were reduced to Fe^0 and precipitated on Ti cathode [113]. A similar study was performed with PED to obtain nZVI with an average diameter of 19 nm [114]. The previously described spinning disk reactor (SDR) method proposed potential application on nZVI synthesis on the laboratory-scale [115]. Nevertheless, the nZVI production on a large-scale still challenges the routines declared above. We made a comparison of these mentioned methods and presented them in Table 1-1.

Table 1-1 The comparison of various preparation methods

Preparation methods	Process	Characteristic
Liquid-phase reduction	Mixing ferrous or ferric ions with $NaBH_4$ to obtain Fe^0 and then the reduced Fe^0 was loaded on supporters like biochar and bentonite.	The most commonly used method, but the additive of $NaBH_4$ is toxic and the post-treatment for effluent is required regulatorily [116].
Mechanical ball milling	Ball milling iron oxides with Al/Zn to produce Fe^0 or ball milling Fe^0 with supporters like AC.	Easily scaled-up for production, but energy consumption is the main concern [117].
Thermal reduction	Reducing iron oxides/hydroxides to Fe^0 through heating under high temperature reducing gas.	Recycling the scrap iron, however, the high energy consumption and the emission of greenhouse gas are the main disadvantages [118].
CVC	Decomposition of $Fe(CO)_5$	The size of Fe^0 particle is adjustable

	under high-temperature inert gas.	by changing temperature, the cost of raw material and energy consumption are the considerations [119].
PED	Preparing Fe^0 by electrochemical reduction.	The purity and thermal stability of prepared Fe^0 are high and the size is controllable, and the power consumption is the central concern [120].
SDR	Introducing $FeSO_4 \cdot 7H_2O$ and $NaBH_4$ solutions into a rotating disk with desired velocity and feeding position to gain Fe^0.	The size of Fe^0 is controllable by adjusting the rotational speed of the disk and the feeding position of solutions [121].

1.1.2.4. Conventional ZVI Composites for Cr(VI) Treatment

1.1.2.4.1 Carbon-ZVI Composites

Biochar, AC, and carbon nanotube have been extensively employed as iron templates to fabricate reliable iron-containing material [122]. Among them, AC possesses stable characteristics because of the developed pores and higher specific surface area, which provided plenty of vacant sites as the iron carrier [123]. Further, AC derived from various kinds of biomass has presented a superior efficiency as a potential adsorbent for Cr(VI) [27, 124, 125]. Moreover, the AC loaded-iron coupled adsorption with reduction has proved to be the main process for Cr(VI) removal [126]. To prepare homogenized AC supported ZVI, the AC was immersed in ferric chloride hexahydrate solution and then was introduced with $NaBH_4$ solution to reduce ferric to ZVI. Finally, nZVI-loaded AC was obtained after centrifugation, filtration, and drying in the nitrogen gas environment

[127]. It was found that the removal efficiency of Cr(VI) increased with an increase in iron loading and the highest removal efficiency (99%) was obtained with the iron loading of 10.9%. On the contrary, the maximum removal efficiency for AC without iron was only 40 %. Further, the characterization of nZVI-loaded AC after treatment has proved that Cr(VI) could be reduced to Cr(III) and precipitated with oxidized product ferric. To illustrate this phenomenon the cyclic voltammetry curve was conducted and was found that it exists the iron-carbon microcell facilitated the redox reaction between iron and Cr(VI).

Similarly, pristine biochar was derived from cornstalk and was modified with H_2O_2, HCl, and NaOH solution. Further liquid-phase reduction method as described above was employed to synthesis iron-loaded biochar and then it was applied for Cr(VI) removal from solution. The Cr(VI) removal experiments results showed that iron-loaded biochar modified with HCl solution exhibited better Cr(VI) removal efficiency than the other two materials. During the process of Cr(VI) removal, the biochar matrix stimulated the redox reaction of iron and Cr(VI) by electrostatic attractions between positively charged biochar and anion chromate, and faded the side impact of Cr(III)/Fe(III) (oxy) hydroxides deposit on the iron particle [128]. Moreover, the micro-galvanic formed between iron particle and carbon matrix contributed to another mechanism, Thus the role of biochar to serve as an electron-transfer mediator through removing aqueous solution Cr(VI) by silicon-rich biochar-supported ZVI was also verified [129]. Compared to iron-loaded on AC or biochar, magnetite-loaded carbon material could endure the defect of secondary separation for by-product [130], owning to magnetic properties of Fe_3O_4 which has attracted much attention for the separation procedure in Cr(VI) removal [131-135]. However, magnetite can easily be inclined to lose magnetic property as a result of oxidation to ferric oxide under acidic conditions [136]. A group of researchers decorated the multiwall carbon nanotube with magnetite nanoparticles and then modified with 1,6-hexanediamine to treat acidic Cr(VI) solution, this synthesized material presented good magnetic property and nearly reached 95%

removal rate of Cr(VI) at pH 2.0 [137]. In addition to the magnetite, γ-Fe_2O_3 had also shown magnetic properties. Laboratory synthesized γ-Fe_2O_3-carbon hybrids could be separated magnetically after the removal of Cr(VI) from the aqueous solution (Fig. 1-5).

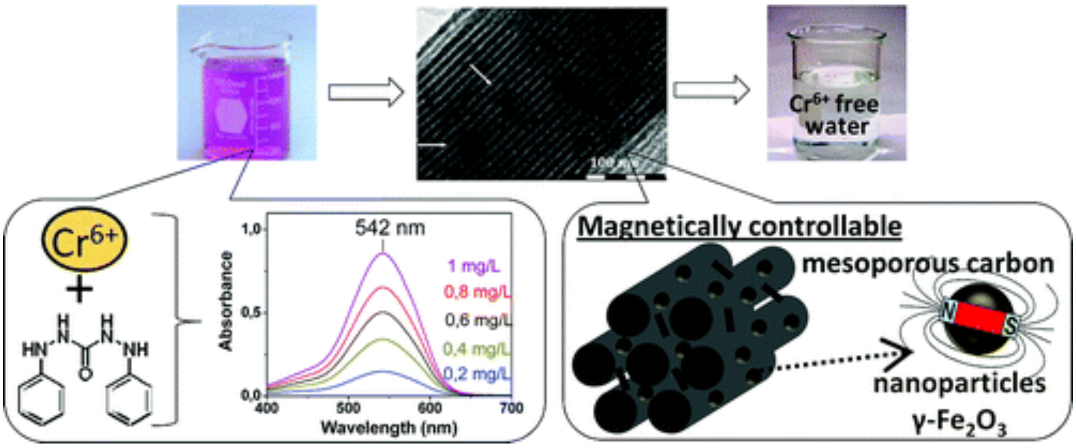

Figure. 1-5 The schematic demonstration of the removal of Cr(VI) by magnetic γ-Fe_2O_3-carbon composite [138], Copyright 2012, ACS Publications.

1.1.2.4.2. Sulfur-ZVI Composites

The reducible species like oxygen, protons [139], and water [140] can consume the electrons originated from ZVI and could damage the utilization efficiency of ZVI to target contaminants. Further, the sulfur compounds modified ZVI could alleviate the unintentional reaction of ZVI with water, and the efficiency of the electron of ZVI could be strengthened as a result. Notably, the findings have demonstrated the essential role of sulfur in the decontamination of trichloroethylene (TCE) [139, 141-143] and florfenicol [144] by S-ZVI. Besides, it has been suggested that sulfur speciation like sulfate radicals specified promising capability on pollutant degradation removal [145]. A team of researchers prepared the S-ZVI composite by mixing the desired amount of iron with elemental sulfur in planetary ball milling within 4 h. Then, the obtained S-ZVI material was employed to treat the Cr(VI) solution under aerobic conditions. The S-ZVI composites appreciably increased the electron effectiveness of iron to Cr(VI) which was 10.7-fold higher than bare iron. The enhancement effect of sulfur species was mainly ascribed to the FeS, which boosted the attachment of chromate onto the surface of S-ZVI and transferred the electrons to chromate [146]. Similarly, the aqueous Cr(VI) was eliminated by S-nZVI composites with a higher S/Fe molar ratio [147], and the removal process has been demonstrated in Fig. 1-6. Based on the prior literature about pollutants elimination by iron under aerobic and anaerobic conditions, it was observed that undesirable hydrogen evolution reaction between iron and water also depleted iron under anaerobic condition, thus decreased the longevity and electron selectivity of iron [148-152]. A comparison between bare iron and sulfur-modified iron was also executed, it was found that the latter implied conservative hydrogen production rate and amount [153]. A plausible explanation for the suppressed reactivity of ZVI to water was that the sulfur-modified ZVI inclined to hydrophobic and the reaction of hydrogen evolution from ZVI and water was mitigated as a result. It made sulfur-modified iron a potential material for anaerobic groundwater remediation. Recent cases also supported the hypothesis that sulfur could fascinate the selectivity and activity of iron to the targeted pollutants [154]. It has been demonstrated that S-nZVI fixed with carboxymethyl cellulose (CMC) presented higher mobility and stability in the sub surfaces for field applications [155].

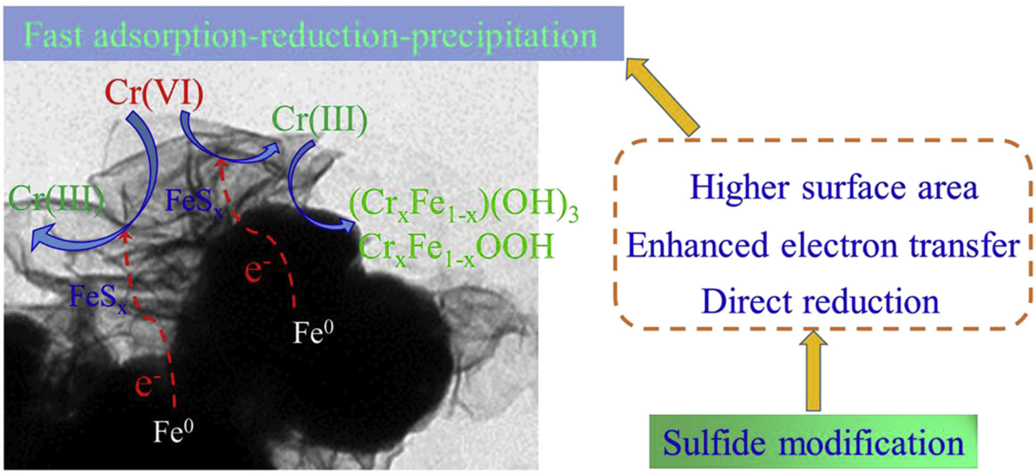

Figure. 1-6 Removal of aqueous Cr(VI) by S-nZVI. The increased surface area after modified with sulfur fascinated the adsorption of Cr(VI), and the FeS_x favored the corrosion of ZVI to target Cr(VI) [147], Copyright 2019, Elsevier.

1.1.2.4.3. Bimetallic Composites

Previous studies have defined bimetal of iron as incorporating the second metal such as Al, Ni, Pt, Ag [156] and Pd [157], Cu [158] with iron. The chemical and electronic properties of the bimetallic materials are optimized evidently as compared to the solitary metals [159]. Table 1-2 is illustrating a summary of the published reports on Cr(VI) removal by ZVI-based bimetallic materials. The main drawback of the bimetallic materials is the employment of noble metals like Ag and Pt or the use of toxic metals such as Ni and Cu as second metals. However, it makes the rarely available metals to fabricate bimetal of iron for pollutants remediation in the large-scale application. Al as the most abundant metallic element on the earth was an ideal candidate for Al-Fe preparation. Besides, the elemental Al has been extensively employed for the removal of a variety of pollutants such as Cr(VI) [160-163], bromate [164], TCE [165] and phenol [166]. The Fe-Al bimetallic particles were fabricated via depositing iron on the Al surface for Cr(VI) removal. The desired mass of Al was added to deionized water, which was priorly mixed with the desired concentration of $FeSO_4$ solution. Then it was rinsed and dried after stirred for 30 min. Different ratio of Al/Fe was obtained by regulating the dose of Al and Fe, the synthesized Fe-Al material was the Al-cored particle and Fe was deposited on its outer layer. The galvanic cell based on Fe as anode and Al as cathode for the electrode potential of Fe (-0.44V) was higher than Al (-1.67V). For this reason, the Cr(VI) was reduced by electrons donated by the Al core and transferred through the iron shell. The iron accelerated the electrons transfer from Al to Cr(VI) and higher removal efficiency was achieved over a wide range of pH (3.0 to 11.0) [72]. Similar studies of the galvanic effect of Al-Fe bimetallic particles for Cr(VI) elimination from aquatic environments was conducted by [167]. In contrast to earlier findings, however, Al-Fe bimetallic that ZVI coated with zero-valent Al has shown lower Cr(VI) removal capacity. However, another research team found that Fe/Al bimetallic material has demonstrated 21 folds higher Cr(VI) removal efficiency than Al/Fe bimetallic [168]. It was due to the oxidation of the Al layer by Cr(VI). Then, the electrons from Al and ZVI was quarantined from contaminants, but concerning iron-coated Al particle, the pathway of electron transfer from Al to Fe was unaffected by contaminants. The oxidized Fe^{2+} by Cr(VI) could be reduced to Fe^0 by Al spontaneously. A similar galvanic cell effect on Fe/Co bimetallic has been demonstrated in Fig. 1-7.

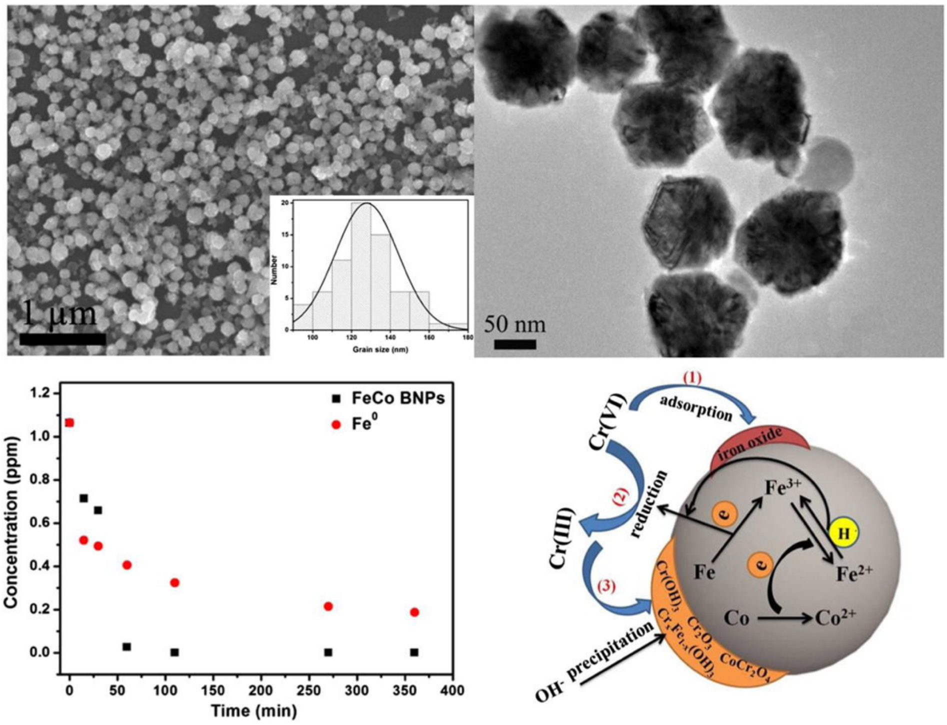

Figure. 1-7 The removal process of Cr(VI) by Fe-Co bimetallic coated by tea-polyphenol. The removal efficiency enhanced after incorporated with Co, ZVI was depleted by Cr(VI) and the Co can maintain the activity for ZVI that electron derived from Co can reduce Fe^{3+} to Fe^{2+}. The reduced Cr(III) separated from the solution by precipitated as $Cr(OH)_3$ and $Cr_xFe_{1-x}(OH)_3$ with Fe^{3+} [169], Copyright 2016, Elsevier.

As compared to the laboratory scale liquid reduction method, the melting and ball milling techniques for synthesis of bimetals exhibited higher homogeneity, superior mechanical stability, and greater potential in large-scale applications [170-173]. Typically, the desired ratio of Al and Fe powder in MgO crucible is melted in a vacuum melting furnace, and then the obtained Al-Fe was crushed into particles for further applications in the removal of targeted contaminants [173]. It was noticed that Al-Fe particles consisting of 20% Fe prepared through melting method has indicated favorable removal performance of Cr(VI) [174]. According to the available literature, ball milling is the most widely used mechanical procedure for the preparation of bimetallic materials for pollutants elimination [175-178]. The bimetallic materials produced by ball milling have demonstrated some advantages, such as simple operation, easy scaling up, and time-saving. However, as far as we know, most of the researches up till now did not focus on the preparation of Fe-Al particles through high energy ball milling, thus, the study would be more beneficial if a wider range of ball milling procedure for Fe-Al preparation is explored, especially for Cr(VI) eradication.

Table 1-2 ZVI-based bimetallic materials for Cr(VI) removal

Bimetals	Synthesis methods	Reducing agents	Removal (%)	Operational pH	Removal mechanism	Refs(s)
Ni-ZVI	Liquid-phase reduction	KBH_4	96.33-60.31	2.0-7.0	Reduction, adsorption, and precipitation	[179]
Ni-ZVI	Liquid-phase reduction	$NaBH_4$	100	1.0-3.0	Reduction, adsorption	[180]
Mont-supported Ni-ZVI	Liquid-phase reduction	$NaBH_4$	100	1.0-3.0	Reduction	[180]
Ni-ZVI	Chemical vapor deposition	H_2	83	N/A	Reduction, adsorption	[181]
Cu-ZVI	Liquid-phase reduction	$NaBH_4$	50.57	2.0	Reduction, adsorption	[182]
Pd-ZVI	Liquid-phase reduction	$NaBH_4$	95.5-73.0	3.0-8.0	Reduction, adsorption, and precipitation	[183]
Cu-ZVI	Liquid-phase reduction	Extract of green tea	94.7	5.0	Reduction, adsorption, and precipitation	[184]
Cu-SZVI	Liquid-phase reduction	Fe	97.9	8.0	Reduction	[185]
Al-Fe	Liquid-phase reduction	Al	90.0	7.0	Reduction, Precipitation	[167]

N/A. Not available

1.1.2.4.4. Magnetite-ZVI Composites

Magnetite or ferrosoferric oxide (Fe_3O_4) is commonly found in nature and characterized by properties like conductivity, magnetism, high surface area, and reducibility. Its importance in literature has been recognized in the elimination of targeted contaminants [71, 186-192]. It was reported that Cr(VI) could directly reduce by magnetite [193]. Further, the coupling of magnetite with iron for the degradation/reduction of contaminants would not only accelerate the corrosion of iron but also easily separate from aqueous solutions [194-196]. The structural Fe^{2+} of magnetite can act as an electron channel from iron to pollutants. Briefly, Fe^{2+}(s) in the octahedral site of magnetite could be oxidized by targeted contaminants to Fe^{3+}(s), and then the oxidized Fe^{3+}(s) could be reduced back to Fe^{2+}(s) by accepting electrons from Fe^0 and this process is thermodynamically favorable, as suggested by standard electrode potential, which is expressed as in Eq (1-5) [197], and without construal constrain [198, 199]. Regarding this, Fig. 1-8 is showing synergistic effects of Fe_3O_4/Fe on Cr(VI) removal.

$$2Fe^{3+}(aq) + Fe^0(s) = 3Fe^{2+}(aq) \quad \Delta E^0=1.21V \qquad (1\text{-}5)$$

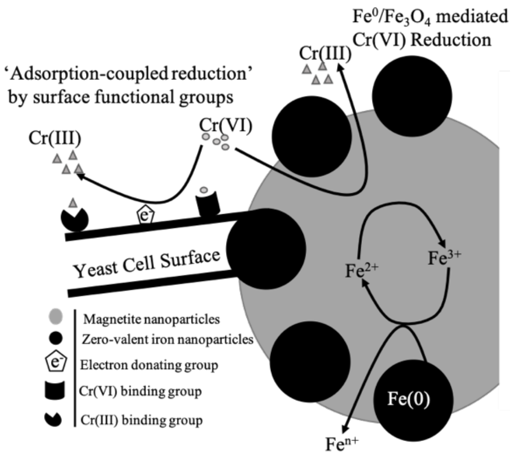

Figure. 1-8 The Yarrowia modified Fe_3O_4-Fe^0 employed for Cr(VI) elimination. The oxidized Fe^{3+}(s) from Fe_3O_4 by Cr(VI) converted to Fe^{2+} (s) by Fe^0 [200200], Copyright 2013, Elsevier.

To determine the effect of Fe^{2+}(s) of magnetite on Cr(VI) removal by Fe_3O_4-Fe^0, the removal performances of Fe^0-α-Fe_2O_3, Fe^0-γ-Fe_2O_3, and Fe^0-FeOOH were compared with Fe^0/Fe_3O_4. The Fe^0/Fe_3O_4 composite depicted a higher Cr(VI) conversion rate (65%) as compared to the other three composites. In contrast, the bare Fe^0 and Fe_3O_4 only converted 15% and 25% Cr(VI), respectively [201]. Moreover, the conventional Fe^0/Fe_3O_4 composite failed to consider the long-term impact of neutral or alkaline conditions. For instance, the Cr(VI) removal efficiency by Fe^0/Fe_3O_4 composite dropped significantly from 100% to 35.88 % as pH increased from 7 to 10 [202]. Furthermore, a previous study reported that the reduction of aqueous Cr(VI) by magnetite was ceased after 10-20 Å surface of magnetite was oxidized into maghemite (γ-Fe_2O_3) at pH 7.0 [203]. It was might be due to the surface passivation effect. Recently, a hydroxyl-modified Fe^0-Fe_3O_4 was fabricated with the addition of Na_2EDTA complexation, and then it was employed for the removal of Cr(VI). The results indicated that the concentration of Cr(VI) was lessened continuously, which could be attributed to the contribution of complexation of Na_2EDTA with Fe^{3+} and Cr^{3+} [178]. Moreover, the EDTA ligand assisted sequestration procedure has gained much attention presently due to its cost-effectiveness and its outstanding capability in the elimination of various contaminants like heavy metals, organic matters, etc. [204-209]. Nevertheless, the existing accounts have failed to resolve the contradiction between in-situ application and environment protection, the degradation of EDTA is important before its discharging to prevent the environment from EDTA toxicity [210]. Thus, more research efforts would be required to find out eco-friendly ligands which can assist the removal of Cr(VI) from the environment by Fe^0/Fe_3O_4 composites.

1.1.2.5. Mechanism of Cr(VI) Sequestration by ZVI-based materials

The route of Cr(VI) removal by ZVI-based materials is mainly controlled with the combination of reduction, adsorption, and co-precipitation, wherein the leading reduction process is effected essentially by pH and DO. The reduction capacity of pristine iron was inhibited due to the intrinsic defect caused by the passivation layer under alkaline and aerobic/anaerobic conditions. The resulting constitution of ZVI after treating with Cr(VI) could clearly be described by two linear dimensions [211]. Deliberately formulated ZVI-based materials have been used to preclude the passivation on the surface of ZVI to promote the electron efficiency and permanence of iron. In the current review, we predominantly consider the mechanism of encouraged Cr(VI) reduction potential of ZVI after incorporated into AC/biochar-ZVI, ZVI-based bimetal, sulfur-ZVI, and magnetite-ZVI composites.

The effect of the galvanic cell has been evidenced to be the main path for Cr(VI) reduction by AC-supported iron [212] and ZVI-based bimetal [213]. The electrons derived from ZVI could be transferred to the target contaminant via AC and the corrosion of ZVI was facilitated, consequently. The produced secondary reductant Fe^{2+} accompanied with the oxidation of Fe^0 could further reduce Cr(VI), and the Cr(III) could be precipitated with Fe^{3+} because the improved pH of the aqueous solution was initialed by redox couple of Cr(VI)-Fe^0/Fe^{2+}. Moreover, the adsorption property of AC on Cr(VI) could advance the reduction process.

Based on the reduction potential difference between Fe^0 and another metal in the bimetallic pair, Fe^0 could serve as an anode in the galvanic cell when coupling with less active metal and could also act as a cathode instead when coupling with the higher active metal [214]. The electrons transported directly from anode Fe^0 or indirectly through less active metal to contaminant, this pathway was greatly related to the configuration of ZVI-based bimetallic particles. In general, these two electron relocation channels were both driven by reduction potential difference of Fe^0-pollutants or Fe^0-Cu/Ni couples when Fe^0 dispersive homogeneously in bimetallic [215, 216]. The electrons originated from the Fe^0 core could simply be transferred indirectly through inert shell metal like Cu or Ni to Cr(VI), conversely. And the core-shell structure could deteriorate the undesirable effect of the passivation layer on Fe^0 [158, 217]. The effect of Cu layer on iron endurance to contaminant transformed from positive to negative when increased the mass of planting Cu on the iron core from heterogeneous and loose to dense and uniform film, owing to the galvanic corrosion of Fe-Cu was readily formed with loose Cu layer [218]. While Fe^0 performs as a cathode in bimetallic material, the reduction of contaminants arisen from three kinds of electron transportations; electrons from Fe^0, higher active metal (e.g., Al), and the galvanic cell of bimetallic [219]. Fe-Al bimetallic prepared by liquid reduction method or replacement reaction suggested a desirable Cr(VI) removal efficiency over a wide pH range (3-11), three electron assignment paths mentioned above contributed appreciably to the Cr(VI) reduction and the subsequent precipitation removal [72].

The reduction of Cr(VI) by sulfur-modified ZVI involved two phases, Cr(VI) reduced directly by Fe^0 and indirectly by the regenerated Fe^{2+} from redox of Fe^{3+}/Fe^0 couple [220]. The sulfured iron film on the surface of the iron core could enhance the corrosion of Fe^0 via the electron transfer from Fe^0 to oxidized Fe^{3+}. Meanwhile, the Cr(VI) reduction performance would be un-favored once excess sulfur was introduced as the core Fe^0 would be covered by a dense sulfidation iron layer [221]. It was also found that the regeneration of Fe^{2+} was absent in the reduction of Cr(VI) by excess sulfur modified iron, it can inference that the iron core was overlaid completely by the outer FeS layer and constrained the regeneration of Fe^{2+} from soluble aqueous Fe^{3+} [222]. Besides, the surface area of iron increased after the sulfidation, which helped in the adsorption of Cr(VI) and succeeding reduction. Corresponding to the passivation of ZVI, the virgin magnetite was also expected to be passivated with maghemite, goethite, and/or $Cr_{1-x}Fe_xOOH$ under alkaline pH during reaction with Cr(VI) which inhibited the reduction of Cr(VI), subsequently [71]. Similarly, a research study implied that the removal efficiency of Cr(VI) on magnetite-ZVI composite was 96.4 %, while about 18.8 % and 48.8 % were noticed by ZVI and Fe_3O_4, respectively [202]. It speculated that the regeneration of Fe^{2+} in magnetite sponsored the enhancement of Cr(VI) sequestration in magnetite-ZVI composite compared to bare ZVI [223]. The octahedrally located Fe^0 on Fe_3O_4 cycled the oxidized Fe^{3+} in magnetite to Fe^{2+} for the further reduction of Cr(VI) with Fe^0. The enhancement of electron selectivity of Fe^0 to Cr(VI), acceleration of corrosion of Fe^0, and the regeneration of Fe^{2+} are the main mechanisms that contribute to the superior Cr(VI) removal capacity by ZVI-based materials. The effect of galvanic cell and the conductive layer covered on Fe^0 accelerate the electron transfer from Fe^0 to Cr(VI), particularly.

1.1.2.6. Comparison with others iron-based materials

The Fe(II)-containing minerals such as pyrite (FeS_2), ferrous sulfide (FeS), and green rusts (GRs) established promising properties on the environmental remediation technologies [224-226]. The GRs as the layer structured Fe(II)-Fe(III) hydroxides possessed an outstanding competence on pollutants reductive removal owing to having a higher content of Fe(II). Meanwhile, the GRs were unstable and the stability modification was essential to lengthen the endurance. Green rust chloride immobilized with silicate (Si), phosphate (P), fulvic acid (FA), CMC, and bone char (BC) were used for Cr(VI) removal, and the results indicated that the release of Fe(II) was retarded after immobilization and fast removal of Cr(VI) was noticed by using over 90% of Fe(II) [227]. Bae et al., (2020) studied the capacity of Fe(II)-phosphate mineral (i.e., vivianite) on Cr(VI) removal, it found that Cr(VI) was reduced by structural Fe(II) in vivianite and then formed a complex with the generated mixed-valence Fe-phosphate [228]. Recently, the FeS_2 particles presented an effective Cr(VI) eradication over a wide pH range (6.0-9.5) [229]. To reinforce the removal of Cr(VI), the FeS-loaded titanate nanotubes were prepared hydrothermally, the Cr(VI) was reduced efficiently by FeS and the produced Cr(III) was adsorbed on titanate nanotubes simultaneously [230]. In general, a wider scope of iron-based materials that are not limited to ZVI-based materials or Fe(II)-containing minerals would help us to extend the application of iron-based materials on Cr(VI) sequestration.

1.1.3. The governing conditions for ZVI performance

1.1.3.1. pH

The speciation and oxidation states of Cr(VI) are greatly dependent on the value of solution pH. The species of Cr(VI) in aqueous solution consists of chromic acid (H_2CrO_4), bichromate ion ($HCrO_4^-$), chromate ion (CrO_4^{2-}), and dichromate ion ($Cr_2O_7^{2-}$), to illustrate the formation process of Cr(VI) complexes, the equations can be seen in Eqs (1-6)-(1-8) [231].

$CrO_4^{2-} + H^+ = HCrO_4^-$ $\quad pK_1=6.51 \quad (1\text{-}6)$

$CrO_4^{2-} + 2H^+ = H_2CrO_4$ $\quad pK_2=5.65 \quad (1\text{-}7)$

$2CrO_4^{2-} + 2H^+ = Cr_2O_7^{2-} + H_2O$ $\quad pK_3=14.56 \quad (1\text{-}8)$

The speciation of hexavalent chromium (1000 ppm) as a function of pH was calculated based on the value of pK, the Fig. 1-9 reveals that the predominant species of Cr(VI) are $HCrO_4^-$ and CrO_4^{2-} which exists at below pH 5.0 and up to pH 8.0, respectively.

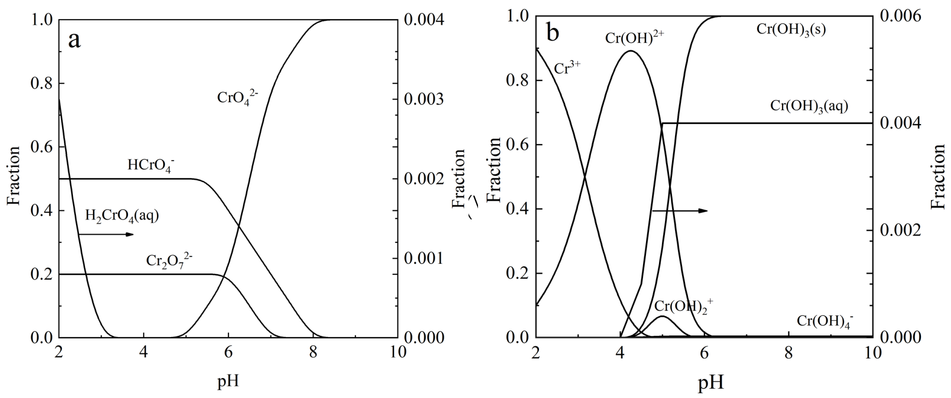

Figure. 1-9 Speciation diagram of (a) Cr(VI) and (b) Cr(III) at different pH

Further, the half-cell reactions of Cr(VI) under acidic and alkaline conditions are expressed as in Eqs (1-9)-(1-10), respectively [232]. Acidic solution favors the oxidation state of Cr(VI), on the contrary, Cr(VI) presents the least significant oxidation state under neutral and alkaline conditions. It was demonstrated that the reduction rate of Cr(VI) by Fe^0 increased notably for near 20 times from pH 7.5 to 5.5, and a negligible Cr(III) was detected after pH increased to 8.0. While, the logarithmic value of the first-order rate coefficient of Cr(VI) removal as a function of pH value is highly linear fitted which the slope is 0.72 ± 0.07 [233]. Further, a team of researchers stated that their data strongly supported the view of Alowitz et al. (2002) that the H^+ accelerated the corrosion of iron and promoted the Cr(VI) reduction. It was found that the removal efficiency of Cr(VI) was significantly declined from 97 % to 50 % as pH increased from 4.0 to 10.0 [234].

$Cr_2O_7^{2-} + 6e^- + 14H^+ \rightarrow 2Cr^{3+} + 7H_2O$ E_0=1.36V (1-9)

$CrO_4^{2-} + 4H_2O + 3e^- \rightarrow Cr(OH)_4^- + 4OH^-$ E_0=-0.13V (1-10)

$Fe^0 + HCrO_4^- + 7H^+ = Fe^{3+} + Cr^{3+} + 4H_2O$ Acidic conditions (1-11)

$Fe^0 + CrO_4^{2-} + 2H_2O = Fe^{3+} + Cr^{3+} + 4OH^-$ Alkalic conditions (1-12)

It should be noted that redox reactions between Fe^0 and Cr(VI) (Eqs (1-11)-(1-12)) were varied substantially as pH. Furthermore, the pH of the solution will increase as the redox reaction carried on either due to the protons consumed or hydroxyl ions (OH^-) generated. Referred to the theory of point of zero charge (pzc), the material presents the positive charge when the pH of the aqueous solution is below the pH of pzc (pH_{pzc}), it exhibits the negative charge when solution pH surpasses the value of pH_{pzc}, conversely [235]. Previously the pH_{pzc} value of ZVI was reported around 7.7-8.3 [236-239]. Thus, it can be concluded that ZVI will be negatively charged at pH over 8.3 and the transport of anion chromate in bulk solution to ZVI surface will be inhibited due to electrostatic repulsion.

To further demonstrate the alkaline condition post side effect on Cr(VI) removal, nano-ZVI was synthesized by the liquid reduction method and was applied for Cr(VI) elimination. It was observed that the removal rate of Cr(VI) decreased around 3-fold from pH range 3.0-4.0 to pH 9.0, meanwhile, the pH of the solution was increased from 3.0 to 6.2 within 60 min [240]. Contrary to the previous findings that increasing pH has a post negative effect on Cr(VI) removal, however, the removal efficiency of Cr(VI) was higher at pH 5.0 under Fe^0/H_2O system between pH 4.0 and 6.0. Comparing to pH 5.0, iron showed a higher reduction capacity at pH 4.0 but the reduced product of Cr(III) was soluble and remained in solution. Furthermore, at pH 6.0, the reduction rate of Cr(VI) was declined greatly due to the minor availability of free protons [85]. Here, the major source of uncertainty is the applied method for the evaluation of the removal performance of Cr(VI) by iron. Generally, the removal mechanism includes the combination of reduction, adsorption, and co-precipitation. Regarding monometallic iron, the removal was mainly contributed by reduction and adsorption at acidic conditions, reduction and co-precipitation under neutral or alkaline conditions. Most accepted equations for removal capacity of Cr(VI) can be seen in Eqs (1-13)-(1-14).

$$q_1=(c_0-c_{Cr(VI)})/c_0 \quad (1\text{-}13)$$

$$q_2=(c_0-c_{total\ Cr})/c_0 \quad (1\text{-}14)$$

Wherein, q_1 and q_2(mg/g) are the removal capacity, c_0(mg/L) is the initial concentration of Cr(VI), $c_{Cr(V)}$ and $c_{total\ Cr}$ (mg/L) are the concentrations of Cr(VI) and total chromium (Cr(VI), respectively. For the Eq (13), it was observed that the value of q_1 decreases gradually as the increase of pH because of the drop of Cr(VI) reduction rate, whereas the variation of q_2 as pH was affected by Cr(VI) and the reduced product Cr(III) for the Eq (14). In brief, reduced soluble Cr(III) decreased gradually as pH increase and started to precipitate when pH over 5.0, and the residual concentration of Cr(VI) increased as pH. Therefore, the value of q_2 was not linearly related to pH. This illustrated the optimal pH for the removal of Cr(VI) by Fe^0 was not the lower value when employed Eq (14). Although extensive research has been carried out to assess the capability of iron for Cr(VI) elimination, however only a few researchers have been able to draw a systematic approach [241-245]. Thus, it was found that a much more systematic approach would result in the identification of reduction and removal capability of iron, a complete removal process should involve the conversion of Cr(VI) to Cr(III) and the final separation of Cr(III) from solution.

1.1.3.2. Dissolved Oxygen

The erosion of iron is highly affected by dissolved oxygen (DO) in aqueous solution, the oxidation product can be seen in Eqs (1-15)-(1-17), it was demonstrated that in the presence of a high concentration of DO in solution, ferrous ion (Fe^{2+}) can be further oxidized to ferric ion (Fe^{3+}) and then could be precipitated with hydroxide (OH^-) [246]. While, Fe^0 is reported as an effective reductant for Cr(VI) [247, 248].

$2Fe^0 + O_2 + 4H^+ = 2Fe^{2+} + 2H_2O$ (1-15)

$4Fe^{2+} + 4H^+ + O_2 = 4Fe^{3+} + 2H_2O$ (1-16)

$Fe^{3+} + 3OH^- = Fe(OH)_3(s)$ (1-17)

It was documented that iron erosion under anaerobic implies a slower rate than that under aerobic, as shown in the Eqs (1-18)-(1-19), due to the formation of ferrous (oxy) hydroxides ($Fe(OH)_2$) instead of ferric (oxy) hydroxides (FeO(OH)). It was found that $Fe(OH)_2$ remained stable in free oxygen and at low temperature [150, 249].

$Fe^0 + 4H_2O = Fe^{2+} + 2H_2 + 4OH^-$ (1-18)

$Fe^{2+} + 2OH^- = Fe(OH)_2(s)$ (1-19)

In general, oxygen may compete for the available sites and electrons of iron with contaminants like Cr(VI) and reduce the efficiency of the electron. On the other hand, the desired concentration of DO stimulated the generation of soluble Fe^{2+} and promoted the elimination of pollutants [250].

The Fe^{2+} was stable under acidic conditions in the presence of oxygen but could easily be oxidized by oxygen under alkaline conditions. The reaction kinetics of Fe^{2+} with Cr(VI) under pH 2.0 was higher than those under pH 6.0 for two orders of magnitude [246, 251, 252]. It meant that Fe^{2+} predominant the redox reaction with Cr(VI) under acidic solution in the presence of oxygen. To further demonstrate the role of Fe^{2+} on Cr(VI) removal under acid/anaerobic solution, 1,10-phenanthroline was introduced as a populated indicator for Fe^{2+} into Cr(VI)/Fe^0 system to complexes strongly with Fe^{2+}. Hence, the availability of Fe^{2+} to Cr(VI) was inhibited, and the results indicated that the removal of Cr(VI) was substantially suppressed in the presence of 1,10-phenanthroline [220]. Similar reports were also supported this idea by adding 1,10-phenanthroline to isolate Fe^{2+} from acid/anaerobic aqueous solution [204, 221, 253]. The generated Fe^{2+} abound in bulk solution which verified by the results that removal rate of Cr(VI) impeded after introducing 1,10-phenanthroline complex. Notably, the data from several sources have identified that the increase in removal performance of Cr(VI) resulted from the produced Fe^{2+} under oxic solution that associated with the Fe^0 surface-bound with Fe^{2+}, not just the free Fe^{2+} in bulk solution [220, 254].

The reduction product of Fe^0 in Cr(VI) solution favors forming the γ-FeOOH or α-FeOOH over α-Fe_2O_3 or γ-Fe_2O_3 [255-257]. Wherein the iron oxyhydroxides (goethite and lepidocrocite) had shown relatively high specific surface, and the reduced Cr(III) could easily be adsorbed on them [258]. The iron oxyhydroxides incorporated with Cr(III) could further transform to sparingly soluble $Cr_xFe_{1-x}(OH)_3$ [259, 260]. This claim has been completed by many researchers [85, 261, 262]. Briefly, it was found that the product was different under oxic and anoxic conditions of Fe^0/Cr(VI) setup, meanwhile, the removal efficiency under oxic was much better than those under anoxic conditions. The porosity of the $FeCr_2O_4$ layer was predominantly covered on iron under oxic/acidic conditions, while the compact layer of hydroxide/oxyhydroxides of Fe(III) and Cr(III) was produced under anoxic/acid condition. The redox product of $FeCr_2O_4$ under oxic/acid conditions substantially coincided with the product of Fe^{2+} and Cr(VI) [263]. It can be concluded that the governing mechanism for Cr(VI) removal by iron under oxic/acid conditions was due to the generation of Fe^{2+} from iron with oxygen and then reacted with Cr(VI).

A recent study concluded a converse view that $FeCr_2O_4$ was formed under anoxic/acid condition, while the iron/chromium oxyhydroxides appeared in the presence of oxygen under acid condition, nevertheless, the presence of oxygen impaired the removal rate of Cr(VI) by iron [240]. The most likely cause of either positive effect or negative effect of DO on Cr(VI) removal under acid condition was the transformation of redox product of Fe^0/Cr(VI) with DO concentration. Typically, the desired amount of oxygen could accelerate the corrosion of iron and the generation of reductant Fe^{2+} accompanied with reserved protons depletion, and the Cr(VI)/Fe^{2+}(aq) and Cr(VI)/Fe^{2+}(s) (bounded on Fe^0) couples could generate loose $FeCr_2O_4$. Adversely, the excess oxygen could deteriorate the effectiveness of iron through further oxidation of Fe^{2+} to Fe^{3+} by

Fenton reaction [264], and the consumed protons could produce compact $Cr_xFe_{1-x}(OH)_3$, simultaneously. Thus, more efforts are required to find the exact critical value of DO concentration. Previous studies about oxygen influence did not focus on its concentration in solution, and most of the attempts were made to compare the aerobic and anaerobic by aeration with oxygen or nitrogen gas [265, 266]. Furthermore, the passivation layer composed of hydroxide/oxyhydroxides of Fe(III)/Cr(III) on the surface of iron hindered the electrons transfer from iron to Cr(VI) under over oxygen content [83]. The shielding effect of the passivation layer formed in the presence of oxygen is evidenced [254].

Altogether, the effect of DO on Cr(VI) removal by ZVI was not only dependent on solution pH but also relied on its concentration. It could be divided into the following five pathways: (1) The important intermediate reducing agent Fe^{2+} that originates from Fe^0 contributed to the elimination of Cr(VI) under lower DO and acidic conditions; (2) the higher value of DO under acid conditions could oxidize immoderately Fe^{2+} to Fe^{3+} and weaken the electron efficiency of Fe^0; (3) under anaerobic/acid conditions, the protons accelerated the erosion of Fe^0 and the produced Fe^{2+} could participate in the reduction of Cr(VI); (4) Due to the instability of Fe^{2+} under aerobic/alkaline conditions and the generated compact precipitate covered on the Fe^0, and the durability of Fe^0 deteriorated accordingly; (5) The Fe^0 and the produced Fe^{2+} both were involved in the reduction of Cr(VI) in the deficiency of DO under alkaline conditions, which improved the removal efficiency of Cr(VI). The specific information about the co-effect between DO and pH is shown in Table 1-3.

Table 1-3 The co-effect of DO and pH on Cr(VI) removal by iron

Operation conditions	Aerobic/acid		Anaerobic/acid	Aerobic/alkaline	Anaerobic/alkaline
	Low DO	High DO			
Effect	Strengthen the performance of iron	Deteriorate performance of iron	Strengthen the performance of iron	Deteriorate performance of iron	Strengthen the performance of iron
Mechanism	$2Fe^0 + O_2 + 4H^+ = 2Fe^{2+} + 2H_2O$ $Fe^0 + HCrO_4^- + 7H^+ = Fe^{3+} + Cr^{3+} + 4H_2O$ $Fe^{2+} + HCrO_4^- + 7H^+ = Fe^{3+} + Cr^{3+} + 4H_2O$	$4Fe^0 + 3O_2 + 12H^+ = 4Fe^{3+} + 6H_2O$	$Fe^0 + 2H^+ = Fe^{2+} + H_{2(gas)}$ $3Fe^{2+} + HCrO_4^- + 7H^+ = 3Fe^{3+} + Cr^{3+} + 4H_2O$ $Fe^0 + HCrO_4^- + 7H^+ = Fe^{3+} + Cr^{3+} + 4H_2O$	$2Fe^0 + 2H_2O + O_2 = 2Fe^{2+} + 4OH^-$ $4Fe^{2+} + O_2 + 2H_2O = 4Fe^{3+} + 4OH^-$	$Fe^0 + 4H_2O = Fe^{2+} + 2H_2 + 4OH^-$ $Fe^0 + CrO_4^{2-} + 2H_2O = Fe^{3+} + Cr^{3+} + 4OH^-$ $3Fe^{2+} + CrO_4^{2-} + 4H_2O = 3Fe^{3+} + Cr^{3+} + 8OH^-$

1.1.4. Practical Applications of ZVI-based materials

Since it was reported in 1925, permeable reactive barrier (PRB) is attracting a lot of interest in the remediation of groundwater pollutants such as organic matters, heavy metals, inorganic matters [267, 268]. It was recorded in 2009 that there were 13 full-scale PRB present worldwide. From them, 6 PRBs were equipped with ZVI as reactive media [269]. The field-scale of PRB was operated under more complicated conditions as compare to the laboratory-scale, such as they did face fairly slow flow, low dissolved oxygen, relatively high pH value, lower temperature, low contaminants concentration, and a range of inorganic anions like CO_3^{2-}, SO_4^{2-}, NO_3^- [270, 271]. In the laboratory studies, the principal mechanism for Cr(VI) removal by ZVI-PRB was presumed to be the redox reaction between Cr(VI) and Fe^0, which could be undermined by the formation of insoluble Fe(III)/Cr(III) (oxy) hydroxides phase [272]. While the removal process for Cr(VI) under field sites would be uncertain owning to the other competitive ions. In general, more attempts are needed to transfer laboratory-based theory to field-scale application.

Longevity and reactivity are the two major considerations in the long-term operation capability of PRB [273]. An early example of research into the reactivity of ZVI PRB has demonstrated that the intensively reducing process and high pH value could be associated with the diminish of reactive media due to the precipitation of inorganic species, which consequently clogged the permeable pore of PRB [274]. Further, about 0.88%/year decline in porosity of ZVI PRB was noticed, which hinted that the loss of carbonates (90%), calcium (82%), and sulfate (69%) in groundwater flow through the PRB [275]. Moreover, the column experiments with various groundwater geochemistry for sequestration Cr(VI) through ZVI were also investigated to elucidate the effects of hardness and carbonate on Cr(VI) removal by ZVI in groundwater, and their results indicated that the capability of ZVI dropped slightly in the presence of calcium hardness. Notably, the Cr(VI) removal capacity of ZVI decreased by 17% under magnesium solution. Furthermore, it was found that a 33% decrease in ZVI performance was noticed in the co-present of hardness and carbonate in columns [276]. Similar research implied the bicarbonate gave the mildest impact on Cr(VI) removal by ZVI compared to calcium, magnesium ions, whereas bicarbonate together with calcium posted the greatest impact on ZVI efficiency for Cr(VI) removal [277]. On the other hand, not all deposits on the barrier are unfavorable for the reactivity of ZVI media, the ferrous precipitates like magnetite and green rust could transfer electrons from ZVI to pollutants [278, 279]. It can therefore be assumed that the permeability of PRB could drop gradually due to the formation of precipitate on the surface of ZVI particles, but the reactivity of ZVI could either reduce or enhance with time, which can be correlated with the geochemical conditions of groundwater like DO and pH.

The longevity of ZVI PRB could be referred to as its potential to maintain the reactivity of filling media and hydraulic performance, while the hydraulic performance was related to the residence time of plume pass through the barrier [280]. Construction methods, reactive material, and groundwater constituents affected the life cycle of PRB. The data from several sources have identified that the trench-based construction method showed significant remediation capacity on Cr(VI) compared to the caisson-based construction method. Notably, the ZVI and iron oxide-coated sand could reduce the environmental impact on PRB. Natural organic matters (NOM) in groundwater could lower the PRB capability due to the depletion of the higher amount of ZVI [281]. For instance, no significant reduction in the performance of PRB was observed even after continuous operation for 13 years [61, 282].

In contrast, the study of Bronstein, et al (2005) noticed a significant fluctuation in the removal performance of Cr(VI) after the operation of one year [283]. Thus, It has been presumed that the uneven depletion of ZVI in plume could decline the longevity in the PRB over time [284]. Apart from the study aimed at the construction method, groundwater constituents, and media reactivity, more comprehensive hydrology of groundwater should be examined. Therefore, the contaminants concentration distribution and flow velocity changes should be taken into account for PRB design and installation. Besides the bare ZVI used for PRB reactive media, the ZVI-based materials like S-nZVI and nZVI-SBA-15 have been developed as the substitute material for Cr(VI) isolation in groundwater at pilot-scale or field trials [285, 286]. Compared to single ZVI, ZVI-based materials could prevent the reactivity loss of nZVI that results from congregating. Various surveys have shown that the permeable reactive columns filled with activated carbon fiber supported nZVI have exhibited a higher Cr(VI) removal efficiency [287]. Therefore, more research efforts are needed in this direction for shifting ZVI-based materials PRB from laboratory-based data to practical implantation.

Moreover, the injection well technology is another most used method excluding PRB technology for groundwater remediation [288]. The media particles were prepared as slurry before injecting into the polluted source sites or plume, in which the extensively utilized media are ZVI and bimetallic particles of iron [271]. Remarkably, the Cr(VI) concentration declined substantially from 4-8 mg/L to 0.015 mg/L by employing a composite of ferrous sulfate (Fe_2SO_4) combined with sodium dithionite ($Na_2S_2O_4$) as the reactive media in the injection well [289]. Sodium dithionite could prevent the premature oxidization of Fe^{2+}, and could prevent the clogging of injected media, and maintained effective hydraulic conductivity. Similarly, an over 96% degradation ratio of TCE was noticed by injecting bimetallic particles of Fe-Pd gravitationally into the groundwater [290]. The particles were supplied at an optimal rate, which presented ideal mobility and diffusion. However, the in-site remediation cases all required the ZVI-based materials prepared on the spot, for example, the CMC-stabilized Fe-Pd composite was synthesized on the site through liquid reduction right before injection into the wells to minimize the reactivity loss of filling material [291]. Thus, the transport, storage, and cost of the raw materials are the potential impediments. Besides, long-term activity, persistence, and dispersion of ZVI-based materials, the stability and mobility of the treated contaminants both entail the advanced, easy-synthesis, and low-cost ZVI-based materials [292-294].

1.1.5. Barriers in Market Penetration of ZVI-Based Materials in Removing Cr (VI)

From the acquisition of raw material, the preparation and performance evaluation of ZVI-based materials from laboratory-scale to commercial applications, the barriers in market penetration are remained mainly attributed to the technology challenges, toxicity assessment to ecosystems, and the cost. The performance of ZVI-based materials in field trials or full-scale applications is rarely documented excluding nZVI. A pilot-scale in-situ remediation test was conducted with commercially available nZVI at Kortan in Hradek nad Nisou. The findings depicted that the concentration of Cr(VI) and total chromium in groundwater were substantially decreased after injecting nZVI with no observed effect on groundwater properties [295]. While, a lot of laboratory-based data has supported that template-supported nZVI or modified nZVI could prevent the agglomeration of the nZVI particles and impair non-target reactions [296, 297]. However, the longevity, reactivity, and removal mechanism of ZVI-based materials for Cr(VI) removal in field remediation are still unclear and act as an obstacle to the market penetration of this technology. The unintentional migration of nZVI through the soil, water, and air can threaten the ecosystem, especially for plant cells, animal cells, and microorganism cells [298, 299]. Thus, the toxicological effects of nZVI on organisms should be addressed in future research [300, 301]. In the commercialized application cases of ZVI, some companies prepared ZVI suspension with organic additives and dispersants to promote diffusion and delivery of ZVI. However, more organic additives are needed in terms of nZVI for the higher surface area and smaller particle size [288]. There would be more regulation considerations on the organic additives and dispersants to the ecosystem. Due to the presence of aggregation of nZVI in the subsurface environment, the nZVI has shown inferior migration than surface-modified nZVI, It was found that the migration of nZVI could be enhanced significantly after coated with starch and polyacrylic acid [302]. However, the potential environmental risks of ZVI-based materials are still unknown. Hence strategies to balance the potential environmental risks and expected environmental interests of ZVI-based materials would be required in clarifying the migration and toxicological impacts at specific sites. Further, as can be seen in Table 1-4, the demand amount of ZVI for a project was so high. Given price was \$0.55-15/lbs for ZVI from 325 μm to below 1 μm. It's a comparative high expenditure for the ZVI during the remediation project. Compared to ZVI produced directly from the smelter, the ZVI derived from scrap iron and recycled material could lower the expenses remarkably. Regarding the sparing information about the actual cost for producing ZVI-based materials like sulfur-ZVI, Cu-ZVI, AC-ZVI, it's urgent to evaluate the cost for the synthesis of ZVI-based materials with scrap iron.

Table 1-4 ZVI remediation cases and the consumption (https://hepure.com/product-list/case-studies/)

Site background	Contaminant	Mode of application	In-situ or ex-situ	Dosage
Vadose zone soils beneath a large manufacturing facility	Cr(VI)	Hydraulic injection	In-situ	64,000 lbs
The facility had operated for 50 years as a machine shop where parts were degreased by a variety of solvents	PCE[a], TCE	PRB and injection	In-situ	154,000 lbs
Former Dry Cleaner	PCE	Injection	In-situ	401,310 lbs
Located in North Central Ohio	PCE, TCE, and VC[b]	Injection	In-situ	145,000 lbs

[a] Tetrachloroethene

[b] Vinyl Chloride

1.1.6. Conclusions

Altogether, the ZVI-based materials have been well-recognized and comprehensively employed for pollutants sequestration. This review has discussed four conventional ZVI-based materials (ZVI-AC/biochar, ZVI-sulfur, ZVI-magnetite, and bimetal of ZVI), two prevailing preparation methods (liquid reduction method and mechanical ball milling procedure), and their applications on Cr(VI) removal. The removal mechanisms have mainly involved the reduction, adsorption, and co-precipitation. Besides, the developed performance of ZVI-based materials regarding the pristine ZVI could be attributed to the galvanic cell effect for ZVI-AC/biochar and bimetals of ZVI, and the regeneration of ferrous ions for sulfur-ZVI and magnetite-ZVI. Especially, the electron selectivity of ZVI to Cr(VI) was substantially controlled by the DO and pH of the solution. One of the most significant findings of this review is that the transfer of electrons from ZVI to Cr(VI) was appreciably dominated by five pathways. Briefly, the acidic/low oxygen condition facilitated the removal capacity of ZVI by generating more reductants, and the removal efficiency of ZVI on Cr(VI) was suppressed under acidic/oxygen-rich conditions due to the over-exhaustion of iron by oxygen, conversely. On the other hand, acidic/anaerobic conditions promoted the Cr(VI) removal through accelerating ZVI hydrogen-evolution erosion, and the erosion product aqueous ferrous ions were an effective reducing agent. The Cr(VI) removal rate was deteriorated under alkaline/aerobic conditions due to the more susceptible oxidation of Fe^{2+} by oxygen under alkaline conditions compared to acid conditions. The last pathway of DO and pH on iron capability under alkaline/anaerobic was that the produced Fe^{2+} contributed to the reduction of Cr(VI), which improved the removal efficiency of Cr(VI). The insights gained from this study may assist in groundwater remediation through PRB. Limited PRB field applications overlooked to consider the distribution of Cr(VI) concentration and flow velocity gradient in groundwater, which could help in optimizing the PRB dimension and avoid the uneven loss of ZVI media. More information on technology challenges, potential ecosystem risk, and cost of ZVI-based materials would help us to establish a greater degree of accuracy on the commercialization of this technology. The following are the key suggestions for future applications of ZVI-based materials:

- The selection of suitable ZVI-based materials is needed to reduce the unintentional consumption of ZVI by O_2, water, or other untargeted pollutants
- The solution chemistry of contaminated sites should be vigilantly evaluated because the utilization efficiency and selectivity to the aimed contaminants of ZVI in ZVI-based materials is greatly affected by pH and DO
- The large-scale and low-cost production of ZVI-based materials is necessary.

Although many ZVI-based materials have shown superior performance in the laboratory-scale or pilot stage, the practical performance is rarely available, like the PRB of ZVI-based materials

- Migration and toxicology of ZVI-based materials in the aquatic environment or soil are the potential ecological risk, thus the treated sites with ZVI-based materials would require long-term monitoring, and the used ZVI-based materials should be disposed of safely.

1.2. Mechanical ball milling prepared iron-based material and their application on contaminants removal

1.2.1. Introduction

The versatile and developing zero-valent iron (ZVI) has been extensively applied to pollutants removal, including toxic heavy metals and organic matters, for over two decades. Since the first full-scale field application for contaminated groundwater remediation at the U.S. Coast Guard (USCG) Support Center near Elizabeth city in June 1996 [61], the ZVI technology has received considerable development in aquatic pollution management and control. However, the intrinsic drawbacks of ZVI such as agglomeration, easy oxidation, surface passivation, and the selectivity to the aqueous conditions challenge the further penetration of the market [83, 303, 304]. The iron-based materials (IBMs) that impregnate ZVI in activated carbon (AC) or biochar exhibit promising competence in deregulating the limitations of ZVI. When compared to its single counterpart, the capability of ZVI on As(V) removal was significantly improved after incorporation in AC at pH 7. The accelerated corrosion rate of ZVI after doped into AC is primarily responsible for the improved performance on As(V) [305]. Previous studies performed with ZVI/AC exhibited potential application in nitrate removal. The galvanic cell effect of ZVI/AC accounts for the higher nitrate reduction capacity [306]. Besides, the adsorption property of AC also accounts for the enhanced degradation performance of IBMs.

Several processes for preparing IBMs have been developed over the last two decades, including liquid reduction [307], thermal reduction [308-310], and ball milling [311]. The developing ball milling technique for IBMs synthesis has distinct advantages in terms of manufacturing cost and scale-up. In contrast to liquid and thermal reduction procedures, ball milling is a simple to use and free-solvent method [13]. Mechanical ball milling with additive under programmed rotation direction, velocity, and duration could be used to create the desired particle size and specified surface IBMs. After deformation, disintegration, and cold-welding of individual particles during mechanical grinding, the intensive impact between milling media and substrate refined particle size [103]. The energy of the collision was accumulated in the defects of prepared materials, which stimulated a chemical reaction that was unfavorable at the ambient temperature. Palo Matteazi et al. successfully produced ZVI by ball milling a hematite and aluminum combination at ambient temperature [110]. The dispersed homogenous iron oxides on biochar after grounding improved the interface of iron oxides with aqueous Cr(VI) and the findings revealed the removal capacity of Cr(VI) was 48.1 mg/g, which was higher than that of other biochar/iron composites [312]. Except for the newly produced chemical material after mechanical ball milling, the refined particle size and the increased specific surface area contribute to the reliable and innovative IBMs material as well [313]. After ball milling, the surface area of the magnetic biochar/Fe_3O_4 material was nearly 12 times that of pristine biochar, with maximal carbamazepine and tetracycline adsorption capacities of 62.7 mg/g and 94.2 mg/g, respectively [314]. Furthermore, as a result of improved dispersion, hydrophilicity, and decreased zeta potential of carbonaceous after the introduction of surface functional groups within ball milling, more active sites were exposed to the contaminants that have an affinity for water [315, 316].

Recently, IBMs modified by ball milling with sulfur, elemental metals, and organic matters for environmental applications were reported. An extensive literature investigation showed just a handful of reviews on ball milling for IBMs synthesis, particularly those that focused on performance enhancement and pollutants removal.

Therefore, it's important to systematically summarize the development of the ball milling prepared IBMs and their application on incapacitating the inherent properties of ZVI such as low electron efficiency, agglomeration, and easy deactivation. The challenge of IBMs in-field implementation was being discussed carefully and indicated the research direction for pragmatic-oriented IBMs. Habitually ignored agitation intensity and flow velocity of contamination removal tests by IBMs under laboratory conditions were deliberated, specifically.

1.2.2. Approaches for IBMs preparation

There has been a lengthy history of mechanochemical research. The first reported mechanochemical reaction was in Theophrastus's book One Stones, written in the 4th century B.C. [317]. Peters et al. defined mechanochemical in 1952 [318]. From the 1970s onwards, mechanochemical was widely used for environmental applications. Apparatuses for mechanochemical are commonly known as planetary ball mills, vibratory ball mills, and stirring ball mills. The planetary ball mill is mostly used in laboratory-scale trials due to the fact that no land is required, and it can be used with single or multiple grinding vials. The spin direction and velocity of the grinding vial including the rotation of the vial and the reverse revolution of the so-called sun wheel, motivate impact and shear force between the grinding medium balls and substrate [13]. Mechanical energy is partly converted to chemical energy and stored in the refined substrate particles due to lattice deformation and dislocation.

We compared ball milling with thermal reduction and liquid phase reduction based on the properties of the resulting material and the preparation conditions, as seen in Table 1-5. The ball milling technique shows edges at a mild reaction temperature and free of toxic solvent. In addition, the increased surface area and homogenously distributed Fe and the secondary material after grinding contribute to the enhanced reactivity of Fe.

Table 1-5 The comparison of ball milling with other approaches on representative IBMs preparation for contaminants removal

Materials / Methods	Biochar-iron			Sulfur-iron			Bimetallic Fe-Ni particle		
	Properties	Conditions	Refs.	Properties	Conditions	Refs.	Properties	Conditions	Refs.
Ball milling	Increase surface area and zeta potential. Equalize the size distribution.	Ambient conditions without solvent.	[319]	Restricted agglomeration, homogenous Fe and S distribution, improved reactivity with pollutant, lower HER, and scaled-up for field application.	Ambient condition with elemental Fe and S.	[143]	Controlled particle size, homogeneously distributed Ni, high activity, and stability, but passivated once pH exceeds 7.0.	Metallic Fe and Ni.	[88]
Liquid phase reduction	Restricted agglomeration and increased reactivity.	Toxic $NaBH_4$ as a reductant.	[287]	Controlled particle size and corrosion degree of metallic iron.	Toxic $NaBH_4$ as a reductant.	[320]	Low activity and stability.	Ni^{2+} solution and metallic Fe.	[88]
Thermal reduction	Stable in air	H_2 500 ℃ or C carrier 700 ℃				n.a			n.a

n.a = not available

1.2.3. Development of ball milling prepared IBMs

Using the tool of RStudio, we plotted the three-fields (author country, keywords, and source) of IBMs development with ball milling. As seen in Fig. 1-10, dechlorination and heavy metal removal have been the primary research issues, and China has contributed the most work. The main advancement of ball milling prepared IBMs on contaminants removal is shown in Fig.1-11.

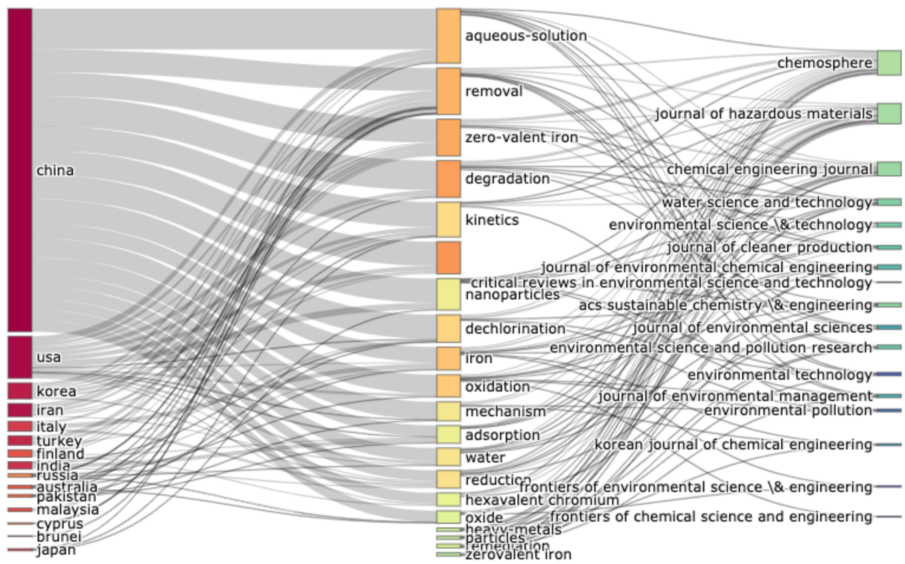

Figure. 1-10 The three-fields plot of the development of ball milling prepared IBMs and application on pollutants removal (Web of Science databases referenced 114 articles and period from 2006 to 2021)

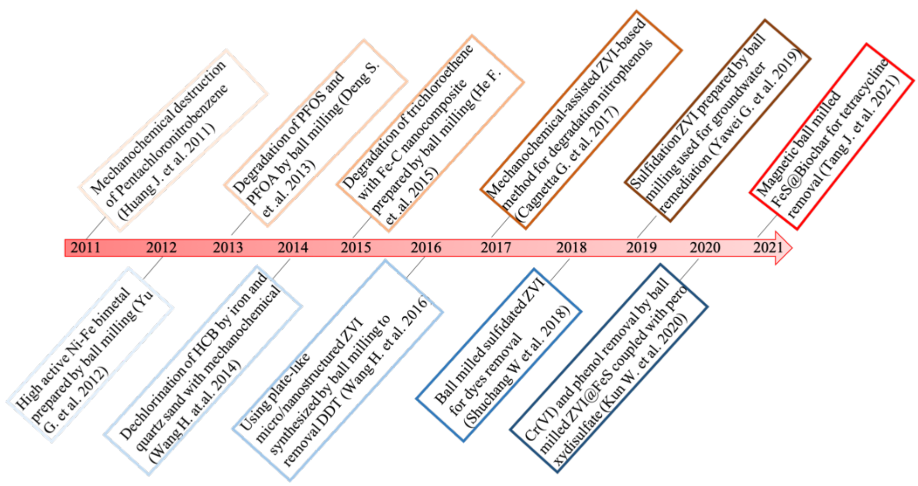

Figure. 1-11 The development of IBMs synthesized through the ball milling method for environmental applications (2011-2021) [154, 170, 321-329].

The grinding product was highly dependent on the milling duration, speed, size of the milling medium, milling atmosphere, and temperature. Higher milling temperatures produced higher solubility of N atoms into ZVI when the temperature was increased from 863K to 973K, leading to the solubility being amplified nearly 45-folds [330]. As a result of particle agglomeration, the specific surface area of the ground substrate initially increases and then gradually decreases as a function of milling duration [331]. To further refine the particle size and improve the surface area, the grinding aid is used to reduce the effect of the agglomeration of newly formed particles. Yonghao Tan et al. (2021) explored the use of oleic acid as a grinding aid to synthesize finer ZrH_2 particles. The results indicated that the particle size decreased from 9.1 μm to 3.21 μm with oleic acid addition [332]. Homogeneously dispersed Ni nanoparticles (50-100 nm) in bulk ZVI were obtained by increasing the ratio of Ni/Fe and increasing the grinding duration, and the Ni-doped ZVI bimetal material indicated higher activity in 4-chlorophenol degradation than that Ni-ZVI synthesized through the chemical solution deposition method [170]. However, the endurance of Ni-ZVI bimetal declined as pH increased due to the passivation effect. Zhe Yang et al. (2019) employed the ball milling method to produce $Fe/Fe_3O_4/FeCl_2$ micro-composite. The passivation effect of the iron oxide layer was deteriorated by the $Fe_3O_4/FeCl_2$ shell and the ferrous ions, and the reactivity of the resulting material on nitrobenzene reduction was about 30-folds higher than the pristine ZVI [333].

IBMs have been extensively used to remove hazardous heavy metals, as well as emerging organic pollutants. Water pollution and soil contamination remediation are two of the most common applications for IBMs produced by ball milling. The optimized ratio of Fe/S mixture fabricated by ball milling was used for the immobilization of Cr(VI) in soil, and the exchangeable species of Cr(VI) in soil was fixed as the less soluble Fe-Mn-Cr compound [334]. The corrosion of ZVI was accelerated after the ball-milled with FeS_2 and commenced a fast removal rate of As; besides, the surface area of ZVI/ FeS_2 was higher than that of virgin ZVI [335]. Because the species of pollutants in aqueous solution differ from those in soil, aqueous contaminants are adsorbed/reduced/oxidized/co-precipitated by IBMs, whereas poisonous metal contaminants in the solid phase complex with IBMs and are then fixed in the soil, and hazardous organics are reduced/oxidized to harmless matters.

[336-338]. He Juan et al. (2021) applied ball-milled biochar-templated FeS to the oxidative removal of TC in water with the additive of persulfate, and the removal efficiency reached 87.4% after 30 min. The biochar worked as an agglomeration inhibitor of FeS, the electron transfer between FeS and TC, and the adsorbent during the TC oxidation process [329]. 1,1,1-trichloro-2,2-bis (4-chlorophenyl) ethane (DDT) contaminated soil was remediated by ball-milled sub-microstructured ZVI, the results suggested that the degradation efficiency of 5 mg/L DDT by the resulting material (50 mg/g) was achieved 95% within 80 min, and the DDT was mainly degraded into less toxic DDD [338]. The ball-milled IBMs have shown a promising substitute for the sequestration of perilous pollutants in solution as well as in soil.

1.2.4. Representative IBMs

1.2.4.1. Carbon-Fe composite

Carbonaceous materials, such as activated carbon and biochar, were used as a common template for IBMs synthesis due to their low cost, ease of availability, and exceptional adsorption properties [339-342]. The synergistic effect of activated carbon or biochar with ZVI dominantly participates in the removal of toxic matters. Laboratory-scale synthesized micro ZVI-carbon composite through ball milling endured surface passivation after adsorption of Cr(VI) under acid and anaerobic conditions. The consumed protons and increased pH resulted in the activity loss of ZVI. Meanwhile, the corrosion rate of ZVI in the ZVI-carbon couple was promoted compared to the virgin ZVI, and the removal ratio of Cr(VI) reached 94.04% within 2 hours [106]. Surface functional groups were introduced into the biochar during ball milling and inclined to be more hydrophilic and dispersive in aqueous solution, and more reaction sites contributed to the improved reactivity with target pollutants [315]. When biochar/activated carbon-Fe_3O_4 composites are ball-milled, they are expected to introduce more oxygen-containing functional groups as well as improve their hydrophilicity. The adsorption capacity of ball-milled biochar/activated carbon-Fe_3O_4 composites was enhanced by 27- and 3-folds in a wide pH range, respectively [343]. There have been conflicting results from other studies on ball-milled carbon. It became more hydrophobic when activated carbon with ZVI was added to the milling jar. This property turned the ZVI-carbon composite prepared by ball milling into a promising reactive material for the degradation of dense non-aqueous phase liquids (DNAPLs), such as TCE contaminated groundwater [324]. Since there are few related studies, the different surface properties of the carbon matrix IBMs after ball milling may come from the cracking and re-agglomeration of carbon particles during physical ball milling. Briefly, the refined carbon particles expose more oxygen-containing functional groups and enhance hydrophilicity. However, as the grinding time increased to the desired value, the carbon particle re-agglomerated and the surface functional groups become blocked. Meanwhile, due to the precipitation of iron hydroxides and other metals, the narrow pH range (pH 2-3) that favors the aging of ZVI-carbon limits its practical utilization.

A recently published work synthesized a core/shell structural ZVI-carbon composite from metal-organic frameworks (MOFs) through mechanical grinding that the outer shell of carbon can reduce the oxidation of ZVI during the storage and transportation, and prevent the precipitation of ferrous and ferric ions on the surface of ZVI [344]. When compared to ZVI-ethylenediaminetetraacetic acid (EDTA) and ZVI-melamine composites, a similar core/shell structural ZVI-carbon material was fabricated by mechanical grinding ZVI with aminoterephthalic acid (ATA). The produced material demonstrated reasonable catalytic ability for sulfamethazine degradation, great stability, and reusability [345].

In the separation of carbon-based IBMs following contamination elimination, magnetic Fe_3O_4 is a well-established technique. Magnetic activated carbon was manufactured by mechanical ball milling with Fe_3O_4 to separate powdered activated carbon following the degradation of perfluorinated compounds (PFCs). It is possible to re-use the magnetic activated carbon for PFCs uptake more than five times without substantial performance loss [346]. Wheat straw was impregnated in a mixture solution of $FeCl_2$ and $FeCl_3$ to obtain the Fe-impregnated wheat straw, and then the Fe_3O_4-loaded wheat straw-derived biochar was acquired in a high-temperature N_2 atmosphere. For superior separation properties after adsorptive removal of the Hg(II) and TC, the magnetic biochar was ball-milled for 12 hours, and saturation magnetization increased from 10.76 to 15.39 emu/g due to the formed crystalline superparamagnetic Fe_3O_4 particles after ball milling and the detailed information presented in Fig.1-12. In general, the couples of carbon-ZVI and carbon-Fe_3O_4 employed for water purification primarily involve the stability of ZVI and enhancement of the dispersion in the bulk phase of pollutants. In terms of water treatment, it appears that ZVI-carbon, with its magnetic core-shell structure, holds promise.

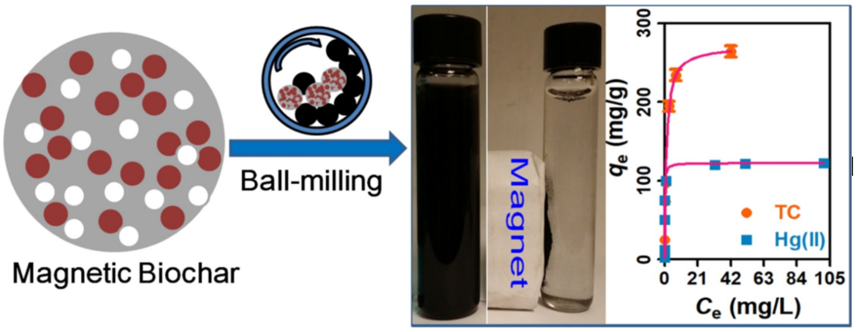

Figure. 1-12 The preparation of magnetic biochar through ball milling and used for the elimination of aqueous TC and Hg(II) together with the post-separation by the magnet [347]. Copyright 2020, Elsevier.

1.2.4.2. S-FeS$_x$ composite

The narrow working pH for iron limits the implementation scope due to the surface self-formed ferric/ferrous (hydro)oxides layer under alkaline conditions hindering the electron transfer [348-350]. Ball milling fabricated sulfur-modified iron maintained high degradation efficiency of TCE over a wide pH range of 6-10 when compared to bare ball-milled iron. The characterization results indicated that the passivation layer on sulfidated iron particles was less compact than that on ball-milled iron without sulfur [154]. Another similar study proved that the surface-formed iron sulfide can alleviate the passivation caused by dissolved oxygen [351].

The regeneration of Fe^{2+} produced by the oxidation of Fe can greatly extend the longevity of Fe, to rule out the possibility that pyrite can improve the durability of ZVI towards the reductive removal of Cr(VI), an innovative mixture of pyrite (FeS_2) and ZVI was examined for Cr(VI) reduction. The removal efficiency of Cr(VI) was kept at >90% in column experiments in presence with higher regenerated Fe^{2+} and much higher than that single ZVI [352]. Several lines of evidence suggest that the sulfur-modified iron could facilitate the corrosion of ZVI [353-355]. In an investigation into the removal of As(III) by ball-milled, sulfidated iron, Min et al. (2017) found that the resulting material present effective removal of As over a wide range of pH, and the As(III) was oxidized to As(V) and then adsorbed on the surface of Fe-FeS_2 [356]. Similar research confirmed that the Fe-FeS_2 composite produced by ball milling had a promising heavy metal Sb(V) elimination capacity (≥ 99.18%) in an aqueous solution over a wide pH range (2.6-10.6) [357].

The features of produced Fe-S composites, including selectivity and electron efficiency to the target contaminants, are governed by their structure. The removal capacity of TCE and electron efficiency rose nearly 11-fold and 7-fold, respectively, in the shell-core structural IBMs with ZVI covered by conductive FeS layer [358]. The electrons from ZVI were transported to TCE via a multilayer FeS shuttle, enhancing TCE dichlorination. Meanwhile, due to quicker electron transfer, the thickness of the FeS layer has a beneficial effect on the activity of ZVI [359]. Meanwhile, the surface coated FeS/FeS_2 layer can reduce the depletion of iron from water [360], the schematic diagram is shown in Fig. 1-13. Another reported structure of FeS_2 template distributed with ZVI particles manufactured by mechanical ball milling left a promising alternative to remove aqueous Cr(VI) over single ZVI or FeS_2, the undermined iron oxide layer on Fe-FeS_2 composite by grinding advanced the durability [89]. Different sulfur precursors,

$S_2O_4^{2-}$ and S^{2-}/S_6^{2-} had distinct effects on the properties of sulfidated iron, with Fe-FeS_2 (with a precursor of $S_2O_4^{2-}$) being more hydrophobic and reactive with TCE than Fe-FeS (with a precursor of S^{2-}/S_6^{2-}). The iron precursors also had an effect on the performance of sulfidated iron; materials made from Fe^{3+} had higher reactivity with water and TCE than those made from Fe^{2+} [361].

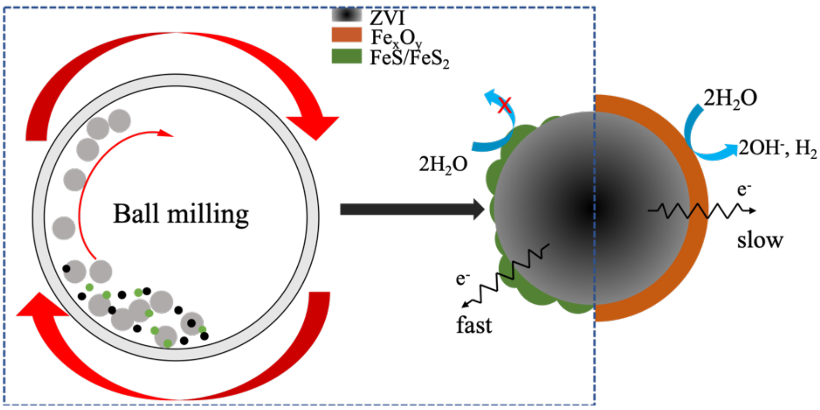

Figure. 1-13 The sulfidated iron prepared from ball milling showed fast electron transfer and higher electron efficiency.

The duration of sulfidation, precursors, and the S/Fe ratio had a big impact on the structure and morphology of Fe-FeSx composites. As a result, the characteristics of Fe-FeSx could be customized for use on corresponding pollutants based on the ratio and milling time. In a nutshell, Fe-FeSx materials with hydrophilic or hydrophobic orientations could be produced to sequester pollutants that are soluble or insoluble in an aqueous solution.

1.2.4.3. Bimetals of Fe-Me

Secondary metals such as Co, Zr, Pb, Cu, and Ni were alloyed with Fe to create materials that were superior in terms of pollution degradation and removal.[362-366]. Those secondary metals enhanced the performance of iron through stabilization, less agglomeration, and the effect of cell-galvanic. In particular, the stabilization was highly dependent on the structure of the bimetal. Ball milling procedure synthesized bimetallic iron materials exhibited higher mechanical stability, stronger adhesion of iron to the second compound, and superior homogeneity of alloyed materials compared to the traditional methods of chemical solution deposition (CSD) [367]. Using ball milling to synthesize Ni-Fe bimetal to decompose monochloroacetic acid (MCA), Zhu Hong and his colleagues (2015) showed that the material maintained high activity even after 10 cycles of treatment. [368]. The elimination rate of 4-chlorophenol (4-CP) by ball-milled Fe-Cu bimetal was nearly 10-fold faster than that by CSD. The evenly distributed Fe and Cu, the increased surface area from 3.21 m^2/g to 78.62 m^2/g, and the generated rough surface were responsible for the favorable removal rate [369]. Well-dispersed biochar supported Fe-Ni bimetal nanoparticles in water exhibited a high degradation capacity of 1,1,1-trichloroethane [370]. In summary, the strategy of loading bimetallic iron particles on the support argues that it can enhance the reductive capacity of elemental iron free of the agglomeration problem.

To improve the durability of magnetite, bimetallic iron oxides of Fe_3O_4-Mn_3O_4 demonstrated a large surface area and a higher content of structural Fe(II) than commercial Fe_3O_4. Surface-bound Fe(II) oxidized toxic As(III) to less toxic As(V) via a Fenton-like pathway [371]. Currently, there is little research about the synthesis of bimetallic iron oxides by mechanical ball milling because of the introduced amorphization triggered by the extensively repetitive collision of the particles during ball milling, which makes the structural Fe(II) in minerals unstable. Ground magnetite was coated by a thick layer of hematite (α-Fe_2O_3) without the additive of oleic acid, while no structure transition of magnetite was noticed in the presence of oleic acid after ground [372]. Recently, research on ball-milled magnetite has been limited to its adsorption ability, which was stimulated by increased surface area and zeta potential [373]. Nevertheless, the oxidation removal through Fenton route being shielded with the surface oxidized magnetite after ball milling and the contaminants such as As(III) remains toxic even been adsorbed. A greater focus on iron oxide bimetal composites prepared by ball milling with non-toxic additives like oleic acid could produce good adsorption and reduction capacity that account more for the significance of Fe(II)-bearing minerals in the removal of pollutants.

1.2.4.4. Other IBMs

Bentonite is a suitable choice for support because of its large surface area, well-distributed pore size, and reasonable price [95]. Bentonite-supported nZVI materials have been widely studied to improve the stability and performance of iron in aqueous solutions [70, 374, 375]. The Fe(II) ions were immobilized between the layers of bentonite during the mechanical ball milling process, and the performance and stability of the prepared material on ethyl xanthate catalytic degradation reached 97.88% even after 4 times recycling, according to the characterization results [376]. Naturally ubiquitous Fe(II)-bearing minerals like pyrite (FeS_2), ferrous sulfide, magnetite, ferruginous smectite, and green rust have shown significance in environmental remediation [189, 377-380]. It has been demonstrated that FeS_2 degraded to FeS after being ground with iron, and the iron was coated by the produced FeS shell [381]. However, FeS_2 remains dominant when ground with biochar and homogenously distributed [382]. Therefore, it seems that biochar could minimize the release of sulfur from FeS_2 throughout the ball milling process.

MOFs have demonstrated their versatility in environmental applications such as water treatment, gas adsorption, and catalysis [383, 384]. Mechanical ball milling prepared MOFs such as MOF-5, ZIF-8, HKUST-, MIL-101, and UiO-66 have a higher specific surface area than conventional chemical ligand methods [385]. It was found that iron-based organic frameworks MIL-88B, synthesized using dry ball milling with the addition of ethanol, had a maximum adsorption capacity of 156.7 mg/g for aqueous arsenate [386]. The stability of MOFs and their resistance to water are the prime concerns for use. To enhance the stability of MIL-100(Fe), conductive polyaniline was applied to modified MIL-100(Fe) with the aid of ball milling, and the produced material displayed good reusability and stability in the aqueous solution [387]. Furthermore, the action of ball milling could reconstruct the decomposed and phase transferred MOFs upon hydration in the aqueous solution, and extend their lifespan [388].

1.2.5. Challenges in the practical application of IBMs

The intrinsic imperfections of metallic iron like agglomeration in solution, low dispersion, and low electron efficiency could be addressed through bimetallic iron particles, doping with sulfur, and supporting on a substrate. However, those countermeasures are not the final solutions due to critical limitations like secondary contamination of dissolved iron, hydrogen evolution, and oxidation in air. Moreover, the impractical mixing intensity and flow velocity in laboratory-scale would result in the performance disparity of IBMs.

1.2.5.1. Secondary contamination

The dissolution of metals from IBMs like bimetallic materials would degrade the water quality [389]. To the best of our understanding, previous studies apparently failed to discuss the second contamination of materials [183, 368]. The most representative iron species, FeOOH crystals, collected from drinking water distribution systems (DWDSs) by pipe flushing, have been verified to have noticeable liver toxicity [390]. Ferric iron was discovered to be chronically toxic to aquatic organisms in North America [391]. In 3-week, 4380 μg/L Fe(II) caused a 16% reproduction impairment in *Daphnia Magna* [392].

The inorganic ions NO_3^- influenced the dissolution of iron, ball milling prepared ZVI and sulfidated ZVI particles both released higher aqueous Fe(II) after the addition of NO_3^- [393]. Similarly, ball-milled ZVI/FeS_2 dissolved higher content of iron and sulfur than that of FeS_2. the detailed information of the higher release of Fe and S from ball-milled ZVI/FeS_2 composite is shown in Fig.1-14. Additionally, in neutral/anoxic circumstances, the dissolution of nZVI was significantly increased when it was doped with Ag and Cu elements using the liquid reduction technique, with total dissolved iron reaching 9.22, 11.98, and 32.08 mg/L within 10 minutes at 3 g/L doses of nZVI and Fe-Ag and Fe-Cu, respectively [394]. The improved surface area, the discontinuous layer, and the galvanic effect mainly contributed to the enhanced corrosion of iron. To effectively remove 28 μg/L CCl_4 under 0.1 mol/L Na_2SO_4 electrolyte at pH 7.98, Al-Fe20 (Fe mass ratio is 20%) bimetal was prepared and the corrosion potential was shown to be favorably related to the removal efficiency, wherein the corrosion potential of Al-Fe20, Al and Fe were -1.11, -0.62, and -0.64 V, respectively. Moreover, the higher the content of Fe, the higher the corrosion potential [389]. According to the Tafel polarization curve analysis, the Fe corrosion current of Fe-Ag bimetal composite at pH 3 was 14-fold greater than at pH 7, and increased 2.3 times as the temperature increased from 31 to 85 °C [395]. While the higher corrosion potential may cause more iron dissolution, the corrosion potential of ZVI was -0.66 V and shifted to -0.75 V after modification with EDTA through ball milling, more ferrous ions and total iron ions were dissolved compared to the bare ZVI particles [336].

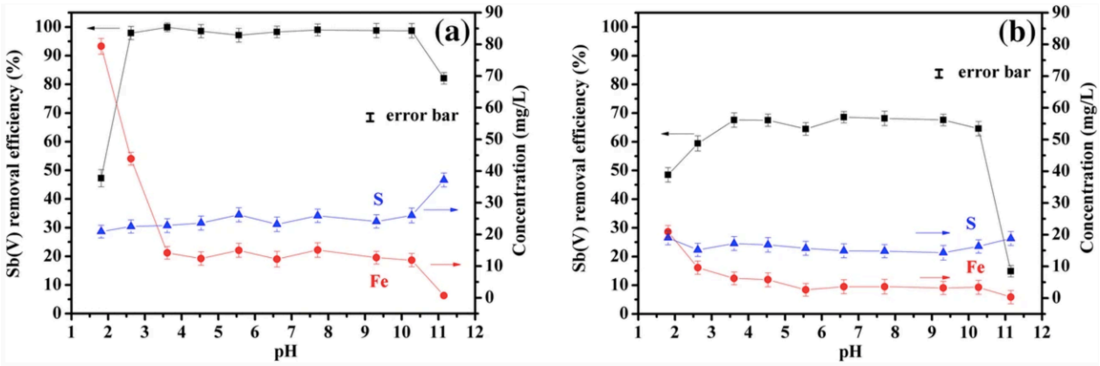

Figure. 1-14 The removal of Sb(V) and the evolution profile of dissolved Fe and S at different pH by (a) ball-milled ZVI-FeS_2 and (b) FeS_2 [357]. Copyright 2020. Springer.

The release of iron was also observed in the elimination of As(V) by Fe-biochar composite, with pH and dissolved oxygen (DO) being responsible for the strength of iron release. In summary, the concentration of iron dropped as DO fell and rose as pH increased, then reduced once pH reached 6 [396]. Cr(VI) elimination by Fe-biochar showed that dissolution of iron and removal efficiency of Cr(VI) reached the maximum at pH 2 [397]. It appears that the appropriate pH value for the treatment of aqueous Cr(VI) conflicts with the discharge obligation of effluent iron content. A similar finding was observed that ball milling prepared Ni-Fe bimetal showed a high degradation efficiency on MCA at a low pH in the presence of the high dissolution of iron [368]. A low dissolved iron (0.21 mg/L) concentration was detected at pH 5.5, and the lowest Cr(VI) concentration was observed between pH 4 and 5.5 from the Fe-biochar composite made by ball milling. Meanwhile, the observations revealed that iron dissolution was also caused by iron oxides and Cr(III)-Fe(III) precipitate [107]. It suggests that the pre-treated Fe-biochar by ball milling can obtain the maximum elimination of contaminants and the minimum release of iron at the same time at a limited pH value.

In addition to secondary contamination caused by the release of iron ions, the generated hydroxyl radical •OH contaminates the water as well. Ball-milled prepared ZVI would produce much more hydroxyl radicals •OH after the addition of an acidic solution [325]. The strategy of coating with carboxymethyl cellulose (CMC) to diminish the ecotoxicity of aqueous iron has been proven to be an effective method. As substantiated by the pronounced results, the decreased hydroxyl radical (•OH) by CMC scavenger is proposed to be the main mechanism of nZVI's mitigated cytotoxicity towards bacteria Agrobacterium sp. PH-08 after stabilization with CMC [398]. A similar finding was reported in the cytotoxicity assessment of CMC coated nZVI on *Escherichia coil* [399].

1.2.5.2. Atmospheric oxidation

The resistance to oxidation of IBMs in the air is critical for their endurance during synthesis, storage, and transportation, especially for the nano-sized ZVI. As iron's applications are explored and expanded, it's been a challenge to increase their stability under ambient circumstances while maintaining their reactivity to the target contaminants. Pretreatments of iron with the acid wash or hydrogen gas to remove the atmospheric oxide scale were reported in recent studies [400-402]. Whereas it is not applicable in large-scale field remediation to pretreat tons of iron with an acid wash or hydrogen gas reduction. The scalable technique of ball milling seems applicable to the pretreatment of iron. However, the oxide scale on iron would be recreated once in contact with air. Nano-ZVI powders prepared by ball milling showed enormous instability in a hermetic mini-environment and a significant decrease in oxygen gas was noticed [403]. The potential substitute composite of sulfidated iron can preserve the reactivity and electron efficiency of ZVI, but the precursor of Fe and S for the synthesis of the Fe/FeS_2 composite would be partially oxidized during ball milling [356].

The surface of Fe/Cu bimetal particles prepared by ball milling was oxidized, and the dominant species of iron were Fe(II) and Fe(III) which was verified by the result of XPS analysis. The elemental mappings after grinding likewise indicated the surface oxidation, seen in Fig. 1-15. Cathodically protecting iron by coating it with a higher activity secondary metal like aluminum to perform as an anode in galvanic cell corrosion can delay the oxidation of iron [219]. Tang et al. (2007) found that core-shell structure Fe-Al powder was synthesized efficaciously by a ball milling procedure after 15 hours, and the shell of Al mixed homogenously with Fe after 20 hours [404]. The cluster and shell-core structures are the main configurations for bimetallic materials of iron. The milling duration contributes to the resulting materials' physical structure chemistry properties. The Fe-coated Al composite exhibited higher Cr(VI) removal efficiency than the Al-coated Fe composite due to the Al-core maintaining the reductive capacity of iron by electron transfer, whereas the former structural iron had limited resistance to oxidation in the air [168]. Meanwhile, no iron ions were released over a pH range of 3.0-11.0 in the iron shell structural Fe-Al bimetal, and Al^{3+} was barely identified in acidic and neutral conditions [72]. The reductive capacity on pollutants of iron via the bimetallic approach appears to clash with its anti-oxidation ability in the atmosphere.

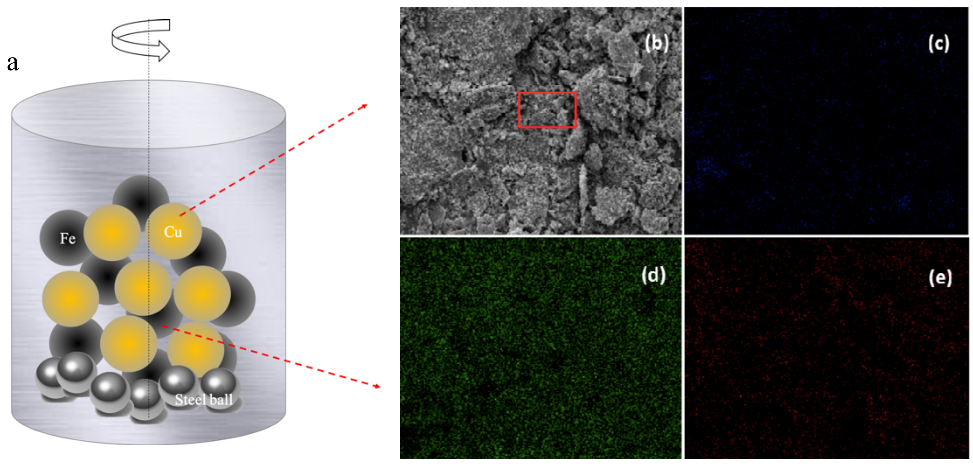

Figure. 1-15 (a) Iron and copper powder mixed and ground for 2 hours and the SEM (b) and elemental mappings of (c) Cu, (d) Fe, and (e) O of the resulting materials [369]. Reproduced with permission from Wiley Online Library, 2019.

Loading iron particles on the stable substrate such as activated carbon, biochar, calcium alginate, bentonite, *etc*. to enhance the stability and mitigate the agglomeration as well as increase the dispersion in the aqueous solution [405-408]. Chitosan-coated nZVI showed a slight decline in acid fuchsine removal although exposed in air for 2 months compared to pristine chitosan-coated nZVI. The homocentric layered structural chitosan polymer proved to prevent the oxidation of air [409]. A comparable core-shell structure of $CaCO_3$ coated ZVI was obtained after ball milling. Characterization results showed the surface iron oxide of the raw material was removed and the freshly exposed ZVI was covered by a fine $CaCO_3$ layer which could prevent the oxidation of iron. Moreover, the $CaCO_3$ layer automatically peeled off when contacted with the pollutant solution [410]. In sum, the approaches to control the oxidation of ZVI during preparation and storage, covering a protective layer on ZVI core seems workable.

1.2.5.3. Hydrogen evolution reaction

The undesirable reaction of iron with water (hydrogen evolution reaction, HER) or anaerobic corrosion results in low electron efficiency (defined as the ratio of electrons used for the reduction of a target pollutant) and escalates the remediation cost [411, 412]. Evidently, produced hydrogen gas blocked the injection zone of iron in groundwater remediation and initiated the diversion of water flow. Furthermore, the immigration of contaminants was fascinated by the hydrogen gas bubble and thus deteriorated the elimination efficiency of contaminants [413]. Besides, the microbial community would be altered by the generated hydrogen gas [414]. In addition, as an inherent feature, the single iron particle's low electron efficiency was unaffected by the surroundings [415]. A study on TCE dechlorination by nZVI found that the rate constant of HER increased 27 folds when solution pH decreased from 8.9 to 6.5, while the rate constant of dechlorination only increased 2 times [416]. Hendrik Paar et al. (2015) evaluated the HER using spherical nZVI and ball-milled flaky nZVI in anaerobic column experiments. The results showed that the use of mechanical ground flaky nZVI slowed the rate of HER [149]. To strengthen Cr(VI) removal, hydroxyl-functionalized ball-milled ZVI/Fe_3O_4 compelled the material to have more affinity for water-soluble contaminants, and higher Cr(VI) removal was obtained; however, the noticeable hydrophilicity of ball-milled material would induce the reaction of ZVI with water [417]. Oxalic acid-modified ZVI through ball milling formed a ferrous oxalate dihydrate layer on the ZVI surface instead of iron oxides which would prevent the oxidation of core ZVI [418]. The same structural composite that ferrous oxalate dihydrate coated ZVI was produced by ball milling, but more hydrogen (3.5 μmol/L) was generated from oxalic acid-modified ZVI than bare ZVI (1.0 μmol/) due to the high proton conductivity of the $FeC_2O_4{\cdot}2H_2O$ layer [419].

For bimetallic IBMs, the extensively discussed composites of bimetallic Pd-Fe accelerate the oxidation of iron through the galvanic cell while in parallel to the high HER with H_2O/H^+ and the low service longevity, thus curtailing the lifespan of iron [420]. A producible observation was also reported with bimetallic Pd-Fe particles [421]. Sulfidation pretreatment has been proved to be a pronounced method for deteriorating the HER as well as improving the electron efficiency of iron to target contaminants [140, 422-424]. Sulfidation of iron showed a promising advantage in limiting HER and enhancing the dechlorination rate, with electron utilization efficiency increasing from 2% to 72% while HER was inhibited. Meanwhile, bimetallic composites of iron like Fe-Pd, Fe-Cu, Fe-Ni, and Fe-Ag all improved the HER [425]. The explanation for the sulfidation of iron can enhance contaminants' removal rate together with reduced HER may be attributed to the hydrophobicity of iron increased after sulfidation and reduced contact with water. In the meantime, the conductive layer of iron sulfides (FeS or FeS_2) can transfer electrons from iron and mediate the degradation of pollutants. The increased hydrophobicity and electron transfer were observed in mechanical ball milling synthesized S-ZVI as well [426]. Fig. 1-16 shows how the contact angle affects the HER, the soluble NO_3^- and insoluble TCE removal. The intensity of hydrophobicity highly depends on the content of incorporated sulfur in a sulfidated iron composite, and the speciation of sulfur also differentiates the hydrophobicity. Research indicates that FeS_2 coated or doped iron behaves with higher hydrophobicity than those with FeS [422]. When the ratio of S/Fe increased from 0.01 to 0.05, a significant decline of HER was noticed [139].

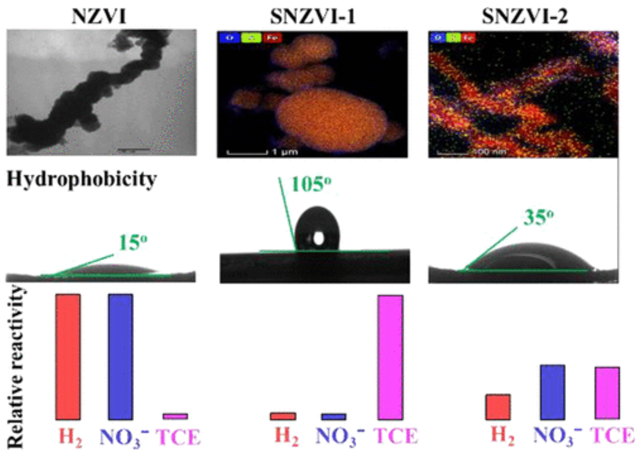

Figure. 1-16 The relationship of HER, NO_3^- and TCE removal between contact angle of nZVI and sulfidated iron. Adapted with permission from [153]. Copyright 2019, America Chemical Society.

Nevertheless, the merits of sulfidation of iron are all based on laboratory results [142]. A key uncertainty for the application of sulfidated iron is the complex geochemistry circumstances of groundwater, which may shadow the field implementation due to the properties of sulfidated iron being more susceptible to the typical inorganic ions like Cu^{2+}, Mn^{2+}, Ca^{2+}, Mg^{2+}, NO_3^-, HCO_3^-, Cl^-, PO_4^{3-}, and SO_4^{2-} [427-429]. HER was promoted obviously and the electron efficiency of ball-milled ZVI and S-ZVI decreased by 17 − 73% in the presence of PO_4^{3-}. Meanwhile, HCO_3^- also elevated HER and decreased the electron efficiency of ball-milled S-ZVI and ZVI by 1.9 and 22%, respectively [430]. On the other hand, there was a scarcity of evaluation of sulfidated iron's long-term performance; most laboratory or field investigations were conducted in the short term, spanning from 2 hours to 17 days [431-433].

1.2.5.4. Impractical agitation intensity and flow rate

When pertinently employing IBMs for field remediation, a certain bias in the actual performance of IBMs would be generated as a result of the surface oxide layer being disturbed by the impractical mixing strength in batch experiments and flow velocity in column studies [434]. We tabulated the flow rate of column tests with IBMs, detailed information seen in Table 1-6. Based on a field remediation case of TCE contaminated groundwater with PRB (permeable reactive barrier), the estimated flow rate range was 0.004-0.04 mL/min [435]. It is apparent that most of the adopted flow rates in the laboratory were higher than the authentic values. Additionally, the flow velocity in the upper layer is slow while the deeper portion of the aquifer is fast, and the pH and ORP of groundwater change as the water level changes, which may cause the uneven aging of IBMs [436]. The low flow velocity of groundwater would result in the corrosion products of iron hydroxides attaching to the vicinity of IBMs and reduce the permeability of PRB and restrain the mass transport of contaminants to the reactive surface of the iron. Moreover, the lifetime and durability of PRB filled with IBMs may be exhausted prematurely.

Table 1-6 The flow rate of column tests in pollutants removal with iron-based materials

Filling materials	Contaminants	Flow rate (mL/min)	References
ZVI and glass beads	Perchlorate	0.017	[437]
Cast iron	RDX	10	[438]
ZVI and sand	TCE	0.063-0.25	[439]
ZVI and sand	NB	0.25-2.0	[440]
ZVI, FeS_2, and sand	Cr(VI)	0.5	[352]
ZVI and sand	As(III), As(VI)	158 and 100	[441]
ZVI, bentonite and sand	Cr(VI)	0.5	[442]
ZVI, Fe_2O_3 coated sand, and sand	As(V), Cr(VI)	0.1	[5]
Zeolite, ZVI	Cr(VI)	4.0, 2.0, 0.6	[443]
ZVI and sand	phenol	3.4	[444]
Acid washed ZVI and aluminum	Cr(VI, Cd^{2+}	1.0	[445]
Bimetal of Fe-Al	CCl_4	0.75	[446]

RDX = royal demolition explosive; NB = nitrobenzene

1.2.6. Conclusions and suggestions

The present review has explicitly outlined the development of the ball milling technique on IBMs preparation and the frequently argued concerns about elevating the electron efficiency and durability of ZVI through doping or homogenously mixing with secondary components such as activated carbon or biochar, sulfur, and metals. The particle size, surface area, and structure of IBMs were highly dependent on the grinding parameters and atmosphere of the grinding. Meanwhile, the mechanical energy stored partially in the ground particles contributed to the improved corrosion rate of ZVI. The enhanced surface area, regulated hydrophilicity, and stable structure of activated carbon/biochar supported ZVI, surfidated ZVI, and bimetallic ZVI created by ball milling outperformed liquid phase reduction and thermal reduction. However, the emerging new hitches (poor stability in air, release of iron, and HER) with manufactured IBMs by ball milling in the laboratory in terms of toxic matter sequestration and the unrealistic mixing intensity and flow rate shadowed the implementation of IBMs. Specific IBMs like bimetallic iron can accelerate the corrosion of iron but boost the HER as well. Sulfidated iron seems like an encouraging option for the controlled HER and high reactivity on pollutants removal. However, its performance is sensitive to the surroundings. The present research on ball milling fabricated activated carbon/biochar-Fe composite emphasized the enhancement of reactivity, not reducing the HER and dissolution of iron.

The practicable IBMs for field remediation should involve four critical aspects, which are: i) resistance to atmospheric oxidation; ii) enhanced electron efficiency; iii) limited iron dissolution; and v) controlled HER with H_2O/H^+ that accompany the whole process of utilization of iron from preparation, storage, transportation, and application. Previously reported IBMs of synthesized Fe-Si/Mg-Al by mechanical ball milling exhibited good stability under ambient conditions, high reactivity on dechlorination of TCAA (trichloroacetic acid), the negligible release of Fe, Al, and Mg, and no detectable

HER below the potential of -0.95V at potentiostatic electrolysis test [367]. Considerably more work will need to be done to fill the data gap and equalize the four essential criteria above for developing IBMs, and more information on the long-term performance of IBMs would help us to establish a greater degree of accuracy on this matter.

Chapter II. **Highly surface activated carbon to remove Cr(VI) from aqueous solution with adsorbent recycling**

2.1. Introduction

Chromium is a highly toxic contaminant in the effluents of electroplating and tanning factories, threatening the health of humans by bioaccumulation in the food chain [447]. Cr(VI) and Cr(III) are the two main chromium species. Cr(VI) shows a higher solubility, mobility, and toxicity as compared to Cr(III) [448]. There are not sparingly soluble Cr(VI) compounds, but in the case of Cr(III), Cr_2O_3 is a compound that has a very low solubility. Therefore to remove Cr(VI), it is a common practice to reduce soluble anion Cr(VI) to Cr(III) followed by precipitation. Conventional reducing agents for Cr(VI) are sulfur compounds and iron salts [447], which are effective in acidic conditions. Under these conditions, the predominant Cr(VI) species are $HCrO_4^-$ [449]. Salts with the sulfoxy species SO_3^{2-}, $S_2O_5^{2-}$ as well as $SO_2(g)$ are the most common reducing agents and rapidly reduce Cr(VI) at pH 2.5 [450, 451]. Fe^{2+} ions also reduce Cr(VI) at a high rate at low pH [452]. Under acidic conditions, Cr^{3+} ions are predominant, and aqueous solution pH should be increased with lime or base compounds to precipitate them as $Cr(OH)_3(s)$. The optimum removal conditions for Cr(VI) and Cr(III) are different from each other. $Cr(OH)_3(s)$ precipitates as ultrafine particles with low flocculation, settling, and filtration rates. As a result, the generated residue is a sludge with high moisture content and is difficult to dispose of as a green discharge. Other techniques have been proposed to remove Cr(VI) from aqueous solutions such as electrodialysis followed by precipitation and electroreduction [453-456], ion exchange [457], bioremediation [457] and modified zero-valent iron (ZVI) and zeolite materials [458, 459]. These techniques have the disadvantage of being of high energy consumption and high cost to produce the synthetic adsorbents.

AC has aroused attention for the removal of heavy metals because of its low cost and easy handling [460, 461]. AC presents a high specific surface area and surface functional groups and electron donors to convert Cr(VI) to Cr(III) [462-466]. It has been found that removal of Cr(VI) is effective at acid conditions in the range of pH 2-4 [27, 37, 467]. At low pH, the AC surface functional groups are protonated, present a high reduction performance [231] and Cr(VI) reduces to Cr(III) and precipitates as $Cr_2O_3(s)$ [468-470]. The high performance of AC for Cr(VI) reduction at low pH is similar to that shown by protonated *Ecklonia* biomass, which was 3.7 times higher than $FeSO_4 \cdot 7H_2O$ [471].

Most waters and soils contaminated with Cr(VI) possess a pH higher than 3.0 so their pH needs to be lowered to about 3 to remove the Cr(VI) according to these studies [472, 473]. Once the adsorption step is completed, the pH then has to be raised to around neutral values to reuse the water and soil. These two steps of pH adjustments could be avoided if the Cr(VI) removal were carried out at near-neutral pH. Under these conditions Cr(VI) is predominantly as CrO_4^{2-} and Cr(III) as $Cr(OH)_3(s)$. After an extensive literature survey, we found that Cr(VI) removal from water at near-neutral pH has not been investigated in detail. Neither has been studied the Cr(VI) desorption from the AC and the AC recycling.

The main aim of this study was to establish the most suitable conditions for the removal of Cr(VI) with AC at near-neutral pH using an AC with a high density of functional groups to enhance the Cr(VI) adsorption and regenerating the AC for its recycling to the adsorption step. It is worth mentioning that this the first work facing these two aspects for the processing of waters contaminated with Cr(VI). Batch Cr(VI) adsorption tests were carried out at pH 6 and 7 with fresh and regenerated AC. The functional groups on the AC were characterized by electrokinetics and surface titration while the Cr species on the AC were identified by SEM (scanning electron microscopy) coupled to an EDX (energy-dispersive X-ray spectroscopy). AC with the high density of functional groups was prepared by high-intensity ball milling [315, 474].

2.2. Materials and methods

2.2.1. Adsorbents and chemicals

Granular coconut shell AC was purchased from Calgon Company. Its chemical composition was 97% C and 3% inorganic residues [469]. The HAC was prepared by ball milling -20 μm size particles of AC for 60 min, using a planetary mono mill (Pulverisette 6, Fritsch, Germany) with steel balls of 5 mm in size as the grinding media. 10 g AC was mixed with the steel balls and milled at a speed of 300 rpm. This milled product is referred to highly activated carbon (HAC) throughout this manuscript. Its D_{80} (particle size of cumulative undersize at 80%) size of the HAC was found to be 4μm, the specific surface area was 928.5 m^2/g, and the mean pore size was 15.3 Å. The HAC was dried at 60 ^oC for 24 hours, then kept in a plastic flask in a glass desiccator. Analytical grade potassium dichromate ($K_2Cr_2O_7$) was the source of Cr(VI) and acquired from J.T.Baker. A stock solution with a concentration of 1,000 mg/L Cr(VI) was prepared for all the adsorption tests. All aqueous solutions were prepared with deionized water of 18.2 Ω, which was obtained by passing distilled water through a Barnstead E-pure II Water Purification Systems, Thermo Scientific, USA. 1.0 mol/L aqueous solutions of both sulfuric acid and sodium hydroxide were used to adjust the pH in the adsorption tests. All other inorganic chemical reagents such as H_2SO_4, H_3PO_4, NaOH, and $NaHCO_3$ were of analytical grade.

2.2.2. Adsorbent characterization

Adsorbed chromium species on HAC were determined through SEM coupled to an EDAX. The surface functional carboxyl and hydroxyl (phenolic, hydroxyl, and lactols) groups of the AC and HAC were quantified by Boehm's titration method [475]. Briefly, the method is as follows: stir 200 mg AC in 100mL deionized water with the desired $NaHCO_3$ and NaOH concentration for 20 hours, take a 50 mL aliquot and titrate it with a normalized HCl aqueous solution. The content of carboxyl and hydroxyl groups was determined from the loss of $NaHCO_3$ and the loss difference of NaOH and $NaHCO_3$, respectively.

A Zeta Probe equipment (Colloidal Dynamics, USA) was employed to determine the zeta potential of AC and HAC. For these measurements, a 3 g sample was stirred ultrasonically in 100 mL with a 0.01mol/L NaCl concentration at 150 rpm for 5 min. For the zeta potential measurements, 0.1 mol/L of both HCl and NaOH aqueous solutions titrated automatically the carbon suspension for pH adjustment throughout the zeta potential quantification. All these measurements were performed at 22°C. The equipment uses the electrokinetic sonic amplitude (ESA) to determine the zeta potential of particles in suspensions. Two electrodes with a high-frequency electric field are immersed in the suspension. For the moment, the particles oscillate back and forth with the electric field and most of the particle oscillations cancel one another out, but the oscillation does not take place near the electrodes, and a sound wave is generated from there. The sound wave would hit a transducer along the delay rod. Therefore, the transducer will produce a sinusoidal voltage signal by vibration. The generated amplitude value of the sinusoidal voltage signal equals the ESA number. The mathematic relation between ESA and dynamic mobility (μ_d) is given by Eq (2-1) [476, 477].

$$\mathrm{ESA} = \mathrm{A}(\omega)\varphi\frac{\Delta\rho}{\rho}Zu_d \tag{2-1}$$

where A(ω) is the instrument calibration factor, which can be determined by calibration with potassium silico tungstate solution (KSiW), φ is the particle volume fraction (3% in our study), Δρ is the density difference between particle (1.91 g/cm^3) and solvent (1.00 g/cm^3), ρ is the solvent density and Z is a factor related to the acoustic impedance of suspension and delay rod of the instrument. Finally, u_d was converted to zeta potential (ζ) by Henry's equation, represents as Eq (2-2) [478]:

$$u_d = \left(\frac{2\varepsilon\zeta}{3\eta}\right)f(\kappa a) \tag{2-2}$$

where ε is the dielectric constant, η is the water viscosity, f(κa) is Henry's factor. A simple value for f(κa) is 1.5, referred to the modified Smoluchowski equation [479]

The specific surface area and pore size of HAC before and after Cr(VI) adsorption were determined by gas adsorption measurement using an Autosorb-1, Quantachrome instrument. A desired amount of sample was heated and degassed at 80 °C before analysis, then nitrogen adsorption and desorption were conducted at 77.3 K liquid nitrogen. The multipoint BET, BJH methods were used to calculate the specific surface area and pore size, respectively.

Raman spectra (DXR, Thermo scientific, USA) were utilized to obtain the detailed carbon structure change caused by ball milling and XPS (X-ray photoelectron spectroscopy) was used to determine the C, N, S, and O elements content.

2.2.3. Cr(VI) uptake experiments

Adsorption kinetics studies were performed with 5g adsorbent and 100 ml, 1000 mg/L Cr(VI) at pH 6 and 7. A 20 μL aliquot was withdrawn from the aqueous solution at various time intervals such as 0.25, 0.5, 1, 3, 5, 7, 9, 12, 15, 30, 60, 120 mins. The aliquot was analyzed for Cr(VI) and total Cr. Adsorption isotherms were built within a Cr(VI) concentration range of 800 to 2000 mg/L at 295, 308, and 323 K by contacting the adsorbent with the Cr(VI) for 24 h. Before the addition of Cr(VI), the AC and HAC were pre-treated for the equilibrium of their surface groups with the aqueous solution as follows: 5 g adsorbent was mixed with 100 mL deionized water, and the pH was stabilized at 6 and 7 until the pH did not change, which occurred at about 30 mins. Then, potassium dichromate was introduced to the suspensions at the desired Cr(VI) concentration.

The HAC suspension was stirred in a 250 mL Erlenmeyer flask using a Thermo scientific magnetic stirrer at 400 rpm at 22 ^{o}C. An aliquot of 100 μL was withdrawn from the aqueous suspension and centrifuged at 8,000 rpm for 10 min using an Allegra^{TM} 21 Centrifuge (Beckman coulter, USA). The supernatant was analyzed for total Cr and Cr(VI). Total Cr was determined through atomic absorption spectrophotometry, while the Cr(VI) by a colorimetric method using a UV/Vis spectrophotometer (Thermo Scientific, USA. with a light path of 1 cm) at 540 nm. 1,5–diphenylcarbazide was used as an indicator [480]. The concentration of Cr(III) was determined by the difference between total Cr and Cr (VI). Unless otherwise stated, all the adsorption experiments were performed with a blank control at 22^{o}C.

2.2.4 Cr desorption from HAC after treatment with Cr(VI)

Cr (VI) desorption from the HAC and HAC surface regeneration was carried out by acid and alkali elution experiments. First, HAC and pristine AC were repeatedly contacted (four times) with a 1,000 mg/L Cr(VI) aqueous solution to obtain a Cr-loaded material. The Cr-loaded HAC (0.5g) and Cr-loaded AC (0.5g) were then treated with 0.2 mol/L H_2SO_4 (50 ml) and 0.1 mol/L NaOH (50 ml) aqueous solutions. The amount of desorbed chromium (mg/g) after elution was determined as follows;

$$q = \frac{C_t V}{m} \tag{2-3}$$

where q (mg/g) is the chromium content desorbed from the carbon materials, C_t (mg/L) is the chromium concentration in the eluted solution at time t, V (L) is the volume of the elution solution and m (g) is the mass of the material.

2.2.5 Regeneration and reusability of HAC

Consecutive adsorption tests were conducted to investigate the reusability of HAC on Cr(VI) (1000mg/L) adsorption. The HAC was contacted with an H_2SO_4 solution of 0.1 mol/L for 24 hours stirring the suspension at 400 rpm in a magnetic stirrer to regenerate the surface of the HAC treated with Cr(VI) solution [481]. This regenerated material was then used in the next Cr(VI) adsorption test.

2.3. Results and discussions

2.3.1. Effect of ball milling on Cr(VI) sequestration

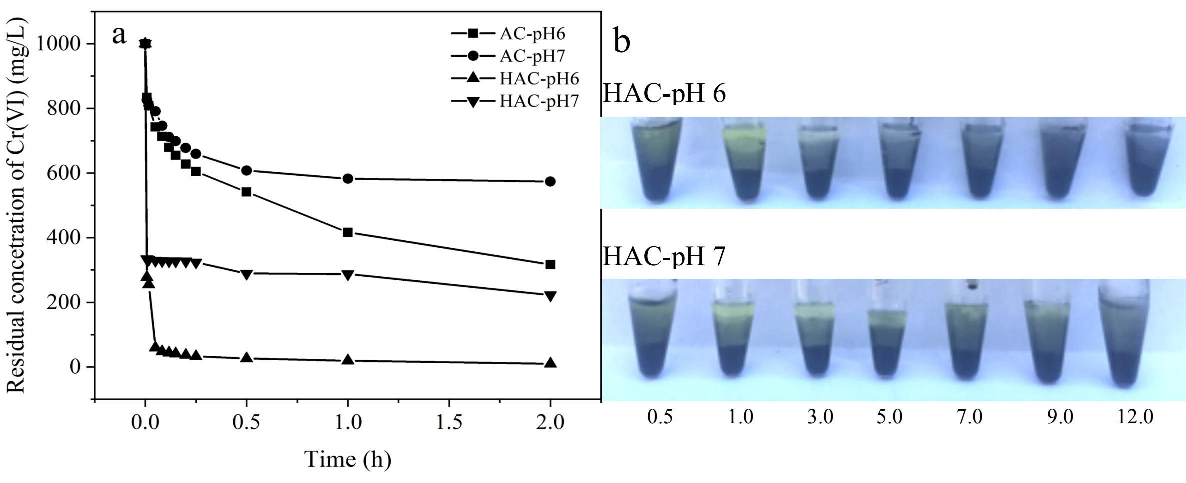

Figure. 2-1 (a) The depletion curve of Cr(VI) by AC and HAC under pH 6 and 7 as

time (AC average size is 20μm, HAC average size is 4μm, dose 5g/100ml, 1000mg/L Cr(VI), RPM=350, 295K); (b) The aqueous solution color change as time of Cr(VI) removal by HAC.

Fig. 2-1 (a) depicts the depletion of Cr(VI) concentration as a function of time at pH 6 and 7. It is seen that for both pHs, the Cr(VI) concentration depletion was very fast in the first 0.25 hour, being this depletion larger at pH 6. The Cr(VI) removal by HAC was 99.0% and 77.8% at pH 6 and 7 after 2 hours, respectively. These Cr(VI) removals were larger than those on pristine AC (68.3% at pH 6 and 42.7% at pH 7). Thus, a significant increase in Cr(VI) removal was achieved with the HAC. The figure also shows photos of the Cr(VI) aqueous solutions at various times at the two pH values. The increase in Cr(VI) adsorption can be associated with the increase of the functional groups on the AC. In Fig. 2-1 (b), it is noted that the color of the Cr(VI) aqueous solution became more crystal clear at pH 6 than at pH 7, clearly indicating that more Cr(VI) was removed at pH 6.

2.3.2 Characterization of materials

2.3.2.1 Surface and texture chemistry of materials

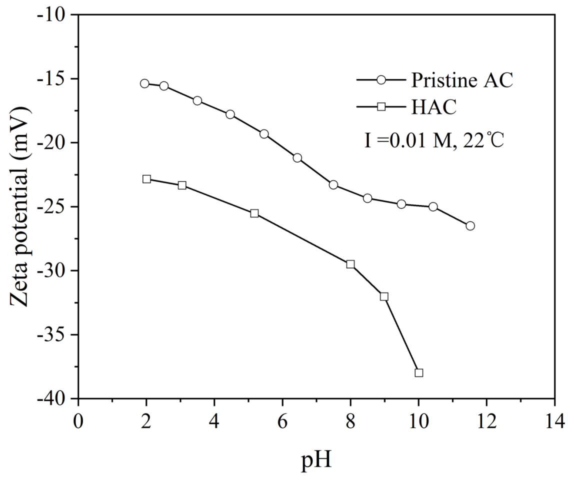

Figure. 2-2 Zeta Potential of AC (20μm) and HAC (4μm) as a function of pH

Fig.2-2 shows the zeta potential of pristine AC and HAC as a function of pH. It is seen that the zeta potential decreased negatively as the pH increased, as reported elsewhere [482, 483]. The negative zeta potential of AC and HAC is due to the dissociation of their acidic functional groups [484] and Chingombe et al. (2005) have reported that the zeta potential of AC becomes more negative as the acid functional groups increased. As noted in Fig. 2-2, the zeta potential of HAC is more negative than that of AC, indicating that the ball milling promoted the formation of acid functional groups of the carboxylic type. This was confirmed by determining the surface density of the functional groups before and after milling. Table 1 presents the surface density of the total acidic and alkaline functional group before and after milling, as well as after adsorption of Cr(VI). It is noted that the total acidic group of the AC increased from 1.31 mmol/g to 1.84 mmol/g after grinding, due mainly to the increase of COOH groups. Our results are consistent with those of Lyu et al. (2018) who have reported that the total acidic groups in biochar increased from 0.3 mmol/g to 1.35 mmol/g after high intensity grinding of the biochar [485]. Recent studies proved that more oxygen/hydrogen functional groups were introduced into activated carbon during the ball milling and increased the hydrophilicity of activated carbon [13, 16]. As noted in Table 2-1, after Cr(VI) adsorption no carboxylic groups were detected on the HAC. This can be accounted for by the shielding of these groups by adsorbed Cr(VI) as explained below. Therefore, the COOH groups played a vital role in Cr(VI) adsorption. The increase in hydroxyl surface density after adsorption is due to $Cr(OH)_3$, which is formed from the reduction of Cr(VI).

Table 2-1 The surface chemical properties before and after ball milling AC and HAC treated with Cr(VI)

Sample	Total acidic group (mmol/g)	Carboxyl (mmol/g) -COOH	Phenolic, hydroxyl, lactols (mmol/g) -OH
Pristine AC	1.31	0.31	1.00
AC after milling HAC	1.84	0.97	0.87
HAC after Cr(VI) adsorption	1.94	ND	1.94

ND is no detectable

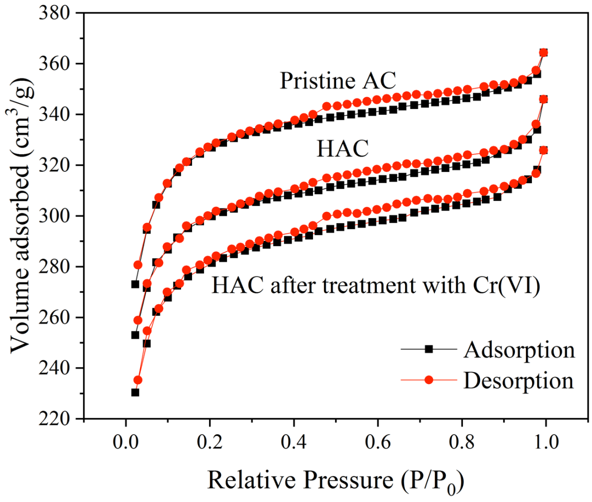

Figure. 2-3 N_2 adsorption-desorption isotherms (BET) of pristine AC, HAC and HAC treated with Cr(VI).

The N_2 adsorption and desorption isotherms and pore size of pristine AC, HAC, and after adsorption are shown in Fig. 2-3. Referring to the classification of physisorption isotherms [486], the N_2 adsorption and desorption curves of the three materials fitted well with the type IV adsorption isotherm (IUPAC classification). The hysteresis loop in Fig.2-3 ascribed to H4 type means a narrow slit-like pore structure, commonly seen in micropore activated carbon materials [487]. The higher surface area of HAC can be associated with its smaller particle size in comparison to that of AC. After adsorption of Cr(VI), the surface area of HAC decreased and the pore size increased, which is due to the filling of adsorbed Cr in the pores. Figs. 2-4 and 2-5 show SEM photomicrographs of Cr-loaded HAC. As noted, there is chromium on the surface and inside of the HAC, being the content of chromium on the surface much higher than that inside the particle. A similar texture to that seen in Fig. 2-5 has been reported by Wang et al. (2020). They reported the formation of an eskolaite (Cr_2O_3) layer on the AC surface, which lowers the Cr(VI) adsorption capacity of AC and the diffusion of Cr(VI) to the interior of the AC particle.

Table 2-2 Pore structural parameter of AC, HAC, and HAC after Cr(VI) adsorption

Materials	Average particle size (μm)	Specific surface area (m^2/g) (BET)	Pore size (Å) (BJH)
Pristine AC	20	846	19.0
HAC	4	929	15.3
HAC after Cr(VI) adsorption	4	876	18.5

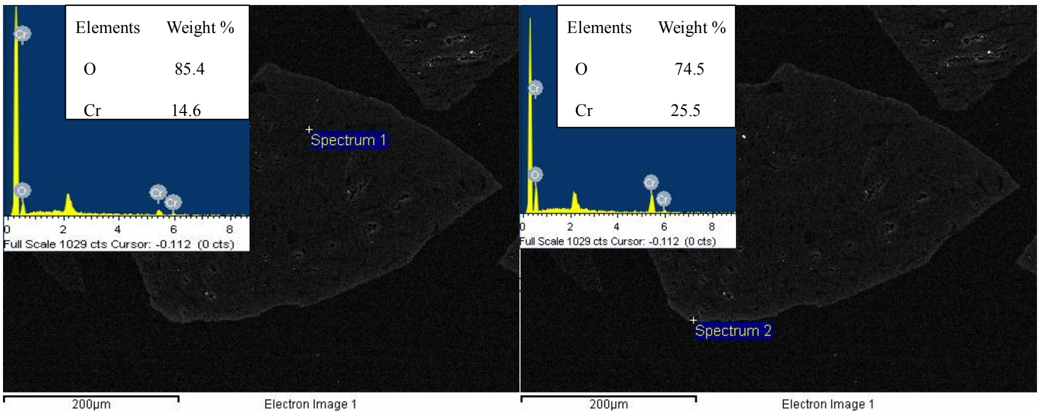

Figure. 2-4 SEM photomicrograph and quantitative analysis EDX pattern after HAC adsorption at pH 7.

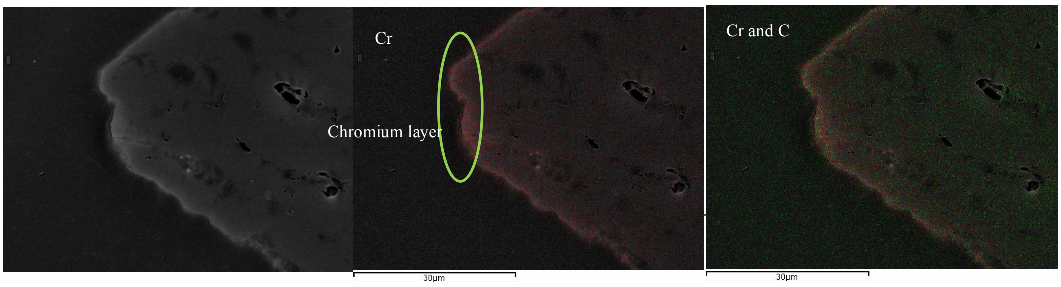

Figure. 2-5 SEM figure and SEM-EDX elements mapping of HAC after adsorption at pH 7.

As can be seen in Figs 2-4 and 2-5, chromium was detected on the surface and inside of the HAC particle, being the content of chromium on the surface much higher than that inside the particle. Table 2-2 compares the summary statistics of surface area and pore size analysis results, it noticeable from this table that the chromium in the HAC lowered the specific surface area and mean pore size of the HAC from 929 m^2/g

to 876 m^2/g and 15.3 Å to 18.5 Å, respectively. A similar texture to that seen in Fig. 2-5 has been reported by Wang et al. (2020) in Cr-loaded AC particles after adsorption at pH 3 [468]. They reported the formation of an eskolaite (Cr_2O_3) layer on the AC surface, which lowers the Cr(VI) adsorption capacity of AC and the diffusion of Cr(VI) to the interior of the AC particle. Besides, the increased BET surface area of HAC generated by ball milling may be explained by the decreased particle size and the deformation of the carbon structure.

2.3.2.2 Raman spectra investigation

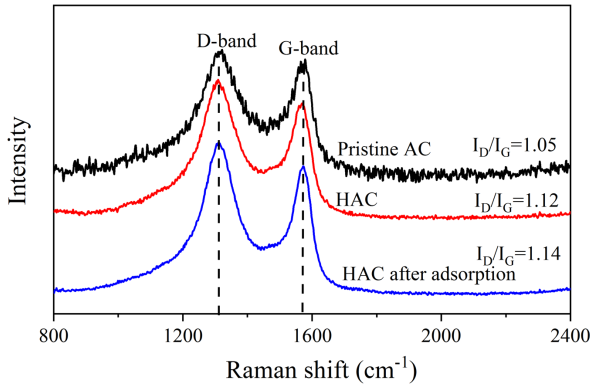

Figure. 2-6 Raman spectra of pristine AC, HAC and HAC after adsorption of Cr(VI).

Fig. 2-6 shows the Raman spectra of AC, HAC, and HAC after Cr(VI) adsorption. the D-band (1320cm^{-1}) and G-band (1563cm^{-1}) in the spectra reveal the degree of lattice distortion of any carbon material, The D-band represents the stretch vibration of sp^3 hybridized carbon, while the G-band is related to the sp^2 graphited carbon [488]. It has been reported that the ratio of the intensity of D-band versus G-band (I_D/I_G) indicates the level of graphitization or structural order of carbon materials [489]. As noted in Fig 2-6, the I_D/I_G of HAC increased from 1.05 for pristine AC to 1.12 and further increased to 1.14 after adsorption of Cr(VI). The increase of I_D/I_G for HAC revealed that ball milling enhanced the formation of sp^3 defects in the carbon structure. Moreover, the increase of sp^3-bonding hybridized carbon atoms of HAC after Cr(VI adsorption may due to the reduction of surface oxygen-containing functional groups [490]. Various studies have demonstrated that the reduction of surface oxygen-containing functional groups caused the formation of amorphous carbon structure [491, 492]. The increase of surface functional groups for HAC by ball milling seems to be contradictory with the increase of disorder of structural carbon. This inconsistency may be due to the relatively more produced hybridized carbon atoms by ball milling compare to the increase of oxygen-containing groups.

The content of C, O, N, and S in HAC and HAC after Cr(VI) adsorption was determined through XPS and the results are presented in Table 2-3. It is seen that the C content decreased after Cr(VI) adsorption and the O element increased. The decrease of carbon content can be related to the decline of C-containing surface functional groups, coupled to the reduction of Cr(VI) to Cr(III). The increase of O content can be associated with the chromium oxide resulting from the Cr(VI) reduction, proving that a chromium species containing oxygen formed from the Cr(VI) reduction.

Table 2-3 The elements analysis of HAC and treated HAC with Cr(VI)

	C	N	O	S
HAC (%)	91.24	0.93	6.86	0.97
Treated HAC (%)	84.58	0.50	13.01	1.91

2.3.3. Adsorption kinetic

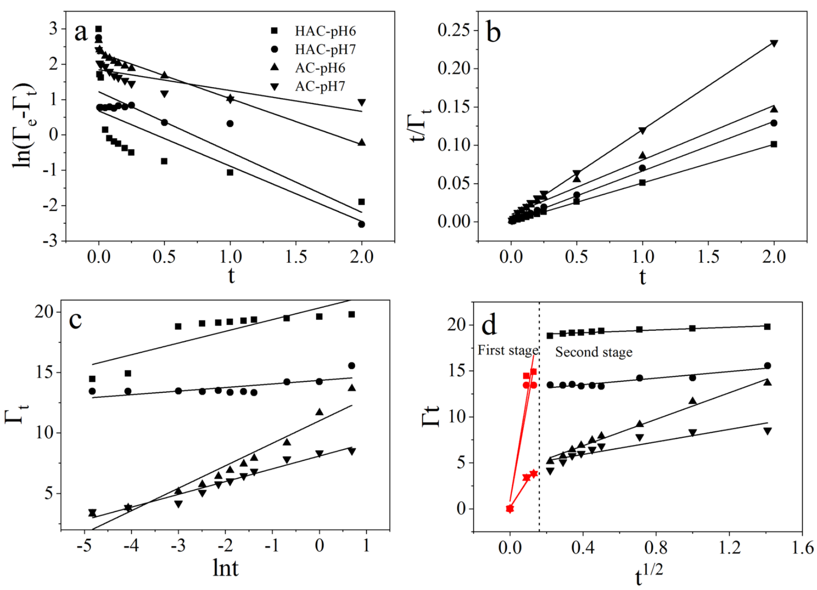

Figure. 2-7 The linear fit for experimental date of Cr(VI) removal by HAC and AC under pH 6 and 7, (a) Pseudo-first order, (b)Pseudo-second order, (c) Elovich, (d) Interparticle diffusion

To investigate the adsorption kinetics of aqueous Cr(VI) adsorption on pristine AC and HAC, and recognize the divergence of the rate constant before and after ball milling. The kinetics models of Pseudo-first order, Pseudo-second order, interparticle diffusion, and Elovich were employed and the general forms as Eqs (2-4)-(2-7) [493, 494].

Pesudo-first order model

$$\ln(\Gamma_e - \Gamma_t) = \ln\Gamma_e - k_1 t \quad (2\text{-}4)$$

Pseudo-second order model

$$\frac{t}{\Gamma_t} = \frac{t}{\Gamma_e} + \frac{1}{k_2\Gamma_e^2} \quad (2\text{-}5)$$

Weber-Morris Interparticle diffusion model

$$\Gamma\mathrm{t} = k_3 t^{1/2} + I \quad (2\text{-}6)$$

Elovich model

$$\Gamma_t = \beta\ln(\alpha\beta) + \beta\ln t \quad (2\text{-}7)$$

where Γe(mg/g) is the adsorption density at equilibrium, Γt(mg/g) is adsorption density at time t, k_1 (h^{-1}) is the rate constant of Pesudo-first order model, k_2 (mg/g·h) is the rate constant of Pesudo-second order, k_3 and I are the constants of interparticle diffusion, α (mg g^{-1} h^{-1}) and β (g mg^{-1}) are the initial sorption rate of adsorbate and desorption constant, respectively.

As shown in Figs. 2-7, the Cr(VI) adsorption data were linearly fitted with adsorption kinetic models, the detailed parameters for models were presented in Table 4. The Cr(VI) removal is described well with Pseudo-second order kinetic model for HAC and AC under pH 6 and pH 7 with higher correlation coefficients (r^2), suggesting that the interaction between the Cr(VI) and the functional groups of the HAC and AC is of the chemical type. As described in Table 2-4, the rate constant of k_2 at pH 6 was nearly 3 times greater than that at pH 7 for HAC, and the rate constant for HAC under pH 6 and 7 both increased after ball milling compared to the pristine AC. Indicating that the adsorption rate was highly favorable with the hydrogen ion strength and the developed Cr(VI) removal capacity on HAC was associated with the quicker chemical reaction between Cr(VI) and surface functional groups. Besides, the chemical reaction associated with the Cr(VI) adsorption was significantly related to the proton concentration, in agreement with studies reported previously [27, 471, 495-497].

Table 2-4 The adsorption kinetic model parameters for Cr(VI) removal by AC and HAC under pH 6 and 7

	HAC		Pristine AC	
Models	pH6	pH7	pH6	pH7
Pseudo-first order				
Γe (mg/g)	1.97	3.39	10.28	6.36
k_1 (h^{-1})	1.56	1.71	1.30	0.59
r^2	0.461	0.746	0.972	0.627
Pseudo-second order				
Γe (mg/g)	20	15.38	14.08	8.77
k_2 (mg/g·h)	8.39	2.88	0.53	2.23
r^2	1.000	0.998	0.983	0.999
Elovich				
α ($mg\ g^{-1}\ h^{-1}$)	1.3×10^{9}	1.9×10^{21}	199.0	1946.5
β ($g\ mg^{-1}$)	0.97	0.30	1.86	1.06
r^2	0.755	0.951	0.978	0.985
Interparticle diffusion				
k_{id1}	122.39	111.24	30.64	30.94
I_1	0.81	0.81	0.13	0.16
r_1^2	0.924	0.910	0.967	0.951
k_{id2}	0.73	1.78	7.20	3.40
I_2	18.86	12.79	3.98	4.55
r_2^2	0.880	0.892	0.986	0.799

The diffusion process of aqueous adsorbate into adsorbent can be elucidated by the Interparticle diffusion model. Briefly, the adsorbate ions transfer through bulk solution into the external surface of the adsorbent and then transfer into the internal surface followed by adsorption in the active sites of adsorbent [498]. As can be seen in Fig. 2-7 (d), the diffusion route of Cr(VI) into AC and HAC contains two steps. The first stage of adsorption dominants the removal rate of Cr(VI) by AC and HAC since the interparticle diffusion rates at the first stage (k_{id1}) for AC and HAC were both higher than that of the second stage (k_{id2}). The k_{id1} of HAC under pH 6 and 7 were nearly 4 times higher than that of AC, this finding has identified that the rate of Cr(VI) transfers from the bulk solution to the surface of AC was improved after ball milling pretreatment.

2.3.4 Adsorption isotherm

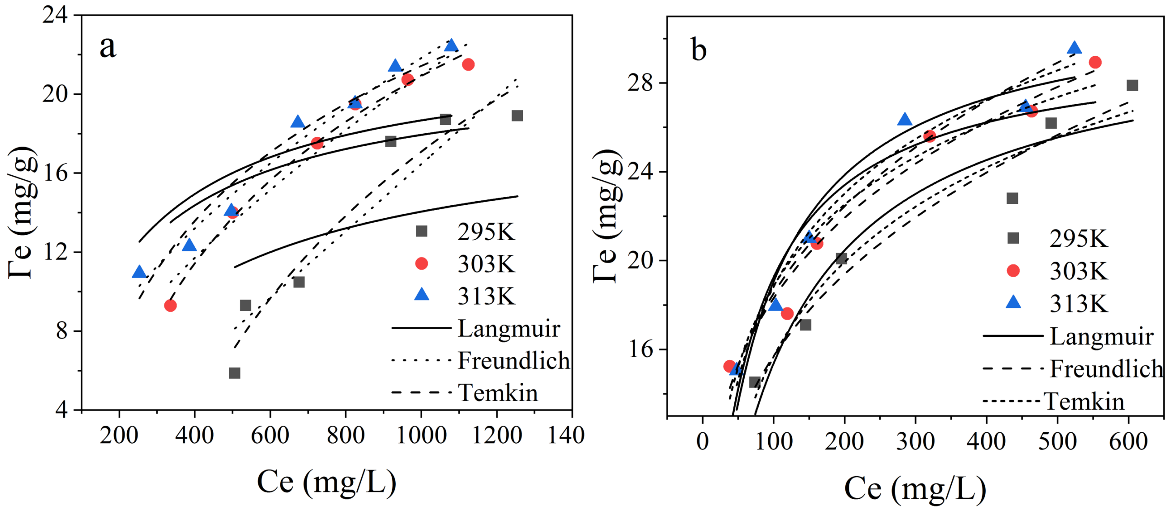

Figure. 2-8 Non-linear fit of adsorption isotherm models (a) AC (b) HAC (pH 7, 50g/L).

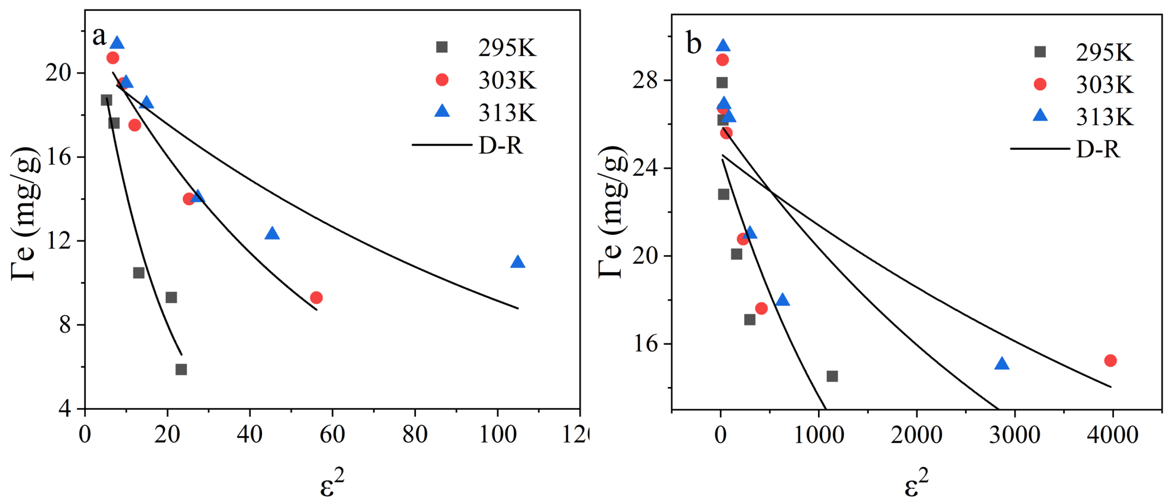

Figure. 2-9 Non-linear fit of D-R model for (a) AC and (b) HAC (pH 7, 50g/L).

Langmuir, Freundlich, Dubinin-Radushkevich (D-R), and Temkin models were employed to delineate the adsorption behavior of Cr(VI) [499], the non-linear equations of those models were presented as follows;

Langmuir equation

$$\Gamma e = \frac{K_L \Gamma_0 C_e}{1+K_L C_e} \quad (2\text{-}8)$$

Freundlich equation

$$\Gamma e = K_F C_e^{1/n} \quad (2\text{-}9)$$

Temkin equation

$$\Gamma e = \frac{RT}{b_T} \ln{(K_T C_e)} \tag{2-10}$$

D-R equation

$$\Gamma e = \Gamma_{max} e^{-K_D \varepsilon^2} \quad \varepsilon = RT \ln\left(1 + \frac{1}{C_e}\right) \tag{2-11}$$

where Γe (mg/g) is the equilibrium adsorption density, Γ_0 (mg/g) is the theoretical monolayer adsorption density, K_L (L/g) is the Langmuir constant, K_F is the Freundlich isotherm constant, Ce (mg/L) is equilibrium concentration, n is the Freundlich isotherm exponent, R (8.314 J/mol/K) is the universal gas constant, T (K) is the absolute temperature, b_T (J/mol) is the Temkin isotherm constant, K_T (L/g) is the Temkin isotherm equilibrium binding constant, Γmax (mg/g) is the theoretical saturation density, K_D ($mol^2\ kJ^{-2}$) is the D-R isotherm constant, ε is the Polanyi potential.

Figs. 2-7 and 2-8 were the non-linear fit of Langmuir, Freundlich, Temkin, and D-R isotherm models, the computed theoretical parameters of the models were provided in Table 2-5. The higher correlation coefficients of the Freundlich model fitted the experimental data satisfactorily and this observation could support the hypothesis that the adsorption of Cr(VI) on AC and HAC was multi-layer. The values of n for HAC were all over 2 while values of n for AC were all below 2, which indicated the adsorption was favorable for HAC under ambient temperature [500]. Table 2-6 listed the adsorption density comparison of different AC materials with this study.

Table 2-5 The parameters of adsorption isotherm models for HAC and AC

		AC			HAC		
Models		295	303	313K	295	303	313K
Langmuir	Γ_0 (mg/g)	18.9	21.5	22.4	31.6	31.7	32.6
	K_L (L/mg)	0.003	0.005	0.005	0.014	0.009	0.014
	r^2	0.438	0.600	0.704	0.919	0.851	0.947
Freundlich	K_F	0.002	0.158	0.441	3.843	5.523	5.179
	1/n	1.303	0.714	0.567	0.306	0.260	0.277
	r^2	0.942	0.982	0.973	0.962	0.970	0.971
Temkin	b_T (J/mol)	153.2	239.6	310.0	423.7	491.8	429.6
	K_T (L/g)	0.003	0.007	0.013	0.128	0.353	0.224
	r^2	0.904	0.997	0.945	0.949	0.941	0.971
D-R	Γmax (mg/g)	25.5	22.5	20.68	24.64	24.66	25.99
	K_D (mol^2 kJ^{-2})	0.058	0.017	0.008	5.9E-4	1.4E-4	2.4E-4
	r^2	0.950	0.977	0.793	0.706	0.545	0.697

Table 2-6 Comparison of Cr(VI) adsorption density onto various AC materials

Adsorbents	Adsorption density (mg/g)	pH	Refs
Commercial AC	20.0	7	[501]
Polysulfide rubber modified AC	8.9	4	[502]
Pomegranate husk AC	10.0	6	[503]
Chestnut oak shells AC	6.0	7	[504]
Tannic acid immobilized AC	0.5	7	[505]
Hazelnut shell AC	8.0	8	[506]
Granular AC	7.2	7	[507]
Fe-modified AC prepared from Trapa natans husk	2.5	7	[508]
Micron-scale iron modified AC	1.3	6	[106]
AC derived from seagrass	0	≥4	[509]
Ball milled AC	28.9	7	This study

2.3.5. Adsorption thermodynamic

The thermodynamic parameters enthalpy change (ΔH) and entropy change (ΔS) can be calculated by the function of $\ln K_C$ versus 1/T, the equation shown in Eq (2-12). Gibb's free energy change (ΔG) can be determined through the Van't Hoff equation (Eq (2-13)).

$$\ln K_c = \frac{\Delta S}{R} - \frac{\Delta H}{RT} \quad (2\text{-}12)$$

$$\Delta G = -RT\ln K_c \quad (2\text{-}13)$$

Where ΔH (kJ/mol) and ΔS (J/mol k) were established by the slope and intercept of Eq(12). The adsorption process is endothermic if the value of ΔH is positive, otherwise, it's exothermic. Equilibrium constant K_C equal to Γe/Ce [27] or the intercept of the plot of ln(Γe/Ce) versus Γe [510], the negative value of ΔG (kJ/mol) means the adsorption process prolongs spontaneously under ambient conditions.

The detailed values of ΔH, ΔS, and ΔG of Cr(VI) adsorption on HAC and AC are given in Table 2-7. The values of ΔG for HAC and AC were both negatives, signifying that the adsorption of Cr(VI) was spontaneous and the values ΔG of HAC under different temperatures were both higher than that of AC, which implied the spontaneity of adsorption was unfavorable energetically and more spontaneity for HAC after ball milling [511]. The value of ΔH was positive for HAC and AC indicated the Cr(VI) adsorption process was endothermic. Positive values of ΔS of HAC and AC related to the disorderliness of the system.

Table 2-7 The adsorption kinetic model parameters for Cr(VI) removal by AC and HAC under pH 6 and 7

Adsorbents	T (K)	ΔG (kJ/mol)	ΔH (kJ/mol)	ΔS (kJ/mol k)
	295	-11.80		
HAC	303	-12.12	0.001	0.04
	313	-12.52		
	295	-17.69		
AC	303	-18.17	0.01	0.06
	313	-18.77		

2.3.6 Cr(VI) removal mechanism

2.3.6.1 The pH-speciation of Cr(III) and Cr(VI)

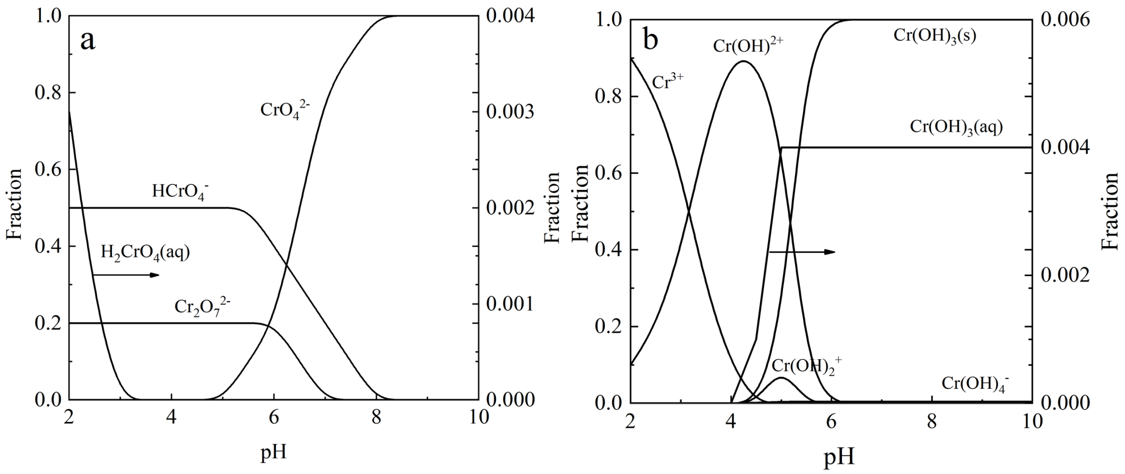

Figure. 2-10 The speciation diagram of (a) Cr(VI) and (b) Cr(III).

Fig. 2-10 is the pH-speciation diagram for 1000 mg/L Cr(VI) and Cr(III), which were built using equations (14)-(21). $HCrO_4^-$ and CrO_4^{2-} are predominant at pH 6, while CrO_4^{2-} predominates at pH 7. As shown in Figure 2-10 (b), $Cr(OH)_3(s)$ is the predominant species both at pH 6 and pH 7. The aqueous solution chemistry equilibriums for Cr(VI) and Cr(III) species are shown in Eqs (2-14) to (2-21) [512-514], where k is the chemical reaction equilibrium constant [515].

$H_2CrO_4 = HCrO_4^- + H^+$	$k = 10^{-0.43}$	(2-14)
$HCrO_4^- = CrO_4^{2-} + H^+$	$k = 10^{-6.49}$	(2-15)
$2HCrO_4^- = Cr_2O_7^{2-} + H_2O$	$k = 10^{1.55}$	(2-16)
$Cr^{3+} + H_2O = Cr(OH)^{2+} + H^+$	$k=10^{-3.56}$	(2-17)
$Cr(OH)^{2+} + H_2O = Cr(OH)^+_2 + H^+$	$k=10^{-6.27}$	(2-18)
$Cr(OH)^+_2 + 2H_2O = Cr(OH)_3(aq) + H^+$	$k=10^{-2.61}$	(2-19)
$Cr(OH)_3(aq) + H_2O = Cr(OH)_4^- + H^+$	$k=10^{-10.33}$	(2-20)
$Cr(OH)_3(aq) = Cr(OH)_3(s)$	$k=10^{4.17}$	(2-21)

It is noteworthy to remark that most studies on Cr(VI) removal have been undertaken at acidic conditions where $HCrO_4^-$ and Cr^{3+} are the predominant species. Under these pH conditions, $Cr_2O_3(s)$ has been reported to be the end chromium product on AC [468-470]. Our work was carried out at pH 6 and 7. Under these pH conditions, $Cr(OH)_3(s)$ was the chromium product on the AC as discussed below.

2.3.6.2 Chromium species on HAC

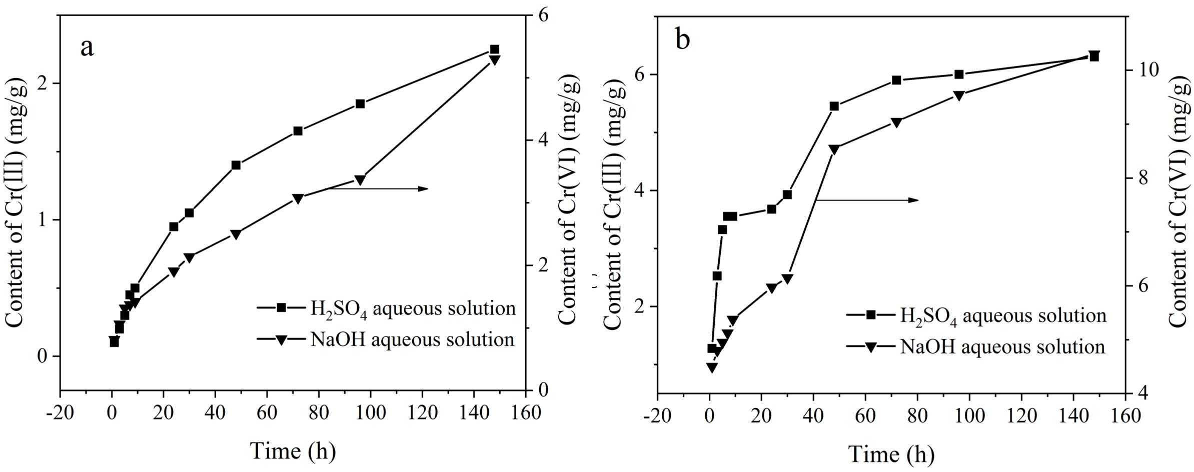

Figure. 2-11 The elution experiments with chromium-loaded virgin AC (a) and HAC (b) after adsorption at pH 7 (1.0 g/100ml treated pristine AC or HAC, 0.2 M H_2SO_4 and 0.1 M NaOH, 295K)

Fig. 2-11(a) and (b) show the amount of Cr(III) and Cr(VI) desorbed from AC and HAC, after treatment with Cr(VI) at pH 7, using a 0.2 M H_2SO_4 and 0.1 M NaOH aqueous solution. Firstly, it is noted that Cr(III) desorbed from the carbons at acidic pH conditions, while Cr(VI) desorbed at basic pH. The Cr(III) in the eluants at acidic conditions likely results from the dissolution of $Cr(OH)_3$, leading to say that this is the Cr(III) species which formed from Cr(VI) adsorption. Cr(VI) in the eluants at basic conditions suggests that Cr(VI) co-adsorbed with the $Cr(OH)_3(s)$ as CrO_4^{2-}. At basic pH, OH^- ions deprotonated the surface COOH groups, which is turned into the electrically negative COO- group. As a result, the adsorbed CrO_4^{2-} on the COOH is repelled and migrated to the aqueous solution. Desorbed Cr(VI) was 10.3 mg/g from HAC, much greater than the Cr(VI) desorbed from AC, which was 5.3 mg/g. Dissolved Cr^{3+} from HAC reached 6.3 mg/g, almost 3 times greater than the Cr^{3+} desorbed from AC. The much greater amount of chromium desorbed from the HAC in comparison to that desorbed from AC confirmed that high-intensity ball milling improved the adsorption performance of AC. More functional groups, especially carboxyl, were created on the AC surface, which in agreement with the work reported by [17, 485]

The chromium elution under acidic and alkaline solution can be stated as Eqs (2-22) and (2-23), respectively.

$$HAC\cdots Cr(OH)_3(s) + 3H^+ \rightarrow HAC + Cr^{3+} + 3H_2O \qquad (2\text{-}22)$$

$$HAC\text{-}COOH\cdot\cdot CrO_4^{2-} + OH^- \rightarrow CrO_4^{2-} + HAC\text{-}COO^- + H_2O \qquad (2\text{-}23)$$

2.3.6.3 Proposal on chromium removal mechanism

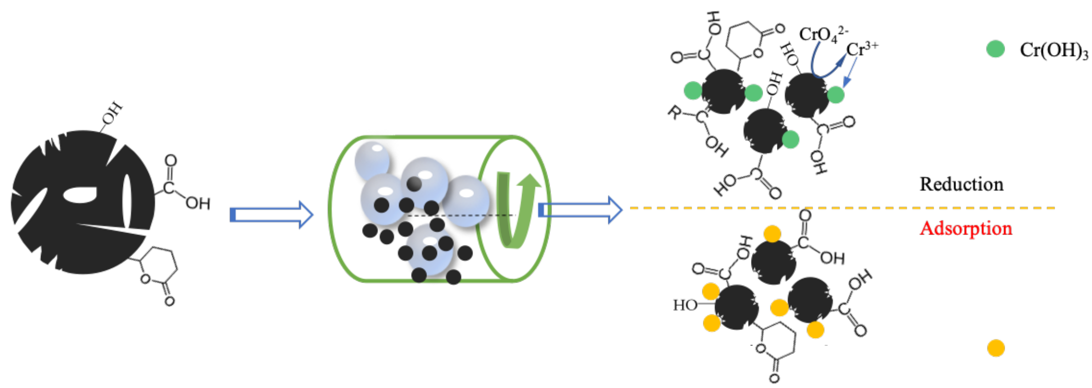

Figure. 2-12 Schematic of Cr(VI) removal by HAC induced by ball milling.

The tests on chromium elution from the Cr-loaded HAC showed that Cr(III) as $Cr(OH)_3$(s) and Cr(VI) as CrO_4^{2-} were on the surface of HAC. The $Cr(OH)_3$(s) formed a layer on the HAC particle, as seen in Figs 2-4 and 2-5. This $Cr(OH)_3$(s) resulted from the reduction of adsorbed Cr(VI) to Cr(III). According to Fig 2-10(b), $Cr(OH)_3$(s) is the stable Cr(III) species at pH 6 and 7. The reduction of Cr(VI) to Cr(III) has been proposed to be due to π-electron in activated-carbon-basal planes [516-518]. The reduction of Cr(VI) to Cr(III) and the surface precipitation of $Cr(OH)_3$ can be expressed as follows:

$$CrO_4^{2-} + 8H^+ + 3e^- = Cr^{3+}(aq) + 4H_2O \qquad (2\text{-}24)$$

$$Cr^{3+} + 3H_2O = Cr(OH)_3(s) + 3H^+ \qquad (2\text{-}25)$$

Adsorption of Cr(VI) may proceed through hydrogen bonding on the surface COOH groups, as follows:

$$HAC\text{-}COOH + CrO_4^{2-} = HAC\text{-}COOH\cdot\cdot CrO_4^{2-} \quad (2\text{-}26)$$

The encouraged capability of HAC on Cr(VI) sequestration was dominantly contributed by the increased surface oxygen-containing functional groups and the refined particle size in the presence of higher surface area. Meanwhile, the reduction of surface oxygen-containing functional groups was verified by the results obtained from Raman spectra and Boehm's titration. Additionally, the adsorption thermodynamic revealed that the spontaneity of Cr(VI) adsorption on HAC increased after ball milling. Fig. 28 shows a schematic representation of the increase in functional groups on the AC after high-intensity grinding and the adsorption of the chromium species on the functional groups.

2.3.7 Reusability and regeneration of HAC

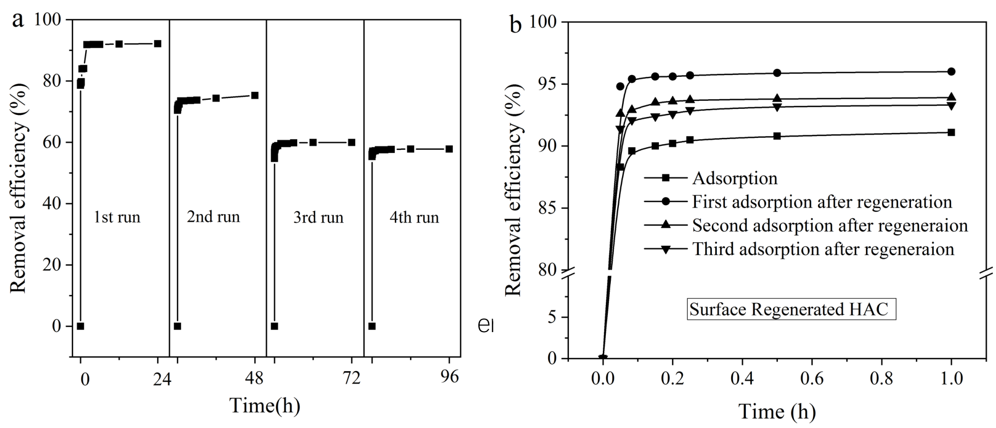

Figure. 2-13 The (a) reusability and (b) regeneration of HAC under pH 7.0 (5 g/100ml HAC, 1000mg/L Cr(VI), 295K)

Fig. 2-13(a) shows the Cr(VI) removal efficiency of HAC as a function of time subjecting the HAC to several consecutive adsorption runs at pH 7, the HAC was recycled to the next adsorption step without removing the loaded chromium. Cr(VI) removal was 92% when the HAC first contacted the Cr(VI) aqueous solution. This removal efficiency decreased steadily with the number of adsorption cycles, being 75% for the first cycle and 60% and 57% for the following. As noted in Figs 2-4 and 2-5, $Cr(OH)_3$(s) is reported in the HAC pores and as a layer on the HAC surface. It follows that $Cr(OH)_3(s)$ was definitively responsible for this decrease in removal efficiency as the number of cycles increased. The $Cr(OH)_3(s)$ blocked off the diffusion of Cr(VI) to the interior of the HAC particle. As noted in Fig. 2-11, at acid conditions, soluble Cr^{3+} is the predominant species, so with an acid wash, it is expected that the $Cr(OH)_3(s)$ in the pores and surface of the HAC will be removed leaving a particle with a free path for diffusion and further adsorption of Cr(VI). This was confirmed by subjecting the Cr loaded HAC to an acid wash then the regenerated HAC was subjected to another cycle of adsorption. Fig. 2-13(b) shows that the removal efficiency of Cr (VI) by HAC increased from 92.2% to 96.3% after acid regeneration. The uptake efficiency of Cr(VI) on HAC decreased with the recycling due to the formation of $Cr(OH)_3(s)$ as foregoing discussed.

2.4. Conclusions

The density of surface functional groups of activated carbon can be significantly improved by high-intensity grinding. Thus, the sequestration capability of commercial AC on Cr(VI) increases, and the removal of aqueous Cr(VI) can be undertaken under near-neutral pH. The feasibility and potential of HAC modified by ball milling on the practical application were developed. Besides, carrying out the Cr(VI) adsorption at near-neutral pH leads to the formation of $Cr(OH)_3(s)$ on HAC. $Cr(OH)_3(s)$ can be easily removed off by acid washing through which the HAC surface is regenerated and thereby regains its original adsorption capacity, and can be recycled to the Cr(VI) adsorption step. Once the adsorbent material has been regenerated, it can be used up to three stages without significantly losing its absorption capacity. The results obtained in this work showed that Cr(VI) adsorption of HAC at near-neutral pH proceeds through two mechanisms. One mechanism is the reduction of Cr(VI) to Cr(III) and hydrogen bonding of CrO_4^{2-} with COOH surface functional groups, and another is the Cr(III) precipitation to $Cr(OH)_3(s)$ in pores and surface of the HAC. This $Cr(OH)_3(s)$ could be removed by acid washing of the HAC, while the $Cr_2O_4^{2-}$ was removed by alkaline washing of the HAC. The studies of adsorption kinetic and isotherm show that the

Pseudo-second order model and Freundlich fitted the adsorption data well, implying the chemisorption and multi-layer adsorption of Cr(VI) on HAC and AC. The intraparticle model study confirmed that the transfer rate of Cr(VI) from the bulk solution to the surface of AC was increased after ball milling. The thermodynamic study indicated that the adsorption of Cr(VI) by HAC and AC is endothermic and the spontaneity of Cr(VI) adsorption on HAC was higher. The Work is yet needed to further improve the removal efficiency of the HAC for its recycling. This involved determining the performance of the HAC after a two-step treatment of the Cr-loaded HAC, under acidic and alkaline conditions.

Chapter III. **A new insight into the restriction of Cr(VI) removal performance of activated carbon under neutral pH condition**

3.1. Introduction

Chromium abounds in nature and is highly toxic in the form of CrO_4^{2-} and $Cr_2O_7^{2-}$ through bioaccumulation [519]. The chromium pollution of water, land, and environment has attracted the interest of experts as electroplating plants, stainless steel manufacturing plants, leather manufacturing plants, and refractory plants have progressively appeared [417, 520, 521]. Cr(III) presents less mobility, toxicity, and solubility than Cr(VI) and generates sparingly soluble chromium hydroxides [522]. The reduction of Cr(VI) to Cr(III) is rapid at acidic conditions, meanwhile, the readily available electron is required for the reduction process [523, 524]. It is well known that removing Cr(VI) from water by reduction and precipitation is a viable option [447, 525-527]. Conventional reducing agents are sulfur and iron salts [528, 529], post-treated effluent contained sulfate, and iron salts would contaminate water and soil. Furthermore, the mandatory wastewater discharge would result in high costs.

The bulk of published studies on Cr(VI) removal by low-cost and readily accessible activated carbon (AC) demonstrated that removal capacity was greater in acidic conditions than alkaline conditions. This suggests that the Cr(VI) elimination is strongly pH-dependent [27, 48, 530]. The removal efficiency of Cr(VI) by activated carbon prepared from teakwood sawdust was 100% at pH 2 while it was below 20 % at pH 10 [531]. Table 3-1 shows the capacity of several ACs to remove Cr(VI) in acidic and alkaline environments. At low pH, the removal capacity was favored because the positively charged surface of Cr(VI) advanced the adsorption of anion Cr(VI) [532]. It is worth noting that the pH-speciation of Cr(VI) reveals that $HCrO_4^-$ dominated below pH 6, whereas CrO_4^{2-} dominates above pH 7 [533]. Furthermore, prior studies have found that positively charged AC produced by protonation at a low pH value tends to attract chromate anions, which is thought to be the main mechanism for Cr(VI) adsorption [534]. It was discovered that as pH dropped, the reduction and adsorption process enhanced simultaneously.

Table 3-1 Comparison of Cr(VI) removal under different pH by various carbon materials

Carbon materials	Cr(VI) removal capacity (mg/g)		Refs
	Acid condition	Alkali condition	
AC derived from *Posidonia Oceanica* seagrass	30.5 (pH 3)	0 (pH > 4)	535
Biochar derived from corn straw	125(pH 2)	50 (pH 6)	536
Powdered AC	46 (pH 2)	8 (pH 7)	491
Biochar derived from waste glue residue	206.7 (pH 2)	90 (pH 6)	537
AC prepared by calcination wheat bran	22 (pH 2)	0 (pH 10)	538
Commercial AC	21 (pH 2.5)	13 (pH 5.5)	539
KOH activated porous corn straw	98.3 (pH 3)	33.7 (pH 7)	45
AC derived from an acrylonitrile-divinylbenzene copolymer	80 (pH 2)	9 (pH 8)	540

To our understanding, there have been few investigations on systematic chromium adsorption and reduction study when pH rises over 7, to shed light on a substantial drop in AC performance. Most studies have only focused on the unfavorable effect of electrostatic repulsion between chromate anions and negatively charged AC surface at high pH values [45, 504, 541]. Besides, an earlier study failed to elucidate the removal paths at pH higher than 6 because the surface negatively charged bamboo bark-based AC that unfavored the adsorption of Cr(VI) anions, hence the reduction process of Cr(VI) to Cr(III) at high pH was omitted [542]. Cr(III) speciation as a function of pH was depicted clearly by Lopez-Valdivieso's study showing that $Cr(OH)_3$(s) predominates at pH over 6.4 [303]. The effect on the removal of Cr(VI) under alkaline conditions of the AC surface loaded Cr(III) precipitate was especially neglected. Early reported studies on the synthesis of eskolaite (α-Cr_2O_3) nanoparticles through AC following adsorption of Cr(VI) have shown that Cr_2O_3 was the reduced species of Cr(VI) on AC [469, 543]. Recently study showed that the Cr_2O_3 reduced the adsorption rate of Cr(VI) significantly [468].

Compared to the consensus that the electrostatic repulsion led to the poor Cr(VI) removal efficiency of AC at alkaline conditions, the effect of AC surface coated Cr_2O_3 precipitate on removal performance was not fully understood. This work aimed to study the effect of powdered AC (PAC) surface formed Cr_2O_3 precipitate on Cr(VI) removal, SEM-EDX (scanning electron microscope-energy dispersive X-ray analysis), and XPS (X-ray photoelectron spectroscopy) were used to investigate the surface morphology and the chemical properties. Desorption and regeneration experiments were used to confirm the role of Cr_2O_3. The insight gained from this study would help to expand the longevity of AC and the recovery of Cr via AC.

3.2. Materials and methods

3.2.1. Characterization of PAC particle

To scrutinize the composition of loaded-chromium on PAC after Cr(VI) removal, three types of de-passivation agents were examined to desorb the adsorbed/reduced chromium on PAC. The formation process of the chromium layer on PAC at pH 3 and 7 was inspected by carrying out consecutive desorption tests following each Cr(VI) adsorption. SEM-EDX (JSM-6610LV, JEOL, Japan) and XPS (K-Alpha, Thermo Scientific, USA) were employed to characterize the distribution of chromium and the chemical species of Cr and C on PAC at pH 3 and 7, respectively. The difference of removal mechanisms under the two pH values was delineated by XPS and Raman spectroscopy (DXR, Thermo Scientific, USA).

3.2.2. Materials

All the chemicals were analytical grade and the aqueous solutions were prepared with deionized water through Barnstead pure II water purification system (Thermo Scientific, USA). Potassium dichromate ($K_2Cr_2O_7$) was purchased from J.T.Baker and used for preparing 1000 mg/L Cr(VI) as a stock solution. 1.0 M H_2SO_4 and 1.0 M NaOH were used to adjust the pH of the aqueous solutions. H_2SO_4, NaOH, KCl, and 1,5–diphenylcarbazide were provided by J.T.Baker. Commercial available AC was provided by Calgon company, its chemical composition was 97% carbon and 3% inorganic residual. The AC was treated by ball milling and obtained a PAC with an average size of 4 μm, a specific surface area of 929 m^2/g, and a pore radius of 15.9 Å, PAC used in this study was reported in our previous work [523]. Following the grinding step, the PAC was dried and stored in a desiccator.

3.2.3. Comparison of Cr(VI) removal at different pH

A comparison was conducted for the PAC removal efficiency at pH 3, 7, and 9 [544]. The desired mass of PAC (5 g) was mixed with deionized water (100 mL) for 1 h, then the pH was adjusted to 3, 7, and 9 using 1.0 M H_2SO_4 and NaOH aqueous solutions and monitoring the pH with an Orion 3 star pH meter (Thermo Scientific, USA). 0.2829 g $K_2Cr_2O_7$ reagent was added to the PAC suspension to prepare a 1000 mg/L solution once the pH was stable. To follow the Cr(VI) uptake a 200 μL aliquot was withdrawn from the aqueous solution at 3, 5, 9, 15, 30, 60, 360, 1440 min. The withdrawn aliquot was centrifuged in a centrifuge (Allegra™ 21, Beckman coulter, USA) for 15 min prior to analysis. The Cr(VI) removal capacity was calculated through Eq (3-1) [545], wherein Γ(mg/g) is the removal capacity, C_0 (mg/L) is the initial concentrations and C_t is the concentration at time t, V (L) and M (g) are the volume of solution and dose of PAC, respectively.

$$\Gamma = (C_0 - C_t)V/M \qquad (3\text{-}1)$$

3.2.4. Selection of desorption agents

Three kinds of desorption agents were evaluated to determine their effectiveness for desorbing the adsorbed chromium species on PAC. Analytical grade $K_2Cr_2O_7$ acted as a precursor of the chromium layer on PAC. To obtain adequate loaded chromium on PAC for assessment, consecutive uptake experiments were undertaken. 5.0 g PAC was mixed with 1000 mg/L Cr(VI) aqueous solution at a fixed pH of 7 in a glass volumetric flask. This suspension was stirred magnetically (Thermo scientific, USA) at 100 rpm to prevent deteriorating of the chromium layer formed on the PAC. A 200 μL sample was withdrawn from the suspension at 0.25, 0.5, 1, 3, 5, 7, 9, 12, 15, 30, 60, 120, 1440 min to determine the concentration of Cr(VI), then the suspension was filtered to collect the PAC, which was rinsed with deionized water, and dried before the following removal experiments. Consecutive removal steps were performed with 1000 mg/L Cr(VI). Dried chromium-load PAC after four repetitive adsorption runs was used for the desorption testing. All the batch experiments were conducted in duplicate under ambient conditions. The adsorption capacity at equilibrium for Cr on PAC was expressed as Eq (3-2)

$$q_p = \sum(1000 - Ce_i)V_i/M_i \qquad (3\text{-}2)$$

where q_p (mg/g) is the content of chromium on PAC, Ce_i (mg/L), V_i (mL) and M_i (g) (i=1, 2, 3, 4) are the equilibrium concentration, solution volume and mass of PAC of each removal cycle, respectively.

To desorb the loaded chromium from the PAC, 0.2M KCl, 0.2M H_2SO_4, and 0.1M NaOH were employed. 0.5g chromium-loaded PAC was mixed with 50 ml of the desorption agent solution in a glass volumetric flask and stirred at 200 rpm, the concentration of desorbed chromium after 1, 3, 5, 7, 9, 24, 30, 48, 72, 96, 148 h was determined, the efficiency of desorption was determined through Eq (3-3).

$$\eta = 100 \times (C_t V)/(q_p M) \qquad (3\text{-}3)$$

where η (%) is desorption efficiency, C_t (mg/L) is the dissolved chromium concentration at t time, V (L) and M (g) are the volumes of desorption solution and dose of PAC correspondingly. In addition, the performance of PAC treated with Cr(VI) after desorption with different chemical agents was evaluated.

3.2.5. The formation process of chromium layer at pH 3 and 7

To ascertain the route of the chromium layer formed on PAC, the chromium speciation after consecutive adsorption runs was analyzed with selected desorption agents (0.2M H_2SO_4 and 0.1M NaOH solution). Four desorption tests followed four successive removal cycles were performed and the increment content of loaded chromium on PAC between two successive adsorption runs was determined by Eq (3-4).

$$\Delta q = (C_{ii} - C_i)V/M \quad (3\text{-}4)$$

where Δq (mg/g) is the increased content of chromium on PAC, C_{ii} and C_i (mg/L) are the equilibrium concentration of desorbed chromium after the two successive elution tests, V (ml) and M (g) are the volume of desorption solution and the dose of PAC after adsorption of Cr(VI).

The adsorption capacity of PAC loaded with chromium on Cr(VI) after the last elution assessment was examined, and all the adsorption experiments were conducted with 1000 mg/L Cr(VI).

3.2.6. Analytical method

A colorimetric approach employing 1,5–diphenylcarbazide and a UV-Visible spectrophotometer (Thermo Scientific, USA) coupled with a 1 cm quartz cell was used to determine Cr(VI). 100 μL filtered solution was diluted to 10 ml and mixed with 0.1 mL 49% H_2SO_4, 0.1 mL 42.5% H_3PO_4, and 0.4 mL 0.2 % 1,5–diphenylcarbazide solution, sequentially. The mixed solution stood for 10 min and was then measured by a UV-Visible spectrophotometer under 540 nm. The absorbance of deionized water was used as a reference. With prepared 0, 0.02, 0.05, 0.1, 0.2, 0.4, 0.6, 0.8, and 1.0 mg/L Cr(VI), a standard curve of concentration versus absorbance was constructed, this standard curve was used to determine the Cr(VI) concentration of the sample. The total concentration of aqueous Cr was analyzed by atomic absorption spectrometry (AAS, Varian Spectra 220FS), a 50μL filtered solution was diluted to 10 mL and then sprayed into the flame of air-acetylene. The chromium ground state atoms formed under a high-temperature flame produce selective absorption of the 357.9 nm characteristic spectrum of chromium hollow cathode lamps, and the absorbance value is proportional to the concentration of Cr. The standard curve of total Cr was built in the same way as Cr(VI), and the concentration of total was determined by the standard curve as well. The presence of soluble Cr species in the solution was Cr(III) and Cr(VI), the concentration of aqueous Cr(III) was confirmed by the difference between total Cr and Cr(VI).

3.3. Results and discussion

3.3.1 Particle characterization

3.3.1.1 Surface morphology

The surface morphology of PAC after Cr(VI) adsorption under pH 7 was characterized by SEM-EDX and elements mapping. As seen in Fig.3-1, a chromium layer adsorbed mostly on the PAC surface. A similar observation was reported recently [468].

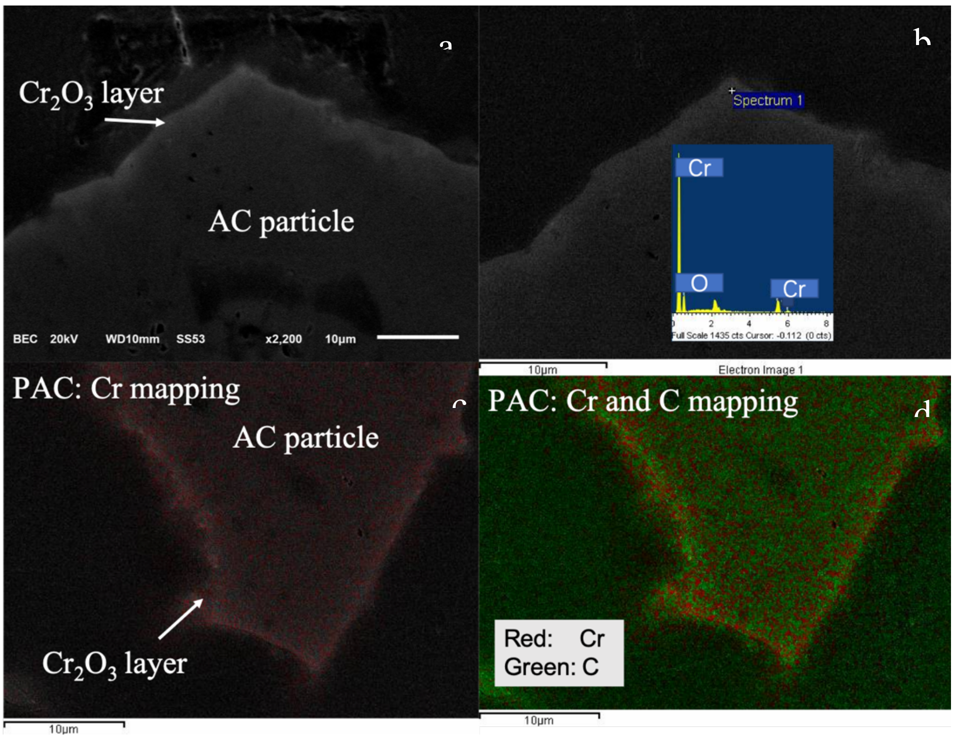

Figure. 3-1 SEM-EDX micrographs (a and b) and SEM coupling with elements mappings (c and d) of PAC after Cr(VI) adsorption at pH 7.

3.3.1.2 XPS spectra analysis

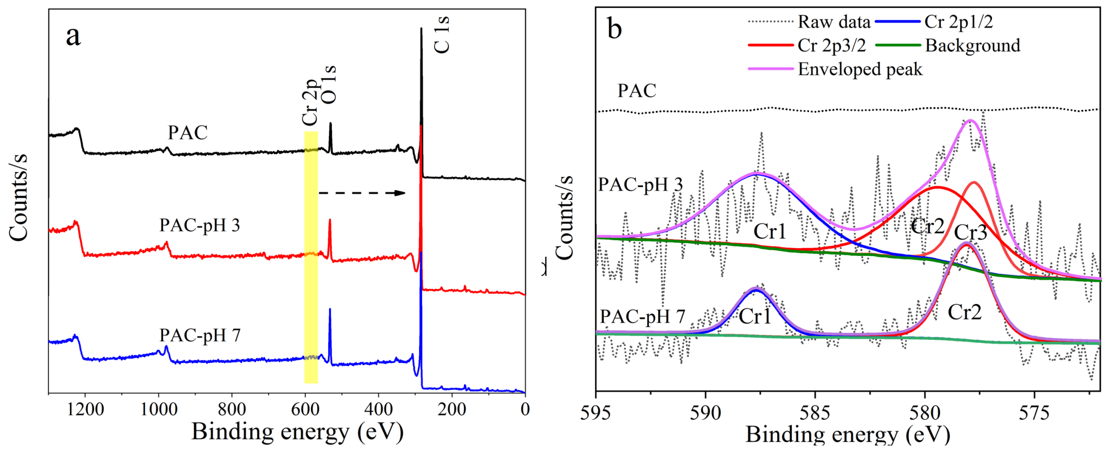

Figure. 3-2 The XPS spectra of PAC treated with Cr(VI) under pH 3 (PAC-pH 3), pH 7 (PAC-pH 7), and fresh PAC; (a) XPS survey, (b) scan of Cr 2p

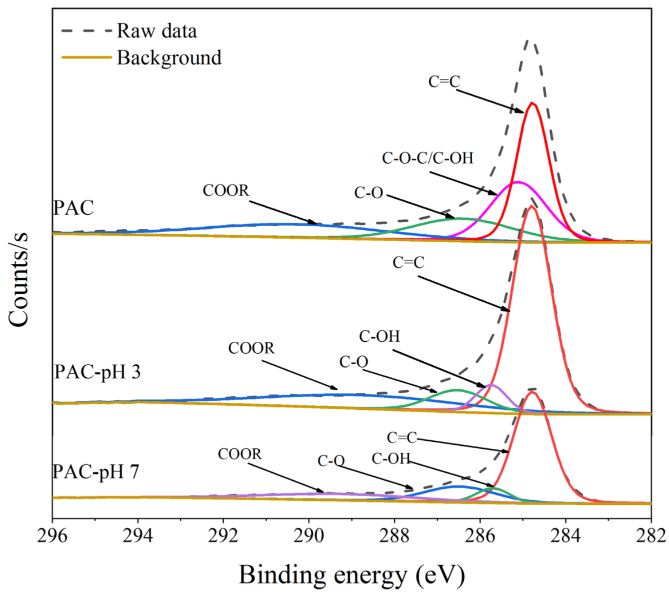

Figure. 3-3 High resolution C 1s spectra of PAC, PAC-pH 3, and PAC-pH 7.

To further inspect the chemical species of Cr on the surface of PAC, the XPS analysis was employed. Figs 3-2(a) and (b) showed the XPS spectra, which were fitted and deconvoluted into multiple peaks by CasaXPS (version 2.3.23). The peak referenced as C 1s at 284.8 eV, the Shirley type was designated as the background subtraction. As presented in Fig. 3-2(a), the Cr 2p peak due to Cr(VI), denoted that the Cr(VI) was adsorbed onto PAC. The XPS spectrum of PAC after being treated with Cr(VI) at pH 3 (PAC-pH 3) and 7 (PAC-pH 7) was built as presented in Fig.2(b). The

Cr 2p region of the photoelectron spectrum was both detected for PAC-pH 3 and PAC-pH 7, which was consistent with the EDX spectrum shown in Fig. 3-1. Cr 2p involves two energy levels, 2p 1/2 and 2p 3/2. The XPS spectrum of PAC-pH 3 can be divided into the Cr1, Cr2, and Cr3 peaks, where the binding energies (BE) value of Cr1 peak of PAC-pH 3 was 587.5 eV, which was very close to that of Cr_2O_3 (587.4 eV ± 0.2) [546]. The BE for Cr2 and Cr3 of PAC-pH 3 were 579.2 and 577.8 eV, respectively, which can be attributed to Cr(VI) [547-549]. Two contributions of Cr1 and Cr2 for the Cr 2p region of PAC-pH 7 were 587.7 and 578.0 eV, matching well with the binding energy for Cr(VI) and Cr_2O_3 [549-551]. Due to XPS detection depth was no more than 4 nm from the sample surface, it can be said that the chromium layers on the surface of PAC-pH 3 were mainly constituted by Cr(VI) and PAC-pH 7 was mainly constituted by Cr_2O_3(s) [552]. Consistent with the present results, previous studies have demonstrated that the reduction and adsorption participated principally in the Cr(VI) removal on biomass [553, 554]. Moreover, the peak area ratio (Cr1 versus total peaks) as determined by CasaXPS was 69.93% and 39.91% Cr_2O_3(s) on the surfaces of PAC-pH 7 and PAC-pH 3, respectively. This higher content of Cr_2O_3 on PAC-pH 7 clearly evidenced that more Cr_2O_3 formed on the PAC at pH 7 than at pH 3, impeding the diffusion of Cr(VI) into the PAC, leading to a lower level of Cr(VI) removal. Besides, the ratio of O/C on PAC, PAC-pH 3, and PAC-pH 7 were 0.075, 0.113, and 0.157, respectively (Table 2). This indicates more O on the PAC after adsorption at pH 7 than at pH 3, due to more Cr_2O_3 precipitate. As noted in Table 3-2, the ratio of Cr/C on PAC-pH 3 was higher than that on PAC-pH 7, which further substantiated that Cr(VI) removal efficiency under pH 3 was superior to that under pH 7 and indicated that not only there was Cr_2O_3 on the PAC surface but also Cr(VI).

Table 3-2 XPS analysis of PAC before and after treatment with Cr(VI)

Materials	O/C	Cr/C
PAC	0.075	0
PAC-pH 3	0.113	0.005
PAC-pH 7	0.157	0.004

The surface functional groups of PAC before and after Cr(VI) adsorption were investigated using high resolution C1s spectra. The deconvolution of C 1s produced four peaks, as shown in Fig. 3-3. For PAC, there were four components: C=C (284.8 eV), C-O-C/C-OH (285.5 eV), C-O (286.7 eV), and COOR (286.7 eV) (290.0 eV) [555]. Similarly, the four peaks of PAC-pH 3 were assigned to the C=C (284.8 eV), C-OH (285.8eV), C-O (286.5 eV), and COOR (288.7 eV) [556, 557]. Meanwhile, the four peaks for PAC-pH 7 were allocated to C=C (284.8 eV), C-OH (285.8eV), C-O (286.5 eV), and COOR (289.5 eV) [558]. The relative percentages of C-OH for PAC, PAC-pH 3, and PAC-pH 7 were 23.62%, 6.77%, and 6.53%, respectively, which suggested that the group of C-OH contributed to the removal of Cr(VI). The oxidation of C-OH to C-O by Cr(VI) caused the increase of the C-O group [460]. Nonetheless, following Cr(VI) adsorption at pH 3, the relative percentage of COOR on PAC rose from 15.22% to 20.56% and dropped to 10.41% after Cr(VI) adsorption at pH 7. This inconsistency may be due to Cr(VI) oxidized the surface of PAC at pH 3 and introduced more COOR groups [559], while the Cr(VI) exhibited weak oxidative capacity at higher pH [560], and the removal of Cr(VI) under pH 7 consumed the COOR groups through the complex.

3.3.1.3 Raman spectra analysis

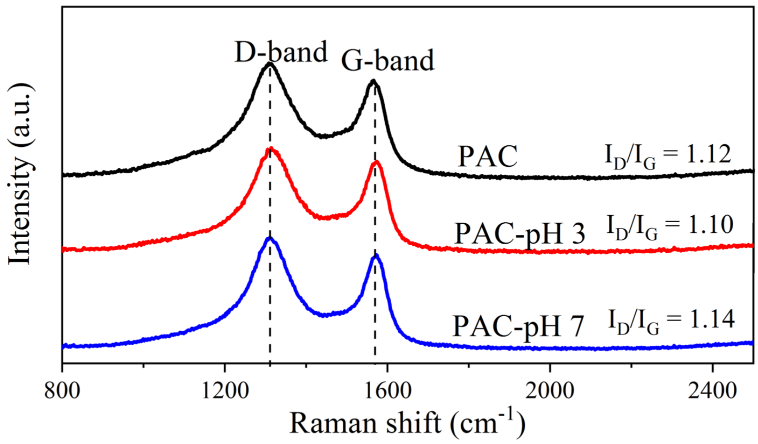

Figure. 3-4 Raman spectra investigation for pristine PAC, after removal of Cr(VI) at pH 3 and 7.

Raman spectroscopy investigation was carried out to evaluate the degree of structural order in carbonaceous PACs, as well as to investigate the difference in Cr(VI) removal mechanisms at pH 3 and pH 7. As depicted in Fig. 3-4, the two sharp and strong bands are associated with the D-band (1319cm^{-1}. defect with sp^3 bonding) and G-band (1563cm^{-1}, graphitization with sp^2 bonding) [488]. The intensity ratio of D-band (I_D) versus G-band (I_G) is often used to assess the degree of disorder in graphite structure in carbon materials [561]. The value of I_D/I_G declined from 1.12 to 1.10 after treatment at pH 3 but increased from 1.12 to 1.14 after treatment at pH 7. As a result, the existence of defects in PAC was strengthened under pH 7, while at pH 3, a well-organized carbon structure formed. This divergence could be explained by the different Cr(VI) adsorption mechanisms at pH 3 and 7. In general, the reduction of surface oxygen-containing functional groups resulted in the increase of amorphous carbon at pH 7 [490, 492, 562, 563], while the oxidation of hybridized carbon atoms caused structural order to grow at pH 3 [564].

3.3.2. Adsorption performance of PAC at pH 3 and 7

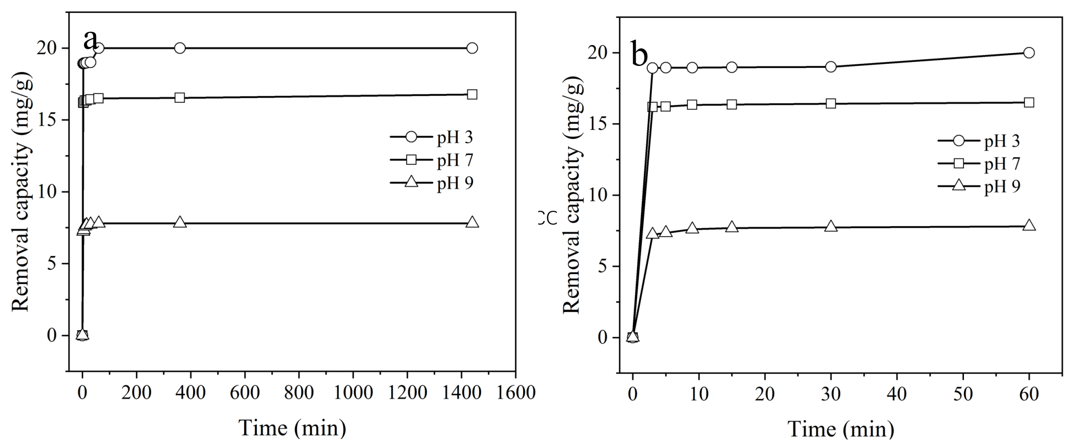

Figure. 3-5 The adsorption capacities comparison at pH 3, 7, and 9, (a) the full profile of adsorption, (b) the first 60 min adsorption profile (Initial concentration 1000 mg/L, 50g/L PAC, 295K)

Fig. 3-5 shows a comparison of adsorption performance at pH 3, 7, and 9 for 1000 mg/L initial concentration of Cr(VI). Adsorption at those three pH values both reached pseudo-equilibrium immediately after 10 mins. Removal capacities for PAC at pH 7 and 3 were 16.8 mg/g and 20 mg/g, respectively, equivalent to 83.86% and nearly 100% removal efficiency. And adsorption capacity under pH 9 was 7.8 mg/g which was much lower than that at pH 3 and 7. It indicated that the removal performance of PAC on

Cr(VI) was higher at low pH, PAC is probably protonated and attracted more anionic Cr(VI).

3.3.3. Desorption performance of Cr-loaded PAC with chemical agents

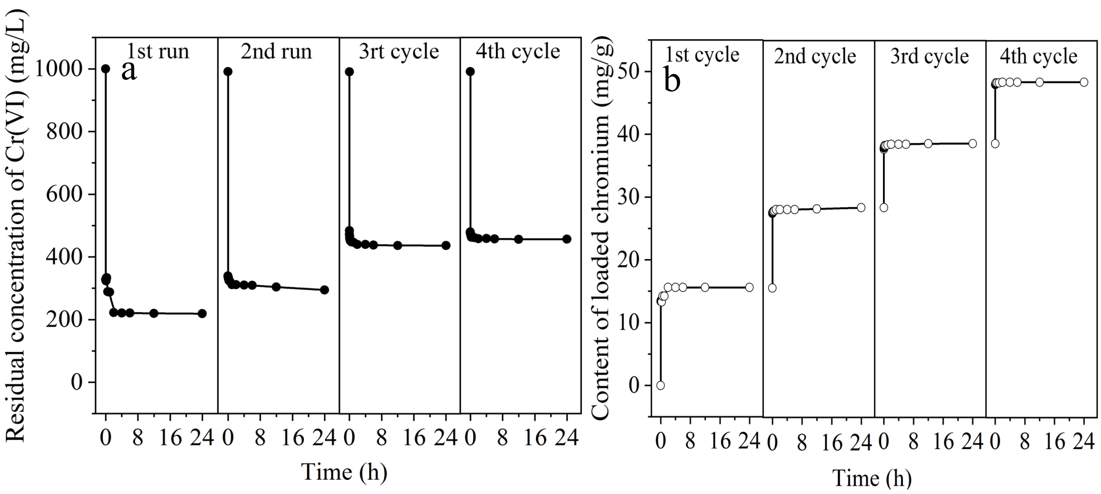

Figure. 3-6 The preparation of chromium-loaded PAC, (a) The residual concentration of Cr(VI) at each Cr(VI) adsorption cycle, (b) the content of loaded chromium as cycling (1000mg/L Cr(VI), 295K, 50g/L, pH 7)

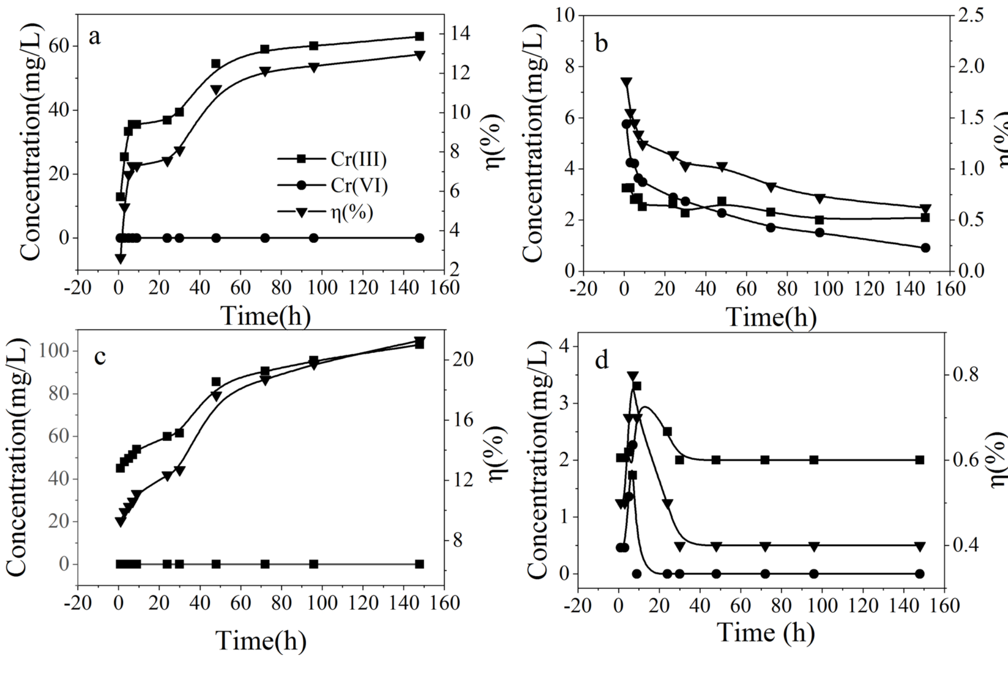

Figure. 3-7 The effect of chemical agents on desorption performance of Cr-loaded PAC (a) H_2SO_4 (b) KCl (c) NaOH (d) H_2O (0.2M KCl, 0.2M H_2SO_4, 0.1M NaOH, 1g/100mL Cr-loaded PAC, 298K)

The desorption of chromium from the Cr-loaded PAC was evaluated using various chemical agents including H_2SO_4, KCl, and NaOH. Abundant chromium-loaded PAC was prepared at pH 7. As shown in Fig. 3-6, the Cr(VI) elimination experiment using PAC was repeated four times. The duration time for every removal cycle was 24 hours. The next removal cycle began once the previous cycle was completed. After four consecutive repetitive adsorption cycles, the content of chromium on PAC reached 48.6mg/g. The results of the desorption analysis using the three reagents are shown in Fig. 3-7. It is noted that only Cr(III) was dissolved in H_2SO_4 aqueous solutions, whereas Cr(VI) was only desorbed in NaOH aqueous solutions. Negligible Cr(III) or Cr(VI) were detected in the KCl solution when compared to acidic and alkaline aqueous solutions. These findings agree well with Ouki and Neufeld's (1997) findings that 3 g/L Cr(III) and 8.4 g/L Cr(VI) were recovered when exhausted carbon was regenerated under acidic and alkaline conditions, respectively [565]. Due to the great stability of the adsorbed chromium on the PAC, desorption of Cr(VI) and Cr(III) from the Cr-loaded PAC with deionized water was minimal. Our results are also in line with those of Jing et al. (2011), who found that the desorption rate of Cr-loaded AC was low with distilled water [566].

As shown in Fig. 3-7(a), Cr(III) precipitate dissolved gradually in 0.2 M H_2SO_4, and 13.0 % Cr(III) precipitate was removed under acidic conditions, this process was depicted by Eq (3-5).

$$Cr_2O_3 + 6H^+ \rightarrow 2Cr^{3+} + 3H_2O \quad (3\text{-}5)$$

With the NaOH aqueous solution (Fig.3-7 (c)), 21.3 % Cr(VI) was desorbed, which was higher than the dissolved Cr(III) by the H_2SO_4 aqueous solution. This seems to contradict the XPS conclusion that less Cr(VI) adsorbed on PAC-pH 7 surface. A possible explanation for this might be that more internal adsorbed Cr(VI) in PAC particles were desorbed by alkaline elution. Cr(VI) adsorbed on AC was previously shown to be bound to the surface functional groups [567]. An ion-exchange mechanism could explain the desorption of adsorbed CrO_4^{2-} (the dominant chromium species under alkaline conditions) on surface functional groups by NaOH aqueous solutions, the OH^-

ions substitute for CrO_4^{2-} anions, as demonstrated in Eq (3-6) [568].

$$PAC\text{-}(COOH_2^{+})_2\cdots CrO_4^{2-}\ (s) + 2OH^{-} \rightarrow PAC\text{-}(COOH)\ (s) + CrO_4^{2-} + H_2O \quad (3\text{-}6)$$

These findings could be useful in the development of a selective recovery method of Cr(III) and Cr(VI) using acid and alkali aqueous solutions.

3.3.4. Formation process of chromium layer at pH 3 and 7

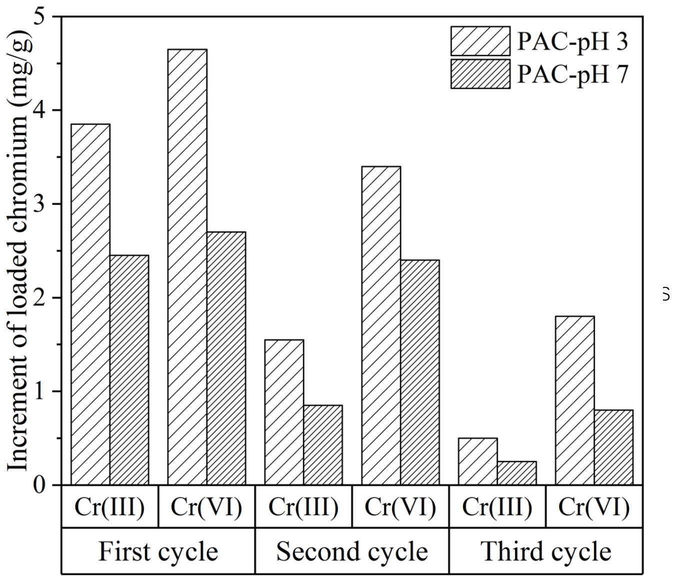

Figure. 3-8 The increment of chromium loaded on PAC as consecutive Cr(VI) removal cycle (295K, 50g/L)

To clarify the influence of pH on the development process of chromium layer on PAC, H_2SO_4, and NaOH desorption agents were used to determine the content of Cr(III) and Cr(VI) adsorbed on PAC-pH 3 and PAC-pH 7. Fig. 3-8 compares the results obtained from elution tests of PAC-pH 3 and PAC-pH 7 after three consecutive adsorption cycles. It is apparent from the figure that the increment of adsorbed Cr(VI) is higher than reduced Cr(III) at each cycle for both PAC-pH 3 and PAC-pH 7. Hence it is conceivable to suggest that the adsorption process prevailed for Cr(VI) elimination. This finding was also reported by Daneshvar et al. (2019) [568]. Another significant observation was that for PAC-pH 3 and PAC-pH 7, the adsorbed Cr(VI) and reduced Cr(III) decreased as the cycles progressed. PAC-pH 3 showed higher Cr(VI) adsorption and reduction capacity. This may be due to the more generated Cr(III) precipitate accumulating on the PAC surface over time at the neutral condition, sheltering the PAC active sites from Cr(VI adsorption.

3.3.5. Performance of Cr-loaded PAC after desorption

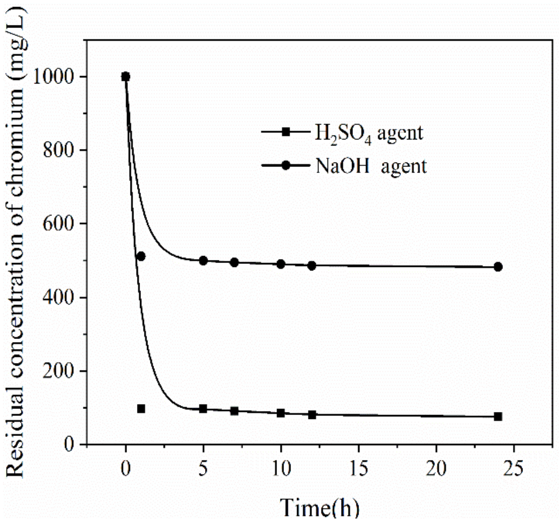

Figure. 3-9 The activity of chromium-loaded PAC-pH 7 after treated with H_2SO_4 and NaOH (1000mg/L Cr(VI), pH 7)

The performance of the PAC for Cr adsorption was assessed after chromium was desorbed from the PAC using the H_2SO_4 and NaOH. Re-adsorption experiments were conducted following the third cycle desorption step. As can be seen in Fig. 3-9, 92.43% removal efficiency of Cr(VI) was achieved by PAC-pH 7 after washing with H_2SO_4, whereas only 51.72% removal was attained using NaOH aqueous. Therefore, it can be inferred that the Cr(III) precipitate is mainly responsible for the poor performance of PAC under neutral conditions. The removal performance after acid washing (92.43%) was higher than the preliminary removal efficiency (83.86%); this result indicated that the acid desorption procedure modified PAC properties and introduced surface functional groups. These results are consistent with those of Guolin Huang et al. (2009), who improved AC's Cr(VI) removal capacity by modifying it with nitric acid [463]. As a result, it is proved that PAC's limited removal capability for Cr(VI) at pH 7 was mostly due to Cr(III) precipitate that formed on the surface of PAC. This finding backs with the XPS results in that chromium oxide piled up mostly on PAC under neutral conditions. The sulfuric acid proved to be a potential chemical agent for the regeneration of Cr-loaded PAC after treating water contaminated with Cr(VI).

3.4. Conclusions

This study aimed to determine the mechanism of the limited sequestration capability of PAC on Cr(VI) under neutral conditions compared to acidic conditions. SEM-EDX substantiated that a chromium layer was formed on PAC, while XPS spectra corroborated the higher Cr_2O_3 content on PAC under alkaline conditions, resulting in poor Cr(VI) removal performance. Conversely, a lower Cr_2O_3 content on PAC under acid conditions is related to the higher Cr(VI) removal capacity. Desorption tests with H_2SO_4 and NaOH solution revealed that the precipitated Cr_2O_3 and adsorbed Cr(VI) can be selectively desorbed, proving that adsorption and reduction processes contributed significantly to the Cr(VI) removal. Consecutive desorption assays proved that the reduction and adsorption capability at 7 declined with time and were both lower than at pH 3. This is due to Cr(III) precipitate and adsorbed Cr(VI) blocking active sites. The superior performance on Cr(VI) removal of Cr-loaded PAC after desorption by H_2SO_4 further confirmed that the restricted removal performance under neutral conditions was ascribed to the formation of Cr_2O_3 passivation layer on the surface of PAC particle. The insights gained from this work may be of assistance to the recycling of chromium from exhausted AC and extend the lifespan of AC.

Chapter IV. **Mechanochemical remove Cr(VI) with micro-Fe^0/Fe_2O_3 over a wide pH range**

4.1. Introduction

Hexavalent chromium (Cr(VI)) contamination in soil and aquatic environment has become a persisting social problem because toxic Cr(VI) (CrO_4^{2-} and $Cr_2O_7^{2-}$) would post serious threatens to human's health [569, 570]. And this kind of environmental risk would sustain for a good while since the characteristic of non-biodegradability and mobility [571]. Trivalent chromium (Cr(III)) shows less toxicity and could form sparingly soluble chromium oxide, so the strategy of reduction coupled precipitation seems feasible to eliminate Cr(VI). Meanwhile, much more emphasis has been placed on Cr(VI) reduction with various inorganic and organic reducing agents [59, 527, 572, 573]. It just come to the attention of researchers by the easily available and high performance of zerovalent iron (ZVI or Fe^0) on handling of heavy metals pollution [155, 303, 527]. While the readily atmospheric oxidation, rapid agglomeration, and quick passivation in aqueous severely restricted the reactivity and longevity of Fe^0 [574, 575]. Many effects, such as template-supported Fe^0 [576, 577], bimetallic Fe^0 particles [158, 578], sulfidated Fe^0 [360], and acid pretreatment [277] have been devoted to circumvent these disadvantages. Compared to pristine Fe^0, carboxymethyl (CMC)-embodied Fe^0 demonstrated higher dispersity, elevated stability, and increased Cr(VI) removal efficiency from 54% to 97% which was dominated with reductive removal [579]. Meanwhile, the lower initial pH favored Cr(VI) removal. Near 99.9 % Cr(VI) was eliminated by biochar-supported Fe^0 under pH 2 [580], whereas the surface formed passivation layer deactivated biochar-supported Fe^0 under higher pH and the removal efficiency was only 39.5% within 48 h [581]. Similarly, during the removal of Cr(VI), sulfur-modified Fe^0 by mechanical ball milling (BM) was quickly covered by a non-conductive layer under alkaline conditions, and the estimated electron efficiency of Fe^0 was less than 1% [582]. Cr(VI) sequestration by sulfur modified iron or carbon-supported iron material was confined to a pH range of 4 to 6, after which the removal capability decreased as pH increased [73, 248]. All the studies reviewed so far, however, suffer from the fact that the working pH must be kept at a narrow range to maintain the longevity and reactivity of Fe^0. It would be more practical to develop a strategy with Fe^0 to sequestrate Cr(VI) throughout a broad pH range as well as high reactivity and lifespan.

The emerging technology of mechanochemical procedure prepared iron composites exhibit satisfactory consequence on Cr(VI) removal [519]. Particles undergo propagate cracked, deformation, and disintegration during impact, and the mechanical energy partly stored in distorted lattice throughout the collision and extrusion of balls and particles which meditated the high reactivity surface of iron-based materials [583]. Nevertheless, once prepared iron composites by BM contacted with chromium solution, a passivation layer formed consequently and this defect still remain unresolved [584]. It's plausible that introduce chromium-containing effluent into the jar of BM with Fe^0 additive to sequestrate hazardous Cr(VI), the mechanical force could continuously flake the oxides layer adhered on additive and hence exposed the fresh Fe^0 to Cr(VI) solution, and the redox reaction between Fe^0 and targeted Cr(VI) ignited immediately.

In this study, to study the feasibility of BM on eradicate the surface passivation layer of Fe^0 on contaminants removal over a wide pH range. Surface oxidized micro-sponge iron powder (micro-Fe^0/Fe_2O_3) as Fe^0 precursor milled with high concentration Cr(VI) solution in planetary ball milling under different conditions with controlled DO, the removal route of Cr(VI) under different milling atmosphere was investigated specifically. The effect of milling parameters like rotated speed of milling jar, aqueous solution pH, dosage of micro-Fe^0/Fe_2O_3, milling atmosphere, initial concentration of Cr(VI) on removal performance were inspected.

4.2. Experiments

4.2.1. Materials and regents

Micro-Fe^0/Fe_2O_3 particles as Fe^0 precursor which obtained from Mexico mine and refined to 28.3 μm by BM. Potassium dichromate was purchased from J.T Baker and prepared for 1000 mg/L Cr(VI) stock solution with deionized water. 1,10-phenathroline

(1,10-phen) and 1,5-diphenylcarbohydrazide were acquired from Sigma-Aldrich. Glacial acetic acid (HAc), sodium acetate anhydrous (NaAc), hydrochloride acid (HCl), sulfuric acid (H_2SO_4), phosphoric acid (H_3PO_4), acetone and ferrous ammonium sulfate hexahydrate ($(NH_4)_2Fe(SO_4)_2{\cdot}6H_2O$) were purchased from J.T Baker. All chemical reagents were analytical grade. High purity nitrogen gas and oxygen gas were used to adjust the milling atmosphere of chromium solution, and the flow rate of aeration was fixed at 20 cm^3/min. The volume of stainless-steel milling jar is 400 ml and outfitted with two upper valves to evacuate and purge gas, the mass of steel balls as milling medium is 200 g and the diameters are 20, 10 and 5 mm, respectively, wherein the mass ratio is 1:2:7. Six bolts and rubber gasket were attached to keep the airtight of milling jar during operation.

4.2.2. Removal of Cr(VI) by micro-Fe^0/Fe_2O_3 with BM

Milling jar filled with Cr(VI) solution was purged with nitrogen or oxygen gas to adjust the dissolved oxygen (DO), and then subjected to programed planetary ball milling (Fritsch, Pulverisette 6, Germany) with settled speed and direction. Some experiments were performed under unbuffered solution with initial pH of 4 and 7, and the rest were buffered with HAc/NaAc solution of pH 4. To investigate the effect of rotation speed, dose of Micro-Fe0/Fe_2O_3, initial Cr(VI) concentration and milling atmosphere on chromium removal performance, rotation speed was fixed at 150,350, 550 rpm, micro-Fe^0/Fe_2O_3 dose was controlled at 0, 0.05, 0.1, 0.2, 0.4, 0.6, 0.8, 1.0 g, initial concentration of Cr(VI) was prepared at 100, 200, 400, 600, 800, 1000 mg/L, milling atmosphere of chromium solution (DO were fixed at 12.8, 3.2 and 1.9 mg/L), the pH of experiments were unbuffered with initial value adjusted to 7. All these experiments were conducted with duplicate and performed under ambient environmental if not specially stated, and an aliquot of sample (2mL) was withdrawn at an interval of 30 min, centrifuged at 8000 rpm for 10 min (Beckman coulter, USA) prior to the immediate analysis of aqueous chromium and iron. During the removal of Cr(VI) by micro-Fe^0/Fe_2O_3, iron in the steel jar and milling balls would dissolve inadvertently as a consequence of mechanical impact, raising the ferrous and ferric ion concentrations. To account for this issue, a blank BM experiment in the absence of micro-Fe^0/Fe_2O_3 was performed in advance.

4.2.3. Analytical method

The concentration of total Fe and Fe^{2+} was analyzed through flame atomic adsorption spectrometric (FAAS) and spectrophotometric method with 1,10-phen as indictor by UV/Vis spectrophotometer (Thermo scientific, USA) under 510 nm. 1,5-diphenylcarbazide as indictor for the determination of Cr(VI) by spectrophotometric method under 540 nm, total concentration of aqueous Cr was determined by FAAS and the difference of total Cr and Cr(VI) was aqueous Cr(III). The DO, pH and oxidation-reduction potential (ORP) were monitored respectively by dissolved oxygen meter (Starter 300D, OHRUS, model of electrode is STD011), pH meter (Orion 4 star, Thermo scientific) and ORP meter (Oakton, 10N 700).

4.2.4. Characterization of liquid and solid phase

The precipitate of ground Cr(VI) solution with micro-Fe^0/Fe_2O_3 was analyzed by Raman spectra (DXR, Thermo scientific, USA), the size distribution of ball milled micro-Fe^0/Fe_2O_3 in Cr(VI) solution was investigated by laser particle size analyzer (BT-9300S, China), scanning electron microscopy-energy dispersive X-ray spectroscopy (SEM-EDS) (JSM-6610LV, JEOL) coupled with elements mapping was employed to observe the transformation of surface morphologies of material particles and the chromium distribution. The Cr and Fe species on the surface of particles before and after ball milling for 1 hour and 2 hours were characterized by X-ray photoelectron spectroscopy (XPS) (K Alpha, Thermo Scientific, USA), XPS investigation was conducted with Al K alpha radiation. The binding energies of samples were calibrated to the C 1s peak at binding energy of 284.8 eV, the survey scans and the high resolution scans were performed at an energy step of 1.0 eV and 0.1 eV with the pass energy of 100 eV and 50 eV, respectively.

4.3. Results and discussion

4.3.1. Effect of BM on Cr(VI) sequestration

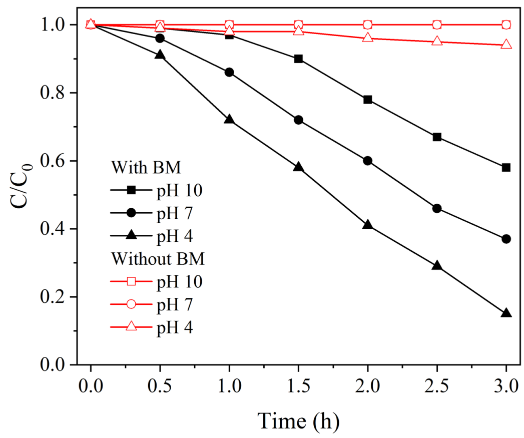

Figure. 4-1 Performance of micro-Fe^0/Fe_2O_3 on Cr(VI) sequestration under different pH with or without BM (non-buffer solution, 0.4g micro-Fe^0/Fe_2O_3/100ml, C_0=1000mg/L Cr(VI), 350 rpm if ground).

As shown in Fig. 4-1, no observed concentration decline of Cr(VI) and negligible decrease of Cr(VI) in absence of BM under pH 10, 7, and 4, respectively. Meanwhile, the performances of micro-Fe^0/Fe_2O_3 under pH 10, 7, and 4 were enhanced significantly with BM. This discrepancy could be attributed to the surface covered Fe_2O_3 on Fe^0 has been peeled off by the abrasive motion of iron balls and the fresh surface of core Fe^0 exposed to Cr(VI), therefore, the capability of micro-Fe^0/Fe_2O_3 on Cr(VI) removal increased substantially. It is apparent from this figure that the removal of Cr(VI) by micro-Fe^0/Fe_2O_3 with BM was pH-independent under non-buffer solution. However, the findings of the current study do not support the previous research that the lower pH value initiated the higher Cr(VI) removal efficiency by ZVI or sulfur modified ZVI [585, 586]. The solution pH values throughout the BM was monitored and we found that the pH increased immediately near 10 after 30 mins and were fully independent from various conditions such as initial pH, DO, and rotation speed, seen in Figure S1. It can be inferred that the action of BM invalidated the effect of pH under non-buffer solution by drastically elevating the pH immediately.

4.3.2. Characterization of pristine and used micro-Fe^0/Fe_2O_3 particles

4.3.2.1. Surface morphology

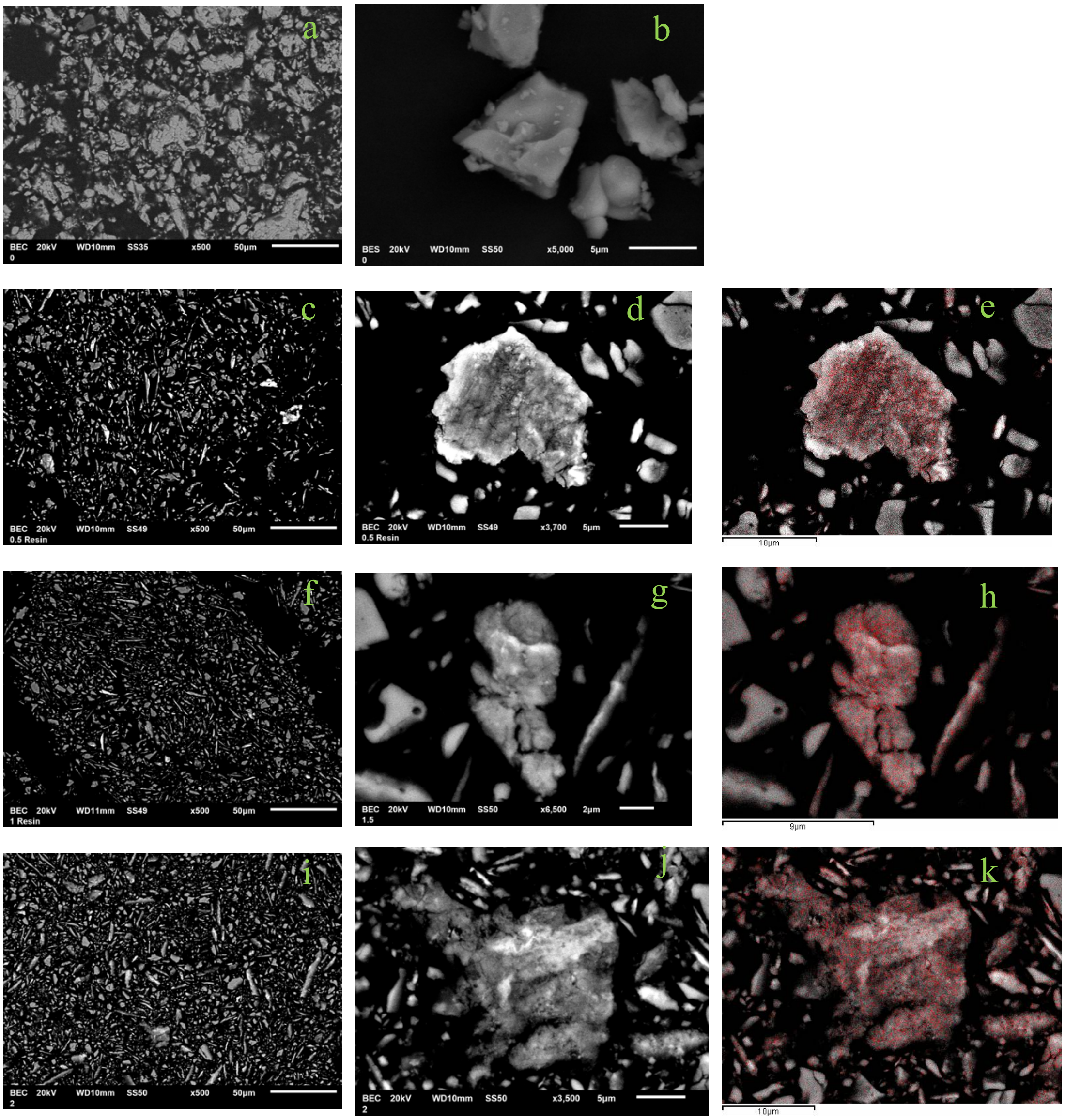

Figure. 4-2 SEM images and element mappings of Cr on micro-Fe^0/Fe_2O_3 particles after grinding with Cr(VI) solution

(0 h (a-b), 0.5 h (c-e), 1.0 h (f-h), and 2 h (i-k). Reaction conditions: micro-Fe^0/Fe_2O_3 = 0.4 g, $Cr(VI)_{initial}$ = 1000 mg/L, unbuffered solution of pH 7, rotation velocity = 350 rpm, T = 22℃, DO = 3.2 mg/L.)

The surface characterization of pristine micro-Fe^0/Fe_2O_3 shows irregular shapes (Fig.4-2 (a-b)), while the produced needle-sharped particles gradually dominants after milling 0.5 h and 1.0 h (Fig.2 c and f), then radically dwindled after 2 h (Fig. 4-2 i). Meanwhile, the particles size diminished as duration (Fig. 4-2 a, c, f, and i) which is consistent with the results of particle size analysis (Fig. S2). It should be noted that the roughness of the particles surface enhanced as milling (Fig. 4-2 b, d, g and j), the corrosion of micro-Fe^0/Fe_2O_3 towards Cr(VI) solution may contribute to this occurrence. To investigate the distribution of eliminated Cr on micro-Fe^0/Fe_2O_3 particles, element mappings of Cr were performed after 0.5 h, 1 h, and 2 h, as seen at Fig. 4-2 e, h, and k, respectively. The surface precipitated Cr accumulated as time and in tune with the declined Cr(VI) concentration of grinding solution.

4.3.2.2. Raman spectra

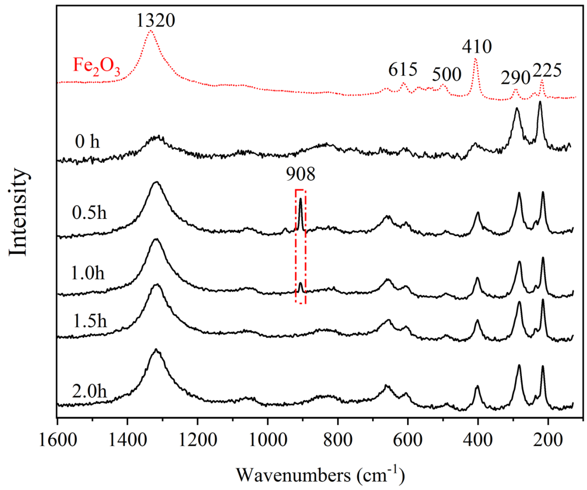

Figure. 4-3 Raman spectra of Fe^0/Fe_2O_3 after contact with Cr(VI) under BM. Reaction conditions: micro-Fe^0/Fe_2O_3 = 0.4 g, $Cr(VI)_{initial}$ = 1000 mg/L, unbuffered solution of pH 7, rotation velocity = 350 rpm, T = 22℃, DO = 3.2 mg/L.

Fig. 4-3 compares the measurement results of *in situ* Raman spectroscopy of micro-Fe^0/Fe_2O_3 after contact with Cr(VI) throughout BM. The vibrational modes at 1320, 615, 500, 410, 290 and 225 cm^{-1} of the α-Fe_2O_3 were remained in ground micro-Fe^0/Fe_2O_3 crystalline phase [587], whereas the bandwidth of those characteristic peaks increased throughout BM. This observation suggested that the modification of material structure that the decrease in particle size, similarly, prior study showed that the bandwidth of those peaks of γ- Fe_2O_3 decreased with particles size increase as the heated temperature increased [588, 589]. Appeared vibrational band of 908 cm^{-1} after 0.5 and 1.0 h is associated with dichromate and bichromate signals [590], and this band disappeared after 1.5 h which validated the removal of Cr(VI).

4.3.2.3. XPS spectra

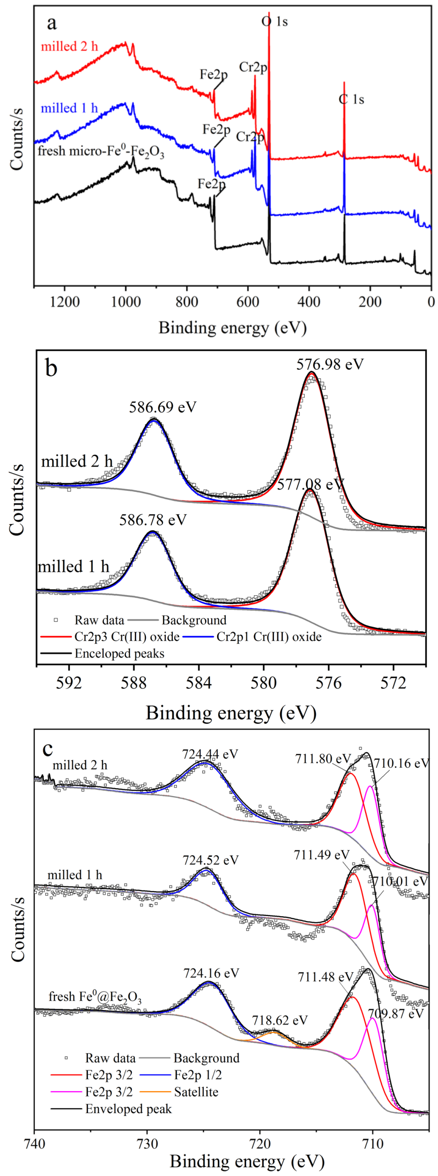

Figure. 4-4 The XPS spectra of micro-Fe^0/Fe_2O_3 particle before and after grinding with Cr(VI) solution. (a) survey scans, (b) high resolution scans of Cr 2p, and (c) high resolution scans of Fe 2p. Reaction conditions: micro-Fe^0/Fe_2O_3 = 0.4 g, $Cr(VI)_{initial}$ = 1000 mg/L, unbuffered solution of pH 7, rotation velocity = 350 rpm, T = 22℃, DO = 3.2 mg/L.

XPS spectra was used to qualitatively and half-quantitatively determine the surface composites of micro-Fe^0/Fe_2O_3 particles. A typical broad peak of Cr 2p was detected after grinding for 1 h and 2 h (Fig. 4-4 a), and the photoelectron line of Cr 2p were deconvoluted into Cr $2p_{1/2}$ and Cr $2p_{3/2}$ two peaks that indicated individual components

(Fig.4-4 b). According to Moulder et al. [591], Cr(III) oxides occur at binding energy range of ~ 576.4 to ~ 579.6 eV, the characteristics peaks of Cr(III) oxides were found at 577.08 and 576.98 eV after milling 1 and 2 h, respectively. The binding energies at 586.78 and 586.69 eV of Cr $2p_{1/2}$ peak for milled 1 and 2 h particles are both in good agreement with the characteristics of Cr(III) hydroxide [260], which denoted the reduction of Cr(VI) to Cr(III) was the prevailing elimination process by micro-Fe^0/Fe_2O_3. Meanwhile, the increased atomic ratio of Cr/Fe from 1.6 to 2.0 within 1 h substantiated the effective Cr(VI) removal.

The splitting of photoelectron line of Fe 2p of those three materials into Fe $2p_{1/2}$ and Fe $2p_{3/2}$ two peaks, the binding energies of the splitted peaks were marked on the Fig. 4-4c. A small satellite peak at 718.62 eV of untreated material is observable above the main peak of Fe $2p_{3/2}$ for approximate 8 eV, which assigned to the Fe in Fe_2O_3 [592]. Fe $2p_{1/2,3/2}$ shifted to higher energies and the satellite peak disappeared after 1 and 2 h ball milling (Fig. 3c), these results were consistent with the XPS analysis of α-Fe_2O_3 when it was exposed to a small amount of oxygen or water vapor [593]. A review previous works [594, 595], the binding energies of the shoulder Fe $2p_{1/2}$ peaks were both the characteristic of Fe in Fe_2O_3. The principal peak at 711.48, 711.49, and 711.80 eV can be attributed to the Fe in Fe_2O_3 [596, 597]. The Fe in FeO at binding energies of 709.87, 710.01, and 710.16 eV in the main Fe $2p_{3/2}$ peak were both detected in the materials before and after ball milling [598]. It's suggested that the surface of pristine material coated with a layer of ferric/ferrous oxides. Besides, the computed area ratio of FeO peak decreased slightly as milling, indicating that the Fe(II)(s) in FeO did not participated in the reduction of Cr(VI). Meanwhile, the dominant component of Fe_2O_3 obtained from XPS analysis corroborates the results of Raman studies that the characteristics peaks of Fe_2O_3 obviously remains before and after ball milling.

The removal of Cr(VI) under neutral and acidic conditions were presented as Eqs (4-1)-(4-2) and (4-3)-(4-5), respectively [599-601].

$$Fe^0 + CrO_4^{2-} + 4H_2O = Fe(OH)_3 + Cr(OH)_3 + 2OH^- \quad (4\text{-}1)$$

$$xFe(OH)_3 + (1-x)Cr(OH)_3 = (Fe_xCr_{1-x})(OH)_3 \quad (4\text{-}2)$$

$Fe^0 + 2HCrO_4^- + 14H^+ = 3Fe^{2+} + 2Cr^{3+} + 8H_2O$ (4-3)

$3Fe^{2+} + HCrO_4^- + 7H^+ = 3Fe^{3+} + Cr^{3+} + 4H_2O$ (4-4)

$Fe^0 + HCrO_4^- + 7H^+ = Fe^{3+} + Cr^{3+} + 4H_2O$ (4-5)

Given that the atomic ratio of Cr/Fe is 2.0 after milling for 2 h, the ending product of Cr and Fe here is expected to have the chemical formula of $Fe_xCr_{1-x}(OH)_3$ where x is predictably about 0.33. Previous work conducted with nanoscale zerovalent iron to remediate Cr(VI) aqueous solution reported the same formula of the mixture precipitate of Cr and Fe [116].

4.3.3. Effect of DO

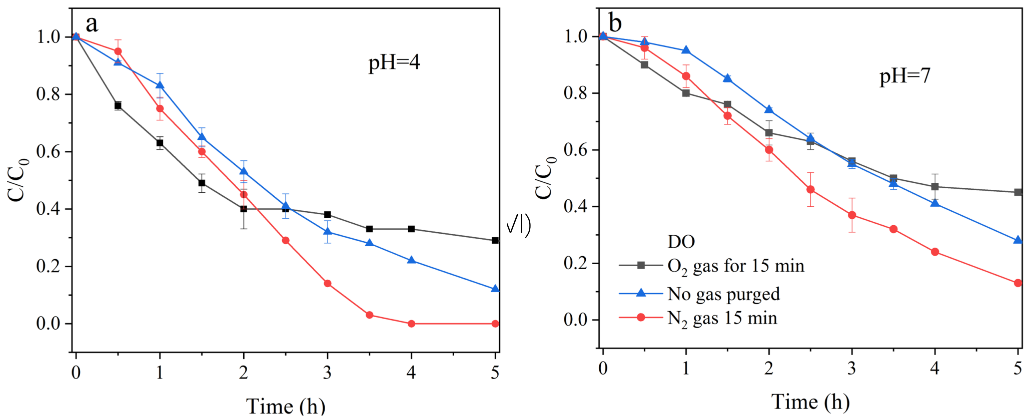

Figure.4-5 The effect of DO on Cr(VI) removal under different non-buffer solution (a) pH 4 (b) pH 7

To determine the effect of milling atmosphere on Cr(VI) removal under different pH, as shown in Fig. 4-5, the removal of Cr(VI) can be divided into two segments under different DO at pH 4 and 7. The removal performances were both increased obviously after purging with O_2 gas for 15 min before 2 and 1.5 hours under pH 4 and 7, respectively. This result supports evidence from previous observations that performance of Cr(VI) sequestration by ZVI was higher under oxic conditions with respect to anoxic conditions [236]. Prior work hold the view that DO fascinated the generation of Fe(II) ions which directly participated the reduction of Cr(VI) at acid solution, and the removal rate of Cr(VI) is coincided with the evolution rate of Fe^{2+} in absence of Cr(VI) solution [250]. However, the removal rate increased as the decrease of DO after 2 and 0.5 as seen in Fig. 4-5 a and b. Meanwhile, the divergence of Cr(VI) removal under different DO enhanced gradually at second segment. Denoting that the O_2 molecules partially consumed the electrons from Fe^0 and diminished the removal rate of Cr(VI). This finding was also reported by Lee et al. [602]. Potential reductants for Cr(VI) in the reaction system other than Fe^0 include Fe^{2+}, considering the Fe^{2+} could be readily oxidized under alkaline condition by DO [251]. Previous work conducted by Lin et al. (1998) also revealed that the reduction of Cr(VI) by Fe^{2+} was greatly suppressed under alkalic conditions in presence of oxygen [603]. This effect discrepancy of DO on Cr(VI) removal might be that the produced Fe^{2+} was unstable and easily oxidized as the solution pH increased throughout the BM. The pH expeditiously increased near 12 after 2.0 and 0.5 hour at pH 4 and 7, respectively (Figure S2), thus the DO gradually weaken the performance of Fe^0 as the increase of solution DO under alkaline conditions. It suggests that anoxic atmosphere has greatly accelerated reduction performance of iron on Cr(VI) under alkalic conditions.

4.3.4. Influencing factors of Cr(VI) removal

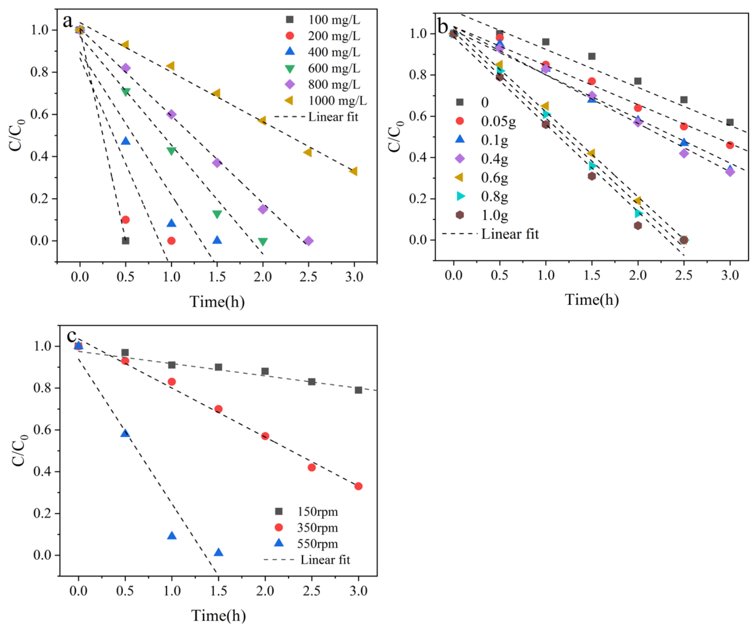

Figure 4-6 C/C_0 as function of time and liner fit of zero-order kinetic model under neutral conditions. (a) initial concentration, (b) dose, (c) rotation speed, (d) DO.

C/C_0 as a function of duration time under different conditions were shown in Fig. 4-6, wherein the C and C_0 (mg/L) were Cr(VI) concentration at time t and 0, respectively. It was found that the experimental data could be fitted adequately with zero-order kinetic model. It presumably ascribed to BM can alleviate the negative effect of iron/chromium (hydro)oxides layer on iron particle surface by abrasive motion of iron balls, meanwhile iron particle uninterruptedly preserved fresh surface and react directly with Cr(VI), which has been supported by the vigorously diminished particle size of micro-Fe^0/Fe_2O_3 that dropped from 28.3 to 3.9 μm within 30 mins (Figure S2).

The zero-order kinetic equation was presented as Eq (4-8), where k_{obs} ($g{\cdot}L^{-1}{\cdot}h^{-1}$) is rate constant and t (h) is time. As illustrated in Table S1, removal rate constants presented partially poor dependence on initial concentration of Cr(VI) below 200 mg/L and above 400 mg/L while increased as initial concentration, and consistent with previous reports that the higher Cr(VI) concentration left the higher removal rate [160, 260, 580]. These results provide further support for the hypothesis that the grinding action continuously uncovered the core iron to relatively deficient aqueous Cr(VI) that compelled the reaction rate independent on low initial concentration, but the comparatively adequate Cr(VI) under high concentration made the removal rate dependent on accessible active sites on iron.

$$\frac{C}{C_0} = 1 - \frac{kt}{C_0} \qquad (4\text{-}8)$$

Attention should be paid that considerably declined of Cr(VI) was been noticed within 6 hours even ground without micro-Fe^0/Fe_2O_3. Additionally, the removal rate increased 2.3 times in presence of 1.0 g micro-Fe^0/Fe_2O_3, admittedly stainless steel jar and iron balls played vital role in Cr(VI) removal. Comparison of Cr(VI) removal under different milling speed indicted that removal rate significantly affected by impact frequency, it is apparent from Table S1 that removal rate under 550 rpm was near an order magnitude higher than that at 150 rpm. In summary, there was a significant positive correlation between collision energy and removal rate.

4.4 Conclusions

Zerovalent iron (Fe^0/ZVI) has versatile properties on contaminated water remediation. However, the surface formed passivation layer restricts its reactivity under alkaline conditions. Here, we show that the inactivation of Fe^0 at high pH can be substantially mitigated by mechanical ball milling. The toxic Cr(VI) was been effectively eliminated over a wide pH of 4-10, while the negligible removal efficiency was noted in absence of ball milling. XPS demonstrated that the removal of Cr(VI) was dominantly contributed by reduction and precipitation. While the performance of Fe^0 significantly decreased as the increase of dissolved oxygen (DO) from 1.9 to 12.8 mg/L over a long time period, but the removal profile at first 2 hours indicated that the higher DO favored the faster removal of Cr(VI). This discrepancy attributed to that DO advanced the generation of Fe(II) that participated in the reduction of Cr(VI) under acidic conditions while the Fe(II) would be oxidized as pH increased throughout the ball milling action. Zero-order kinetic model was adequately fitted the elimination of Cr(VI) under different rotation speed, initial concentration, and dosage over time. This study demonstrates that the mechanical ball milling is a promising approach on quick sequestration of Cr(VI) by Fe^0-containing materials under anoxic conditions.

Supplement materials

Table S1 Zero-order kinetic parameters of Cr(VI) removal under different conditions

	Initial concentration (mg/L)						Dose (g)						
	100	200	400	600	800	1000	0	0.05	0.1	0.4	0.6	0.8	1.0
Correlation efficiency	1	0.824	0.917	0.986	0.997	0.991	0.985	0.997	0.993	0.991	0.996	0.994	0.985
k ($g \cdot L^{-1} \cdot h^{-1}$)	0.2	0.2	0.31	0.31	0.33	0.34	0.18	0.19	0.21	0.34	0.41	0.42	0.42
	Rotational speed (rpm)						DO (mg/L)						
	150	350	550					12.8	3.2	1.9			
Correlation efficiency	0.993	0.991	0.937					0.961	0.991	0.920			
k ($g \cdot L^{-1} \cdot h^{-1}$)	0.06	0.34	0.69					0.09	0.34	0.45			

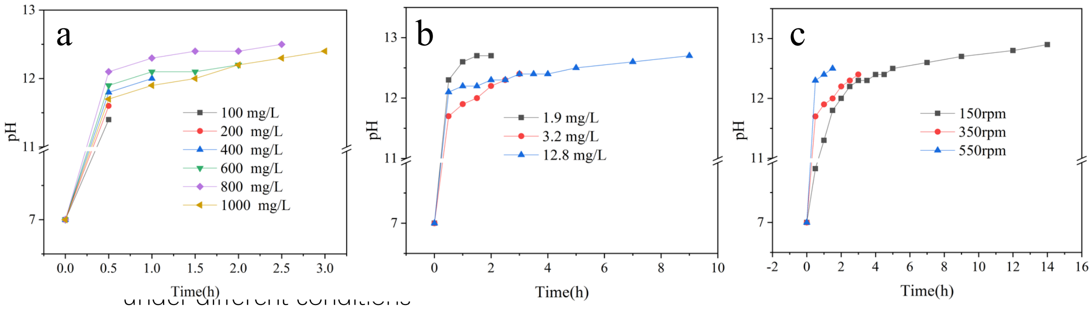

Figure. S1 The pH evolution under different conditions. (a) initial concentration, (b) DO, (c) Rotational speed

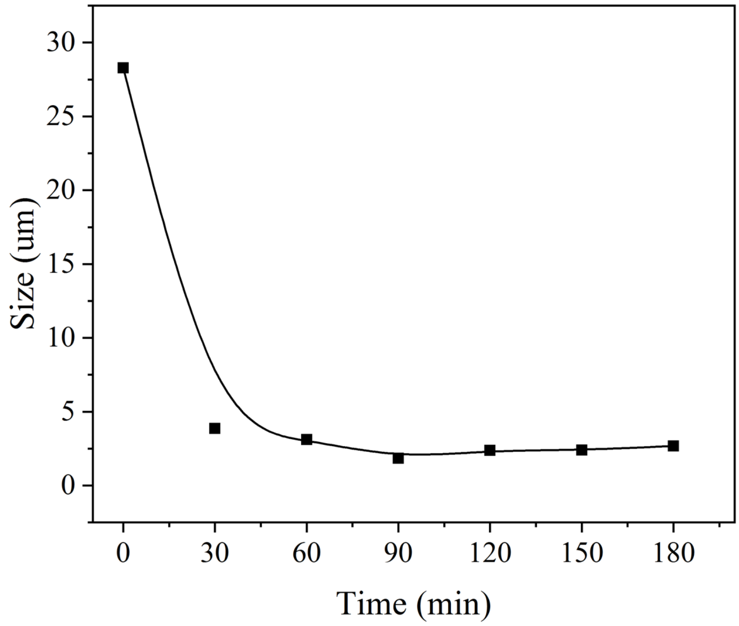

Figure. S2 The particle size (D_{80}) development of Fe^0/Fe_2O_3 as BM

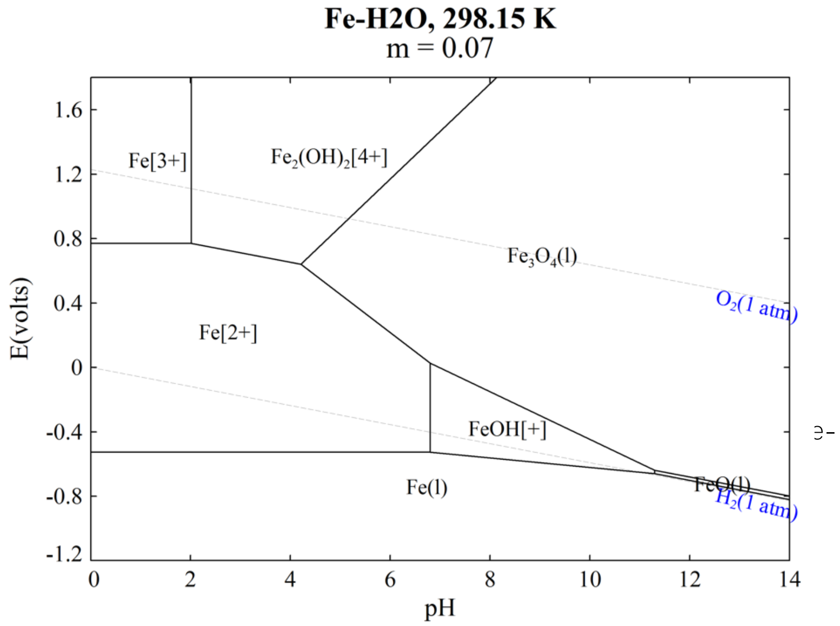

Figure. S3 The Eh-pH (Pourbaix) diagram of Fe-H_2O system build by software FactSage (Education edition)

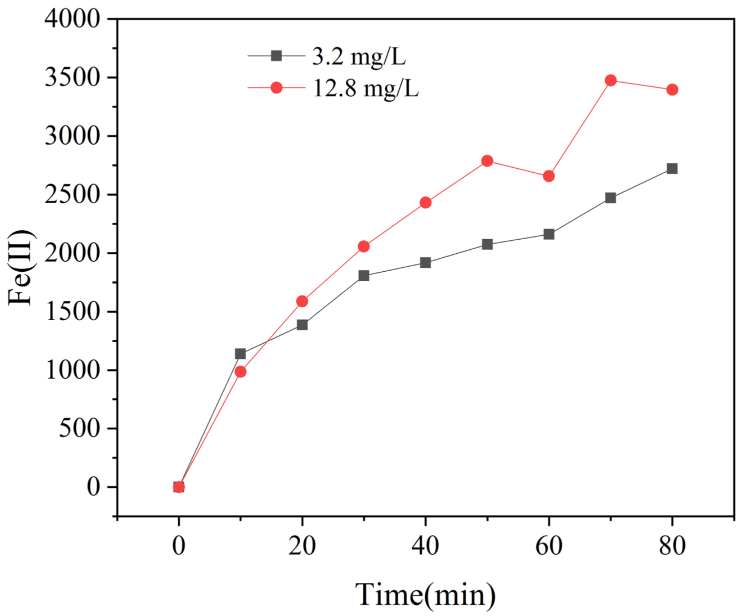

Figure. S4 The generation of Fe(II) without Cr(VI) under buffer solution of pH 4 (DO = 3.2/12.8 mg/L, rotational speed = 350 rpm, dose of Fe/Fe_2O_3 = 0.4g)

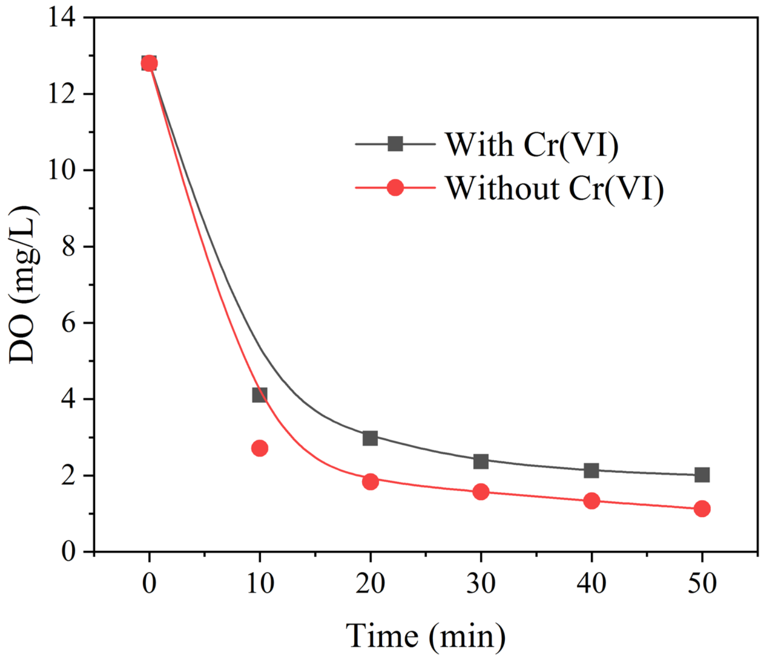

Figure. S5 The DO depletion as time with/without Cr(VI) (initial DO=12.8 mg/L, rotation speed = 350 rpm, dose of Fe/Fe_2O_3 = 0.4g, Cr(VI) concentration = 1000mg/L if added)

Chapter V. **Conclusions**

The pronounced results of the Cr(VI) reduction and precipitation by modified activated carbon proved that the action of ball milling can refine the activated carbon particles and improve the surface area, meanwhile, the enriched surface functional groups accompanied the enhanced hydrophilicity took responsibility for the advanced Cr(VI) removal at neutral and alkaline conditions. The generated Cr(III) precipitated on the surface of activated carbon particles, the elution experiments and re-adsorption test proved that the surface Cr(III) oxides layer caused the low Cr(VI) removal efficiency at higher pH than that at low pH. Moreover, the reduction and adsorption process both declined as time. The activated carbon after treating with Cr(VI) could be rejuvenated by acidic washing and the capacity maintained satisfactory even after three times repetitive Cr(VI) treatment.

The inactivation of Fe^0 at high pH due to the passivation could be solved by the motion of ball milling, the surface formed Fe(III)/Cr(III) (hydro)oxides were peeled off and the fresh core Fe^0 exposed to the Cr(VI) aqueous. The Cr(VI) removal experiments conducted under different DO indicated that the anaerobic conditions mitigated the consumption of Fe^0 by competitive oxidant O^2 and the removal rate was the highest. The DO improve the depletion rate of Cr(VI) at the first segment through the generated Fe(II) by DO, but the Fe(II) ions were further oxidized by DO as pH increased and the removal rate decreased significantly. The analysis of XPS spectra denoted that reduction and precipitation dominant the elimination of Cr(VI) by Fe^0/Fe_2O_3 micro particles.

Appendix

Published Papers during Ph.D

1. **Fang Y**, Wu X, Dai M, et al. The sequestration of aqueous Cr (VI) by zero valent iron-based materials: From synthesis to practical application[J]. Journal of Cleaner Production, 2021: 127678. (Q1, IF 9.297) https://doi.org/10.1016/j.jclepro.2021.127678
2. **Fang Y**, Yang K, Zhang Y, et al. Highly surface activated carbon to remove Cr (VI) from aqueous solution with adsorbent recycling[J]. Environmental Research, 2021, 197: 111151. (Q1, IF 6.498) https://doi.org/10.1016/j.envres.2021.111151
3. **Fang Y**, Yang K, Zhang Y, et al. A new insight into the restriction of Cr (VI) removalperformance of activated carbon under neutral pH condition[J]. Water Science and Technology, 2021. (Q2, IF 1.915) https://doi.org/10.2166/wst.2021.449
4. **Fang Y**, Peng C, Yang K, et al. Adsorptive removal of cationic toxic dyes from aqueous solution: adsorbents development and performance investigation[j]. Fresenius Environmental Bulletin, 2020, 29(7 A): 6072-6081. (Q4, IF 0.489)

Journal of Cleaner Production 312 (2021) 127678

Contents lists available at ScienceDirect

Journal of Cleaner Production

journal homepage: www.elsevier.com/locate/jclepro

The sequestration of aqueous Cr(VI) by zero valent iron-based materials: From synthesis to practical application

Yi Fang [a,b], Xiange Wu [a], Min Dai [a,**], A. Lopez-Valdivieso [b], Saleem Raza [c], Imran Ali [c,d,***], Changsheng Peng [a,d,*], Juying Li [c], Iffat Naz [e,****]

[a] Guangdong Provincial Key Laboratory of Environmental Health and Land Resource, Zhaoqing University, Zhaoqing, 526061, China

[b] Instituto de Metalurgia, Universidad Autónoma de San Luis Potosí, San Luis Potosí, C. P., 78210, Mexico

[c] Department of Environmental Science and Engineering, College of Chemistry and Environmental Engineering, Shenzhen University, Shenzhen, 518060, China

[d] The Key Lab of Marine Environmental Science and Ecology, Ministry of Education, Ocean University of China, Qingdao, 266100, China

[e] Science Unit, Deanship of Educational Services, Qassim University, Buraidah, 51452, Saudi Arabia

A R T I C L E I N F O

Handling editor: Prof. Jiri Jaromir Klemeš

Keywords:
Zero-valent iron (ZVI)-based materials
Fabrication
Hexavalent chromium (Cr (VI))
Removal mechanism
Field implementation
Dissolved oxygen

A B S T R A C T

In recent years, zero-valent iron (ZVI) has been extensively employed for the elimination of organic and inorganic contaminants. However, the performance of ZVI was restrained due to the inherent properties in the process of pollutants sequestration like agglomeration, surface passivation, and sensitivity to the pH and dissolved oxygen (DO) in the environment. To combat these issues, ZVI-based materials were utilized to attenuate the drawbacks of ZVI. Therefore, in this review, the representative hazardous hexavalent chromium (Cr(VI)) was chosen as the target pollutant to discuss the performance, limitations, and future of ZVI-based materials. The prevailing preparation methods of ZVI-based materials could be classified into aqueous reduction and mechanical procedures. Further, the conventional ZVI-based materials were mainly encompassed carbon-ZVI, sulfur-ZVI, bimetallic materials of ZVI, and magnetite-ZVI composites. A new insight into the co-effect of pH and DO on Cr(VI) removal by ZVI through five pathways was also proposed. The mechanism of Cr(VI) elimination by ZVI-based materials was dominant through the combination of reduction, adsorption, and co-precipitation, wherein the enhanced reduction capability of ZVI-based materials compared to their monometallic counterpart was critically scrutinized. Besides, some field applications of ZVI-based materials such as ZVI incorporation into the permeable reactive barrier (PRB) to remediate groundwater have also been examined. Finally, barriers in market penetration of ZVI-based materials in removing Cr(VI) have been highlighted which would open a new window for the researcher to accomplish the research gaps for shifting applications of ZVI-based materials from lab-scale to real or commercial implementations.

1. Introduction

Chromium (Cr) has a wide range of industrial applications such as plating, alloying, leather tanning, metallurgy, textile dyes, and pigments. Thus, Cr-contamination has become a big issue and has attracted the attention of experts to eliminate Cr by employing various kinds of materials like activated carbon (Al-Othman et al., 2012; Fang et al., 2021), alkalic modified activated carbon (Norouzi et al., 2018), green synthesized zero-valent iron (Bavasso et al., 2018; Fazlzadeh et al., 2017; Vilardi et al., 2018b) and well-designed nanocarbon spheres (Zhou et al., 2018). Cr mainly occurs in two different states in nature such as hexavalent chromium (Cr(VI)) and trivalent chromium (Cr(III)). Cr(VI) has mutagenic and carcinogenic effects in humans because of its higher mobile and toxic behavior. It can cause severe diseases such as

* Corresponding author.
** Corresponding author.
*** Corresponding author. Department of Environmental Science and Engineering, College of Chemistry and Environmental Engineering, Shenzhen University, Shenzhen, 518060, China.
**** Corresponding author. The Key Lab of Marine Environmental Science and Ecology, Ministry of Education, Ocean University of China, Qingdao, 266100, China.
E-mail addresses: nikonplussigma@gmail.com (Y. Fang), 316533880@qq.com (X. Wu), Daimin1007@163.com (M. Dai), alopez@uaslp.mx (A. Lopez-Valdivieso), raza@szu.edu.cn (S. Raza), imranali@szu.edu.cn, engrimran56@gmail.com (I. Ali), cspeng@sohu.com, pcs005@ouc.edu.cn (C. Peng), jyli@szu.edu.cn (J. Li), iffatkhattak@yahoo.com, I.Majid@qu.edu.sa (I. Naz).

https://doi.org/10.1016/j.jclepro.2021.127678
Received 23 October 2020; Received in revised form 27 April 2021; Accepted 24 May 2021
Available online 27 May 2021
0959-6526/

kidney circulation, dermatitis, and lung cancer in humans (Norouzi et al., 2018). While, Cr(III) is less mobile, more stable, and less toxic than Cr(VI) (Bencheikh-Latmani et al., 2007). It can be converted into chromium hydroxide ($Cr(OH)_3$), which can be precipitated out at moderately acidic to alkaline pH and can also serve as an essential micronutrient. Therefore, the removal or reduction of Cr(VI) anions to nontoxic and immobile Cr(III) ions is imperative for protecting the environment and public health.

Various conventional methods such as adsorption, reduction, membrane filtration, precipitation, and ion exchange have been employed to remove heavy metals from sewage (Fazlzadeh et al., 2017; Zhao et al., 2020b). Whereas, the reduction and adsorption procedure of Cr(VI) has attracted more attention because of its cost-effectiveness as compared to membrane filtration (Muthukrishnan and Guha, 2008), ion exchange (Peng et al., 2020), and electrochemical treatment technologies (Owlad et al., 2008). Further, iron and modified iron compounds have been extensively applied for Cr(VI) elimination owing to having their higher activity and feasible synthesis protocols such as green technologies (Bavasso et al., 2018; Fazlzadeh et al., 2017; Vilardi et al., 2018b; Zhang et al., 2020), mangrove fungus reduction method (Chatterjee et al., 2020), in-situ growth method (Zhao et al., 2020a) and replacement reactions method (Gheju, 2011).

Further, the nanoparticles of zero-valent iron (ZVI) have shown a great potential application in the treatment of real tannery wastewater and the removal ratio of 100, 70, 73, and 88% were noticed for Cr(VI), TOC, COD, and phenol, respectively (Vilardi et al., 2018a). Since the first exhaustively documented practical application of ZVI on groundwater remediation with the permeable reactive barrier (PRB) in 1996 (Puls et al., 1999), the development of ZVI-based materials has received considerable attention for environmental remediation. Regarding this, Fig. 1 is illustrating a comprehensive summary of the advancements in ZVI-based materials for sewage treatment.

Notably, certain factors such as particle size (Lv et al., 2013), pH value (Katsoyiannis et al., 2008; Mamindy-Pajany et al., 2011), co-existing ions (Vilardi et al., 2017a, 2017c), hydrodynamic filed (Vilardi et al., 2019c) and contaminant concentration were restricted performance of iron (Shi et al., 2011). The passivation layer on the surface of the iron particle formed under alkaline conditions could sequester the electron derived from iron, wherein the passivation layer was mainly contained non-conductive hydroxide of iron and Cr (He et al., 2005). Research efforts have been done on impairing the effect of the passivation layer. For instance, the iron/aluminum bimetallic material presented higher Cr-elimination performance as compared to the elemental iron (Fu et al., 2015a). In addition to unfavorable impacts induced by the surface oxidized layer, nZVI particles are preferred to clump in the aqueous solution where the activities of iron were limited remarkably (Dai et al., 2016). To solve this issue, a stable nZVI containing material was synthesized through embodied nZVI in MCM-41 for the improvement of the performance and longevity of nZVI in solution (Petala et al., 2013). The most common measures to promote the capability of iron include composite bimetallic materials (Al–Fe, Zn–Fe, Pb–Fe, Cu–Fe, Ni–Fe, Ag–Fe) (Koutsospyros et al., 2012; Zhu et al., 2017), loaded iron on carbon template (Hoch et al., 2008), and mixed iron with elemental sulfur or sulfide (Patterson et al., 1997). The preparation procedures for iron-bearing materials fluctuate by considering the limitations caused by poor solution dispersion and easy air oxidation of iron. To enhance the dispersion of nZVI in solution, carbon nanotube-supported nZVI was synthesized through liquid-phase reduction method and Cr removal efficiency was found to be around 36% higher than bare nZVI (Lv et al., 2011). While, the reduction of 10 ppm Cr(VI) solution to ~1 ppm was observed in three days by employing activated carbon-supported iron prepared by carbothermal reduction technique (Hoch et al., 2008). Similarly, the carbon skeleton improved the stability of iron dramatically (Sun et al., 2012).

Therefore, a comprehensive summary of ZVI-based materials development was essential to design a compatible environmental material with practical contamination sites. Even though some review papers have recapitulated the versatile ZVI technology from the synthesis procedure to different countermeasures against the limitations of pristine ZVI (Crane et al., 2012; Zou et al., 2016). While, some researchers have discussed the effect of solution chemistry and operational conditions on ZVI properties (Sun et al., 2016). Rare reviews systematically considered the co-effect of pH and DO on the performance of ZVI-based materials on targeted pollutant sequestration. For example, the efficiency of ZVI towards Cr(VI) removal was suppressed in the presence of oxygen (Flury et al., 2009), but another study discovered the opposing results in the presence of oxygen (Yoon et al., 2011). Briefly, the pH could greatly involve in the corrosion of ZVI and product establishment with DO. Therefore, we delicately evaluated the co-effect of pH (acid or alkaline) and DO (oxic or anoxic) on the capability of ZVI-based materials. Moreover, the literature involved in the preparation methods of ZVI-based materials (liquid-phase reduction and mechanical methods),

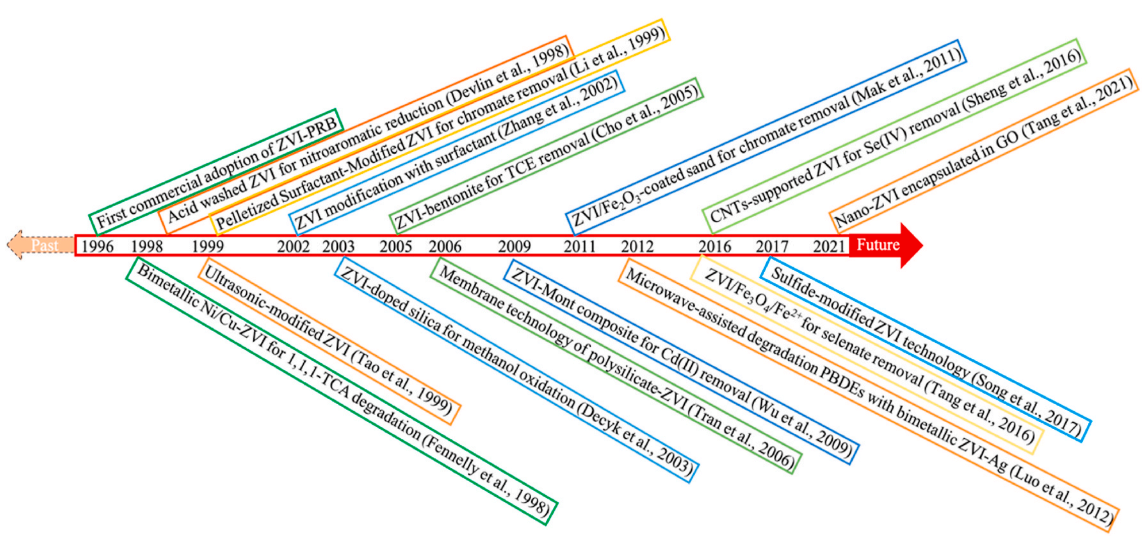

Fig. 1. The major events of ZVI-based materials development over the past 25 years (1,1,1 TCA (1,1,1-trichloroethane), TCE (trichloroethylene), Mont (Montmorillonite), CNTs (carbon nanotubes), PBDEs (polybrominated diphenyl ethers), GO (graphite oxide) (Cho et al., 2005; Decyk et al., 2003; Devlin et al., 1998; Du et al., 2016; Fennelly and Roberts, 1998; Li et al., 1999; Luo et al., 2012; Mak and Lo, 2011; Sheng et al., 2016; Song et al., 2017; Tang et al., 2021; Tao et al., 1999; Tran et al., 2006; Wu et al., 2009; Zhang et al., 2002, 2019e).

four common ZVI-based materials (carbon-ZVI, sulfur-ZVI, bimetal of ZVI, and magnetite-ZVI composites), mechanism of Cr(VI) elimination, field application, and market penetration of ZVI-based materials were carefully discussed herein.

2. Synthesis of ZVI-based materials for the removal of chromium

Various technologies based on the physical and chemical methods are employed for the fabrication of ZVI-based materials to remove Cr from the environment. Chemical reductants such as molecular hydrogen, hydrazine hydrate, $NaBH_4$, CO, etc. are mostly applied for Cr-reduction. While, the physical methods are comprised of mechanical crushing and metal electrode precipitation (Tavakoli et al., 2007). To the best of our knowledge, most of the researches have only focused on the application of chemical reduction methods by using $NaBH_4$ (Wang et al., 2019c) and mechanical milling (He et al., 2020b; Xu et al., 2012).

2.1. Liquid-phase reduction

The liquid-phase reduction or borohydride reduction method is based on ferric and ferrous ions as ZVI precursors and $NaBH_4$ as a reducing agent. The earliest recorded prepared nano-scale ZVI was $FeBr_2$(aq) and $FeBr_3$(aq), which were reduced by $NaBH_4$ in the aqueous solution (Glavee et al., 1995). Similarly, various other researchers synthesized nano-scale ZVI with narrow size distribution (10–100 nm) (Nurmi et al., 2005; Wang et al., 1997) and also coated with oxide shells (Yang et al., 2005). For its preparation, the desired amount of Fe precursor such as degassed $FeCl_3$ solution was dropped with sodium borohydride solution (1 drop/s), the reduction reaction is presented in Eq (1). After the accomplishment of the reaction, the mixed solution was allowed to settle down for 20 min, and then it was centrifuged for collection of ZVI (Hwang et al., 2011). The entire process was conducted under an inert atmosphere as-synthesized ZVI can be easily oxidized in air.

$$4Fe^{3+} + 3BH_4- + 9H_2O \rightarrow 4Fe^0 + 3H_2BO_3- + 12H^+ + 6H_2 \text{ (gas)} \quad (1)$$

Although extensive research has been carried out on bare ZVI preparation, the reactivity of nZVI might be lowered due to agglomerate irreversibly in the solution. ZVI doped on the template such as activated carbon (Mortazavian et al., 2018), biochar (Lyu et al., 2017), graphite (Xu et al., 2018) and chitosan (Liu et al., 2010) has demonstrated outstanding dispersion in the solution. Meanwhile, the removal performance of Cr(VI) was improved considerably for ZVI-loaded material concerning their monometallic counterpart. A team of research investigators successfully fabricated biochar-supported nZVI by liquid reduction technique, wherein nZVI was loaded on biochar through carboxyl and silicon mineral within biochar. The removal capacity for Cr (VI) was 40 mg/g under initial pH 4.0 and could serve as a candidate material for groundwater remediation (Qian et al., 2017). Further, as compared to non-supported nZVI (62.9%), the attapulgite-supported nZVI exhibited 90.6% removal efficiency for Cr(VI). Moreover, the stability and dispersion of nZVI were improved after doping evenly on a supporter of attapulgite (Zhang et al., 2019a). Further, a series of experiments were performed to illustrate that bentonite-supported organosolv lignin stabilized nZVI (BL-nZVI) had a higher removal capacity of Cr(VI) than bare nZVI and bentonite-supported nZVI (B-nZVI) (Wang et al., 2020a). A comprehensive procedure from synthesis to the application has been demonstrated in Fig. 2.

2.2. Mechanical method

The ball milling (BM) procedure has been proved to be an effective method for the preparation of nZVI (Kerekes et al., 2002). Briefly, the iron grains undergo deformation, fracture, and welding repeatedly in the presence of vigorous collision between milling medium balls and iron particles. The size of the produced ZVI is a function of grinding duration time (Ambika et al., 2016). Further, the ZVI fabricated by mechanical milling subjects to the coarse size and unregulated shape, but the BM method can easily be scaled up with reasonable expenditures as compared to other approaches (Huber, 2005). It was reported that the 2 mm grain of ZVI was milled in high energy planetary ball milling for

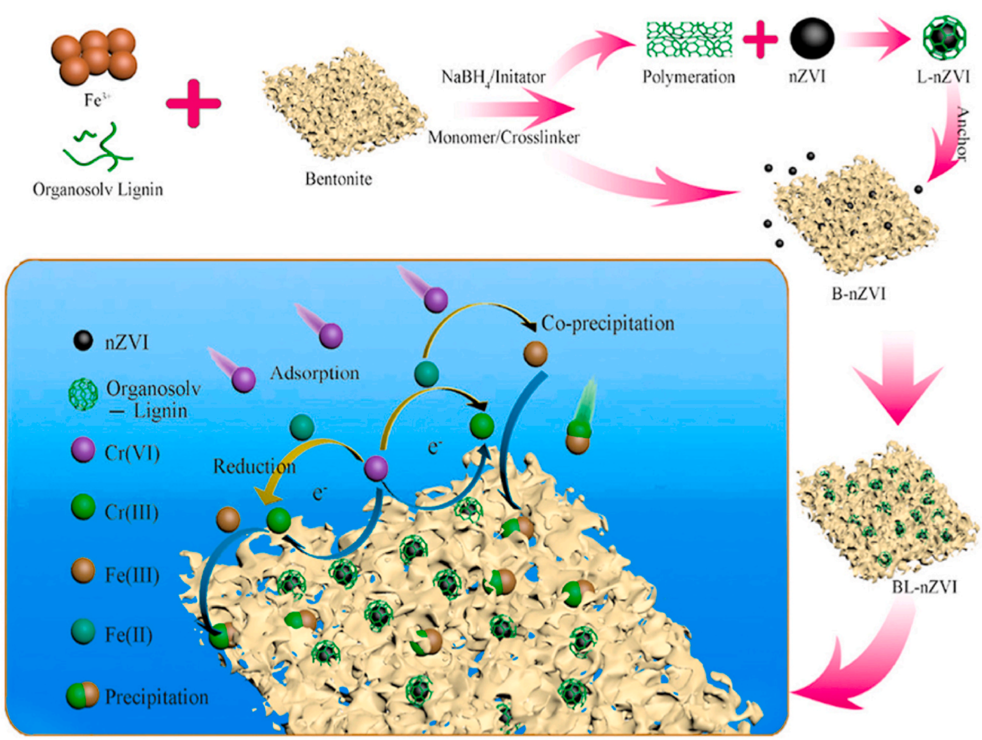

Fig. 2. The schematic illustration of the preparation of BL-nZVI by liquid-phase reduction method, and the removal process of Cr(VI). The Cr(VI) was reduced by loaded-ZVI and followed co-precipitation with Fe(III) (Wang et al., 2020a), Copyright 2020, Elsevier.

10 h, and the resulting 20.9 μm meso-ZVI eradicated Cr(VI) and organic pollutant effectively (Ambika et al., 2020). Recently, it was reported that different masses of AC were combined with 5.6 g of micron-scale ZVI (mZVI) in stainless steel milling jar and then grounded for 30 min at 300 rpm. Thereafter, it was followed by the addition of mZVI-AC in acidic and anaerobic Cr(VI) solution. The removal efficiency of Cr(VI) reached 94.01% within 2 h, it was also found that only 22.1% Cr(VI) was removed by the mixture of ZVI and AC (Wang et al., 2020b). These results verified the findings of a great deal of the previous work of Wang et al. (2020), and their thorough information has been presented in Fig. 3 (Wang et al., 2020c).

Besides, the milling-induced displacement reaction to prepare various sizes of ZVI is a promising technology, as it could enable the recycling of scrap iron. The nanocomposites of ZVI with Al_2O_3 or ZnO were obtained after grinding of a sample of metallic aluminum or zinc with magnetite or hematite (Matteazzi et al., 1992; Pardavi-Horvath et al., 1995; Takacs, 1992). As the reaction processes have been presented in Eqs (2)–(4). Thus, by considering the ease of operation, cost-effectiveness, and readily scaling-up, BM is a promising technology for ZVI preparation.

$$3Fe_3O_4 + 8Al = 3Fe + 4Al_2O_3 \tag{2}$$

$$Fe_3O_4 + 4Zn = 3Fe + 4ZnO \tag{3}$$

$$Fe_2O_3 + 2Al = 2Fe + Al_2O_3 \tag{4}$$

2.3. Other synthetic methods

Apart from the numerous studies about chemical reduction and mechanical milling, there are also other non-widely discussed approaches for ZVI fabrication. For instance, the coal and iron oxide (FeO, Fe_2O_3, Fe_3O_4) were introduced into a silica glass tube equipped with a graphite cylinder radiation heater, the coal reacted with H_2O and CO_2 to produce reductant gas CO and H_2 over 800 °C, and then CO and H_2 reduced iron oxides to ZVI via the thermal reduction method (Liu et al., 2004). Similarly, the goethite was reduced to ZVI by H_2 with heat, nevertheless, the reducing reactant not only included ZVI but also magnetite (Nurmi et al., 2005). Further, the chemical vapor condensation (CVC) process could decompose iron pentacarbonyl ($Fe(CO)_5$) under Ar or He atmosphere to prepare nZVI. Thus, the spherical nZVI (6–25 nm in diameter) was successfully prepared by CVC at 150 °C (Choi et al., 2002). Moreover, pulsed electrodeposition (PED) was adopted to reduce aqueous iron salt to ZVI by desired current and voltage. In short, sacrificial iron anode and inert Ti cathode were immersed in $(NH_4)_2Fe(SO_4)_2$-contained electrolyte and were pulsed continuously. Thus, Fe^{2+} ions were reduced to Fe^0 and precipitated on Ti cathode (Liu et al., 2008). A similar study was performed with PED to obtain nZVI with an average diameter of 19 nm (Natter et al., 2000). The previously described spinning disk reactor (SDR) method proposed potential application of nZVI synthesis at the laboratory-scale (Vilardi et al., 2019b). Nevertheless, the nZVI production on a large-scale still challenges the routines declared above. Thus a comparison of these mentioned methods have been presented in Table 1.

Table 1
The comparison of various preparation methods.

Preparation methods	Process	Characteristics
Liquid-phase reduction	Mixing ferrous or ferric ions with $NaBH_4$ to obtain Fe^0 and then the reduced Fe^0 was loaded on supporters like biochar and bentonite.	The most commonly used method, but the additive of $NaBH_4$ is toxic and the post-treatment for effluent is required regulatorily (Ponder et al., 2000).
Mechanical ball milling	Ball milling iron oxides with Al/Zn to produce Fe^0 or ball milling Fe^0 with supporters like AC.	Easily scaled-up for production, but energy consumption is the main concern (Ribas et al., 2019).
Thermal reduction	Reducing iron oxides/hydroxides to Fe^0 through heating under high temperature reducing gas.	Recycling the scrap iron, however, the high energy consumption and the emission of greenhouse gas are the main disadvantages (Man et al., 2014).
CVC	Decomposition of $Fe(CO)_5$ under high-temperature inert gas.	The size of Fe^0 particle is adjustable by changing temperature, the cost of raw material and energy consumption are the considerations (Choi et al., 2001).
PED	Preparing Fe^0 by electrochemical reduction.	The purity and thermal stability of prepared Fe^0 are high and the size is controllable, and the power consumption is the central concern (Yanez et al., 2017).
SDR	Introducing $FeSO_4{\cdot}7H_2O$ and $NaBH_4$ solutions into a rotating disk with desired velocity and feeding position to gain Fe^0.	The size of Fe^0 is controllable by adjusting the rotational speed of the disk and the feeding position of solutions (Vilardi et al., 2017b).

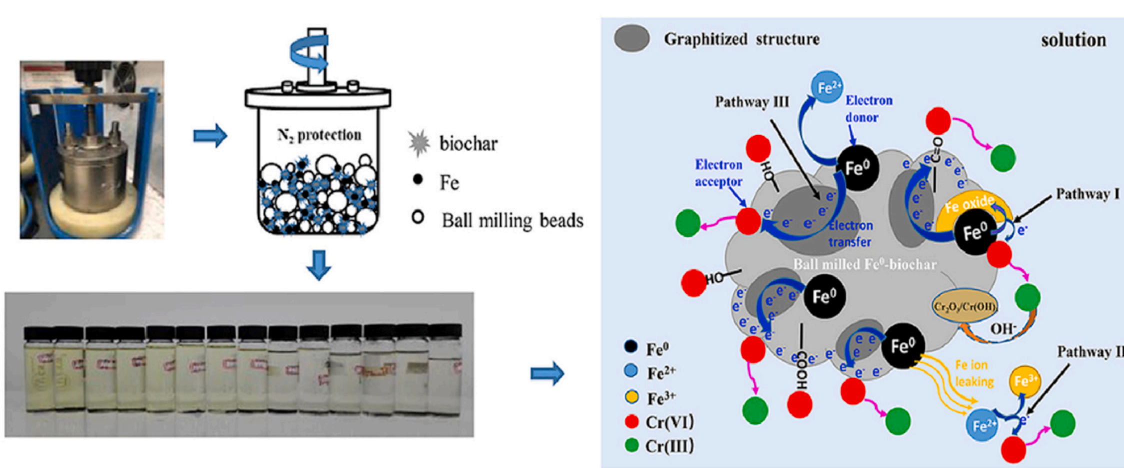

Fig. 3. The schematic illustration of the preparation of the biochar-supported ZVI by mechanical ball milling and its application for the Cr(VI) removal. The adsorbed Cr(VI) on pore channel and surface functional groups of biochar was reduced by Fe^0, meanwhile, part of Cr(VI) reduced in solution (Wang et al., 2020c), Copyright 2020, Elsevier.

2.4. Conventional ZVI composites for Cr(VI) treatment

2.4.1. Carbon-ZVI composites

Biochar, AC, and carbon nanotube have been extensively employed as iron templates to fabricate reliable iron-containing material (Zhou et al., 2014a). Among them, AC possesses stable characteristics because of the developed pores and higher specific surface area, which provided plenty of vacant sites as the iron carrier (Oliveira et al., 2002). Further, AC derived from various kinds of biomass has presented a superior efficiency as a potential adsorbent for Cr(VI) (Al-Othman et al., 2012; Cronje et al., 2011; Karthikeyan et al., 2005). Moreover, the AC loaded-iron coupled adsorption with reduction has proved to be the main process for Cr(VI) removal (Huang et al., 2014). To prepare homogenized AC supported ZVI, the AC was immersed in ferric chloride hexahydrate solution and then was introduced with $NaBH_4$ solution to reduce ferric to ZVI. Finally, nZVI-loaded AC was obtained after centrifugation, filtration, and drying in the nitrogen gas environment (Wu et al., 2013). It was found that the removal efficiency of Cr(VI) increased with an increase in iron loading and the highest removal efficiency (99%) was obtained with the iron loading of 10.9%. On the contrary, the maximum removal efficiency for AC without iron was only 40%. Further, the characterization of nZVI-loaded AC after treatment has proved that Cr(VI) could be reduced to Cr(III) and precipitated with oxidized product ferric. To illustrate this phenomenon the cyclic voltammetry curve was conducted and was found that it exists the iron-carbon microcell facilitated the redox reaction between iron and Cr (VI).

Similarly, pristine biochar was derived from cornstalk and was modified with H_2O_2, HCl, and NaOH solution. Further liquid-phase reduction method as described above was employed to synthesis iron-loaded biochar and then it was applied for Cr(VI) removal from solution. The Cr(VI) removal experiments results have shown that iron-loaded biochar modified with HCl solution exhibited better Cr(VI) removal efficiency than the other two materials. During the process of Cr (VI) removal, the biochar matrix stimulated the redox reaction of iron and Cr(VI) by electrostatic attractions between positively charged biochar and anion chromate, and faded the side impact of Cr(III)/Fe(III) (oxy) hydroxides deposit on the iron particle (Dong et al., 2017a). Moreover, the micro-galvanic formed between iron particle and carbon matrix contributed to another mechanism, Thus the role of biochar to serve as an electron-transfer mediator through removing aqueous solution Cr(VI) by silicon-rich biochar-supported ZVI was also verified (Qian et al., 2019). Compared to iron-loaded on AC or biochar, magnetite-loaded carbon material could endure the defect of secondary separation for by-product (Qiu et al., 2015), owning to magnetic properties of Fe_3O_4 which has attracted much attention for the separation procedure in Cr(VI) removal (Gupta et al., 2011; Huang et al., 2015; Nethaji et al., 2013; Rajput et al., 2016; Salam, 2017). However, magnetite can be easily inclined to lose magnetic property as a result of oxidation to ferric oxide under acidic conditions (Rebodos and Vikesland, 2010). A group of researchers decorated the multiwall carbon nanotube with magnetite nanoparticles and then modified with 1,6-hexanediamine to treat acidic Cr(VI) solution, this synthesized material presented good magnetic property and nearly reached 95% removal rate of Cr(VI) at pH 2.0 (Lu et al., 2017a). In addition to the magnetite, γ-Fe_2O_3 had also shown magnetic properties. Laboratory synthesized γ-Fe_2O_3-carbon hybrids could be separated magnetically after the removal of Cr(VI) from the aqueous solution (Fig. 4).

2.4.2. Sulfur-ZVI composites

The reducible species like oxygen, protons (Han et al., 2016), and water (Fan et al., 2017) can consume the electrons originated from ZVI and could damage the utilization efficiency of ZVI to target contaminants. Further, the sulfur compounds modified ZVI could alleviate the unintentional reaction of ZVI with water, and the efficiency of the electron of ZVI could be strengthened as a result. Notably, the findings have demonstrated the essential role of sulfur in the decontamination of trichloroethylene (TCE) (Fan et al., 2016; Gu et al., 2017; Han et al., 2016; Li et al., 2017) and florfenicol (Cao et al., 2017) by S-ZVI. Besides, it has been suggested that sulfur speciation like sulfate radicals specified promising capability on pollutant degradation removal (Xiao et al., 2020). A team of researchers prepared the S-ZVI composite by mixing the desired amount of iron with elemental sulfur in planetary ball milling within 4 h. Then, the obtained S-ZVI material was employed to treat the Cr(VI) solution under aerobic conditions. The S-ZVI composites appreciably increased the electron effectiveness of iron to Cr(VI) which was 10.7-fold higher than bare iron. The enhancement effect of sulfur species was mainly ascribed to the FeS, which boosted the attachment of chromate onto the surface of S-ZVI and transferred the electrons to chromate (Li et al., 2018). Similarly, the aqueous Cr(VI) was eliminated by S-nZVI composites with a higher S/Fe molar ratio (Lv et al., 2019), and the removal process has been demonstrated in Fig. 5. Based on the prior literature about pollutants elimination by iron under aerobic and anaerobic conditions, it was observed that undesirable hydrogen evolution reaction between iron and water also depleted iron under anaerobic condition, thus decreased the longevity and electron selectivity of iron (Liu et al., 2006; Paar et al., 2015; Rajajayavel et al., 2015; Reardon, 1995, 2005). A comparison between bare iron and sulfur-modified iron was also executed, it was found that the latter implied conservative hydrogen production rate and amount (Xu et al.,

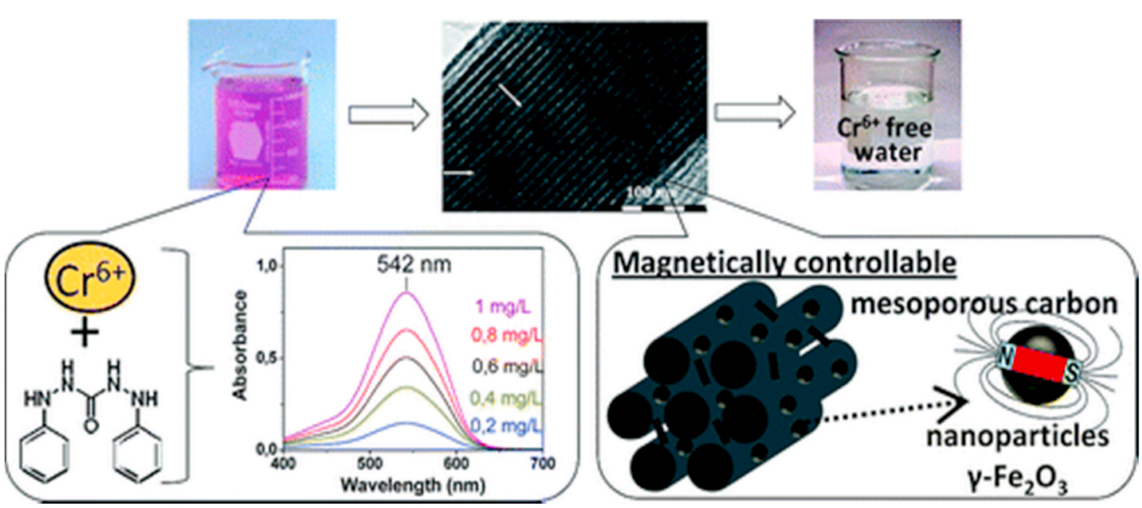

Fig. 4. The schematic demonstration of the removal of Cr(VI) by magnetic γ-Fe_2O_3-carbon composite (Baikousi et al., 2012), Copyright 2012, ACS Publications.

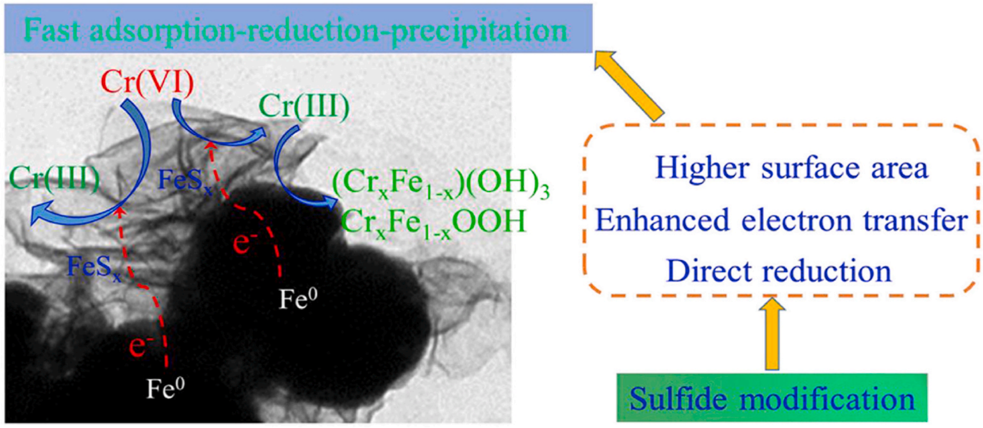

Fig. 5. Removal of aqueous Cr(VI) by S-nZVI. The increased surface area after modified with sulfur fascinated the adsorption of Cr(VI), and the FeS_x favored the corrosion of ZVI to target Cr(VI) (Lv et al., 2019), Copyright 2019, Elsevier.

2019). A plausible explanation for the suppressed reactivity of ZVI to water was that the sulfur-modified ZVI inclined to hydrophobic and the reaction of hydrogen evolution from ZVI and water was mitigated as a result. It made sulfur-modified iron a potential material for anaerobic groundwater remediation. Recent cases also supported the hypothesis that sulfur could fascinate the selectivity and activity of iron to the targeted pollutants (Gu et al., 2019). It has been demonstrated that S-nZVI fixed with carboxymethyl cellulose (CMC) presented higher mobility and stability in the sub surfaces for field applications (Nunez Garcia et al., 2020).

2.4.3. Bimetallic composites

Previous studies have defined bimetal of iron as incorporating the second metal such as Al, Ni, Pt, Ag (Liu et al., 2014) and Pd (Dong et al., 2011), Cu (Hu et al., 2010) with iron. The chemical and electronic properties of the bimetallic materials are optimized evidently as compared to the solitary metals (Gunawardana et al., 2011). Table 2 is illustrating a summary of the published reports on Cr(VI) removal by ZVI-based bimetallic materials. The main drawback of the bimetallic materials is the employment of noble metals like Ag and Pt or the use of toxic metals such as Ni and Cu as second metals. However, it makes the rarely available metals to fabricate bimetal of iron for pollutants remediation in the large-scale application. Al as the most abundant metallic element on the earth was an ideal candidate for Al–Fe preparation. Besides, the elemental Al has been extensively employed for the removal of a variety of pollutants such as Cr(VI) (Jiang et al., 2017; Yang et al., 2017; Yang, Y. et al., 2020; Zhang et al., 2019c), bromate (Lin et al., 2017), TCE (Ren et al., 2018) and phenol (Wu et al., 2020). The Fe–Al bimetallic particles were fabricated via depositing iron on the Al surface for Cr(VI) removal. The desired mass of Al was added to deionized water, which was priorly mixed with the desired concentration of $FeSO_4$ solution. Then it was rinsed and dried after stirred for 30 min. Different ratio of Al/Fe was obtained by regulating the dose of Al and Fe, the synthesized Fe–Al material was the Al-cored particle and Fe was deposited on its outer layer. The galvanic cell based on Fe as anode and Al as cathode for the electrode potential of Fe (−0.44V) was higher than Al (−1.67V). For this reason, the Cr(VI) was reduced by electrons donated by the Al core and transferred through the iron shell. The iron accelerated the electrons transfer from Al to Cr(VI) and higher removal efficiency was achieved over a wide range of pH (3.0–11.0) (Fu et al., 2015a). Similar studies of the galvanic effect of Al–Fe bimetallic particles for Cr(VI) elimination from aquatic environments was conducted by (He et al., 2018). In contrast to earlier findings, however, Al–Fe bimetallic that ZVI coated with zero-valent Al has shown lower Cr(VI) removal capacity. However, another research team found that Fe/Al bimetallic material has demonstrated 21 folds higher Cr(VI) removal efficiency than Al/Fe bimetallic (Ou et al., 2020). It was due to the oxidation of the Al layer by Cr(VI). Then, the electrons from Al and ZVI was quarantined from contaminants, but concerning iron-coated Al particle, the pathway of electron transfer from Al to Fe was unaffected by contaminants. The oxidized Fe^{2+} by Cr(VI) could be reduced to Fe^0 by Al spontaneously. A similar galvanic cell effect on Fe/Co bimetallic has been demonstrated in Fig. 6.

As compared to the laboratory scale liquid reduction method, the melting and ball milling techniques for synthesis of bimetals exhibited higher homogeneity, superior mechanical stability, and greater potential in large-scale applications (Xu, F. et al., 2012; Xu et al., 2017a; Xu et al., 2017b; Zhao et al., 2014). Typically, the desired ratio of Al and Fe

Table 2
ZVI-based bimetallic materials for Cr(VI) removal.

Bimetals	Synthesis methods	Reducing agents	Removal (%)	Operational pH	Removal mechanism	Reference(s)
Ni-ZVI	Liquid-phase reduction	KBH_4	96.33–60.31	2.0–7.0	Reduction, adsorption, and precipitation	Zhou et al. (2014b)
Ni-ZVI	Liquid-phase reduction	$NaBH_4$	100	1.0–3.0	Reduction, adsorption	Kadu et al. (2011)
Mont-supported Ni-ZVI	Liquid-phase reduction	$NaBH_4$	100	1.0–3.0	Reduction	Kadu et al. (2011)
Ni-ZVI	Chemical vapor deposition	H_2	83	N/A	Reduction, adsorption	Lu et al. (2017b)
Cu-ZVI	Liquid-phase reduction	$NaBH_4$	50.57	2.0	Reduction, adsorption	Shao et al. (2019)
Pd-ZVI	Liquid-phase reduction	$NaBH_4$	95.5–73.0	3.0–8.0	Reduction, adsorption, and precipitation	He et al. (2020a)
Cu-ZVI	Liquid-phase reduction	Extract of green tea	94.7	5.0	Reduction, adsorption, and precipitation	Zhu et al. (2018)
Cu-SZVI	Liquid-phase reduction	Fe	97.9	8.0	Reduction	Jia et al. (2019)
Al–Fe	Liquid-phase reduction	Al	90.0	7.0	Reduction, Precipitation	He et al. (2018)

N/A. Not available.

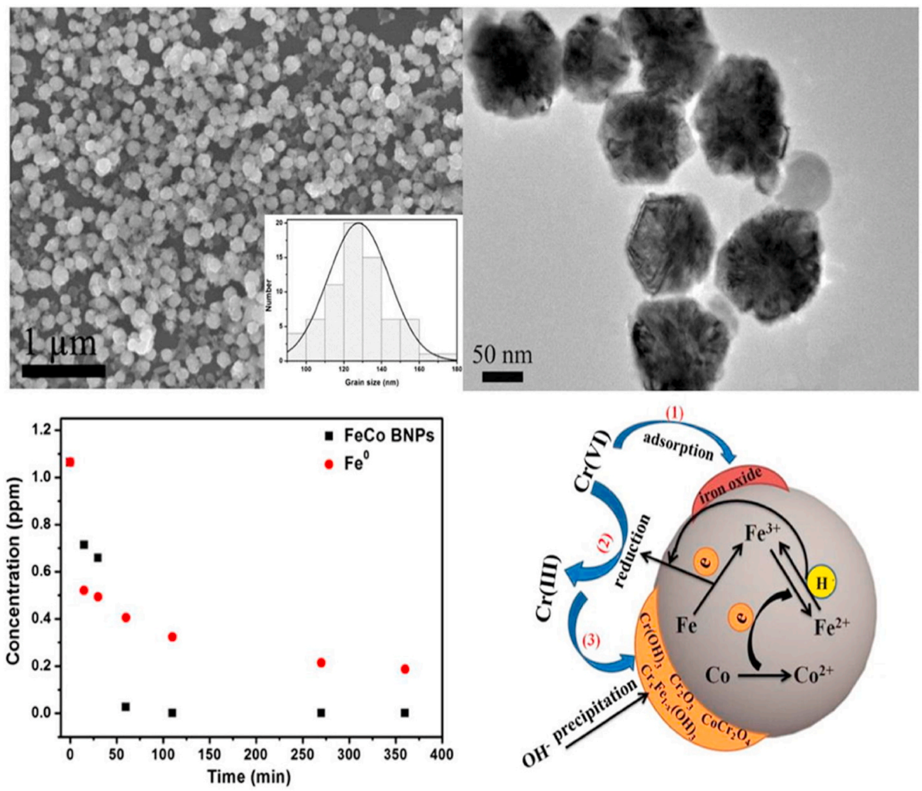

Fig. 6. The removal process of Cr(VI) by Fe–Co bimetallic coated by tea-polyphenol. The removal efficiency enhanced after incorporated with Co, ZVI was depleted by Cr(VI) and the Co can maintain the activity for ZVI that electron derived from Co can reduce Fe^{3+} to Fe^{2+}. The reduced Cr(III) separated from the solution by precipitated as $Cr(OH)_3$ and $Cr_xFe_{1-x}(OH)_3$ with Fe^{3+} (Qin et al., 2016b), Copyright 2016, Elsevier.

powder in MgO crucible is melted in a vacuum melting furnace, and then the obtained Al–Fe was crushed into particles for further applications in the removal of targeted contaminants (Xu et al., 2017a). It was noticed that Al–Fe particles consisting of 20% Fe prepared through melting method has indicated favorable removal performance of Cr(VI) (Zhang et al., 2019b). According to the available literature, ball milling is the most widely used mechanical procedure for the preparation of bimetallic materials for pollutants elimination (Kumar et al., 2011; Sui et al., 2017; Wang et al., 2019b; Yang et al., 2014). The bimetallic materials produced by ball milling have demonstrated some advantages, such as simple operation, easy scaling up, and time-saving. However, as far as we know, most of the researches up till now have not focused on the preparation of Fe–Al particles through high energy ball milling, thus, the study would be more beneficial if a wider range of ball milling procedure for Fe–Al preparation is explored, especially for Cr(VI) eradication.

2.4.4. Magnetite-ZVI composites

Magnetite or ferrosoferric oxide (Fe_3O_4) is commonly found in nature and characterized by properties like conductivity, magnetism, high surface area, and reducibility. Its importance in literature has been recognized in the elimination of targeted contaminants (Crean et al., 2012; Gorski et al., 2010; He et al., 2005; Petrova et al., 2011; Su, 2017; Wiatrowski et al., 2009; Yuan et al., 2009, 2010). It was reported that Cr (VI) could directly reduce by magnetite (Peterson et al., 1996). Further, the coupling of magnetite with iron for the degradation/reduction of contaminants would not only accelerate the corrosion of iron but also easily separate from aqueous solutions (Qu et al., 2019; Rao et al., 2013b; Villacís-García et al., 2015). The structural Fe^{2+} of magnetite can act as an electron channel from iron to pollutants. Briefly, Fe^{2+}(s) in the octahedral site of magnetite could be oxidized by targeted contaminants to Fe^{3+}(s), and then the oxidized Fe^{3+}(s) could be reduced back to Fe^{2+}(s) by accepting electrons from Fe^0 and this process is thermodynamically favorable, as suggested by standard electrode potential, which is expressed as in Eq (5) (Jonoush et al., 2020), and without construal constrain (Moura et al., 2005, 2006). Regarding this, Fig. 7 is showing synergistic effects of Fe_3O_4/Fe on Cr(VI) removal.

$$2Fe^{3+}(aq) + Fe^0(s) = 3Fe^{2+}(aq)\ \triangle E^0 = 1.21V \quad (5)$$

To determine the effect of Fe^{2+}(s) of magnetite on Cr(VI) removal by Fe_3O_4–Fe^0, the removal performances of Fe^0-α-Fe_2O_3, Fe^0-γ-Fe_2O_3, and Fe^0–FeOOH were compared with Fe^0/Fe_3O_4. The Fe^0/Fe_3O_4 composite demostrated a higher Cr(VI) conversion rate (65%) as compared to the other three composites. In contrast, the bare Fe^0 and Fe_3O_4 only

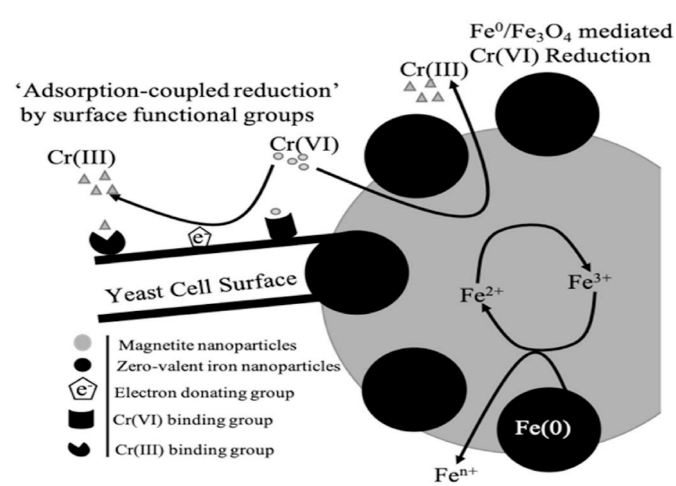

Fig. 7. The Yarrowia modified Fe_3O_4–Fe^0 employed for Cr(VI) elimination. The oxidized Fe^{3+}(s) from Fe_3O_4 by Cr(VI) converted to Fe^{2+} (s) by Fe^0 (Rao et al., 2013a), Copyright 2013, Elsevier.

converted 15 and 25% Cr(VI), respectively (Coelho et al., 2008). Moreover, the conventional Fe^0/Fe_3O_4 composite failed to consider the long-term impact of neutral or alkaline conditions. For instance, the Cr (VI) removal efficiency by Fe^0/Fe_3O_4 composite dropped significantly from 100 to 35.88% as pH increased from 7 to 10 (Lv et al., 2012). Further, it was reported that the reduction of aqueous Cr(VI) by magnetite was ceased after 10–20 Å surface of magnetite was oxidized into maghemite (γ-Fe_2O_3) at pH 7.0 (Peterson et al., 1997). It was might be due to the surface passivation effect. Recently, a hydroxyl-modified Fe^0–Fe_3O_4 was fabricated with the addition of Na_2EDTA complexation, and then it was employed for the removal of Cr(VI). The results indicated that the concentration of Cr(VI) was declined continuously, which could be attributed to the contribution of complexation of Na_2EDTA with Fe^{3+} and Cr^{3+} (Wang et al., 2019b). Moreover, the EDTA ligand assisted sequestration procedure has gained much attention presently due to its cost-effectiveness and its outstanding capability in the elimination of various contaminants like heavy metals, organic matters, etc. (Fu et al., 2013; López et al., 2005; Luo et al., 2010; Wang et al., 2012; Zhang et al., 2010; Zhou et al., 2008). Nevertheless, the existing accounts have failed to resolve the contradiction between in-situ application and environment protection, the degradation of EDTA is important before its discharging to prevent the environment from EDTA toxicity (Englehardt et al., 2007).

Thus, further research efforts are required to find out eco-friendly ligands which can assist the removal of Cr(VI) from the environment by Fe^0/Fe_3O_4 composites.

2.5. Mechanism of Cr(VI) sequestration by ZVI-based materials

The route of Cr(VI) removal by ZVI-based materials is mainly controlled with the combination of reduction, adsorption, and co-precipitation, wherein the leading reduction process is effected essentially by pH and DO. The reduction capacity of pristine iron was inhibited due to the intrinsic defect caused by the passivation layer under alkaline and aerobic/anaerobic conditions. The resulting constitution of ZVI after treating with Cr(VI) could clearly be described by two linear dimensions (Vilardi et al., 2019a). Deliberately formulated ZVI-based materials have been used to preclude the passivation on the surface of ZVI to promote the electron efficiency and permanence of iron. In the current review, the mechanism of encouraged Cr(VI) reduction potential of ZVI after incorporated into AC/biochar-ZVI, ZVI-based bimetal, sulfur-ZVI, and magnetite-ZVI composites is predominantly considered.

The effect of the galvanic cell has been evidenced to be the main path for Cr(VI) reduction by AC-supported iron (Huang et al., 2017) and ZVI-based bimetal (Lugo-Lugo et al., 2014). The electrons derived from ZVI could be transferred to the target contaminant via AC and the corrosion of ZVI was facilitated, consequently. The produced secondary reductant Fe^{2+} accompanied with the oxidation of Fe^0 could further reduce Cr(VI), and the Cr(III) could be precipitated with Fe^{3+} because the improved pH of the aqueous solution was initialed by redox couple of Cr(VI)–Fe^0/Fe^{2+}. Moreover, the adsorption property of AC on Cr(VI) could advance the reduction process.

Based on the reduction potential difference between Fe^0 and another metal in the bimetallic pair, Fe^0 could serve as an anode in the galvanic cell when coupling with less active metal and could also act as a cathode instead when coupling with the higher active metal (Lugo-Lugo et al., 2010). The electrons transported directly from anode Fe^0 or indirectly through less active metal to contaminant, this pathway was greatly related to the configuration of ZVI-based bimetallic particles. In general, these two electron relocation channels were both driven by reduction potential difference of Fe^0-pollutants or Fe^0–Cu/Ni couples when Fe^0 dispersive homogeneously in bimetallic (Jiang et al., 2018). The electrons originated from the Fe^0 core could simply be transferred indirectly through inert shell metal like Cu or Ni to Cr(VI), conversely. And the core-shell structure could deteriorate the undesirable effect of the passivation layer on Fe^0 (Hu et al., 2010; Zhou et al., 2016). The effect of Cu layer on iron endurance to contaminant transformed from positive to negative when increased the mass of planting Cu on the iron core from heterogeneous and loose to dense and uniform film, owing to the galvanic corrosion of Fe–Cu was readily formed with loose Cu layer (Lai et al., 2014). While Fe^0 performs as a cathode in bimetallic material, the reduction of contaminants arisen from three kinds of electron transportations; electrons from Fe^0, higher active metal (e.g., Al), and the galvanic cell of bimetallic (Cheng et al., 2016). Fe–Al bimetallic prepared by liquid reduction method or replacement reaction suggested a desirable Cr(VI) removal efficiency over a wide pH range (3–11), three electron assignment paths mentioned above contributed appreciably to the Cr(VI) reduction and the subsequent precipitation removal (Fu et al., 2015a).

The reduction of Cr(VI) by sulfur-modified ZVI involved two phases, Cr(VI) reduced directly by Fe^0 and indirectly by the regenerated Fe^{2+} from redox of Fe^{3+}/Fe^0 couple (Shao et al., 2018). The sulfured iron film on the surface of the iron core could enhance the corrosion of Fe^0 via the electron transfer from Fe^0 to oxidized Fe^{3+}. Meanwhile, the Cr(VI) reduction performance would be un-favored once excess sulfur was introduced as the core Fe^0 would be covered by a dense sulfidation iron layer (Zhang et al., 2019d). It was also found that the regeneration of Fe^{2+} was absent in the reduction of Cr(VI) by excess sulfur modified iron, it can inference that the iron core was overlaid completely by the outer FeS layer and constrained the regeneration of Fe^{2+} from soluble aqueous Fe^{3+} (Zou et al., 2019). Besides, the surface area of iron increased after the sulfidation, which helped in the adsorption of Cr(VI) and succeeding reduction. Corresponding to the passivation of ZVI, the virgin magnetite was also expected to be passivated with maghemite, goethite, and/or $Cr_{1-x}Fe_xOOH$ under alkaline pH during reaction with Cr (VI) which inhibited the reduction of Cr(VI), subsequently (He et al., 2005). Similarly, a research study implied that the removal efficiency of Cr(VI) on magnetite-ZVI composite was 96.4%, while about 18.8 and 48.8% were noticed by ZVI and Fe_3O_4, respectively (Lv et al., 2012). It speculated that the regeneration of Fe^{2+} in magnetite sponsored the enhancement of Cr(VI) sequestration in magnetite-ZVI composite compared to bare ZVI (Wu et al., 2009). The octahedrally located Fe^0 on Fe_3O_4 cycled the oxidized Fe^{3+} in magnetite to Fe^{2+} for the further reduction of Cr(VI) with Fe^0. The enhancement of electron selectivity of Fe^0 to Cr(VI), acceleration of corrosion of Fe^0, and the regeneration of Fe^{2+} are the main mechanisms that contribute to the superior Cr(VI) removal capacity by ZVI-based materials. The effect of galvanic cell and the conductive layer covered on Fe^0 accelerate the electron transfer from Fe^0 to Cr(VI), particularly.

2.6. Comparison with others iron-based materials

The Fe(II)-containing minerals such as pyrite (FeS_2), ferrous sulfide (FeS), and green rusts (GRs) established promising properties for the environmental remediation technologies (Lian et al., 2021; Perez et al., 2021; Si et al., 2021). The GRs as the layer structured Fe(II)–Fe(III) hydroxides possessed an outstanding competence on pollutants reductive removal owing to having a higher content of Fe(II). Meanwhile, the GRs were unstable and the stability modification was essential to lengthen the endurance. Green rust chloride immobilized with silicate (Si), phosphate (P), fulvic acid (FA), CMC, and bone char (BC) were used for Cr(VI) removal, and the results indicated that the release of Fe(II) was retarded after immobilization and fast removal of Cr(VI) was noticed by using over 90% of Fe(II) (Zhao et al., 2021). Bae et al. (2020) studied the capacity of Fe(II)-phosphate mineral (i.e., vivianite) on Cr (VI) removal, and found that Cr(VI) was reduced by structural Fe(II) in vivianite and then has formed a complex with the generated mixed-valence Fe-phosphate (Bae et al., 2020). Recently, the FeS_2 particles presented an effective Cr(VI) eradication over a wide pH range (6.0–9.5) (Wang et al., 2019a). To reinforce the removal of Cr(VI), the FeS-loaded titanate nanotubes were prepared hydrothermally, the Cr

(VI) was reduced efficiently by FeS and the produced Cr(III) was adsorbed on titanate nanotubes simultaneously (Li et al., 2020). In general, a wider scope of iron-based materials that are not limited to ZVI-based materials or Fe(II)-containing minerals would help us to extend the application of iron-based materials on Cr(VI) sequestration.

3. The governing conditions for ZVI performance

3.1. pH

The speciation and oxidation states of Cr(VI) are greatly dependent on the value of solution pH. The species of Cr(VI) in aqueous solution consists of chromic acid (H_2CrO_4), bichromate ion ($HCrO_4^-$), chromate ion (CrO_4^{2-}), and dichromate ion ($Cr_2O_7^{2-}$), to illustrate the formation process of Cr(VI) complexes, the equations can be seen in Eqs (6)–(8) (Ramos et al., 1994).

$$CrO_4^{2-} + H^+ = HCrO_4^- \; pK_1 = 6.51 \tag{6}$$

$$CrO_4^{2-} + 2H^+ = H_2CrO_4 \; pK_2 = 5.65 \tag{7}$$

$$2CrO_4^{2-} + 2H^+ = Cr_2O_7^{2-} + H_2O \; pK_3 = 14.56 \tag{8}$$

The speciation of hexavalent chromium (1000 ppm) as a function of pH was calculated based on the value of pK, the Fig. 8 reveals that the predominant species of Cr(VI) are $HCrO_4^-$ and CrO_4^{2-} which exists at below pH 5.0 and up to pH 8.0, respectively.

Further, the half-cell reactions of Cr(VI) under acidic and alkaline conditions are expressed as in Eqs 9 and 10, respectively (White et al., 1996). Acidic solution favors the oxidation state of Cr(VI), on the contrary, Cr(VI) presents the least significant oxidation state under neutral and alkaline conditions. It was demonstrated that the reduction rate of Cr(VI) by Fe^0 increased notably for near 20 times from pH 7.5 to 5.5, and a negligible Cr(III) was detected after pH increased to 8.0. While, the logarithmic value of the first-order rate coefficient of Cr(VI) removal as a function of pH value is highly linear fitted which the slope is 0.72 ± 0.07 (Alowitz et al., 2002). Further, a team of researchers stated that their data strongly supported the view of Alowitz et al. (2002) that the H^+ accelerated the corrosion of iron and promoted the Cr(VI) reduction. It was found that the removal efficiency of Cr(VI) was significantly declined from 97 to 50% as pH increased from 4.0 to 10.0 (Cissoko et al., 2009).

$$Cr_2O_7^{2-} + 6e^- + 14H^+ \rightarrow 2Cr^{3+} + 7H_2O \; E_0 = 1.36V \tag{9}$$

$$CrO_4^{2-} + 4H_2O + 3e^- \rightarrow Cr(OH)_4^- + 4OH^- \; E_0 = -0.13V \tag{10}$$

$$Fe^0 + HCrO_4^- + 7H^+ = Fe^{3+} + Cr^{3+} + 4H_2O \text{ Acidic conditions} \tag{11}$$

$$Fe^0 + CrO_4^{2-} + 2H_2O = Fe^{3+} + Cr^{3+} + 4OH^- \text{Alkalic conditions} \tag{12}$$

It should be noted that redox reactions between Fe^0 and Cr(VI) (Eqs (11)-(12)) were varied substantially as pH. Further, the pH of the solution will increase as the redox reaction carried on either due to the protons consumed or hydroxyl ions (OH^-) generated. Referred to the theory of point of zero charge (pzc), the material presents the positive charge when the pH of the aqueous solution is below the pH of pzc (pH_{pzc}), it exhibits the negative charge when solution pH surpasses the value of pH_{pzc}, conversely (Yoon et al., 1979). Previously the pH_{pzc} value of ZVI was reported around 7.7–8.3 (Choi et al., 2012; Giasuddin et al., 2007; Kanel et al., 2005; Sun et al., 2006). Thus, it can be concluded that ZVI will be negatively charged at pH over 8.3 and the transport of anion chromate in bulk solution to ZVI surface will be inhibited due to electrostatic repulsion.

To further demonstrate the alkaline condition post side effect on Cr (VI) removal, nano-ZVI was synthesized by the liquid reduction method and was applied for Cr(VI) elimination. It was observed that the removal rate of Cr(VI) decreased around 3-fold from pH range 3.0–4.0 to pH 9.0, meanwhile, the pH of the solution was increased from 3.0 to 6.2 within 60 min (Zhang et al., 2018). Contrary to the previous findings that increasing pH has a post negative effect on Cr(VI) removal, however, the removal efficiency of Cr(VI) was higher at pH 5.0 under Fe^0/H_2O system between pH 4.0 and 6.0. Comparing to pH 5.0, iron showed a higher reduction capacity at pH 4.0 but the reduced product of Cr(III) was soluble and remained in solution. Furthermore, at pH 6.0, the reduction rate of Cr(VI) was declined greatly due to the minor availability of free protons (Yoon et al., 2011). Here, the major source of uncertainty is the applied method for the evaluation of the removal performance of Cr(VI) by iron. Generally, the removal mechanism includes the combination of reduction, adsorption, and co-precipitation. Regarding monometallic iron, the removal was mainly contributed by reduction and adsorption at acidic conditions, reduction and co-precipitation under neutral or alkaline conditions. Most accepted equations for removal capacity of Cr (VI) can be seen in Eqs (13)-(14).

$$q_1 = (c_0 - c_{Cr(VI)})/c_0 \tag{13}$$

$$q_2 = (c_0 - c_{total\ Cr})/c_0 \tag{14}$$

Wherein, q_1 and q_2(mg/g) are the removal capacity, c_0(mg/L) is the initial concentration of Cr(VI), $c_{Cr(V)}$ and $c_{total\ Cr}$ (mg/L) are the concentrations of Cr(VI) and total chromium (Cr(VI), respectively. For the Eq (13), it was observed that the value of q_1 decreases gradually as the increase of pH because of the drop of Cr(VI) reduction rate, whereas the variation of q_2 as pH was affected by Cr(VI) and the reduced product Cr (III) for the Eq (14). In brief, reduced soluble Cr(III) decreased gradually as pH increase and started to precipitate when pH over 5.0, and the residual concentration of Cr(VI) increased as pH. Therefore, the value of q_2 was not linearly related to pH. This illustrated the optimal pH for the removal of Cr(VI) by Fe^0 was not the lower value when employed Eq

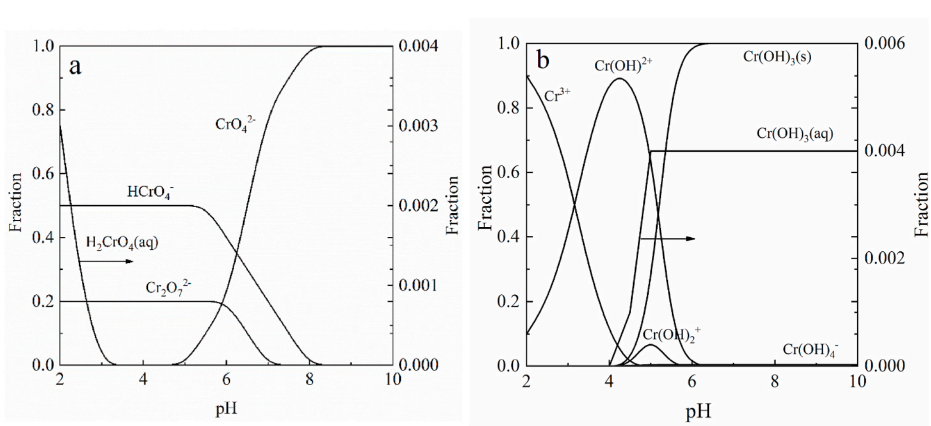

Fig. 8. Speciation illustration of (a) Cr(VI) and (b) Cr(III) at different pH.

(14). Although extensive research has been carried out to assess the capability of iron for Cr(VI) elimination, however only a few researchers have been able to draw a systematic approach (Alidokht et al., 2011; Fan et al., 2020; Fang et al., 2011; Nahuel Montesinos et al., 2014; Zhang et al., 2013). Thus, it was found that a much more systematic approach would result in the identification of reduction and removal capability of iron, a complete removal process should involve the conversion of Cr (VI) to Cr(III) and the final separation of Cr(III) from solution.

3.2. Dissolved oxygen

The erosion of iron is highly affected by dissolved oxygen (DO) in aqueous solution, the oxidation product can be seen in Eqs (15)-(17), it was demonstrated that in the presence of a high concentration of DO in solution, ferrous ion (Fe^{2+}) can be further oxidized to ferric ion (Fe^{3+}) and then could be precipitated with hydroxide (OH^-) (Rivero-Huguet et al., 2010). While, Fe^0 is reported as an effective reductant for Cr(VI) (Guan et al., 2011; Wang et al., 2018).

$$2Fe^0 + O_2 + 4H^+ = 2Fe^{2+} + 2H_2O \tag{15}$$

$$4Fe^{2+} + 4H^+ + O_2 = 4Fe^{3+} + 2H_2O \tag{16}$$

$$Fe^{3+} + 3OH^- = Fe(OH)_3(s) \tag{17}$$

It was documented that iron erosion under anaerobic implies a slower rate than that under aerobic, as shown in the Eqs (18)-(19), due to the formation of ferrous (oxy) hydroxides ($Fe(OH)_2$) instead of ferric (oxy) hydroxides (FeO(OH)). It was found that $Fe(OH)_2$ remained stable in free oxygen and at low temperature (Noubactep, 2009; Reardon, 1995).

$$Fe^0 + 4H_2O = Fe^{2+} + 2H_2 + 4OH^- \tag{18}$$

$$Fe^{2+} + 2OH^- = Fe(OH)_2(s) \tag{19}$$

In general, oxygen may compete for the available sites and electrons of iron with contaminants like Cr(VI) and reduce the efficiency of the electron. On the other hand, the desired concentration of DO stimulated the generation of soluble Fe^{2+} and promoted the elimination of pollutants (Qin et al., 2016a).

The Fe^{2+} was stable under acidic conditions in the presence of oxygen but could easily be oxidized by oxygen under alkaline conditions. The reaction kinetics of Fe^{2+} with Cr(VI) under pH 2.0 was higher than those under pH 6.0 for two orders of magnitude (Fendorf et al., 1996; Lewis, 1997; Rivero-Huguet et al., 2010). Thus the Fe^{2+} predominated the redox reaction with Cr(VI) under acidic solution in the presence of oxygen. To further demonstrate the role of Fe^{2+} on Cr(VI) removal under acid/anaerobic solution, 1,10-phenanthroline was introduced as a populated indicator for Fe^{2+} into Cr(VI)/Fe^0 system to complexes strongly with Fe^{2+}. Hence, the availability of Fe^{2+} to Cr(VI) was inhibited, and the results indicated that the removal of Cr(VI) was substantially suppressed in the presence of 1,10-phenanthroline (Shao et al., 2018). Similar reports were also supported this idea by adding 1, 10-phenanthroline to isolate Fe^{2+} from acid/anaerobic aqueous solution (Lan et al., 2006; Zhang et al., 2019d; Zhou et al., 2008). The generated Fe^{2+} abound in bulk solution which verified by the results that removal rate of Cr(VI) impeded after introducing 1,10-phenanthroline complex. Notably, the data from several sources have identified that the increase in removal performance of Cr(VI) resulted from the produced Fe^{2+} under oxic solution that associated with the Fe^0 surface-bound with Fe^{2+}, not just the free Fe^{2+} in bulk solution (Mu et al., 2015b; Shao et al., 2018).

The reduction product of Fe^0 in Cr(VI) solution favors the formation of the γ-FeOOH or α-FeOOH over α-Fe_2O_3 or γ-Fe_2O_3 (Astrup et al., 2000; Manning et al., 2007; Pratt et al., 1997). Whereas the iron oxyhydroxides (goethite and lepidocrocite) had shown relatively high specific surface, and the reduced Cr(III) could easily be adsorbed on them (Komárek et al., 2013). The iron oxyhydroxides incorporated with Cr (III) could further transform to sparingly soluble $Cr_xFe_{1-x}(OH)_3$ (Li et al., 2008; Mu et al., 2015a). This claim has been accomplished by many researchers (Gheju et al., 2011; Liu et al., 2016; Yoon et al., 2011). Briefly, it was found that the product was different under oxic and anoxic conditions of Fe^0/Cr(VI) setup, meanwhile, the removal efficiency under oxic was much better than those under anoxic conditions. The porosity of the $FeCr_2O_4$ layer was predominantly covered by iron under oxic/acidic conditions, while the compact layer of hydroxide/oxyhydroxides of Fe(III) and Cr(III) was produced under anoxic/acid condition. The redox product of $FeCr_2O_4$ under oxic/acid conditions substantially coincided with the product of Fe^{2+} and Cr(VI) (He et al., 2004). It can be concluded that the governing mechanism for Cr(VI) removal by iron under oxic/acid conditions was due to the generation of Fe^{2+} from iron with oxygen and then reacted with Cr(VI).

A recent study concluded a converse view that $FeCr_2O_4$ was formed under anoxic/acid condition, while the iron/chromium oxyhydroxides appeared in the presence of oxygen under acid condition, nevertheless, the presence of oxygen impaired the removal rate of Cr(VI) by iron (Zhang et al., 2018). The most likely cause of either positive effect or negative effect of DO on Cr(VI) removal under acid condition was the transformation of redox product of Fe^0/Cr(VI) with DO concentration. Typically, the desired amount of oxygen could accelerate the corrosion of iron and the generation of reductant Fe^{2+} accompanied with reserved protons depletion, and the Cr(VI)/Fe^{2+}(aq) and Cr(VI)/Fe^{2+}(s) (bounded on Fe^0) couples could generate loose $FeCr_2O_4$. Adversely, the excess oxygen could deteriorate the effectiveness of iron through further oxidation of Fe^{2+} to Fe^{3+} by Fenton reaction (Ai et al., 2013), and the consumed protons could produce compact $Cr_xFe_{1-x}(OH)_3$, simultaneously. Thus, more efforts are required to find the exact critical value of DO concentration. Previous studies about oxygen influence did not focus on its concentration in solution, and most of the attempts were made to compare the aerobic and anaerobic by aeration with oxygen or nitrogen gas (Diao et al., 2016; Jeen et al., 2008). Further, the passivation layer composed of hydroxide/oxyhydroxides of Fe(III)/Cr(III) on the surface of iron hindered the electrons transfer from iron to Cr(VI) under over oxygen content (Sun et al., 2016). The shielding effect of the passivation layer formed in the presence of oxygen is evidenced (Mu et al., 2015b).

Altogether, the effect of DO on Cr(VI) removal by ZVI was not only dependent on solution pH but also relied on its concentration. It could be divided into the following five pathways: (1) The important intermediate reducing agent Fe^{2+} that originates from Fe^0 contributed to the elimination of Cr(VI) under lower DO and acidic conditions; (2) the higher value of DO under acid conditions could oxidize immoderately Fe^{2+} to Fe^{3+} and weaken the electron efficiency of Fe^0; (3) under anaerobic/acid conditions, the protons accelerated the erosion of Fe^0 and the produced Fe^{2+} could participate in the reduction of Cr(VI); (4) Due to the instability of Fe^{2+} under aerobic/alkaline conditions and the generated compact precipitate covered on the Fe^0, and the durability of Fe^0 deteriorated accordingly; (5) The Fe^0 and the produced Fe^{2+} both were involved in the reduction of Cr(VI) in the deficiency of DO under alkaline conditions, which improved the removal efficiency of Cr(VI). The specific information about the co-effect between DO and pH is shown in Table 3.

4. Practical applications of ZVI-based materials

Since it was reported in 1925, permeable reactive barrier (PRB) is attracting a lot of interest in the remediation of groundwater pollutants such as organic matters, heavy metals, inorganic matters (Blowes et al., 2000; Rhodes et al., 1925). It was recorded in 2009 that there were 13 full-scale PRB present worldwide. From them, 6 PRBs were equipped with ZVI as reactive media (ITRC, 2011). It was observed that field-scale PRB are operated under more complicated conditions as compare to the laboratory-scale, such as they face fairly slow flow, low dissolved oxygen, relatively high pH value, lower temperature, low contaminants

Table 3
The co-effect of DO and pH on Cr(VI) removal by iron.

Operation conditions	Aerobic/acid		Anaerobic/acid
	Low DO	High DO	
Effect	Strengthen	Deteriorate	Strengthen
Mechanism	$2Fe^0 + O_2 + 4H^+ = 2Fe^{2+} + 2H_2O$ $Fe^0 + HCrO_4^- + 7H^+ = Fe^{3+} + Cr^{3+} + 4H_2O$ $Fe^{2+} + HCrO_4^- + 7H^+ = Fe^{3+} + Cr^{3+} + 4H_2O$	$4Fe^0 + 3O_2 + 12H^+ = 4Fe^{3+} + 6H_2O$	$Fe^0 + 2H^+ = Fe^{2+} + H_2$ $3Fe^{2+} + HCrO_4^- + 7H^+ = 3Fe^{3+} + Cr^{3+} + 4H_2O$ $Fe^0 + HCrO_4^- + 7H^+ = Fe^{3+} + Cr^{3+} + 4H_2O$
Operation conditions	Aerobic/alkaline		Anaerobic/alkaline
Effect	Deteriorate		Strengthen
Mechanism	$2Fe^0 + 2H_2O + O_2 = 2Fe^{2+} + 4OH^-$ $4Fe^{2+} + O_2 + 2H_2O = 4Fe^{3+} + 4OH^-$		$Fe^0 + 4H_2O = Fe^{2+} + 2H_2 + 4OH^-$ $Fe^0 + CrO_4^{2-} + 2H_2O = Fe^{3+} + Cr^{3+} + 4OH^-$ $3Fe^{2+} + CrO_4^{2-} + 4H_2O = 3Fe^{3+} + Cr^{3+} + 8OH^-$

concentration, and a range of inorganic anions like CO_3^{2-}, SO_4^{2-}, NO_3^- (Cundy et al., 2008; Obiri-Nyarko et al., 2014). In the laboratory studies, the principal mechanism for Cr(VI) removal by ZVI-PRB was presumed to be the redox reaction between Cr(VI) and Fe^0, which could be undermined by the formation of insoluble Fe(III)/Cr(III) (oxy) hydroxides phase (Blowes et al., 1997). While the removal process for Cr(VI) under field sites would be uncertain owning to the other competitive ions. In general, more attempts are needed to transfer laboratory-based theory to field-scale application.

Longevity and reactivity are the two major considerations in the long-term operation capability of PRB (Wilkin et al., 2003). An early example of research into the reactivity of ZVI PRB has demonstrated that the intensively reducing process and high pH value could be associated with the diminish of reactive media due to the precipitation of inorganic species, which consequently clogged the permeable pore of PRB (Phillips et al., 2003). Further, about 0.88% per year decline in porosity of ZVI PRB was noticed, which has demonstrated the loss of carbonates (90%), calcium (82%), and sulfate (69%) in groundwater flow through the PRB (Lai et al., 2006). Moreover, the column experiments with various groundwater geochemistry for sequestration Cr(VI) through ZVI were also investigated to elucidate the effects of hardness and carbonate on Cr(VI) removal by ZVI in groundwater, and their results indicated that the capability of ZVI dropped slightly in the presence of calcium hardness. Notably, the Cr(VI) removal capacity of ZVI decreased by 17% under magnesium solution. Further, it was found that a 33% decrease in ZVI performance was noticed in the co-present of hardness and carbonate in columns (Lo et al., 2006). Similar research implied the bicarbonate gave the mildest impact on Cr(VI) removal by ZVI compared to calcium, magnesium ions, whereas bicarbonate together with calcium posted the greatest impact on ZVI efficiency for Cr(VI) removal (Lai et al., 2008). On the other hand, not all deposits on the barrier are unfavorable for the reactivity of ZVI media, the ferrous precipitates like magnetite and green rust could transfer electrons from ZVI to pollutants (Ritter et al., 2002; Roh et al., 2000). Thus it can be assumed that the permeability of PRB could drop gradually due to the formation of precipitate on the surface of ZVI particles, but the reactivity of ZVI could either reduce or enhance with time, which can be correlated with the geochemical conditions of groundwater like DO and pH.

The longevity of ZVI PRB could be referred to as its potential to maintain the reactivity of filling media and hydraulic performance, while the hydraulic performance was related to the residence time of plume pass through the barrier (Carniato et al., 2012). Construction methods, reactive material, and groundwater constituents affected the life cycle of PRB. The data from several sources have identified that the trench-based construction method showed significant remediation capacity of Cr(VI) compared to the caisson-based construction method. Notably, the ZVI and iron oxide-coated sand could reduce the environmental impact on PRB. Natural organic matters (NOM) in groundwater could lower the PRB capability due to the depletion of the higher amount of ZVI (Mak et al., 2011). For instance, no significant reduction in the performance of PRB was observed even after continuous operation for 13 years (Puls et al., 1999; Wilkin et al., 2005).

In contrast, a significant fluctuation in the removal performance of Cr(VI) was reported after the operation of one year (Bronstein et al., 2005). Thus, It has been presumed that the uneven depletion of ZVI in plume could decline the longevity in the PRB over time (Henderson et al., 2007). Apart from the study aimed at the construction method, groundwater constituents, and media reactivity, more comprehensive hydrology of groundwater should be examined. Therefore, the contaminants concentration distribution and flow velocity changes should be taken into account for PRB design and installation. Besides the bare ZVI used for PRB reactive media, the ZVI-based materials like S-nZVI and nZVI-SBA-15 have been developed as the substitute material for Cr (VI) isolation in groundwater at pilot-scale or field trials (Fu et al., 2015b; Sun et al., 2014). Compared to single ZVI, ZVI-based materials could prevent the reactivity loss of nZVI that results from congregating. Various surveys have shown that the permeable reactive columns filled with activated carbon fiber supported nZVI have exhibited a higher Cr (VI) removal efficiency (Qu et al., 2017). Therefore, more research efforts are needed for shifting ZVI-based materials PRB from laboratory-based data to practical implantation.

Moreover, the injection well technology is another most used method excluding PRB technology for groundwater remediation (Mueller et al., 2012). The media particles were prepared as slurry before injecting into the polluted source sites or plume, in which the extensively utilized media are ZVI and bimetallic particles of iron (Cundy et al., 2008). Remarkably, the Cr(VI) concentration declined substantially from 4 to 8 to 0.015 mg/L by employing a composite of ferrous sulfate (Fe_2SO_4) combined with sodium dithionite ($Na_2S_2O_4$) as the reactive media in the injection well (Ludwig et al., 2007). Sodium dithionite could prevent the premature oxidization of Fe^{2+}, and could prevent the clogging of injected media, and maintained effective hydraulic conductivity. Similarly, an over 96% degradation ratio of TCE was noticed by injecting bimetallic particles of Fe–Pd gravitationally into the groundwater (Elliott et al., 2001). The particles were supplied at an optimal rate, which presented ideal mobility and diffusion. However, the in-site remediation cases all required the ZVI-based materials prepared on the spot. Such as, the CMC-stabilized Fe–Pd composite was synthesized on the site through liquid reduction right before injection into the wells to minimize the reactivity loss of filling material (He et al., 2010). Thus, the transport, storage, and cost of the raw materials are the potential impediments. Besides, long-term activity, persistence, and dispersion of ZVI-based materials, the stability and mobility of the treated contaminants both entail the advanced, easy-synthesis, and low-cost ZVI-based materials (He et al., 2007; Kocur et al., 2016; Yang et al., 2020).

5. Barriers in market penetration of ZVI-Based materials for Cr (VI) removal

From the acquisition of raw material, the preparation and performance evaluation of ZVI-based materials from laboratory-scale to commercial applications, the barriers in market penetration are remained mainly attributed to the technology challenges, toxicity assessment to ecosystems, and the cost. The performance of ZVI-based materials in field trials or full-scale applications is rarely documented excluding nZVI. A pilot-scale in-situ remediation test was conducted with commercially available nZVI at Kortan in Hradek nad Nisou. It was found that the concentration of Cr(VI) and total chromium in groundwater were substantially decreased after injecting nZVI with no observed effect on groundwater properties (Němeček et al., 2014). While, a lot of laboratory-based data has supported that template-supported nZVI or modified nZVI could prevent the agglomeration of the nZVI particles and impair non-target reactions (Dong et al., 2017b; Hu et al., 2019). However, the longevity, reactivity, and removal mechanism of ZVI-based materials for field scale Cr(VI) remediation are still unclear and act as an obstacle to the market penetration of this technology. The unintentional migration of nZVI through the soil, water, and air can threaten the ecosystem, especially plants, animals, and microorganisms' cells (Lefevre et al., 2016; Xue et al., 2018). Thus, the toxicological effects of nZVI on organisms should be addressed in future research (Brasili et al., 2020; El-Temsah et al., 2012). In the commercial application cases of ZVI, some companies prepared ZVI suspension with organic additives and dispersants to promote diffusion and delivery of ZVI. However, more organic additives are needed in terms of nZVI for the higher surface area and smaller particle size (Mueller et al., 2012). There would be more regulation considerations on the organic additives and dispersants to the ecosystem. Due to the presence of aggregation of nZVI in the subsurface environment, the nZVI has shown inferior migration than surface-modified nZVI, It was found that the migration of nZVI could be enhanced significantly after coated with starch and polyacrylic acid (Dong et al., 2016). However, the potential environmental risks of ZVI-based materials are still unknown. Hence strategies to balance the potential environmental risks and expected environmental interests of ZVI-based materials would be required in clarifying the migration and toxicological impacts at specific sites. Further, as can be seen in Table 4, the demand amount of ZVI for a project was so high. Given price was $0.55–15/lbs for ZVI from 325 μm to below 1 μm. It's a comparative high expenditure for the ZVI during the remediation project. Compared to ZVI produced directly from the smelter, the ZVI derived from scrap iron and recycled material could lower the expenses remarkably. Regarding the sparing information about the actual cost for producing ZVI-based materials like sulfur-ZVI, Cu-ZVI, AC-ZVI, it's urgent to evaluate the cost for the synthesis of ZVI-based materials with scrap iron.

6. Conclusions

Altogether, the ZVI-based materials have been well-recognized and comprehensively employed for pollutants sequestration. This review has discussed four conventional ZVI-based materials (ZVI-AC/biochar, ZVI-sulfur, ZVI-magnetite, and bimetal of ZVI), two prevailing preparation methods (liquid reduction method and mechanical ball milling procedure), and their applications for Cr(VI) removal. The removal mechanisms have mainly involved the reduction, adsorption, and co-precipitation. Besides, the developed performance of ZVI-based materials regarding the pristine ZVI could be attributed to the galvanic cell effect for ZVI-AC/biochar and bimetals of ZVI, and the regeneration of ferrous ions for sulfur-ZVI and magnetite-ZVI. Especially, the electron selectivity of ZVI to Cr(VI) was substantially controlled by the DO and pH of the solution. One of the most significant findings of this review is that the transfer of electrons from ZVI to Cr(VI) was appreciably dominated by five pathways. Briefly, the acidic/low oxygen condition facilitated the removal capacity of ZVI by generating more reductants, and the removal efficiency of ZVI on Cr(VI) was suppressed under acidic/oxygen-rich conditions due to the over-exhaustion of iron by oxygen, conversely. On the other hand, acidic/anaerobic conditions promoted the Cr(VI) removal through accelerating ZVI hydrogen-evolution erosion, and the erosion product aqueous ferrous ions were an effective reducing agent. The Cr(VI) removal rate was deteriorated under alkaline/aerobic conditions due to the more susceptible oxidation of Fe^{2+} by oxygen under alkaline conditions compared to acid conditions. The last pathway of DO and pH on iron capability under alkaline/anaerobic was that the produced Fe^{2+} contributed to the reduction of Cr(VI), which improved the removal efficiency of Cr(VI). The insights gained from this study may assist in groundwater remediation through PRB. Limited PRB field applications overlooked to consider the distribution of Cr(VI) concentration and flow velocity gradient in groundwater, which could help in optimizing the PRB dimension and avoid the uneven loss of ZVI media. More information on technology challenges, potential ecosystem risk, and cost of ZVI-based materials would help us to establish a greater degree of accuracy on the commercialization of this technology. The following are the key suggestions for future applications of ZVI-based materials:

- The selection of suitable ZVI-based materials is needed to reduce the unintentional consumption of ZVI by O_2, water, or other untargeted pollutants
- The solution chemistry of contaminated sites should be vigilantly evaluated because the utilization efficiency and selectivity to the aimed contaminants of ZVI in ZVI-based materials is greatly affected by pH and DO
- The large-scale and low-cost production of ZVI-based materials is necessary. Although many ZVI-based materials have shown superior performance at the laboratory-scale or pilot stage, the practical performance is rarely available, like the PRB of ZVI-based materials
- Migration and toxicology of ZVI-based materials in the aquatic environment or soil are the potential ecological risk, thus the treated sites with ZVI-based materials would require long-term monitoring, and the used ZVI-based materials should be disposed of safely.

Table 4
ZVI remediation cases and the consumption (https://hepure.com/product-list/case-studies/).

Site background	Contaminant	Mode of application	In-situ or ex-situ	Dosage
Vadose zone soils beneath a large manufacturing facility	Cr(VI)	Hydraulic injection	In-situ	64,000 lbs
The facility had operated for 50 years as a machine shop where parts were degreased by a variety of solvents	PCE[a], TCE	PRB and injection	In-situ	154,000 lbs
Former Dry Cleaner	PCE	Injection	In-situ	401,310 lbs
Located in North Central Ohio	PCE, TCE, and VC[b]	Injection	In-situ	145,000 lbs

[a] Tetrachloroethene.

[b] Vinyl Chloride.

Declaration of competing interest

The authors declare that they have no known competing financial interests or personal relationships that could have appeared to influence the work reported in this paper.

Acknowledgments

This work was financially supported from CONACYT (Consejo Nacional de Ciencia y Tecnología de Mexico) project (No. 900339), the Technology Innovation Project of Zhaoqing (201904030103) and the Guangdong College Students' Innovative Project (pdjh2021b0538, X201910580158).

References

Ai, Z., Gao, Z., Zhang, L., He, W., Yin, J.J., 2013. Core–shell structure dependent reactivity of Fe@ Fe2O3 nanowires on aerobic degradation of 4-chlorophenol. Environ. Sci. Technol. 47 (10), 5344–5352.

Al-Othman, Z.A., Ali, R., Naushad, M., 2012. Hexavalent chromium removal from aqueous medium by activated carbon prepared from peanut shell: adsorption kinetics, equilibrium and thermodynamic studies. Chem. Eng. J. 184, 238–247.

Alidokht, L., Khataee, A.R., Reyhanitabar, A., Oustan, S., 2011. Reductive removal of Cr (VI) by starch-stabilized Fe0 nanoparticles in aqueous solution. Desalination 270 (1), 105–110.

Alowitz, M.J., Scherer, M.M., 2002. Kinetics of nitrate, nitrite, and Cr(VI) reduction by iron metal. Environ. Sci. Technol. 36 (3), 299–306.

Ambika, S., Devasena, M., Nambi, I.M., 2016. Synthesis, characterization and performance of high energy ball milled meso-scale zero valent iron in Fenton reaction. J. Environ. Manag. 181, 847–855.

Ambika, S., Devasena, M., Nambi, I.M., 2020. Single-step removal of Hexavalent chromium and phenol using meso zerovalent iron. Chemosphere 248, 125912.

Astrup, T., Stipp, S.L.S., Christensen, T.H., 2000. Immobilization of chromate from coal fly ash leachate using an attenuating barrier containing zero-valent iron. Environ. Sci. Technol. 34 (19), 4163–4168.

Bae, S., Yoon, S., Kaplan, U., Kim, H., Han, S., Lee, W., 2020. Effect of groundwater ions (Ca2+, Na+, and HCO3−) on removal of hexavalent chromium by Fe(II)-phosphate mineral. J. Hazard Mater. 398, 122948.

Baikousi, M., Bourlinos, A.B., Douvalis, A., Bakas, T., Anagnostopoulos, D.F., Tuček, J., Šafářová, K., Zboril, R., Karakassides, M.A., 2012. Synthesis and characterization of γ-Fe2O3/carbon hybrids and their application in removal of hexavalent chromium ions from aqueous solutions. Langmuir 28 (8), 3918–3930.

Bavasso, I., Verdone, N., Di Palma, L., 2018. Cr (VI) removal by green-synthetized iron-based nanoparticles: effect of Cr (VI) concentration and pH condition on adsorption process. Chem. Eng. Trans. 70, 469–474.

Bencheikh-Latmani, R., Obraztsova, A., Mackey, M.R., Ellisman, M.H., Tebo, B.M., 2007. Toxicity of Cr(III) to shewanella sp. strain MR-4 during Cr(VI) reduction. Environ. Sci. Technol. 41 (1), 214–220.

Blowes, D.W., Ptacek, C.J., Benner, S.G., McRae, C.W., Bennett, T.A., Puls, R.W., 2000. Treatment of inorganic contaminants using permeable reactive barriers. J. Contam. Hydrol. 45 (1–2), 123–137.

Blowes, D.W., Ptacek, C.J., Jambor, J.L., 1997. In-situ remediation of Cr (VI)-contaminated groundwater using permeable reactive walls: laboratory studies. Environ. Sci. Technol. 31 (12), 3348–3357.

Brasili, E., Bavasso, I., Petruccelli, V., Vilardi, G., Valletta, A., Bosco, C.D., Gentili, A., Pasqua, G., Di Palma, L., 2020. Remediation of hexavalent chromium contaminated water through zero-valent iron nanoparticles and effects on tomato plant growth performance. Sci. Rep. 10 (1), 1920.

Bronstein, K.J.N.N.o.E.M.S.F., 2005. Permeable Reactive Barriers for Inorganic and Radionuclide Contamination.

Cao, Z., Liu, X., Xu, J., Zhang, J., Yang, Y., Zhou, J., Xu, X., Lowry, G.V., 2017. Removal of antibiotic florfenicol by sulfide-modified nanoscale zero-valent iron. Environ. Sci. Technol. 51 (19), 11269–11277.

Carniato, L., Schoups, G., Seuntjens, P., Van Nooten, T., Simons, Q., Bastiaens, L., 2012. Predicting longevity of iron permeable reactive barriers using multiple iron deactivation models. J. Contam. Hydrol. 142–143, 93–108.

Chatterjee, S., Mahanty, S., Das, P., Chaudhuri, P., Das, S., 2020. Biofabrication of iron oxide nanoparticles using manglicolous fungus Aspergillus Niger BSC-1 and removal of Cr (VI) from aqueous solution. Chem. Eng. J. 385, 123790.

Cheng, Z., Fu, F., Dionysiou, D.D., Tang, B., 2016. Adsorption, oxidation, and reduction behavior of arsenic in the removal of aqueous As(III) by mesoporous Fe/Al bimetallic particles. Water Res. 96, 22–31.

Cho, H.-H., Lee, T., Hwang, S.-J., Park, J.-W., 2005. Iron and organo-bentonite for the reduction and sorption of trichloroethylene. Chemosphere 58 (1), 103–108.

Choi, C.J., Dong, X.L., Kim, B.K., 2001. Characterization of Fe and Co nanoparticles synthesized by chemical vapor condensation. Scripta Mater. 44 (8), 2225–2229.

Choi, C.J., Tolochko, O., Kim, B.K., 2002. Preparation of iron nanoparticles by chemical vapor condensation. Mater. Lett. 56 (3), 289–294.

Choi, K., Lee, W., 2012. Enhanced degradation of trichloroethylene in nano-scale zero-valent iron Fenton system with Cu(II). J. Hazard Mater. 211–212, 146–153.

Cissoko, N., Zhang, Z., Zhang, J., Xu, X., 2009. Removal of Cr(VI) from simulative contaminated groundwater by iron metal. Process Saf. Environ. Protect. 87 (6), 395–400.

Coelho, F.d.S., Ardisson, J.D., Moura, F.C.C., Lago, R.M., Murad, E., Fabris, J.D., 2008. Potential application of highly reactive Fe(0)/Fe3O4 composites for the reduction of Cr(VI) environmental contaminants. Chemosphere 71 (1), 90–96.

Crane, R.A., Scott, T.B., 2012. Nanoscale zero-valent iron: future prospects for an emerging water treatment technology. J. Hazard Mater. 211–212, 112–125.

Crean, D.E., Coker, V.S., van der Laan, G., Lloyd, J.R., 2012. Engineering biogenic magnetite for sustained Cr(VI) remediation in flow-through systems. Environ. Sci. Technol. 46 (6), 3352–3359.

Cronje, K., Chetty, K., Carsky, M., Sahu, J., Meikap, B., 2011. Optimization of chromium (VI) sorption potential using developed activated carbon from sugarcane bagasse with chemical activation by zinc chloride. Desalination 275 (1–3), 276–284.

Cundy, A.B., Hopkinson, L., Whitby, R.L.D., 2008. Use of iron-based technologies in contaminated land and groundwater remediation: a review. Sci. Total Environ. 400 (1), 42–51.

Dai, Y., Hu, Y., Jiang, B., Zou, J., Tian, G., Fu, H., 2016. Carbothermal synthesis of ordered mesoporous carbon-supported nano zero-valent iron with enhanced stability and activity for hexavalent chromium reduction. J. Hazard Mater. 309, 249–258.

Decyk, P., Trejda, M., Ziolek, M., Kujawa, J., Głaszczka, K., Bettahar, M., Monteverdi, S., Mercy, M., 2003. Physicochemical and catalytic properties of iron-doped silica—the effect of preparation and pretreatment methods. J. Catal. 219 (1), 146–155.

Devlin, J.F., Klausen, J., Schwarzenbach, R.P., 1998. Kinetics of nitroaromatic reduction on granular iron in recirculating batch experiments. Environ. Sci. Technol. 32 (13), 1941–1947.

Diao, Z.-H., Xu, X.-R., Chen, H., Jiang, D., Yang, Y.-X., Kong, L.-J., Sun, Y.-X., Hu, Y.-X., Hao, Q.-W., Liu, L., 2016. Simultaneous removal of Cr(VI) and phenol by persulfate activated with bentonite-supported nanoscale zero-valent iron: reactivity and mechanism. J. Hazard Mater. 316, 186–193.

Dong, H., Deng, J., Xie, Y., Zhang, C., Jiang, Z., Cheng, Y., Hou, K., Zeng, G., 2017a. Stabilization of nanoscale zero-valent iron (nZVI) with modified biochar for Cr (VI) removal from aqueous solution. J. Hazard Mater. 332, 79–86.

Dong, H., Deng, J., Xie, Y., Zhang, C., Jiang, Z., Cheng, Y., Hou, K., Zeng, G., 2017b. Stabilization of nanoscale zero-valent iron (nZVI) with modified biochar for Cr(VI) removal from aqueous solution. J. Hazard Mater. 332, 79–86.

Dong, H., He, Q., Zeng, G., Tang, L., Zhang, C., Xie, Y., Zeng, Y., Zhao, F., Wu, Y., 2016. Chromate removal by surface-modified nanoscale zero-valent iron: effect of different surface coatings and water chemistry. J. Colloid Interface Sci. 471, 7–13.

Dong, T., Luo, H., Wang, Y., Hu, B., Chen, H., 2011. Stabilization of Fe–Pd bimetallic nanoparticles with sodium carboxymethyl cellulose for catalytic reduction of para-nitrochlorobenzene in water. Desalination 271, 11–19.

Du, J., Bao, J., Fu, X., Lu, C., Kim, S.H., 2016. Mesoporous sulfur-modified iron oxide as an effective Fenton-like catalyst for degradation of bisphenol A. Appl. Catal. B Environ. 184, 132–141.

El-Temsah, Y.S., Joner, E.J., 2012. Ecotoxicological effects on earthworms of fresh and aged nano-sized zero-valent iron (nZVI) in soil. Chemosphere 89 (1), 76–82.

Elliott, D.W., Zhang, W.-x., 2001. Field assessment of nanoscale bimetallic particles for groundwater treatment. Environ. Sci. Technol. 35 (24), 4922–4926.

Englehardt, J.D., Meeroff, D.E., Echegoyen, L., Deng, Y., Raymo, F.M., Shibata, T., 2007. Oxidation of aqueous EDTA and associated organics and coprecipitation of inorganics by ambient iron-mediated aeration. Environ. Sci. Technol. 41 (1), 270–276.

Fan, D., Lan, Y., Tratnyek, P.G., Johnson, R.L., Filip, J., O'Carroll, D.M., Nunez Garcia, A., Agrawal, A., 2017. Sulfidation of iron-based materials: a review of processes and implications for water treatment and remediation. Environ. Sci. Technol. 51 (22), 13070–13085.

Fan, D., O'Brien Johnson, G., Tratnyek, P.G., Johnson, R.L., 2016. Sulfidation of nano zerovalent iron (nZVI) for improved selectivity during in-situ chemical reduction (ISCR). Environ. Sci. Technol. 50 (17), 9558–9565.

Fan, H., Ren, H., Ma, X., Zhou, S., Huang, J., Jiao, W., Qi, G., Liu, Y., 2020. High-gravity continuous preparation of chitosan-stabilized nanoscale zero-valent iron towards Cr (VI) removal. Chem. Eng. J. 390, 124639.

Fang, Z., Qiu, X., Huang, R., Qiu, X., Li, M., 2011. Removal of chromium in electroplating wastewater by nanoscale zero-valent metal with synergistic effect of reduction and immobilization. Desalination 280 (1), 224–231.

Fang, Yi., Yang, Ke., Zhang, Y., Peng, C., Robledo-Cabrera, A., López-Valdivieso, A., 2021. Highly surface activated carbon to remove Cr(VI) from aqueous solution with adsorbent recycling. Environ. Res. 197, 111151.

Fazlzadeh, M., Rahmani, K., Zarei, A., Abdoallahzadeh, H., Nasiri, F., Khosravi, R., 2017. A novel green synthesis of zero valent iron nanoparticles (NZVI) using three plant extracts and their efficient application for removal of Cr(VI) from aqueous solutions. Adv. Powder Technol. 28 (1), 122–130.

Fendorf, S.E., Li, G., 1996. Kinetics of chromate reduction by ferrous iron. Environ. Sci. Technol. 30 (5), 1614–1617.

Fennelly, J.P., Roberts, A.L., 1998. Reaction of 1,1,1-trichloroethane with zero-valent metals and bimetallic reductants. Environ. Sci. Technol. 32 (13), 1980–1988.

Flury, B., Frommer, J., Eggenberger, U., Mäder, U., Nachtegaal, M., Kretzschmar, R., 2009. Assessment of long-term performance and chromate reduction mechanisms in a field scale permeable reactive barrier. Environ. Sci. Technol. 43 (17), 6786–6792.

Fu, Cheng, Z., Dionysiou, D.D., Tang, B., 2015a. Fe/Al bimetallic particles for the fast and highly efficient removal of Cr(VI) over a wide pH range: performance and mechanism. J. Hazard Mater. 298, 261–269.

Fu, Yang, Y., Xu, Z., Zhang, X., Guo, X., Bi, D., 2015b. The removal of chromium (VI) and lead (II) from groundwater using sepiolite-supported nanoscale zero-valent iron (S-NZVI). Chemosphere 138, 726–734.

Fu, F., Han, W., Tang, B., Hu, M., Cheng, Z., 2013. Insights into environmental remediation of heavy metal and organic pollutants: simultaneous removal of hexavalent chromium and dye from wastewater by zero-valent iron with ligand-enhanced reactivity. Chem. Eng. J. 232, 534–540.

Gheju, M., 2011. Hexavalent chromium reduction with zero-valent iron (ZVI) in aquatic systems. Water, Air, Soil Pollut. 222 (1), 103–148.

Gheju, M., Balcu, I., 2011. Removal of chromium from Cr(VI) polluted wastewaters by reduction with scrap iron and subsequent precipitation of resulted cations. J. Hazard Mater. 196, 131–138.

Giasuddin, A.B.M., Kanel, S.R., Choi, H., 2007. Adsorption of humic acid onto nanoscale zerovalent iron and its effect on arsenic removal. Environ. Sci. Technol. 41 (6), 2022–2027.

Glavee, G.N., Klabunde, K.J., Sorensen, C.M., Hadjipanayis, G.C., 1995. Chemistry of borohydride reduction of iron(II) and iron(III) ions in aqueous and nonaqueous media. Formation of nanoscale Fe, FeB, and Fe2B powders. Inorg. Chem. 34 (1), 28–35.

Gorski, C.A., Nurmi, J.T., Tratnyek, P.G., Hofstetter, T.B., Scherer, M.M., 2010. Redox behavior of magnetite: implications for contaminant reduction. Environ. Sci. Technol. 44 (1), 55–60.

Gu, Y., Gong, L., Qi, J., Cai, S., Tu, W., He, F., 2019. Sulfidation mitigates the passivation of zero valent iron at alkaline pHs: experimental evidences and mechanism. Water Res. 159, 233–241.

Gu, Y., Wang, B., He, F., Bradley, M.J., Tratnyek, P.G., 2017. Mechanochemically sulfidated microscale zero valent iron: pathways, kinetics, mechanism, and efficiency of trichloroethylene dechlorination. Environ. Sci. Technol. 51 (21), 12653–12662.

Guan, X., Dong, H., Ma, J., Lo, I.M.C., Dou, X., 2011. Performance and mechanism of simultaneous removal of chromium and arsenate by Fe(II) from contaminated groundwater. Separ. Purif. Technol. 80 (1), 179–185.

Gunawardana, B., Singhal, N., Swedlund, P., 2011. Degradation of chlorinated phenols by zero valent iron and bimetals of iron: a review. Environ. Eng. Res. 16 (4), 187–203.

Gupta, V., Agarwal, S., Saleh, T.A., 2011. Chromium removal by combining the magnetic properties of iron oxide with adsorption properties of carbon nanotubes. Water Res. 45 (6), 2207–2212.

Han, Y., Yan, W., 2016. Reductive dechlorination of trichloroethene by zero-valent iron nanoparticles: reactivity enhancement through sulfidation treatment. Environ. Sci. Technol. 50 (23), 12992–13001.

He, Y.T., Chen, C.C., Traina, S.J., 2004. Inhibited Cr(VI) reduction by aqueous Fe(II) under hyperalkaline conditions. Environ. Sci. Technol. 38 (21), 5535–5539.

He, Lin, H., Luo, M., Liu, J., Dong, Y., Li, B., 2020a. Highly efficient remediation of groundwater co-contaminated with Cr(VI) and nitrate by using nano-Fe/Pd bimetal-loaded zeolite: process product and interaction mechanism. Environ. Pollut. 263, 114479.

He, Min, X., Peng, T., Zhao, F., Ke, Y., Wang, Y., Jiang, G., Xu, Q., Wang, J., 2020b. Mechanochemically activated microsized zero-valent iron/pyrite composite for effective hexavalent chromium sequestration in aqueous solution. J. Chem. Eng. Data 65 (4), 1936–1945.

He, F., Zhao, D., 2007. Manipulating the size and dispersibility of zerovalent iron nanoparticles by use of carboxymethyl cellulose stabilizers. Environ. Sci. Technol. 41 (17), 6216–6221.

He, F., Zhao, D., Paul, C., 2010. Field assessment of carboxymethyl cellulose stabilized iron nanoparticles for in situ destruction of chlorinated solvents in source zones. Water Res. 44 (7), 2360–2370.

He, Y., Sun, H., Liu, W., Yang, W., Lin, A., 2018. Study on removal effect of Cr(VI) and surface reaction mechanisms by bimetallic system in aqueous solution. Environ. Technol. 1–23.

He, Y.T., Traina, S.J., 2005. Cr(VI) reduction and immobilization by magnetite under alkaline pH Conditions: the role of passivation. Environ. Sci. Technol. 39 (12), 4499–4504.

Henderson, A.D., Demond, A.H., 2007. Long-term performance of zero-valent iron permeable reactive barriers: a critical review. Environ. Eng. Sci. 24 (4), 401–423.

Hoch, L.B., Mack, E.J., Hydutsky, B.W., Hershman, J.M., Skluzacek, J.M., Mallouk, T.E., 2008. Carbothermal synthesis of carbon-supported nanoscale zero-valent iron particles for the remediation of hexavalent chromium. Environ. Sci. Technol. 42 (7), 2600–2605.

Hu, C.Y., Lo, S.L., Liou, Y.H., Hsu, Y.W., Shih, K., Lin, C.J., 2010. Hexavalent chromium removal from near natural water by copper-iron bimetallic particles. Water Res. 44 (10), 3101–3108.

Hu, Y.-b., Zhang, M., Li, X.-y., 2019. Improved longevity of nanoscale zero-valent iron with a magnesium hydroxide coating shell for the removal of Cr(VI) in sand columns. Environ. Int. 133, 105249.

Huang, D., Wang, G., Shi, Z., Li, Z., Kang, F., Liu, F., 2017. Removal of hexavalent chromium in natural groundwater using activated carbon and cast iron combined system. J. Clean. Prod. 165, 667–676.

Huang, L., Zhou, S., Jin, F., Huang, J., Bao, N., 2014. Characterization and mechanism analysis of activated carbon fiber felt-stabilized nanoscale zero-valent iron for the removal of Cr (VI) from aqueous solution. Colloid. Surface. Physicochem. Eng. Aspect. 447, 59–66.

Huang, Z.-n., Wang, X.-l., Yang, D.-s., 2015. Adsorption of Cr(VI) in wastewater using magnetic multi-wall carbon nanotubes. Water Sci. Eng. 8 (3), 226–232.

Huber, D., 2005. Synthesis, properties, and applications of iron nanoparticles. Small 1, 482–501.

Hwang, Y.-H., Kim, D.-G., Shin, H.-S., 2011. Mechanism study of nitrate reduction by nano zero valent iron. J. Hazard Mater. 185 (2), 1513–1521.

ITRC, 2011. Permeable Reactive Barrier: Technology Update. Interstate Technology & Regulatory Council.

Jeen, S.-W., Blowes, D.W., Gillham, R.W., 2008. Performance evaluation of granular iron for removing hexavalent chromium under different geochemical conditions. J. Contam. Hydrol. 95 (1), 76–91.

Jia, T., Zhang, B., Huang, L., Wang, S., Xu, C., 2019. Enhanced sequestration of Cr(VI) by copper doped sulfidated zerovalent iron (SZVI-Cu): characterization, performance, and mechanisms. Chem. Eng. J. 366, 200–207.

Jiang, B., Xin, S., Gao, L., Luo, S., Xue, J., Wu, M., 2017. Dramatically enhanced aerobic Cr(VI) reduction with scrap zero-valent aluminum induced by oxalate. Chem. Eng. J. 308, 588–596.

Jiang, D., Huang, D., Lai, C., Xu, P., Zeng, G., Wan, J., Tang, L., Dong, H., Huang, B., Hu, T., 2018. Difunctional chitosan-stabilized Fe/Cu bimetallic nanoparticles for removal of hexavalent chromium wastewater. Sci. Total Environ. 644, 1181–1189.

Jonoush, Z.A., Rezaee, A., Ghaffarinejad, A., 2020. Electrocatalytic nitrate reduction using Fe0/Fe3O4 nanoparticles immobilized on nickel foam: selectivity and energy consumption studies. J. Clean. Prod. 242, 118569.

Kadu, B.S., Sathe, Y.D., Ingle, A.B., Chikate, R.C., Patil, K.R., Rode, C.V., 2011. Efficiency and recycling capability of montmorillonite supported Fe–Ni bimetallic nanocomposites towards hexavalent chromium remediation. Appl. Catal. B Environ. 104 (3), 407–414.

Kanel, S.R., Manning, B., Charlet, L., Choi, H., 2005. Removal of arsenic(III) from groundwater by nanoscale zero-valent iron. Environ. Sci. Technol. 39 (5), 1291–1298.

Karthikeyan, T., Rajgopal, S., Miranda, L.R., 2005. Chromium (VI) adsorption from aqueous solution by Hevea Brasilinesis sawdust activated carbon. J. Hazard Mater. 124 (1–3), 192–199.

Katsoyiannis, I.A., Ruettimann, T., Hug, S.J., 2008. pH dependence of Fenton reagent generation and as (III) oxidation and removal by corrosion of zero valent iron in aerated water. Environ. Sci. Technol. 42 (19), 7424–7430.

Kerekes, L., Hakl, J., Meszaros, S., Vad, K., Gurin, P., Kis-Varga, M., Uzonyi, I., Szabo, S., Beke, D.J., 2002. Study of magnetic relaxation in partially oxidized nanocrystalline iron. Czech. J. Phys. 52 (1), A89–A92.

Kocur, C.M.D., Lomheim, L., Molenda, O., Weber, K.P., Austrins, L.M., Sleep, B.E., Boparai, H.K., Edwards, E.A., O'Carroll, D.M., 2016. Long-term field study of microbial community and dechlorinating activity following carboxymethyl cellulose-stabilized nanoscale zero-valent iron injection. Environ. Sci. Technol. 50 (14), 7658–7670.

Komárek, M., Vaněk, A., Ettler, V., 2013. Chemical stabilization of metals and arsenic in contaminated soils using oxides – a review. Environ. Pollut. 172, 9–22.

Koutsospyros, A., Pavlov, J., Fawcett, J., Strickland, D., Smolinski, B., Braida, W., 2012. Degradation of high energetic and insensitive munitions compounds by Fe/Cu bimetal reduction. J. Hazard Mater. 219, 75–81.

Kumar, V., Talreja, N., Deva, D., Sankararamakrishnan, N., Sharma, A., Verma, N., 2011. Development of bi-metal doped micro- and nano multi-functional polymeric adsorbents for the removal of fluoride and arsenic(V) from wastewater. Desalination 282, 27–38.

Lai, B., Zhang, Y., Chen, Z., Yang, P., Zhou, Y., Wang, J., 2014. Removal of p-nitrophenol (PNP) in aqueous solution by the micron-scale iron–copper (Fe/Cu) bimetallic particles. Appl. Catal. B Environ. 144, 816–830.

Lai, K., Lo, I., Birkelund, V., Kjeldsen, P., 2006. Field monitoring of permeable reactive barrier for removal of chlorinated organics. J. Environ. Eng. 132.

Lai, K.C., Lo, I.M., 2008. Removal of chromium (VI) by acid-washed zero-valent iron under various groundwater geochemistry conditions. Environ. Sci. Technol. 42 (4), 1238–1244.

Lan, Y.-Q., Yang, J.-X., Deng, B., 2006. Catalysis of dissolved and adsorbed iron in soil suspension for chromium(VI) reduction by sulfide. Pedosphere 16 (5), 572–578.

Lefevre, E., Bossa, N., Wiesner, M.R., Gunsch, C.K., 2016. A review of the environmental implications of in situ remediation by nanoscale zero valent iron (nZVI): behavior, transport and impacts on microbial communities. Sci. Total Environ. 565, 889–901.

Lewis, D.G., 1997. Factors Influencing the Stability and Properties of Green Rusts. Catena Verlag.

Li, J., Zhang, X., Liu, M., Pan, B., Zhang, W., Shi, Z., Guan, X., 2018. Enhanced reactivity and electron selectivity of sulfidated zerovalent iron toward chromate under aerobic conditions. Environ. Sci. Technol. 52 (5), 2988–2997.

Li, J., Zhang, X., Sun, Y., Liang, L., Pan, B., Zhang, W., Guan, X., 2017. Advances in sulfidation of zerovalent iron for water decontamination. Environ. Sci. Technol. 51 (23), 13533–13544.

Li, K., Hanpei, Y., Lina, W., Siqi, C., Ruichen, Z., Junming, W., Xiaona, L., 2020. Facile integration of FeS and titanate nanotubes for efficient removal of total Cr from aqueous solution: synergy in simultaneous reduction of Cr(VI) and adsorption of Cr (III). J. Hazard Mater. 398, 122834.

Li, X.-q., Cao, J., Zhang, W.-x., 2008. Stoichiometry of Cr(VI) immobilization using nanoscale zerovalent iron (nZVI): A study with high-resolution X-ray photoelectron spectroscopy (HR-XPS). Ind. Eng. Chem. Res. 47 (7), 2131–2139.

Li, Z., Jones, H.K., Bowman, R.S., Helferich, R., 1999. Enhanced reduction of chromate and PCE by pelletized surfactant-modified zeolite/zerovalent iron. Environ. Sci. Technol. 33 (23), 4326–4330.

Lian, J., Wang, H., He, H., Huang, W., Yang, M., Zhong, Y., Peng, P.a., 2021. The reaction of amorphous iron sulfide with Mo(VI) under different pH conditions. Chemosphere 266, 128946.

Lin, K.-Y., Lin, C.-H., Yang, H., 2017. Enhanced bromate reduction using zero-valent aluminum mediated by oxalic acid. J. Environ. Chem. Eng. 5, 5085–5090.

Liu, G.-s., Strezov, V., Lucas, J.A., Wibberley, L.J., 2004. Thermal investigations of direct iron ore reduction with coal. Thermochim. Acta 410 (1), 133–140.

Liu, J., Liu, H., Wang, C., Li, X., Tong, Y., Xuan, X., Cui, G., 2008. Synthesis, characterization and re-activation of a Fe0/Ti system for the reduction of aqueous Cr (VI). J. Hazard Mater. 151 (2), 761–769.

Liu, Q., Xu, M., Li, F., Wu, T., Li, Y., 2016. Rapid and effective removal of Cr(VI) from aqueous solutions using the FeCl3/NaBH4 system. Chem. Eng. J. 296, 340–348.

Liu, T., Zhao, L., Sun, D., Tan, X., 2010. Entrapment of nanoscale zero-valent iron in chitosan beads for hexavalent chromium removal from wastewater. J. Hazard Mater. 184 (1), 724–730.

Liu, W.-J., Qian, T.-T., Jiang, H., 2014. Bimetallic Fe nanoparticles: recent advances in synthesis and application in catalytic elimination of environmental pollutants. Chem. Eng. J. 236, 448–463.

Liu, Y., Lowry, G., 2006. Effect of particle age (Fe 0 content) and solution pH on NZVI reactivity: H 2 evolution and TCE dechlorination. Environ. Sci. Technol. 40, 6085–6090.

Lo, I.M.C., Lam, C.S.C., Lai, K.C.K., 2006. Hardness and carbonate effects on the reactivity of zero-valent iron for Cr(VI) removal. Water Res. 40 (3), 595–605.

López, M.L., Peralta-Videa, J.R., Benitez, T., Gardea-Torresdey, J.L., 2005. Enhancement of lead uptake by alfalfa (Medicago sativa) using EDTA and a plant growth promoter. Chemosphere 61 (4), 595–598.

Lu, Li, J., Sheng, Y., Zhang, X., You, J., Chen, L., 2017a. One-pot synthesis of magnetic iron oxide nanoparticle-multiwalled carbon nanotube composites for enhanced removal of Cr(VI) from aqueous solution. J. Colloid Interface Sci. 505, 1134–1146.
Lu, Xu, Y., Zhou, S., 2017b. High saturation magnetization superparamagnetic Fe/Ni core/shell microparticles for chromium removal. RSC Adv. 7, 42363–42369.
Ludwig, R.D., Su, C., Lee, T.R., Wilkin, R.T., Acree, S.D., Ross, R.R., Keeley, A., 2007. In situ chemical reduction of Cr(VI) in groundwater using a combination of ferrous sulfate and sodium Dithionite: A field investigation. Environ. Sci. Technol. 41 (15), 5299–5305.
Lugo-Lugo, V., Barrera-Díaz, C., Bilyeu, B., Balderas-Hernández, P., Ureña-Nuñez, F., Sánchez-Mendieta, V., 2010. Cr(VI) reduction in wastewater using a bimetallic galvanic reactor. J. Hazard Mater. 176 (1), 418–425.
Lugo-Lugo, V., Bernal-Martínez, L.A., Ureña-Núñez, F., Linares-Hernández, I., Almazán-Sánchez, P.T., Vázquez-Santillán, P.d.J.B., 2014. Treatment of Cr(VI) present in plating wastewater using a Cu/Fe galvanic reactor. Fuel 138, 203–214.
Luo, S., Yang, S., Sun, C., Gu, J.-D., 2012. Improved debromination of polybrominated diphenyl ethers by bimetallic iron–silver nanoparticles coupled with microwave energy. Sci. Total Environ. 429, 300–308.
Luo, W., Zhu, L., Wang, N., Tang, H., Cao, M., She, Y., 2010. Efficient removal of organic pollutants with magnetic nanoscaled BiFeO3 as a reusable heterogeneous fenton-like catalyst. Environ. Sci. Technol. 44 (5), 1786–1791.
Lv, D., Zhou, J., Cao, Z., Xu, J., Liu, Y., Li, Y., Yang, K., Lou, Z., Lou, L., Xu, X., 2019. Mechanism and influence factors of chromium (VI) removal by sulfide-modified nanoscale zerovalent iron. Chemosphere 224, 306–315.
Lv, X., Hu, Y., Tang, J., Sheng, T., Jiang, G., Xu, X., 2013. Effects of co-existing ions and natural organic matter on removal of chromium (VI) from aqueous solution by nanoscale zero valent iron (nZVI)-Fe3O4 nanocomposites. Chem. Eng. J. 218, 55–64.
Lv, X., Xu, J., Jiang, G., Tang, J., Xu, X., 2012. Highly active nanoscale zero-valent iron (nZVI)–Fe3O4 nanocomposites for the removal of chromium(VI) from aqueous solutions. J. Colloid Interface Sci. 369 (1), 460–469.
Lv, X., Xu, J., Jiang, G., Xu, X., 2011. Removal of chromium (VI) from wastewater by nanoscale zero-valent iron particles supported on multiwalled carbon nanotubes. Chemosphere 85 (7), 1204–1209.
Lyu, H., Tang, J., Huang, Y., Gai, L., Zeng, E.Y., Liber, K., Gong, Y., 2017. Removal of hexavalent chromium from aqueous solutions by a novel biochar supported nanoscale iron sulfide composite. Chem. Eng. J. 322, 516–524.
Mak, Lo, I.M., 2011. Environmental life cycle assessment of permeable reactive barriers: effects of construction methods, reactive materials and groundwater constituents. Environ. Sci. Technol. 45 (23), 10148–10154.
Mak, M.S.H., Lo, I.M.C., Liu, T., 2011. Synergistic effect of coupling zero-valent iron with iron oxide-coated sand in columns for chromate and arsenate removal from groundwater: influences of humic acid and the reactive media configuration. Water Res. 45 (19), 6575–6584.
Mamindy-Pajany, Y., Hurel, C., Marmier, N., Roméo, M., 2011. Arsenic (V) adsorption from aqueous solution onto goethite, hematite, magnetite and zero-valent iron: effects of pH, concentration and reversibility. Desalination 281, 93–99.
Man, Y., Feng, J.X., Li, F.J., Ge, Q., Chen, Y.M., Zhou, J.Z., 2014. Influence of temperature and time on reduction behavior in iron ore–coal composite pellets. Powder Technol. 256, 361–366.
Manning, B.A., Kiser, J.R., Kwon, H., Kanel, S.R., 2007. Spectroscopic investigation of Cr (III)- and Cr(VI)-Treated nanoscale zerovalent iron. Environ. Sci. Technol. 41 (2), 586–592.
Matteazzi, P., Le Caër, G., 1992. Mechanochemical reduction of hematite by room temperature ball milling. Hyperfine Interact. 68 (1), 177–180.
Mortazavian, S., An, H., Chun, D., Moon, J., 2018. Activated carbon impregnated by zero-valent iron nanoparticles (AC/nZVI) optimized for simultaneous adsorption and reduction of aqueous hexavalent chromium: material characterizations and kinetic studies. Chem. Eng. J. 353, 781–795.
Moura, F.C.C., Oliveira, G.C., Araujo, M.H., Ardisson, J.D., Macedo, W.A.A., Lago, R.M., 2006. Highly reactive species formed by interface reaction between Fe0–iron oxides particles: an efficient electron transfer system for environmental applications. Appl. Catal. Gen. 307 (2), 195–204.
Moura, F.C.C., Oliveira, G.C., Araujo, M.H., Ardisson, J.D., Macedo, W.A.d.A., Lago, R. M., 2005. formation of highly reactive species at the interface Fe°–Iron oxides particles by mechanical alloying and thermal treatment: potential application in environmental remediation processes. Chem. Lett. 34 (8), 1172–1173.
Mu, Y., Ai, Z., Zhang, L., Song, F., 2015a. Insight into core–shell dependent anoxic Cr (VI) removal with Fe@ Fe2O3 nanowires: indispensable role of surface bound Fe (II). ACS Appl. Mater. Interfaces 7 (3), 1997–2005.
Mu, Y., Wu, H., Ai, Z., 2015b. Negative impact of oxygen molecular activation on Cr(VI) removal with core–shell Fe@Fe2O3 nanowires. J. Hazard Mater. 298, 1–10.
Mueller, N.C., Braun, J., Bruns, J., Černík, M., Rissing, P., Rickerby, D., Nowack, B., 2012. Application of nanoscale zero valent iron (NZVI) for groundwater remediation in Europe. Environ. Sci. Pollut. Control Ser. 19 (2), 550–558.
Muthukrishnan, M., Guha, B.K., 2008. Effect of pH on rejection of hexavalent chromium by nanofiltration. Desalination 219 (1), 171–178.
Nahuel Montesinos, V., Quici, N., Beatriz Halac, E., Leyva, A.G., Custo, G., Bengio, S., Zampieri, G., Litter, M.I., 2014. Highly efficient removal of Cr(VI) from water with nanoparticulated zerovalent iron: understanding the Fe(III)–Cr(III) passive outer layer structure. Chem. Eng. J. 244, 569–575.
Natter, H., Schmelzer, M., Löffler, M.S., Krill, C.E., Fitch, A., Hempelmann, R., 2000. Grain-growth kinetics of nanocrystalline iron studied in situ by synchrotron real-time X-ray diffraction. J. Phys. Chem. B 104 (11), 2467–2476.
Němeček, J., Lhotský, O., Cajthaml, T., 2014. Nanoscale zero-valent iron application for in situ reduction of hexavalent chromium and its effects on indigenous microorganism populations. Sci. Total Environ. 485–486, 739–747.
Nethaji, S., Sivasamy, A., Mandal, A., 2013. Preparation and characterization of corn cob activated carbon coated with nano-sized magnetite particles for the removal of Cr (VI). Bioresour. Technol. 134, 94–100.
Norouzi, S., Heidari, M., Alipour, V., Rahmanian, O., Fazlzadeh, M., Mohammadi-Moghadam, F., Nourmoradi, H., Goudarzi, B., Dindarloo, K., 2018. Preparation, characterization and Cr(VI) adsorption evaluation of NaOH-activated carbon produced from Date Press Cake; an agro-industrial waste. Bioresour. Technol. 258, 48–56.
Noubactep, C., 2009. An analysis of the evolution of reactive species in Fe0/H2O systems. J. Hazard Mater. 168 (2), 1626–1631.
Nunez Garcia, A., Boparai, H.K., de Boer, C.V., Chowdhury, A.I.A., Kocur, C.M.D., Austrins, L.M., Herrera, J., O'Carroll, D.M., 2020. Fate and transport of sulfidated nano zerovalent iron (S-nZVI): a field study. Water Res. 170, 115319.
Nurmi, J.T., Tratnyek, P.G., Sarathy, V., Baer, D.R., Amonette, J.E., Pecher, K., Wang, C., Linehan, J.C., Matson, D.W., Penn, R.L., Driessen, M.D., 2005. Characterization and properties of metallic iron Nanoparticles: spectroscopy, electrochemistry, and kinetics. Environ. Sci. Technol. 39 (5), 1221–1230.
Obiri-Nyarko, F., Grajales-Mesa, S.J., Malina, G., 2014. An overview of permeable reactive barriers for in situ sustainable groundwater remediation. Chemosphere 111, 243–259.
Oliveira, L.C.A., Rios, R.V.R.A., Fabris, J.D., Garg, V., Sapag, K., Lago, R.M., 2002. Activated carbon/iron oxide magnetic composites for the adsorption of contaminants in water. Carbon 40 (12), 2177–2183.
Ou, J.-H., Sheu, Y.-T., Tsang, D.C.W., Sun, Y.-J., Kao, C.-M., 2020. Application of iron/aluminum bimetallic nanoparticle system for chromium-contaminated groundwater remediation. Chemosphere 256, 127158.
Owlad, M., Aroua, M.K., Daud, W.A.W., Baroutian, S., 2008. Removal of hexavalent chromium-contaminated water and wastewater: a review. Water Air Soil Pollut. 200 (1–4), 59–77.
Paar, H., Ruhl, A.S., Jekel, M., 2015. Influences of nanoscale zero valent iron loadings and bicarbonate and calcium concentrations on hydrogen evolution in anaerobic column experiments. Water Res. 68, 731–739.
Pardavi-Horvath, M., Takacs, L., 1995. Magnetic nanocomposites by reaction milling. Scripta Metall. Mater. 33 (10), 1731–1740.
Patterson, R.R., Fendorf, S., Fendorf, M., 1997. Reduction of hexavalent chromium by amorphous iron sulfide. Environ. Sci. Technol. 31 (7), 2039–2044.
Peng, H., Guo, J., 2020. Removal of chromium from wastewater by membrane filtration, chemical precipitation, ion exchange, adsorption electrocoagulation, electrochemical reduction, electrodialysis, electrodeionization, photocatalysis and nanotechnology: a review. Environ. Chem. Lett. 18 (6), 2055–2068.
Perez, J.P.H., Schiefler, A.A., Rubio, S.N., Reischer, M., Overheu, N.D., Benning, L.G., Tobler, D.J., 2021. Arsenic removal from natural groundwater using 'green rust': solid phase stability and contaminant fate. J. Hazard Mater. 401, 123327.
Petala, E., Dimos, K., Douvalis, A., Bakas, T., Tucek, J., Zbořil, R., Karakassides, M.A., 2013. Nanoscale zero-valent iron supported on mesoporous silica: characterization and reactivity for Cr (VI) removal from aqueous solution. J. Hazard Mater. 261, 295–306.
Peterson, M.L., Brown, G.E., Parks, G.A., 1996. Direct XAFS evidence for heterogeneous redox reaction at the aqueous chromium/magnetite interface. Colloid. Surface. Physicochem. Eng. Aspect. 107, 77–88.
Peterson, M.L., White, A.F., Brown, G.E., Parks, G.A., 1997. Surface passivation of magnetite by reaction with aqueous Cr(VI): XAFS and TEM results. Environ. Sci. Technol. 31 (5), 1573–1576.
Petrova, T., Fachikov, L., Hristov, J., 2011. The magnetite as adsorbent for some hazardous species from aqueous solutions: a review. Int. Rev. Chem. Eng. 3, 134–152.
Phillips, D., Watson, D., Roh, Y., Gu, B., 2003. Mineralogical characteristics and transformations during long-term operation of a zerovalent iron reactive barrier. J. Environ. Qual. 32, 2033–2045.
Ponder, S.M., Darab, J.G., Mallouk, T.E., 2000. Remediation of Cr(VI) and Pb(II) aqueous solutions using supported, nanoscale zero-valent iron. Environ. Sci. Technol. 34 (12), 2564–2569.
Pratt, A.R., Blowes, D.W., Ptacek, C.J., 1997. Products of chromate reduction on proposed subsurface remediation material. Environ. Sci. Technol. 31 (9), 2492–2498.
Puls, R.W., Blowes, D.W., Gillham, R.W., 1999. Long-term performance monitoring for a permeable reactive barrier at the U.S. Coast guard support center, elizabeth city, North Carolina. J. Hazard Mater. 68 (1), 109–124.
Qian, L., Shang, X., Zhang, B., Zhang, W., Su, A., Chen, Y., Ouyang, D., Han, L., Yan, J., Chen, M., 2019. Enhanced removal of Cr (VI) by silicon rich biochar-supported nanoscale zero-valent iron. Chemosphere 215, 739–745.
Qian, L., Zhang, W., Yan, J., Han, L., Chen, Y., Ouyang, D., Chen, M., 2017. Nanoscale zero-valent iron supported by biochars produced at different temperatures: synthesis mechanism and effect on Cr(VI) removal. Environ. Pollut. 223, 153–160.
Qin, Li, J., Bao, Q., Li, L., Guan, X., 2016a. Role of dissolved oxygen in metal(loid) removal by zerovalent iron at different pH: its dependence on the removal mechanisms. RSC Adv. 6 (55), 50144–50152.
Qin, Zhang, Y., Zhou, H., Geng, Z., Liu, G., Zhang, Y., Zhao, H., Wang, G., 2016b. Enhanced removal of trace Cr(VI) from neutral and alkaline aqueous solution by FeCo bimetallic nanoparticles. J. Colloid Interface Sci. 472, 8–15.
Qiu, B., Wang, Y., Sun, D., Wang, Q., Zhang, X., Weeks, B.L., O'Connor, R., Huang, X., Wei, S., Guo, Z., 2015. Cr(vi) removal by magnetic carbon nanocomposites derived from cellulose at different carbonization temperatures. J. Mater. Chem. 3 (18), 9817–9825.

Qu, G., Kou, L., Wang, T., Liang, D., Hu, S., 2017. Evaluation of activated carbon fiber supported nanoscale zero-valent iron for chromium (VI) removal from groundwater in a permeable reactive column. J. Environ. Manag. 201, 378–387.

Qu, G., Zeng, D., Chu, R., Wang, T., Liang, D., Qiang, H., 2019. Magnetic Fe3O4 assembled on nZVI supported on activated carbon fiber for Cr(VI) and Cu(II) removal from aqueous solution through a permeable reactive column. Environ. Sci. Pollut. Control Ser. 26 (5), 5176–5188.

Rajajayavel, S., Ghoshal, S., 2015. Enhanced reductive dechlorination of trichloroethylene by sulfidated nanoscale zero valent iron. Water Res. 78, 144–153.

Rajput, S., Pittman Jr., C.U., Mohan, D., 2016. Magnetic magnetite (Fe3O4) nanoparticle synthesis and applications for lead (Pb2+) and chromium (Cr6+) removal from water. J. Colloid Interface Sci. 468, 334–346.

Ramos, R.L., Martinez, A.J., Coronado, R.G., 1994. Adsorption of chromium (VI) from aqueous solutions on activated carbon. Water Sci. Technol. 30 (9), 191.

Rao, A., Bankar, A., Kumar, A.R., Gosavi, S., Zinjarde, S., 2013a. Removal of hexavalent chromium ions by Yarrowia lipolytica cells modified with phyto-inspired Fe0/Fe3O4 nanoparticles. J. Contam. Hydrol. 146, 63–73.

Rao, A., Bankar, A., Kumar, A.R., Zinjarde, S., Gosavi, S., 2013b. Phytofabrication of Fe0/Fe3O4 composites for the removal of hexavalent chromium. J. Nanoeng. Nanomanufact. 3 (2), 114–120.

Reardon, E., 1995. Anaerobic corrosion of granular iron: measurement and interpretation of hydrogen evolution rates. Environ. Sci. Technol. 29, 2936–2945.

Reardon, E., 2005. Zerovalent irons: styles of corrosion and inorganic control on hydrogen pressure buildup. Environ. Sci. Technol. 39, 7311–7317.

Rebodos, R.L., Vikesland, P.J., 2010. Effects of oxidation on the magnetization of nanoparticulate magnetite. Langmuir 26 (22), 16745–16753.

Ren, T., Yang, S., Jiang, Y., Sun, X., Zhang, Y., 2018. Enhancing surface corrosion of zero-valent aluminum (ZVAl) and electron transfer process for the degradation of trichloroethylene with the presence of persulfate. Chem. Eng. J. 348.

Rhodes, F., Carty, J., 1925. The corrosion of certain metals by carbon tetrachloride. Ind. Eng. Chem. 17 (9), 909–911.

Ribas, D., Pešková, K., Jubany, I., Parma, P., Černik, M., Benito, J.A., Martí, V., 2019. High reactive nano zero-valent iron produced via wet milling through abrasion by alumina. Chem. Eng. J. 366, 235–245.

Ritter, K., Odziemkowski, M.S., Gillham, R.W., 2002. An in situ study of the role of surface films on granular iron in the permeable iron wall technology. J. Contam. Hydrol. 55 (1), 87–111.

Rivero-Huguet, M., Marshall, W.D., 2010. Impact of various inorganic oxyanions on the removal rates of hexavalent chromium mediated by zero-valent iron. Environ. Chem. 7 (3), 250–258.

Roh, Y., Lee, S., Elless, M.J.E.G., 2000. Characterization of corrosion products in the permeable reactive barriers. Environ. Geol. 40 (1–2), 184–194.

Salam, M.A., 2017. Preparation and characterization of chitin/magnetite/multiwalled carbon nanotubes magnetic nanocomposite for toxic hexavalent chromium removal from solution. J. Mol. Liq. 233, 197–202.

Shao, F., Zhou, S., Xu, J., Du, Q., Chen, J., Shang, J., 2019. Detoxification of Cr(VI) using biochar supported Cu/Fe bimetallic nanoparticles. Desal. Water Treat. 158, 121–129.

Shao, Q., Xu, C., Wang, Y., Huang, S., Zhang, B., Huang, L., Fan, D., Tratnyek, P.G., 2018. Dynamic interactions between sulfidated zerovalent iron and dissolved oxygen: mechanistic insights for enhanced chromate removal. Water Res. 135, 322–330.

Sheng, G., Alsaedi, A., Shammakh, W., Monaquel, S., Sheng, J., Wang, X., Li, H., Huang, Y., 2016. Enhanced sequestration of selenite in water by nanoscale zero valent iron immobilization on carbon nanotubes by a combined batch, XPS and XAFS investigation. Carbon 99, 123–130.

Shi, L.-n., Zhang, X., Chen, Z.-l., 2011. Removal of chromium (VI) from wastewater using bentonite-supported nanoscale zero-valent iron. Water Res. 45 (2), 886–892.

Si, Z., Song, X., Wang, Y., Cao, X., Wang, Y., Zhao, Y., Ge, X., 2021. Natural pyrite improves nitrate removal in constructed wetlands and makes wetland a sink for phosphorus in cold climates. J. Clean. Prod. 280, 124304.

Song, S., Su, Y., Adeleye, A.S., Zhang, Y., Zhou, X., 2017. Optimal design and characterization of sulfide-modified nanoscale zerovalent iron for diclofenac removal. Appl. Catal. B Environ. 201, 211–220.

Su, C., 2017. Environmental implications and applications of engineered nanoscale magnetite and its hybrid nanocomposites: a review of recent literature. J. Hazard Mater. 322, 48–84.

Sui, H., Rong, Y., Song, J., Zhang, D., Li, H., Wu, P., Shen, Y., Huang, Y., 2017. Mechanochemical destruction of DDTs with Fe-Zn bimetal in a high-energy planetary ball mill. J. Hazard Mater. 342, 201–209.

Sun, H., Zhou, G., Liu, S., Ang, H.M., Tadé, M.O., Wang, S., 2012. Nano-Fe0 encapsulated in microcarbon s pheres: synthesis, characterization, and environmental applications. ACS Appl. Mater. Interfaces 4 (11), 6235–6241.

Sun, X., Yan, Y., Li, J., Han, W., Wang, L., 2014. SBA-15-incorporated nanoscale zero-valent iron particles for chromium(VI) removal from groundwater: mechanism, effect of pH, humic acid and sustained reactivity. J. Hazard Mater. 266, 26–33.

Sun, Y., Li, J., Huang, T., Guan, X., 2016. The influences of iron characteristics, operating conditions and solution chemistry on contaminants removal by zero-valent iron: a review. Water Res. 100, 277–295.

Sun, Y.-P., Li, X.-q., Cao, J., Zhang, W.-x., Wang, H.P., 2006. Characterization of zero-valent iron nanoparticles. Adv. Colloid Interface Sci. 120 (1), 47–56.

Takacs, L., 1992. Reduction of magnetite by aluminum: a displacement reaction induced by mechanical alloying. Mater. Lett. 13 (2), 119–124.

Tang, H., Cheng, W., Yi, Y., Ding, C., Nie, X., 2021. Nano zero valent iron encapsulated in graphene oxide for reducing uranium. Chemosphere 278, 130229.

Tao, N.R., Sui, M.L., Lu, J., Lua, K., 1999. Surface nanocrystallization of iron induced by ultrasonic shot peening. Nanostruct. Mater. 11 (4), 433–440.

Tavakoli, A., Sohrabi, M., Kargari, A., 2007. A review of methods for synthesis of nanostructured metals with emphasis on iron compounds. Chem. Pap. 61 (3), 151–170.

Tran, T., Gray, S., Naughton, R., Bolto, B., 2006. Polysilicato-iron for improved NOM removal and membrane performance. J. Membr. Sci. 280 (1), 560–571.

Vilardi, G., Di Palma, L., Verdone, N., 2017a. Competitive reaction modelling in aqueous systems: the case of contemporary reduction of dichromates and nitrates by nZVI. Chem. Eng. Trans. 60, 175–180.

Vilardi, G., Di Palma, L., Verdone, N., 2018a. On the critical use of zero valent iron nanoparticles and Fenton processes for the treatment of tannery wastewater. J. Water Process. Eng. 22, 109–122.

Vilardi, G., Di Palma, L., Verdone, N., 2019a. A physical-based interpretation of mechanism and kinetics of Cr(VI) reduction in aqueous solution by zero-valent iron nanoparticles. Chemosphere 220, 590–599.

Vilardi, G., Ochando-Pulido, J.M., Verdone, N., Stoller, M., Di Palma, L., 2018b. On the removal of hexavalent chromium by olive stones coated by iron-based nanoparticles: equilibrium study and chromium recovery. J. Clean. Prod. 190, 200–210.

Vilardi, G., Stoller, M., Di Palma, L., Boodhoo, K., Verdone, N., 2019b. Metallic iron nanoparticles intensified production by spinning disk reactor: optimization and fluid dynamics modelling. Chem. Eng. Process. Intensification. 146, 107683.

Vilardi, G., Stoller, M., Di Palma, L., Verdone, N., 2019c. CFD model of agitated vessel for the removal of Cr (vi) by nano-hematite particles. Chem. Eng. Trans. 73, 157–162.

Vilardi, G., Stoller, M., Verdone, N., Di Palma, L., 2017b. Production of nano Zero Valent Iron particles by means of a spinning disk reactor. Chem. Eng. Trans. 57, 751–756.

Vilardi, G., Verdone, N., Di Palma, L., 2017c. The influence of nitrate on the reduction of hexavalent chromium by zero-valent iron nanoparticles in polluted wastewater. Desal. Water. Treat. 86, 252–258.

Villacís-García, M., Villalobos, M., Gutiérrez-Ruiz, M., 2015. Optimizing the use of natural and synthetic magnetites with very small amounts of coarse Fe(0) particles for reduction of aqueous Cr(VI). J. Hazard Mater. 281, 77–86.

Wang, Chen, G., Wang, X., Li, S., Liu, Y., Yang, G., 2020a. Removal of hexavalent chromium by bentonite supported organosolv lignin-stabilized zero-valent iron nanoparticles from wastewater. J. Clean. Prod. 267, 122009.

Wang, Hu, B., Wang, C., Liang, Z., Cui, F., Zhao, Z., Yang, C., 2020b. Cr(VI) removal by micron-scale iron-carbon composite induced by ball milling: the role of activated carbon. Chem. Eng. J. 389, 122633.

Wang, Qian, T., Huo, L., Li, Y., Zhao, D., 2019a. Immobilization of hexavalent chromium in soil and groundwater using synthetic pyrite particles. Environ. Pollut. 255, 112992.

Wang, Sun, Y., Tang, J., He, J., Sun, H., 2020c. Aqueous Cr(VI) removal by a novel ball milled Fe0-biochar composite: role of biochar electron transfer capacity under high pyrolysis temperature. Chemosphere 241, 125044.

Wang, Wu, Y., Qu, T., Liu, S., Pi, Y., Shen, J., 2019b. Enhanced Cr(VI) removal in the synergy between the hydroxyl-functionalized ball-milled ZVI/Fe3O4 composite and Na2EDTA complexation. Chem. Eng. J. 359, 874–881.

Wang, Zhao, M., Zhou, M., Li, Y.C., Wang, J., Gao, B., Sato, S., Feng, K., Yin, W., Igalavithana, A.D., Oleszczuk, P., Wang, X., Ok, Y.S., 2019c. Biochar-supported nZVI (nZVI/BC) for contaminant removal from soil and water: a critical review. J. Hazard Mater. 373, 820–834.

Wang, C.-B., Zhang, W.-x., 1997. Synthesizing nanoscale iron particles for rapid and complete dechlorination of TCE and PCBs. Environ. Sci. Technol. 31 (7), 2154–2156.

Wang, M., Wang, N., Tang, H., Cao, M., She, Y., Zhu, L., 2012. Surface modification of nano-Fe3O4 with EDTA and its use in H2O2 activation for removing organic pollutants. Catalysis. Sci. Technol. 2 (1), 187–194.

Wang, Y., Shao, Q., Huang, S., Zhang, B., Xu, C., 2018. High performance and simultaneous sequestration of Cr (VI) and Sb (III) by sulfidated zerovalent iron. J. Clean. Prod. 191, 436–444.

White, A.F., Peterson, M.L., 1996. Reduction of aqueous transition metal species on the surfaces of Fe (II)-containing oxides. Geochem. Cosmochim. Acta 60 (20), 3799–3814.

Wiatrowski, H.A., Das, S., Kukkadapu, R., Ilton, E.S., Barkay, T., Yee, N., 2009. Reduction of Hg(II) to Hg(0) by magnetite. Environ. Sci. Technol. 43 (14), 5307–5313.

Wilkin, R.T., Puls, R.W., Sewell, G.W., 2003. Long-term performance of permeable reactive barriers using zero-valent iron: geochemical and microbiological effects. Ground Water 41 (4), 493–503.

Wilkin, R.T., Su, C., Ford, R.G., Paul, C.J., 2005. Chromium-removal processes during groundwater remediation by a zerovalent iron permeable reactive barrier. Environ. Sci. Technol. 39 (12), 4599–4605.

Wu, Zhang, J., Tong, Y., Xu, X., 2009. Chromium (VI) reduction in aqueous solutions by Fe3O4-stabilized Fe0 nanoparticles. J. Hazard Mater. 172 (2), 1640–1645.

Wu, L., Liao, L., Lv, G., Qin, F., He, Y., Wang, X., 2013. Micro-electrolysis of Cr (VI) in the nanoscale zero-valent iron loaded activated carbon. J. Hazard Mater. 254, 277–283.

Wu, P., Wu, W., Li, S., Xing, N., Zhu, N., Li, P., Wu, J., Yang, C., Dang, Z., 2009. Removal of Cd2+ from aqueous solution by adsorption using Fe-montmorillonite. J. Hazard Mater. 169 (1), 824–830.

Wu, S., Yang, S., Liu, S., Zhang, Y., Ren, T., Zhang, Y., 2020. Enhanced reactivity of zero-valent aluminum with ball milling for phenol oxidative degradation. J. Colloid Interface Sci. 560, 260–272.

Xiao, R., He, L., Luo, Z., Spinney, R., Wei, Z., Dionysiou, D.D., Zhao, F., 2020. An experimental and theoretical study on the degradation of clonidine by hydroxyl and sulfate radicals. Sci. Total Environ. 710, 136333.

Xu, Deng, S., Xu, J., Zhang, W., Wu, M., Wang, B., Huang, J., Yu, G., 2012a. Highly active and stable Ni–Fe bimetal prepared by ball milling for catalytic hydrodechlorination of 4-chlorophenol. Environ. Sci. Technol. 46 (8), 4576–4582.

Xu, C., Yang, W., Liu, W., Sun, H., Jiao, C., Lin, A.-j., 2018. Performance and mechanism of Cr(VI) removal by zero-valent iron loaded onto expanded graphite. J. Environ. Sci. 67, 14–22.
Xu, F., Deng, S., Xu, J., Zhang, W., Wu, M., Wang, B., Huang, J., Yu, G., 2012b. Highly active and stable Ni-Fe bimetal prepared by ball milling for catalytic hydrodechlorination of 4-chlorophenol. Environ. Sci. Technol. 46, 4576–4582.
Xu, J., Pu, Y., Qi, W.-K., Yang, X., Tang, Y., Wan, P., Fisher, A., 2017a. Chemical removal of nitrate from water by aluminum-iron alloys. Chemosphere 166, 197–202.
Xu, J., Pu, Y., Yang, X., Wan, P., Wang, R., Song, P., Fisher, A., 2017b. Rapid removal of chloroform, carbon tetrachloride and trichloroethylene in water by aluminum-iron alloy particles. Environ. Technol. 39, 1–23.
Xu, J., Wang, Y., Weng, C., Bai, W., Jiao, Y., Kaegi, R., Lowry, G.V., 2019. Reactivity, selectivity, and long-term performance of sulfidized nanoscale zerovalent iron with different properties. Environ. Sci. Technol. 53 (10), 5936–5945.
Xue, W., Huang, D., Zeng, G., Wan, J., Cheng, M., Zhang, C., Hu, C., Li, J., 2018. Performance and toxicity assessment of nanoscale zero valent iron particles in the remediation of contaminated soil: a review. Chemosphere 210, 1145–1156.
Yanez, J.E., Wang, Z., Lege, S., Obst, M., Roehler, S., Burkhardt, C.J., Zwiener, C., 2017. Application and characterization of electroactive membranes based on carbon nanotubes and zerovalent iron nanoparticles. Water Res. 108, 78–85.
Yang, Cai, J., Wang, X., Li, Y., Wu, Z., Wu, W.D., Chen, X.D., Sun, J., Sun, S.-P., Wang, Z., 2020a. A bimetallic Fe–Mn oxide-activated oxone for in situ chemical oxidation (ISCO) of trichloroethylene in groundwater: efficiency, sustained activity, and mechanism investigation. Environ. Sci. Technol. 54 (6), 3714–3724.
Yang, B., Zhang, J., Zhang, Y., Deng, S., Yu, G., Wu, J., Zhang, H., Liu, J., 2014. Promoting effect of EDTA on catalytic activity of highly stable Al–Ni bimetal alloy for dechlorination of 2-chlorophenol. Chem. Eng. J. 250, 222–229.
Yang, G.C.C., Lee, H.-L., 2005. Chemical reduction of nitrate by nanosized iron: kinetics and pathways. Water Res. 39 (5), 884–894.
Yang, S., Zheng, D., Ren, T., Zhang, Y., 2017. Zero-valent aluminum for reductive removal of aqueous pollutants over a wide pH range: performance and mechanism especially at near-neutral pH. Water Res. 123.
Yang, Y., Gai, W.-Z., Zhou, J.-G., Deng, Z.-Y., 2020b. Surface modified zero-valent aluminum for Cr(VI) removal at neutral pH. Chem. Eng. J. 395, 125140.
Yoon, I.-H., Bang, S., Chang, J.-S., Gyu Kim, M., Kim, K.-W., 2011. Effects of pH and dissolved oxygen on Cr(VI) removal in Fe(0)/H2O systems. J. Hazard Mater. 186 (1), 855–862.
Yoon, R.H., Salman, T., Donnay, G., 1979. Predicting points of zero charge of oxides and hydroxides. J. Colloid Interface Sci. 70 (3), 483–493.
Yuan, P., Fan, M., Yang, D., He, H., Liu, D., Yuan, A., Zhu, J., Chen, T., 2009. Montmorillonite-supported magnetite nanoparticles for the removal of hexavalent chromium [Cr(VI)] from aqueous solutions. J. Hazard Mater. 166 (2), 821–829.
Yuan, P., Liu, D., Fan, M., Yang, D., Zhu, R., Ge, F., Zhu, J., He, H., 2010. Removal of hexavalent chromium [Cr(VI)] from aqueous solutions by the diatomite-supported/unsupported magnetite nanoparticles. J. Hazard Mater. 173 (1), 614–621.
Zhang, Qian, L., Ouyang, D., Chen, Y., Han, L., Chen, M., 2019a. Effective removal of Cr (VI) by attapulgite-supported nanoscale zero-valent iron from aqueous solution: enhanced adsorption and crystallization. Chemosphere 221, 683–692.
Zhang, Wu, J., Chao, J., Shi, N., Li, H., Hu, Q., Yang, X.J., 2019b. Simultaneous removal of nitrate, copper and hexavalent chromium from water by aluminum-iron alloy particles. J. Contam. Hydrol. 227, 103541.
Zhang, Yang, S., Ren, T., Zhang, Y., Jiang, Y., Xue, Y., Wang, M., Chen, H., Chen, Y., 2019c. Enhancing surface gully erosion of micron-sized zero-valent aluminum (mZVAl) for Cr(VI) removal: performance and mechanism in the presence of carbonate buffer. J. Clean. Prod. 238, 117943.
Zhang, Zhang, Y., Gao, X., Xu, C., 2019d. Insights on the effects of pH and Fe(II) regeneration during the chromate sequestration by sulfidated zero-valent iron. Chem. Eng. J. 378, 122115.
Zhang, Zhao, D., Ding, Y., Chen, Y., Li, F., Alsaedi, A., Hayat, T., Chen, C., 2019e. Synthesis of Fe–Ni/graphene oxide composite and its highly efficient removal of uranium(VI) from aqueous solution. J. Clean. Prod. 230, 1305–1315.
Zhang, P., Tao, X., Li, Z., Bowman, R.S., 2002. Enhanced perchloroethylene reduction in column systems using surfactant-modified zeolite/zero-valent iron pellets. Environ. Sci. Technol. 36 (16), 3597–3603.
Zhang, S.-H., Wu, M.-F., Tang, T.-T., Xing, Q.-J., Peng, C.-Q., Li, F., Liu, H., Luo, X.-B., Zou, J.-P., Min, X.-B., Luo, J.-M., 2018. Mechanism investigation of anoxic Cr(VI) removal by nano zero-valent iron based on XPS analysis in time scale. Chem. Eng. J. 335, 945–953.
Zhang, Y., Jiao, X., Liu, N., Lv, J., Yang, Y., 2020. Enhanced removal of aqueous Cr (VI) by a green synthesized nanoscale zero-valent iron supported on oak wood biochar. Chemosphere 245, 125542.
Zhang, Y., Li, Y., Yang, L.-q., Ma, X.-j., Wang, L.-y., Ye, Z.-F., 2010. Characterization and adsorption mechanism of Zn2+ removal by PVA/EDTA resin in polluted water. J. Hazard Mater. 178 (1), 1046–1054.
Zhang, Y.-Y., Jiang, H., Zhang, Y., Xie, J.-F., 2013. The dispersity-dependent interaction between montmorillonite supported nZVI and Cr(VI) in aqueous solution. Chem. Eng. J. 229, 412–419.
Zhao, F., Liu, Y., Hammouda, S.B., Doshi, B., Guijarro, N., Min, X., Tang, C.-J., Sillanpää, M., Sivula, K., Wang, S., 2020a. MIL-101(Fe)/g-C3N4 for enhanced visible-light-driven photocatalysis toward simultaneous reduction of Cr(VI) and oxidation of bisphenol A in aqueous media. Appl. Catal. B Environ. 272, 119033.
Zhao, F., Yang, Z., Wei, Z., Spinney, R., Sillanpää, M., Tang, J., Tam, M., Xiao, R., 2020b. Polyethylenimine-modified chitosan materials for the recovery of La(III) from leachates of bauxite residue. Chem. Eng. J. 388, 124307.
Zhao, J., Xiong, S., Ai, J., Wu, J., Huang, L.-Z., Yin, W., 2021. Stabilized green rusts for aqueous Cr(VI) removal: fast kinetics, high iron utilization rate and anti-acidification. Chemosphere 262, 127853.
Zhao, W., Zhu, X., Wang, Y., Ai, Z., Zhao, D., 2014. Catalytic reduction of aqueous nitrates by metal supported catalysts on Al particles. Chem. Eng. J. 254, 410–417.
Zhou, Gao, B., Zimmerman, A.R., Chen, H., Zhang, M., Cao, X., 2014a. Biochar-supported zerovalent iron for removal of various contaminants from aqueous solutions. Bioresour. Technol. 152, 538–542.
Zhou, Li, Y., Chen, J., Liu, Z., Wang, Z., Na, P., 2014b. Enhanced Cr(VI) removal from aqueous solutions using Ni/Fe bimetallic nanoparticles: characterization, kinetics and mechanism. RSC Adv. 4, 50699–50707.
Zhou, H., He, Y., Lan, Y., Mao, J., Chen, S., 2008. Influence of complex reagents on removal of chromium(VI) by zero-valent iron. Chemosphere 72 (6), 870–874.
Zhou, L., Zhang, G., Wang, M., Wang, D., Cai, D., Wu, Z., 2018. Efficient removal of hexavalent chromium from water and soil using magnetic ceramsite coated by functionalized nano carbon spheres. Chem. Eng. J. 334, 400–409.
Zhou, X., Jing, G., Lv, B., Zhou, Z., Zhu, R., 2016. Highly efficient removal of chromium (VI) by Fe/Ni bimetallic nanoparticles in an ultrasound-assisted system. Chemosphere 160, 332–341.
Zhu, F., Li, L., Ren, W., Deng, X., Liu, T., 2017. Effect of pH, temperature, humic acid and coexisting anions on reduction of Cr(Ⅵ) in the soil leachate by nZVI/Ni bimetal material. Environ. Pollut. 227, 444–450.
Zhu, F., Ma, S., Liu, T., Deng, X., 2018. Green synthesis of nano zero-valent iron/Cu by green tea to remove hexavalent chromium from groundwater. J. Clean. Prod. 174, 184–190.
Zou, H., Hu, E., Yang, S., Gong, L., He, F., 2019. Chromium(VI) removal by mechanochemically sulfidated zero valent iron and its effect on dechlorination of trichloroethene as a co-contaminant. Sci. Total Environ. 650, 419–426.
Zou, Y., Wang, X., Khan, A., Wang, P., Liu, Y., Alsaedi, A., Hayat, T., Wang, X., 2016. Environmental remediation and application of nanoscale zero-valent iron and its composites for the removal of heavy metal ions: a review. Environ. Sci. Technol. 50 (14), 7290–7304.

Environmental Research 197 (2021) 111151

Contents lists available at ScienceDirect

Environmental Research

journal homepage: www.elsevier.com/locate/envres

Highly surface activated carbon to remove Cr(VI) from aqueous solution with adsorbent recycling

Yi Fang [a], Ke Yang [a], Yipeng Zhang [a], Changsheng Peng [b,**], Aurora Robledo-Cabrera [a], Alejandro López-Valdivieso [a,*]

[a] Instituto de Metalurgia, Universidad Autónoma de San Luis Potosí, Av. Sierra Leona 550, C.P, 78210, Mexico
[b] School of Environmental and Chemical Engineering, Zhaoqing Univerity, Zhaoqing, 526061, China

ARTICLE INFO

Keywords:
Activated carbon
Chromium removal
Adsorption
High-intensity ball milling
Reusability

ABSTRACT

To enhance the inferior removal capability of aqueous Cr(VI) by commercial activated carbon under neutral conditions. The emerging ball milling technology was employed and the removal efficiency of Cr(VI) by ball-milled highly activated carbon (HAC) increased from 68.3% to 99.0% under pH 6 and from 42.7% to 77.8% under pH 7 compared to pristine activated carbon (AC), respectively. Raman spectra and Boehm's titration results signified that the enhanced Cr(VI) removal performance of HAC under neutral conditions was associated with the enriched surface acid functional groups, in which the content of COOH groups increased from 0.31 mmol/g to 0.97 mmol/g. Two Cr(VI) removal mechanisms were proposed established on the acid and alkalic solution washed chromium-loaded HAC, involving the reduction of Cr(VI) to Cr(III) subsequently accompany with the formation of chromium hydroxides on the surface and inside the pores of HAC, and the bonding of CrO_4^{2-} on the surface COOH groups, as confirmed by SEM-EDX element mapping and specific surface area and porosity measurements. The Pseudo-second order model and Freundlich model fitted the adsorption kinetic and isotherm of AC and HAC well severally, suggesting that the specific interaction of Cr(VI) with the HAC surface and the Cr(VI) removal was multi-layer adsorption. Thermodynamic study exhibited the spontaneity of Cr(VI) removal on ball-milled HAC was increased. Reusability and regeneration studies of HAC denoted the potential application on Cr(VI) uptake under neutral conditions.

1. Introduction

Chromium is a highly toxic contaminant in the effluents of electroplating and tanning factories, threatening the health of humans by bioaccumulation in the food chain (Barrera-Diaz et al., 2012). Cr(VI) and Cr(III) are the two main chromium species. Cr(VI) shows a higher solubility, mobility, and toxicity as compared to Cr(III) (Hu et al., 2010). There are not sparingly soluble Cr(VI) compounds, but in the case of Cr (III), Cr_2O_3 is a compound that has a very low solubility. Therefore to remove Cr(VI), it is a common practice to reduce soluble anion Cr(VI) to Cr(III) followed by precipitation. Conventional reducing agents for Cr (VI) are sulfur compounds and iron salts (Barrera-Diaz et al., 2012), which are effective in acidic conditions. Under these conditions, the predominant Cr(VI) species are $HCrO_4^-$ (Acharya et al., 2018). Salts with the sulfoxy species SO_3^{2-}, $S_2O_5^{2-}$ as well as SO_2(g) are the most common reducing agents and rapidly reduce Cr(VI) at pH 2.5 (Jiang et al., 2016; Suzuki, 1999). Fe^{2+} ions also reduce Cr(VI) at a high rate at low pH (Jardine et al., 1999). Under acidic conditions, Cr^{3+} ions are predominant, and aqueous solution pH should be increased with lime or base compounds to precipitate them as $Cr(OH)_3$(s). The optimum removal conditions for Cr(VI) and Cr(III) are different from each other. Cr $(OH)_3$(s) precipitates as ultrafine particles with low flocculation, settling, and filtration rates. As a result, the generated residue is a sludge with high moisture content and is difficult to dispose of as a green discharge. Other techniques have been proposed to remove Cr(VI) from aqueous solutions such as electrodialysis followed by precipitation and electroreduction (Alvarado et al., 2009; Peng et al., 2004, 2005; Velasco et al., 2016), ion exchange (Qin et al., 2020), bioremediation (Qin et al., 2020) and modified zero-valent iron (ZVI) and zeolite materials (Ahmadi et al., 2017; Massoudinejad et al., 2015). These techniques

* Corresponding author.
** Corresponding author.
E-mail addresses: nikonplussigma@gmail.com (Y. Fang), keyang1020@gmail.com (K. Yang), lionsa90@gmail.com (Y. Zhang), cspeng@ouc.edu.cn (C. Peng), acabrera@uaslp.mx (A. Robledo-Cabrera), alopez@uaslp.mx (A. López-Valdivieso).

https://doi.org/10.1016/j.envres.2021.111151
Received 20 November 2020; Received in revised form 20 March 2021; Accepted 6 April 2021
Available online 20 April 2021

have the disadvantage of being of high energy consumption and high cost to produce the synthetic adsorbents.

AC has aroused attention for the removal of heavy metals because of its low cost and easy handling (Kakavandi et al., 2018; Su et al., 2019). AC presents a high specific surface area and surface functional groups and electron donors to convert Cr(VI) to Cr(III) (Herrera-Gonzalez et al., 2019; Huang et al., 2009; Pamphile et al., 2019; Park et al., 2008; Wang et al., 2010). It has been found that removal of Cr(VI) is effective at acid conditions in the range of pH 2–4 (Al-Othman et al., 2012; Anupam et al., 2011; Ghosh, 2009). At low pH, the AC surface functional groups are protonated, present a high reduction performance (Ramos et al., 1994) and Cr(VI) reduces to Cr(III) and precipitates as Cr_2O_3(s) (Cruz-Espinoza et al., 2012; Ibarra-Galván et al., 2014; Wang et al., 2020b). The high performance of AC for Cr(VI) reduction at low pH is similar to that shown by protonated *Ecklonia* biomass, which was 3.7 times higher than $FeSO_4 \cdot 7H_2O$ (Park et al., 2004).

Most waters and soils contaminated with Cr(VI) possess a pH higher than 3.0 so their pH needs to be lowered to about 3 to remove the Cr(VI) according to these studies (Hanson et al., 1993; Vainshtein et al., 2003). Once the adsorption step is completed, the pH then has to be raised to around neutral values to reuse the water and soil. These two steps of pH adjustments could be avoided if the Cr(VI) removal were carried out at near-neutral pH. Under these conditions Cr(VI) is predominantly as CrO_4^{2-} and Cr(III) as $Cr(OH)_3$(s). After an extensive literature survey, we found that Cr(VI) removal from water at near-neutral pH has not been investigated in detail. Neither has been studied the Cr(VI) desorption from the AC and the AC recycling.

The main aim of this study was to establish the most suitable conditions for the removal of Cr(VI) with AC at near-neutral pH using an AC with a high density of functional groups to enhance the Cr(VI) adsorption and regenerating the AC for its recycling to the adsorption step. It is worth mentioning that this the first work facing these two aspects for the processing of waters contaminated with Cr(VI). Batch Cr(VI) adsorption tests were carried out at pH 6 and 7 with fresh and regenerated AC. The functional groups on the AC were characterized by electrokinetics and surface titration while the Cr species on the AC were identified by SEM (scanning electron microscopy) coupled to an EDX (energy-dispersive X-ray spectroscopy). AC with the high density of functional groups was prepared by high-intensity ball milling (Cho et al., 2020; Lyu et al., 2018a).

2. Materials and methods

2.1. Adsorbents and chemicals

Granular coconut shell AC was purchased from Calgon Company. Its chemical composition was 97% C and 3% inorganic residues (Cruz-Espinoza et al., 2012). The HAC was prepared by ball milling −20 μm size particles of AC for 60 min, using a planetary mono mill (Pulverisette 6, Fritsch, Germany) with steel balls of 5 mm in size as the grinding media. 10 g AC was mixed with the steel balls and milled at a speed of 300 rpm. This milled product is referred to highly activated carbon (HAC) throughout this manuscript. Its D_{80} (particle size of cumulative undersize at 80%) size of the HAC was found to be 4 μm, the specific surface area was 928.5 m^2/g, and the mean pore size was 15.3 Å. The HAC was dried at 60 °C for 24 h, then kept in a plastic flask in a glass desiccator. Analytical grade potassium dichromate ($K_2Cr_2O_7$) was the source of Cr (VI) and acquired from J.T.Baker. A stock solution with a concentration of 1000 mg/L Cr(VI) was prepared for all the adsorption tests. All aqueous solutions were prepared with deionized water of 18.2 Ω, which was obtained by passing distilled water through a Barnstead E-pure II Water Purification Systems, Thermo Scientific, USA. 1.0 mol/L aqueous solutions of both sulfuric acid and sodium hydroxide were used to adjust the pH in the adsorption tests. All other inorganic chemical reagents such as H_2SO_4, H_3PO_4, NaOH, and $NaHCO_3$ were of analytical grade.

2.2. Adsorbent characterization

Adsorbed chromium species on HAC were determined through SEM coupled to an EDAX. The surface functional carboxyl and hydroxyl (phenolic, hydroxyl, and lactols) groups of the AC and HAC were quantified by Boehm's titration method (Boehm, 2002). Briefly, the method is as follows: stir 200 mg AC in 100 ml deionized water with the desired $NaHCO_3$ and NaOH concentration for 20 h, take a 50 ml aliquot and titrate it with a normalized HCl aqueous solution. The content of carboxyl and hydroxyl groups was determined from the loss of $NaHCO_3$ and the loss difference of NaOH and $NaHCO_3$, respectively.

A Zeta Probe equipment (Colloidal Dynamics, USA) was employed to determine the zeta potential of AC and HAC. For these measurements, a 3 g sample was stirred ultrasonically in 100 ml with a 0.01 mol/L NaCl concentration at 150 rpm for 5 min. For the zeta potential measurements, 0.1 mol/L of both HCl and NaOH aqueous solutions titrated automatically the carbon suspension for pH adjustment throughout the zeta potential quantification. All these measurements were performed at 22 °C. The equipment uses the electrokinetic sonic amplitude (ESA) to determine the zeta potential of particles in suspensions. Two electrodes with a high-frequency electric field are immersed in the suspension. For the moment, the particles oscillate back and forth with the electric field and most of the particle oscillations cancel one another out, but the oscillation does not take place near the electrodes, and a sound wave is generated from there. The sound wave would hit a transducer along the delay rod. Therefore, the transducer will produce a sinusoidal voltage signal by vibration. The generated amplitude value of the sinusoidal voltage signal equals the ESA number. The mathematic relation between ESA and dynamic mobility (μ_d) is given by Eq. (1) (Carasso et al., 1995; Rao et al., 2009).

$$ESA = A(\omega)\phi\frac{\triangle\rho}{\rho}Zu_d \tag{1}$$

where A(ω) is the instrument calibration factor, which can be determined by calibration with potassium silico tungstate solution (KSiW), ϕ is the particle volume fraction (3% in our study), △ρ is the density difference between particle (1.91 g/cm^3) and solvent (1.00 g/cm^3), ρ is the solvent density and Z is a factor related to the acoustic impedance of suspension and delay rod of the instrument. Finally, u_d was converted to zeta potential (ζ) by Henry's equation, represents as Eq (2) (Hunter, 2001):

$$u_d = \left(\frac{2\varepsilon\zeta}{3\eta}\right)f(\kappa a) \tag{2}$$

where ε is the dielectric constant, η is the water viscosity, f(κa) is Henry's factor. A simple value for f(κa) is 1.5, referred to the modified Smoluchowski equation (Smoluchowski, 1921).

The specific surface area and pore size of HAC before and after Cr(VI) adsorption were determined by gas adsorption measurement using an Autosorb-1, Quantachrome instrument. A desired amount of sample was heated and degassed at 80 °C before analysis, then nitrogen adsorption and desorption were conducted at 77.3 K liquid nitrogen. The multipoint BET, BJH methods were used to calculate the specific surface area and pore size, respectively.

Raman spectra (DXR, Thermo scientific, USA) were utilized to obtain the detailed carbon structure change caused by ball milling and XPS (X-ray photoelectron spectroscopy) was used to determine the C, N, S, and O elements content.

2.3. Cr(VI) uptake experiments

Adsorption kinetics studies were performed with 5g adsorbent and 100 ml, 1000 mg/L Cr(VI) at pH 6 and 7. A 20 μL aliquot was withdrawn from the aqueous solution at various time intervals such as 0.25, 0.5, 1, 3, 5, 7, 9, 12, 15, 30, 60, 120 min. The aliquot was analyzed for Cr(VI)

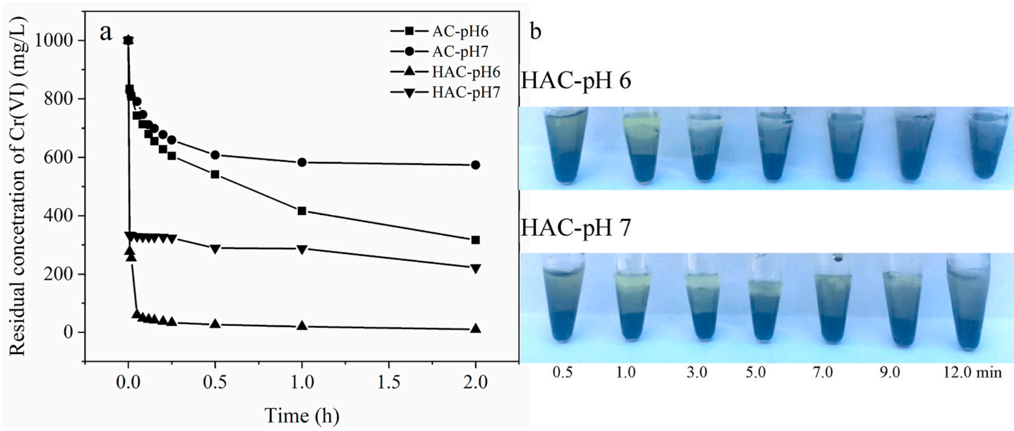

Fig. 1. (a) The depletion curve of Cr(VI) by AC and HAC under pH 6 and 7 as time (AC average size is 20 μm, HAC average size is 4 μm, dose 5g/100 ml, 1000 mg/L Cr(VI), RPM = 350, 295K); (b) The aqueous solution color change as time of Cr(VI) removal by HAC. (For interpretation of the references to color in this figure legend, the reader is referred to the Web version of this article.)

and total Cr. Adsorption isotherms were built within a Cr(VI) concentration range of 800–2000 mg/L at 295, 308, and 323 K by contacting the adsorbent with the Cr(VI) for 24 h. Before the addition of Cr(VI), the AC and HAC were pre-treated for the equilibrium of their surface groups with the aqueous solution as follows: 5 g adsorbent was mixed with 100 ml deionized water, and the pH was stabilized at 6 and 7 until the pH did not change, which occurred at about 30 min. Then, potassium dichromate was introduced to the suspensions at the desired Cr(VI) concentration.

The HAC suspension was stirred in a 250 ml Erlenmeyer flask using a Thermo scientific magnetic stirrer at 400 rpm at 22 °C. An aliquot of 100 μL was withdrawn from the aqueous suspension and centrifuged at 8000 rpm for 10 min using an Allegra™ 21 Centrifuge (Beckman coulter, USA). The supernatant was analyzed for total Cr and Cr(VI). Total Cr was determined through atomic absorption spectrophotometry, while the Cr (VI) by a colorimetric method using a UV/Vis spectrophotometer (Thermo Scientific, USA. with a light path of 1 cm) at 540 nm. 1,5–diphenylcarbazide was used as an indicator (Association et al., 1915). The concentration of Cr(III) was determined by the difference between total Cr and Cr (VI). Unless otherwise stated, all the adsorption experiments were performed with a blank control at 22 °C.

2.4. Cr desorption from HAC after treatment with Cr(VI)

Cr (VI) desorption from the HAC and HAC surface regeneration was carried out by acid and alkali elution experiments. First, HAC and pristine AC were repeatedly contacted (four times) with a 1000 mg/L Cr (VI) aqueous solution to obtain a Cr-loaded material. The Cr-loaded HAC (0.5g) and Cr-loaded AC (0.5g) were then treated with 0.2 mol/L H_2SO_4 (50 ml) and 0.1 mol/L NaOH (50 ml) aqueous solutions. The amount of desorbed chromium (mg/g) after elution was determined as follows;

$$q = \frac{C_t V}{m} \tag{3}$$

where q (mg/g) is the chromium content desorbed from the carbon materials, C_t (mg/L) is the chromium concentration in the eluted solution at time t, V (L) is the volume of the elution solution and m (g) is the mass of the material.

2.5. Regeneration and reusability of HAC

Consecutive adsorption tests were conducted to investigate the reusability of HAC on Cr(VI) (1000 mg/L) adsorption. The HAC was contacted with an H_2SO_4 solution of 0.1 mol/L for 24 h stirring the suspension at 400 rpm in a magnetic stirrer to regenerate the surface of the HAC treated with Cr(VI) solution (Giri et al., 2012). This regenerated material was then used in the next Cr(VI) adsorption test.

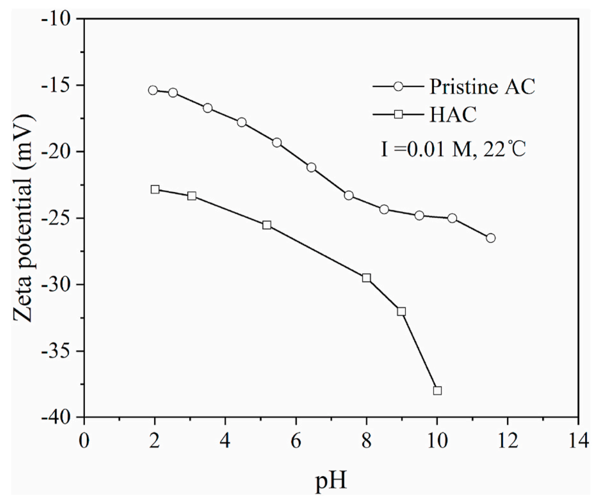

Fig. 2. Zeta Potential of AC (20 μm) and HAC (4 μm) as a function of pH.

3. Results and discussions

3.1. Effect of ball milling on Cr(VI) sequestration

Fig. 1 (a) depicts the depletion of Cr(VI) concentration as a function of time at pH 6 and 7. It is seen that for both pHs, the Cr(VI) concentration depletion was very fast in the first 0.25 h, being this depletion larger at pH 6. The Cr(VI) removal by HAC was 99.0% and 77.8% at pH 6 and 7 after 2 h, respectively. These Cr(VI) removals were larger than those on pristine AC (68.3% at pH 6 and 42.7% at pH 7). Thus, a significant increase in Cr(VI) removal was achieved with the HAC. The figure also shows photos of the Cr(VI) aqueous solutions at various times at the two pH values. The increase in Cr(VI) adsorption can be associated with the increase of the functional groups on the AC. In Fig. 1 (b), it is noted that the color of the Cr(VI) aqueous solution became more crystal clear at pH 6 than at pH 7, clearly indicating that more Cr(VI) was removed at pH 6.

Table 1
The surface chemical properties before and after ball milling AC and HAC treated with Cr(VI).

Sample	Total acidic group (mmol/g)	Carboxyl (mmol/g)	Phenolic, hydroxyl, and lactols (mmol/g)
		-COOH	-OH
Pristine AC	1.31	0.31	1.00
AC after milling HAC	1.84	0.97	0.87
HAC after Cr(VI) adsorption	1.94	ND	1.94

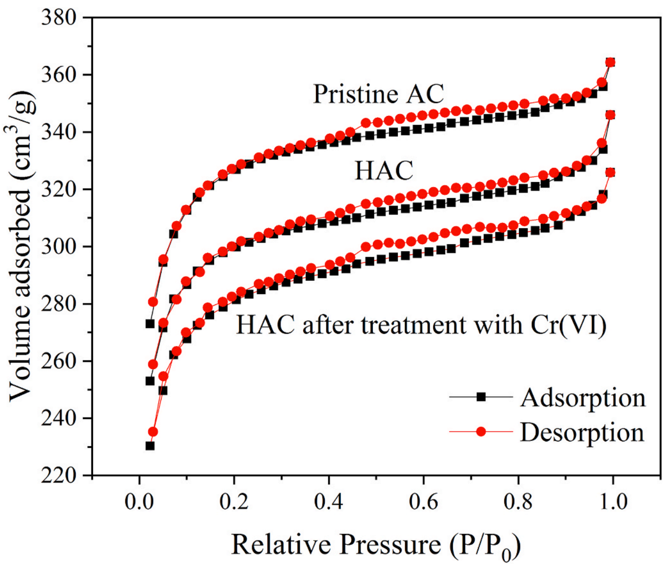

Fig. 3. N_2 adsorption-desorption isotherms (BET) of pristine AC, HAC and HAC treated with Cr(VI).

3.2. Characterization of materials

3.2.1. Surface and texture chemistry of materials

Fig. 2 shows the zeta potential of pristine AC and HAC as a function of pH. It is seen that the zeta potential decreased negatively as the pH increased, as reported elsewhere (Dai, 1994; Julien et al., 1998). The negative zeta potential of AC and HAC is due to the dissociation of their acidic functional groups (Song et al., 2010) and Chingombe et al. (2005) have reported that the zeta potential of AC becomes more negative as the acid functional groups increased. As noted in Fig. 2, the zeta potential of HAC is more negative than that of AC, indicating that the ball milling promoted the formation of acid functional groups of the carboxylic type. This was confirmed by determining the surface density of the functional groups before and after milling. Table 1 presents the surface density of the total acidic and alkaline functional group before and after milling, as well as after adsorption of Cr(VI). It is noted that the total acidic group of the AC increased from 1.31 mmol/g to 1.84 mmol/g after grinding, due mainly to the increase of COOH groups. Our results are consistent with those of Lyu et al. (2018) who have reported that the total acidic groups in biochar increased from 0.3 mmol/g to 1.35 mmol/g after high intensity grinding of the biochar (Lyu et al., 2018b). Recent studies proved that more oxygen/hydrogen functional groups were introduced into activated carbon during the ball milling and increased the hydrophilicity of activated carbon (Lyu et al., 2017; Takaesu et al., 2019). As noted in Table 1, after Cr(VI) adsorption no carboxylic groups were detected on the HAC. This can be accounted for by the shielding of these groups by adsorbed Cr(VI) as explained below. Therefore, the COOH groups played a vital role in Cr(VI) adsorption. The increase in hydroxyl surface density after adsorption is due to $Cr(OH)_3$, which is formed from the reduction of Cr(VI).

The N_2 adsorption and desorption isotherms and pore size of pristine AC, HAC, and after adsorption are shown in Fig. 3. Referring to the classification of physisorption isotherms (Sing, 1985), the N_2 adsorption and desorption curves of the three materials fitted well with the type IV adsorption isotherm (IUPAC classification). The hysteresis loop in Fig. 3 ascribed to H4 type means a narrow slit-like pore structure, commonly seen in micropore activated carbon materials (Guedidi et al., 2013). The higher surface area of HAC can be associated with its smaller particle size in comparison to that of AC. After adsorption of Cr(VI), the surface area of HAC decreased and the pore size increased, which is due to the filling of adsorbed Cr in the pores. Figs. 4 and 5 show SEM photomicrographs of Cr-loaded HAC. As noted, there is chromium on the surface and inside of the HAC, being the content of chromium on the surface much higher than that inside the particle. A similar texture to that seen in Fig. 5 has been reported by Wang et al. (2020). They reported the formation of an eskolaite (Cr_2O_3) layer on the AC surface, which lowers the Cr(VI) adsorption capacity of AC and the diffusion of Cr(VI) to the interior of the AC particle.

Chromium layerAs can be seen in Figs. 4 and 5, chromium was detected on the surface and inside of the HAC particle, being the content of chromium on the surface much higher than that inside the particle. Table 2 compares the summary statistics of surface area and pore size analysis results, it noticeable from this table that the chromium in the HAC lowered the specific surface area and mean pore size of the HAC from 929 m^2/g to 876 m^2/g and 15.3 Å to 18.5 Å, respectively. A similar texture to that seen in Fig. 5 has been reported by Wang et al. (2020) in Cr-loaded AC particles after adsorption at pH 3 (Wang et al., 2020b). They reported the formation of an eskolaite (Cr_2O_3) layer on the AC

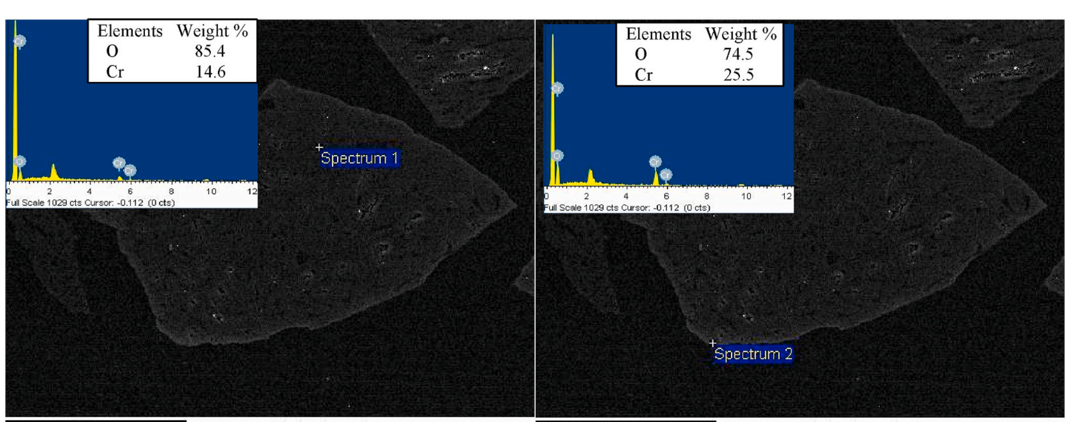

Fig. 4. SEM photomicrograph and quantitative analysis EDX pattern after HAC adsorption at pH 7.

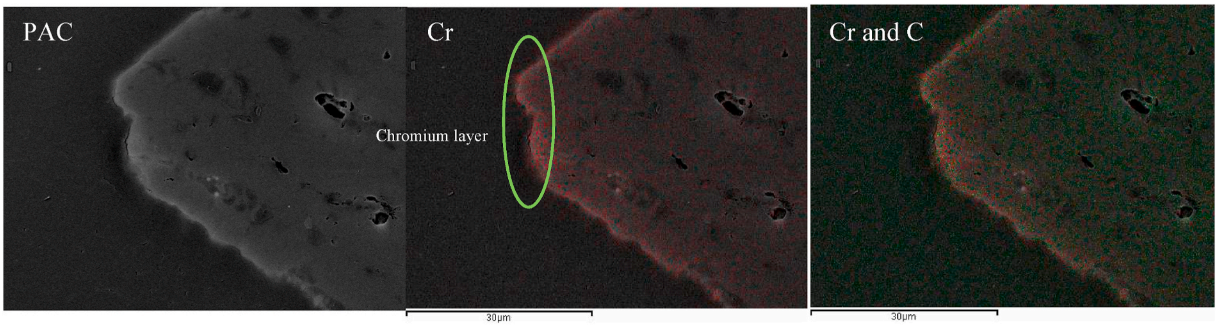

Fig. 5. SEM figure and SEM-EDX elements mapping of HAC after adsorption at pH 7.

Table 2
Pore structural parameter of AC, HAC, and HAC after Cr(VI) adsorption.

Materials	Average particle size (μm)	Specific surface area (m^2/g) (BET)	Pore size (Å) (BJH)
Pristine AC	20	846	19.0
HAC	4	929	15.3
HAC after Cr(VI) adsorption	4	876	18.5

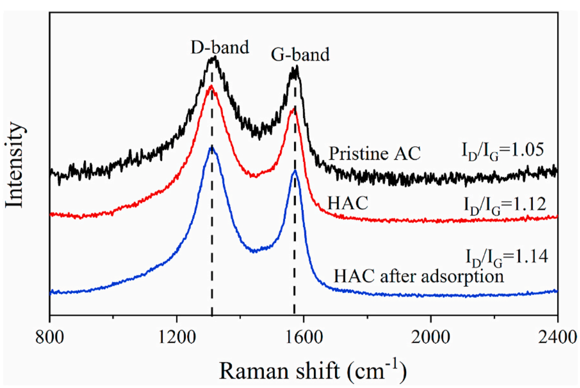

Fig. 6. Raman spectra of pristine AC, HAC and HAC after adsorption of Cr(VI).

surface, which lowers the Cr(VI) adsorption capacity of AC and the diffusion of Cr(VI) to the interior of the AC particle. Besides, the increased BET surface area of HAC generated by ball milling may be explained by the decreased particle size and the deformation of the carbon structure.

3.2.2. Raman spectra investigation

Fig. 6 shows the Raman spectra of AC, HAC, and HAC after Cr(VI) adsorption. The D-band (1320 cm^{-1}) and G-band (1563 cm^{-1}) in the spectra reveal the degree of lattice distortion of any carbon material, The D-band represents the stretch vibration of sp^3 hybridized carbon, while the G-band is related to the sp^2 graphited carbon (Cuesta et al., 1994). It has been reported that the ratio of the intensity of D-band versus G-band (I_D/I_G) indicates the level of graphitization or structural order of carbon materials (Chen et al., 2017). As noted in Fig. 6, the I_D/I_G of HAC increased from 1.05 for pristine AC to 1.12 and further increased to 1.14 after adsorption of Cr(VI). The increase of I_D/I_G for HAC revealed that ball milling enhanced the formation of sp^3 defects in the carbon structure. Moreover, the increase of sp^3-bonding hybridized carbon atoms of HAC after Cr(VI adsorption may due to the reduction of surface oxygen-containing functional groups (Cong et al., 2012). Various studies have demonstrated that the reduction of surface oxygen-containing functional groups caused the formation of amorphous carbon structure (Li et al., 2016; Sangkarak et al., 2020). The increase of surface functional groups for HAC by ball milling seems to be contradictory with the increase of disorder of structural carbon. This inconsistency may be due to the relatively more produced hybridized carbon atoms by ball milling compare to the increase of oxygen-containing groups.

Table 3
The elements analysis of HAC and treated HAC with Cr(VI).

	C	N	O	S
HAC (%)	91.24	0.93	6.86	0.97
Treated HAC (%)	84.58	0.50	13.01	1.91

The content of C, O, N, and S in HAC and HAC after Cr(VI) adsorption was determined through XPS and the results are presented in Table 3. It is seen that the C content decreased after Cr(VI) adsorption and the O element increased. The decrease of carbon content can be related to the decline of C-containing surface functional groups, coupled to the reduction of Cr(VI) to Cr(III). The increase of O content can be associated with the chromium oxide resulting from the Cr(VI) reduction, proving that a chromium species containing oxygen formed from the Cr(VI) reduction.

3.3. Adsorption kinetics

To investigate the adsorption kinetics of aqueous Cr(VI) adsorption on pristine AC and HAC, and recognize the divergence of the rate constant before and after ball milling. The kinetics models of Pseudo-first order, Pseudo-second order, interparticle diffusion, and Elovich were employed and the general forms as Eqs (4)–(7) (Azari et al., 2015a; Sparks, 1998).

Pesudo-first order model

$$\ln(\Gamma_e - \Gamma_t) = \ln\Gamma_e - k_1 t \tag{4}$$

Pseudo-second order model

$$\frac{t}{\Gamma_t} = \frac{t}{\Gamma_e} + \frac{1}{k_2\Gamma_e^2} \tag{5}$$

Weber-Morris Interparticle diffusion model

$$\Gamma t = k_3 t^{1/2} + I \tag{6}$$

Elovich model

$$\Gamma_t = \beta\ln(\alpha\beta) + \beta\ln t \tag{7}$$

where Γe(mg/g) is the adsorption density at equilibrium, Γt(mg/g) is adsorption density at time t, k_1 (h^{-1}) is the rate constant of Pesudo-first order model, k_2 (mg/g·h) is the rate constant of Pesudo-second order, k_{id} and I are the constants of interparticle diffusion, α (mg g^{-1} h^{-1}) and β (g mg^{-1}) are the initial sorption rate of adsorbate and desorption constant, respectively.

As shown in Fig. 7, the Cr(VI) adsorption data were linearly fitted with adsorption kinetic models, the detailed parameters for models were

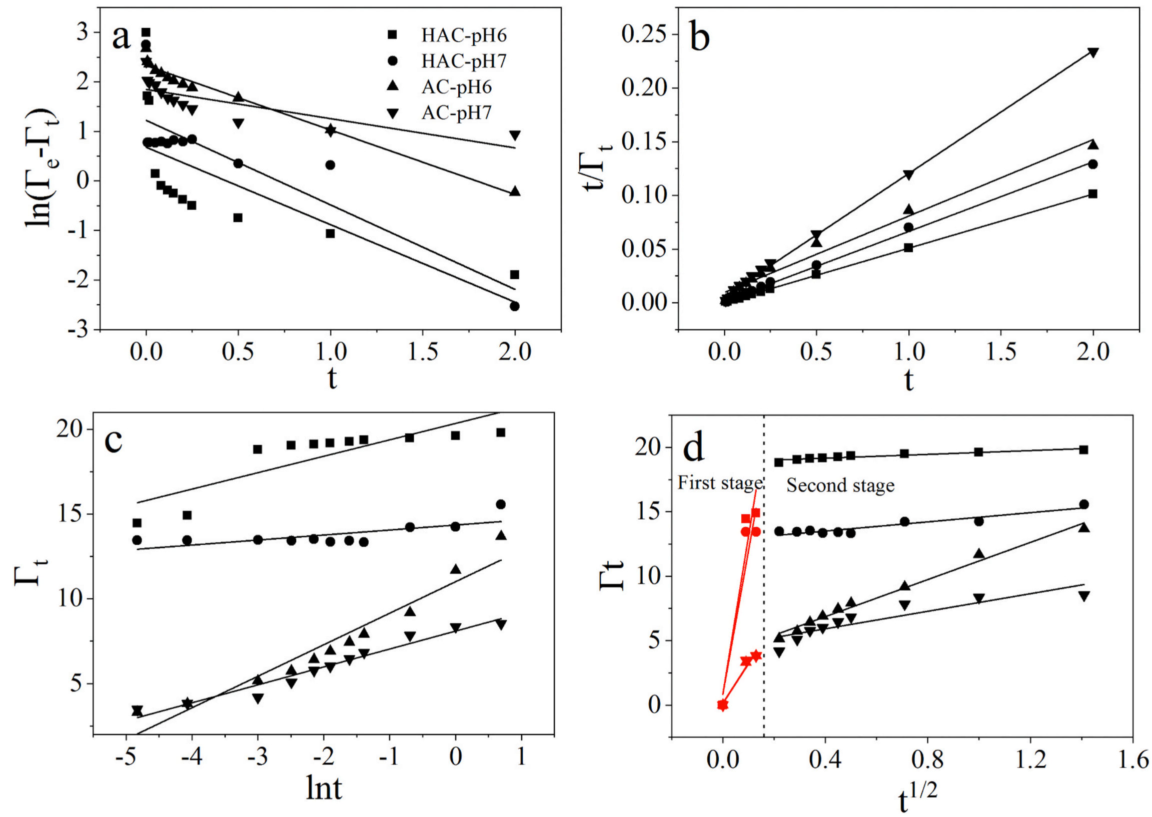

Fig. 7. The linear fit for experimental date of Cr(VI) removal by HAC and AC under pH 6 and 7, (a) Pseudo-first order, (b)Pseudo-second order, (c) Elovich, (d) Interparticle diffusion.

Table 4
The adsorption kinetic model parameters for Cr(VI) removal by AC and HAC under pH 6 and 7.

	HAC		Pristine AC	
Models	pH6	pH7	pH6	pH7
Pseudo-first order				
Γe (mg/g)	1.97	3.39	10.28	6.36
k_1 (h^{-1})	1.56	1.71	1.30	0.59
r^2	0.461	0.746	0.972	0.627
Pseudo-second order				
Γe (mg/g)	20	15.38	14.08	8.77
k_2 (mg/g·h)	8.39	2.88	0.53	2.23
r^2	1.000	0.998	0.983	0.999
Elovich				
α (mg g^{-1} h^{-1})	1.3×10^9	1.9×10^{21}	199.0	1946.5
β (g mg^{-1})	0.97	0.30	1.86	1.06
r^2	0.755	0.951	0.978	0.985
Interparticle diffusion				
k_{id1}	122.39	111.24	30.64	30.94
I_1	0.81	0.81	0.13	0.16
r_1^2	0.924	0.910	0.967	0.951
k_{id2}	0.73	1.78	7.20	3.40
I_2	18.86	12.79	3.98	4.55
r_2^2	0.880	0.892	0.986	0.799

presented in Table 4. The Cr(VI) removal is described well with Pseudo-second order kinetic model for HAC and AC under pH 6 and pH 7 with higher correlation coefficients (r^2), suggesting that the interaction between the Cr(VI) and the functional groups of the HAC and AC is of the chemical type. As described in Table 4, the rate constant of k_2 at pH 6 was nearly 3 times greater than that at pH 7 for HAC, and the rate constant for HAC under pH 6 and 7 both increased after ball milling compared to the pristine AC. Indicating that the adsorption rate was highly favorable with the hydrogen ion strength and the developed Cr (VI) removal capacity on HAC was associated with the quicker chemical reaction between Cr(VI) and surface functional groups. Besides, the chemical reaction associated with the Cr(VI) adsorption was significantly related to the proton concentration, in agreement with studies reported previously (Acharya et al., 2009; Al-Othman et al., 2012; Demiral et al., 2008; Park et al., 2004; Wang, 2018).

The diffusion process of aqueous adsorbate into adsorbent can be elucidated by the Interparticle diffusion model. Briefly, the adsorbate ions transfer through bulk solution into the external surface of the adsorbent and then transfer into the internal surface followed by adsorption in the active sites of adsorbent (Gürses et al., 2006). As can be seen in Fig. 7 (d), the diffusion route of Cr(VI) into AC and HAC contains two steps. The first stage of adsorption dominants the removal rate of Cr (VI) by AC and HAC since the interparticle diffusion rates at the first stage (k_{id1}) for AC and HAC were both higher than that of the second stage (k_{id2}). The k_{id1} of HAC under pH 6 and 7 were nearly 4 times higher than that of AC, this finding has identified that the rate of Cr(VI) transfers from the bulk solution to the surface of AC was improved after ball milling pretreatment.

3.4. Adsorption isotherms

Langmuir, Freundlich, Dubinin-Radushkevich (D-R), and Temkin models were employed to delineate the adsorption behavior of Cr(VI) (Azari et al., 2015b; Babaei et al., 2016), the non-linear equations of those models were presented as follows;

Langmuir equation

$$\Gamma e = \frac{K_L \Gamma_0 C_e}{1 + K_L C_e} \tag{8}$$

Freundlich equation

$$\Gamma e = K_F C_e^{1/n} \tag{9}$$

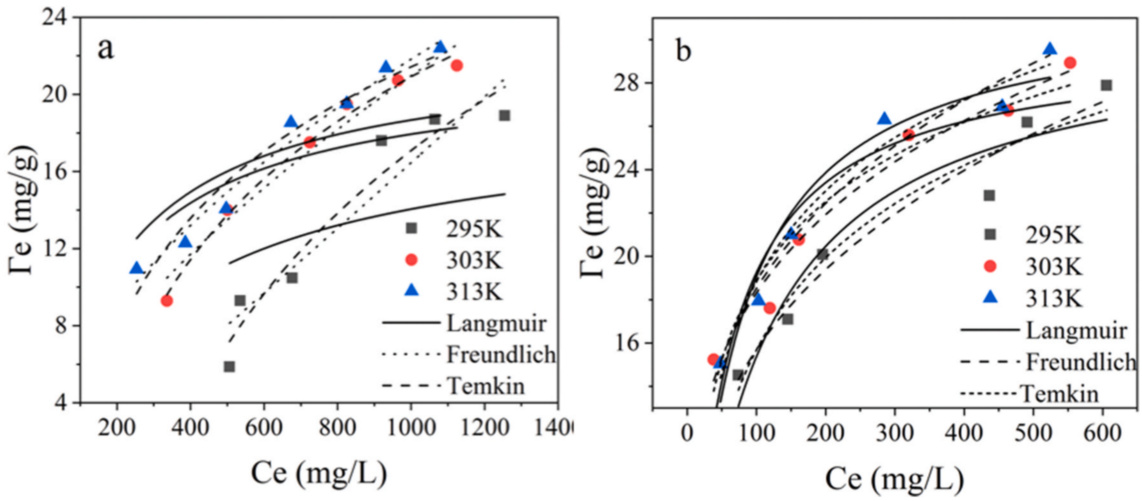

Fig. 8. Non-linear fit of adsorption isotherm models (a) AC (b) HAC (pH 7, 50 g/L).

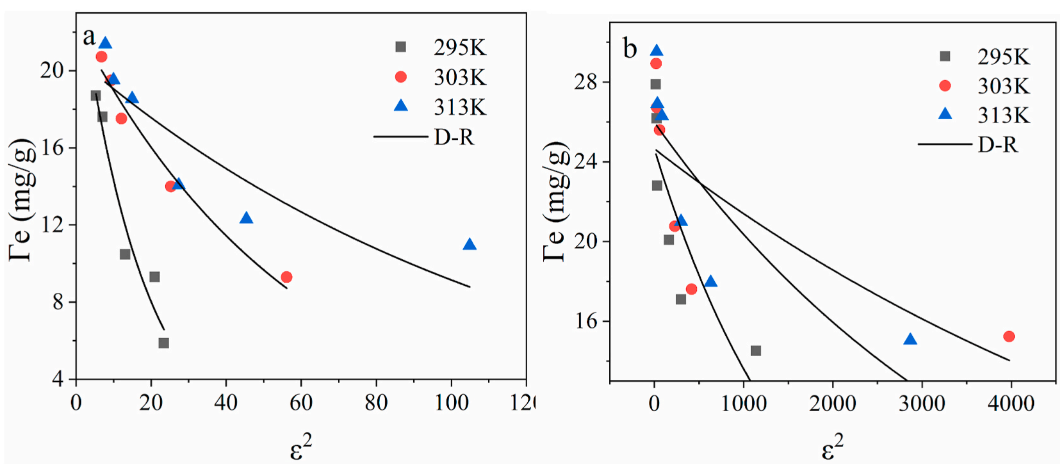

Fig. 9. Non-linear fit of D-R model for (a) AC and (b) HAC (pH 7, 50 g/L).

Table 5
The parameters of adsorption isotherm models for HAC and AC.

		AC			HAC		
Models		295	303	313K	295	303	313K
Langmuir	Γ_0 (mg/g)	18.9	21.5	22.4	31.6	31.7	32.6
	K_L (L/mg)	0.003	0.005	0.005	0.014	0.009	0.014
	r^2	0.438	0.600	0.704	0.919	0.851	0.947
Freundlich	K_F	0.002	0.158	0.441	3.843	5.523	5.179
	1/n	1.303	0.714	0.567	0.306	0.260	0.277
	r^2	0.942	0.982	0.973	0.962	0.970	0.971
Temkin	b_T (J/mol)	153.2	239.6	310.0	423.7	491.8	429.6
	K_T (L/g)	0.003	0.007	0.013	0.128	0.353	0.224
	r^2	0.904	0.997	0.945	0.949	0.941	0.971
D-R	Γmax (mg/g)	25.5	22.5	20.68	24.64	24.66	25.99
	K_D (mol^2 kJ^{-2})	0.058	0.017	0.008	5.9E-4	1.4E-4	2.4E-4
	r^2	0.950	0.977	0.793	0.706	0.545	0.697

Temkin equation

$$\Gamma e = \frac{RT}{b_T}\ln(K_T C_e) \tag{10}$$

D-R equation

Table 6
Comparison of Cr(VI) adsorption density onto various AC materials.

Adsorbents	Adsorption density (mg/g)	pH	References
Commercial AC	20.0	7	Huang and Wu (1977)
Polysulfide rubber modified AC	8.9	4	Mortazavian et al. (2019)
Pomegranate husk AC	10.0	6	Nemr (2009)
Chestnut oak shells AC	6.0	7	Niazi et al. (2018)
Tannic acid immobilized AC	0.5	7	Li et al. (2012)
Hazelnut shell AC	8.0	8	Kobya (2004)
Granular AC	7.2	7	Di Natale et al. (2007)
Fe-modified AC prepared from Trapa natans husk	2.5	7	Liu et al. (2010)
Micron-scale iron modified AC	1.3	6	Wang et al. (2020a)
AC derived from seagrass	0	≥4	Asimakopoulos et al. (2020)
Ball milled AC	28.9	7	This study

Table 7
The thermodynamic parameters for Cr(VI) adsorption on HAC and AC.

Adsorbent	Thermodynamic parameters			
	T (K)	ΔG (kJ/mol)	ΔH (kJ/mol)	ΔS (kJ/mol k)
HAC	295	−11.80	0.001	0.04
	303	−12.12		
	313	−12.52		
AC	295	−17.69	0.01	0.06
	303	−18.17		
	313	−18.77		

$$\Gamma e = \Gamma_{max} e^{-K_D \varepsilon^2} \varepsilon = RT \ \ln\left(1 + \frac{1}{C_e}\right) \quad (11)$$

where Γe (mg/g) is the equilibrium adsorption density, Γ_0 (mg/g) is the theoretical monolayer adsorption density, K_L (L/g) is the Langmuir constant, K_F is the Freundlich isotherm constant, Ce (mg/L) is equilibrium concentration, n is the Freundlich isotherm exponent, R (8.314 J/mol/K) is the universal gas constant, T (K) is the absolute temperature, b_T (J/mol) is the Temkin isotherm constant, K_T (L/g) is the Temkin isotherm equilibrium binding constant, Γmax (mg/g) is the theoretical saturation density, K_D (mol^2 kJ^{-2}) is the D-R isotherm constant, ε is the Polanyi potential.

Figs. 8 and 9 were the non-linear fit of Langmuir, Freundlich, Temkin, and D-R isotherm models, the computed theoretical parameters of the models were provided in Table 5. The higher correlation coefficients of the Freundlich model fitted the experimental data satisfactorily and this observation could support the hypothesis that the adsorption of Cr (VI) on AC and HAC was multi-layer. The values of n for HAC were all over 2 while values of n for AC were all below 2, which indicated the adsorption was favorable for HAC under ambient temperature (McKay et al., 1980). Table 6 listed the adsorption density comparison of different AC materials with this study.

3.5. Adsorption thermodynamics

The thermodynamic parameters enthalpy change (ΔH) and entropy change (ΔS) can be calculated by the function of $\ln K_C$ versus 1/T, the equation shown in Eq (12). Gibb's free energy change (ΔG) can be determined through the Van't Hoff equation (Eq (13)).

$$\ln K_c = \frac{\Delta S}{R} - \frac{\Delta H}{RT} \quad (12)$$

$$\Delta G = -RT\ln K_c \quad (13)$$

Where ΔH (kJ/mol) and ΔS (J/mol k) were established by the slope and intercept of Eq (12). The adsorption process is endothermic if the value of ΔH is positive, otherwise, it's exothermic. Equilibrium constant K_C equal to Γe/Ce (Al-Othman et al., 2012) or the intercept of the plot of ln (Γe/Ce) versus Γe (Lyubchik et al., 2004), the negative value of ΔG (kJ/mol) means the adsorption process prolongs spontaneously under ambient conditions.

The detailed values of ΔH, ΔS, and ΔG of Cr(VI) adsorption on HAC and AC are given in Table 7. The values of ΔG for HAC and AC were both negatives, signifying that the adsorption of Cr(VI) was spontaneous and the values of ΔG for HAC under different temperatures were both higher than that of AC, which implied the spontaneity of adsorption was unfavorable energetically and more spontaneity for HAC after ball milling (Chegrouche et al., 2009). The value of ΔH was positive for HAC and AC indicated the Cr(VI) adsorption process was endothermic. Positive values of ΔS of HAC and AC related to the disorderliness of the system.

3.6. Cr(VI) removal mechanism

3.6.1. The pH-speciation of Cr(III) and Cr(VI)

Fig. 10 is the pH-speciation diagram for 1000 mg/L Cr(VI) and Cr (III), which were built using equations (14)-(21). $HCrO_4^-$ and CrO_4^{2-} are predominant at pH 6, while CrO_4^{2-} predominates at pH 7. As shown in Fig. 10 (b), $Cr(OH)_3$(s) is the predominant species both at pH 6 and pH 7. The aqueous solution chemistry equilibriums for Cr(VI) and Cr(III) species are shown in Eqs (14) to (21) (Fahim et al., 2006; Gherasim et al., 2011; Kocaoba and Akcin, 2002), where k is the chemical reaction equilibrium constant (Butler et al., 1998).

$$H_2CrO_4 = HCrO_4^- + H^+ \ k = 10^{-0.43} \quad (14)$$

$$HCrO_4^- = CrO_4^{2-} + H^+ \ k = 10^{-6.49} \quad (15)$$

$$2HCrO_4^- = Cr_2O_7^{2-} + H_2O \ k = 10^{1.55} \quad (16)$$

$$Cr^{3+} + H_2O = Cr(OH)^{2+} + H^+ \ k = 10^{-3.56} \quad (17)$$

$$Cr(OH)^{2+} + H_2O = Cr(OH)^+{}_2 + H^+ \ k = 10^{-6.27} \quad (18)$$

$$Cr(OH)^+{}_2 + 2H_2O = Cr(OH)_3(aq) + H^+ \ k = 10^{-2.61} \quad (19)$$

$$Cr(OH)_3(aq) + H_2O = Cr(OH)_4^- + H^+ \ k = 10^{-10.33} \quad (20)$$

$$Cr(OH)_3(aq) = Cr(OH)_3(s) \ k = 10^{4.17} \quad (21)$$

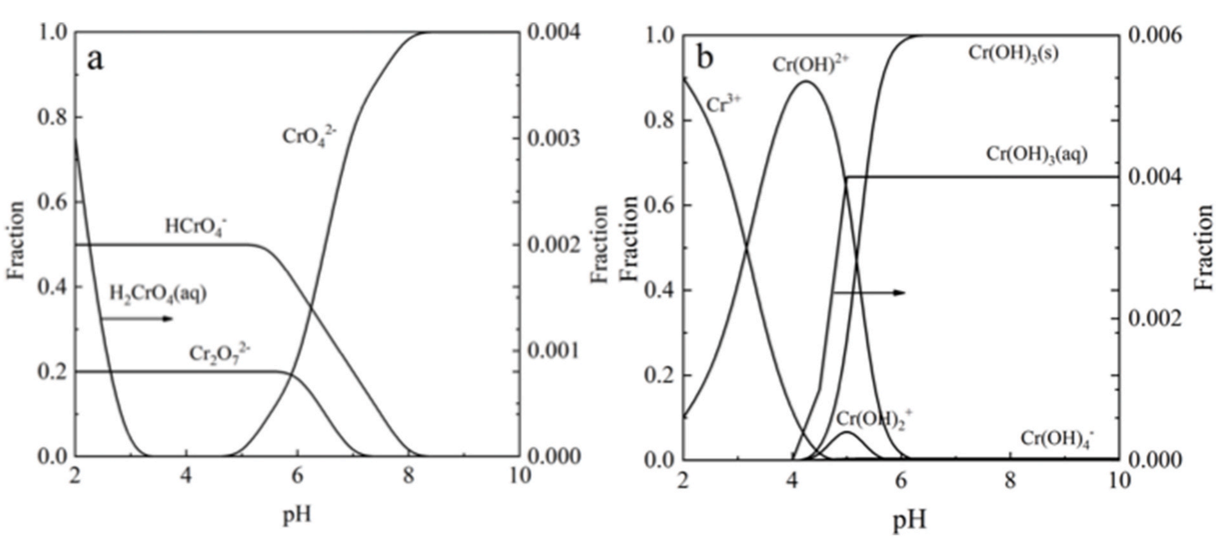

Fig. 10. The speciation diagram of (a) Cr(VI) and (b) Cr(III).

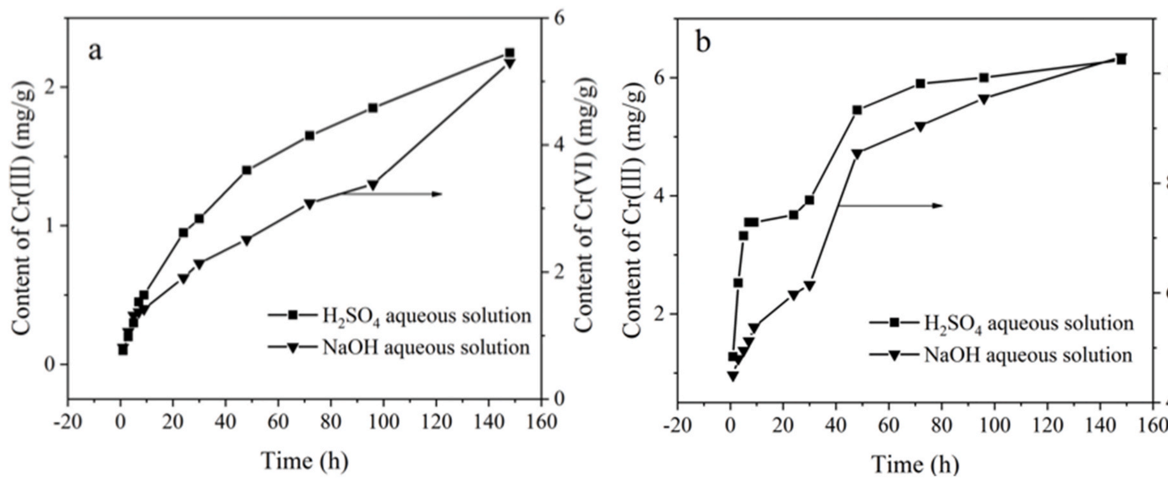

Fig. 11. The elution experiments with chromium-loaded virgin AC (a) and HAC (b) after adsorption at pH 7 (1.0 g/100 ml treated pristine AC or HAC, 0.2 M H_2SO_4 and 0.1 M NaOH, 295K).

It is noteworthy to remark that most studies on Cr(VI) removal have been undertaken at acidic conditions where $HCrO_4^-$ and Cr^{3+} are the predominant species. Under these pH conditions, Cr_2O_3(s) has been reported to be the end chromium product on AC (Cruz-Espinoza et al., 2012; Ibarra-Galván et al., 2014; Wang et al., 2020b). Our work was carried out at pH 6 and 7. Under these pH conditions, $Cr(OH)_3$(s) was the chromium product on the AC as discussed below.

3.6.2. Chromium species on HAC

Fig. 11(a) and (b) show the amount of Cr(III) and Cr(VI) desorbed from AC and HAC, after treatment with Cr(VI) at pH 7, using a 0.2 M H_2SO_4 and 0.1 M NaOH aqueous solution. Firstly, it is noted that Cr(III) desorbed from the carbons at acidic pH conditions, while Cr(VI) desorbed at basic pH. The Cr(III) in the eluants at acidic conditions likely results from the dissolution of $Cr(OH)_3$, leading to say that this is the Cr (III) species which formed from Cr(VI) adsorption. Cr(VI) in the eluants at basic conditions suggests that Cr(VI) co-adsorbed with the $Cr(OH)_3$(s) as CrO_4^{2-}. At basic pH, OH^- ions deprotonated the surface COOH groups, which is turned into the electrically negative COO- group. As a result, the adsorbed CrO_4^{2-} on the COOH is repelled and migrated to the aqueous solution. Desorbed Cr(VI) was 10.3 mg/g from HAC, much greater than the Cr(VI) desorbed from AC, which was 5.3 mg/g. Dissolved Cr^{3+} from HAC reached 6.3 mg/g, almost 3 times greater than the Cr^{3+} desorbed from AC. The much greater amount of chromium desorbed from the HAC in comparison to that desorbed from AC confirmed that high-intensity ball milling improved the adsorption performance of AC. More functional groups, especially carboxyl, were created on the AC surface, which in agreement with the work reported by (Baklanova et al., 2019; Lyu et al., 2018b).

The chromium elution under acidic and alkaline solution can be stated as Eqs (22) and (23), respectively.

$$HAC\cdots Cr(OH)_3(s) + 3H^+ \rightarrow HAC + Cr^{3+} + 3H_2O \quad (22)$$

$$HAC\text{-}COOH\cdot\cdot CrO_4{}^{2-} + OH^- \rightarrow CrO_4{}^{2-} + HAC\text{-}COO^- + H_2O \quad (23)$$

3.6.3. Proposal on chromium removal mechanism

The tests on chromium elution from the Cr-loaded HAC showed that Cr(III) as $Cr(OH)_3$(s) and Cr(VI) as CrO_4^{2-} were on the surface of HAC. The $Cr(OH)_3$(s) formed a layer on the HAC particle, as seen in Figs. 4 and 5. This $Cr(OH)_3$(s) resulted from the reduction of adsorbed Cr(VI) to Cr (III). According to Fig. 6(b), $Cr(OH)_3$(s) is the stable Cr(III) species at pH 6 and 7. The reduction of Cr(VI) to Cr(III) has been proposed to be due to π-electron in activated-carbon-basal planes (Franz et al., 2000; Miretzky and Cirelli, 2010; Yang et al., 2019). The reduction of Cr(VI) to Cr(III) and the surface precipitation of $Cr(OH)_3$ can be expressed as follows:

$$CrO_4{}^{2-} + 8H^+ + 3e^- = Cr^{3+}(aq) + 4H_2O \quad (24)$$

$$Cr^{3+} + 3H_2O = Cr(OH)_3(s) + 3H^+ \quad (25)$$

Adsorption of Cr(VI) may proceed through hydrogen bonding on the surface COOH groups, as follows:

$$HAC\text{-}COOH + CrO_4{}^{2-} = HAC\text{-}COOH\cdot\cdot CrO_4{}^{2-} \quad (26)$$

The encouraged capability of HAC on Cr(VI) sequestration was dominantly contributed by the increased surface oxygen-containing functional groups and the refined particle size in the presence of

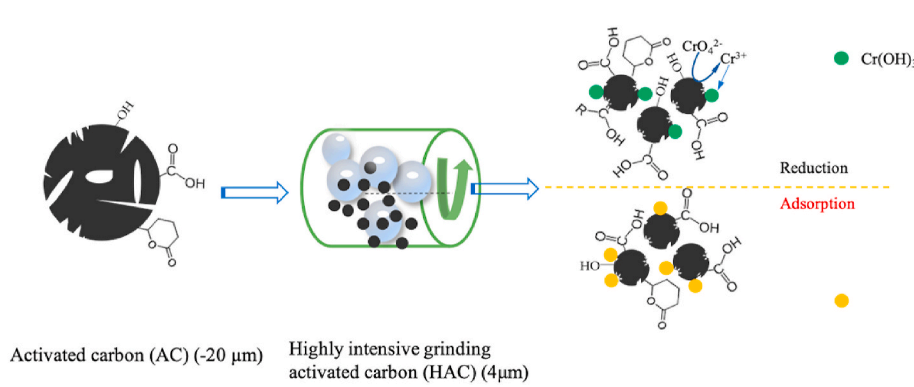

Fig. 12. Schematic of Cr(VI) removal by HAC induced by ball milling.

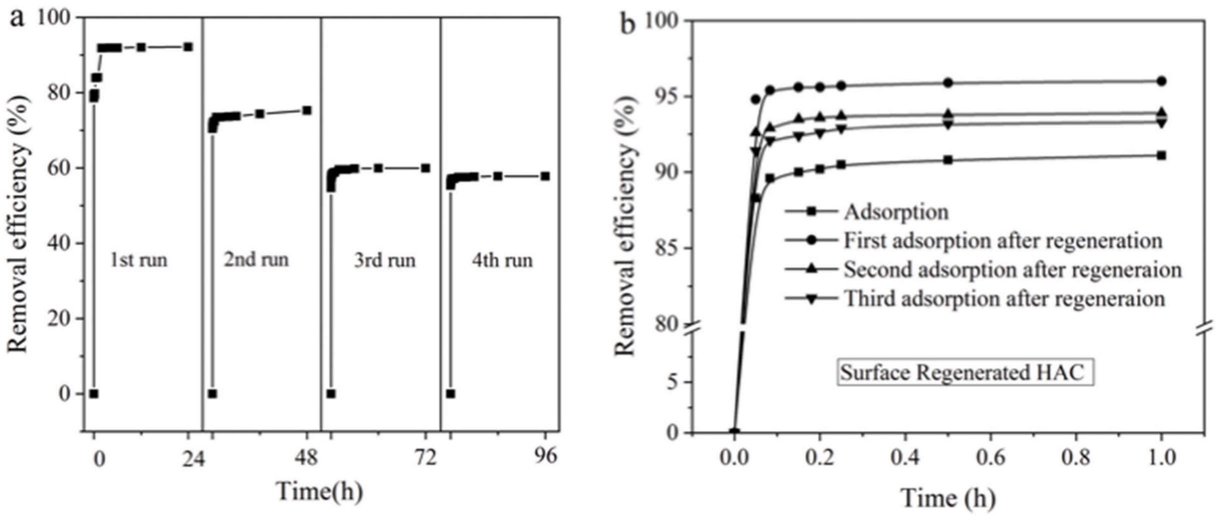

Fig. 13. The (a) reusability and (b) regeneration of HAC under pH 7.0 (5 g/100 ml HAC, 1000 mg/L Cr(VI), 295K).

higher surface area. Meanwhile, the reduction of surface oxygen-containing functional groups was verified by the results obtained from Raman spectra and Boehm's titration. Additionally, the adsorption thermodynamic revealed that the spontaneity of Cr(VI) adsorption on HAC increased after ball milling.

Fig. 12 shows a schematic representation of the increase in functional groups on the AC after high-intensity grinding and the adsorption of the chromium species on the functional groups.

3.7. Reusability and regeneration of HAC

Fig. 13(a) shows the Cr(VI) removal efficiency of HAC as a function of time subjecting the HAC to several consecutive adsorption runs at pH 7, the HAC was recycled to the next adsorption step without removing the loaded chromium. Cr(VI) removal was 92% when the HAC first contacted the Cr(VI) aqueous solution. This removal efficiency decreased steadily with the number of adsorption cycles, being 75% for the first cycle and 60% and 57% for the following. As noted in Figs. 4–5, $Cr(OH)_3(s)$ is reported in the HAC pores and as a layer on the HAC surface. It follows that $Cr(OH)_3(s)$ was definitively responsible for this decrease in removal efficiency as the number of cycles increased. The $Cr(OH)_3(s)$ blocked off the diffusion of Cr(VI) to the interior of the HAC particle. As noted in Fig. 10, at acid conditions, soluble Cr^{3+} is the predominant species, so with an acid wash, it is expected that the $Cr(OH)_3(s)$ in the pores and surface of the HAC will be removed leaving a particle with a free path for diffusion and further adsorption of Cr(VI). This was confirmed by subjecting the Cr loaded HAC to an acid wash then the regenerated HAC was subjected to another cycle of adsorption. Fig. 13(b) shows that the removal efficiency of Cr (VI) by HAC increased from 92.2% to 96.3% after acid regeneration. The uptake efficiency of Cr (VI) on HAC decreased with the recycling due to the formation of $Cr(OH)_3(s)$ as foregoing discussed.

4. Conclusions

The density of surface functional groups of activated carbon can be significantly improved by high-intensity grinding. Thus, the sequestration capability of commercial AC on Cr(VI) increases, and the removal of aqueous Cr(VI) can be undertaken under near-neutral pH. The feasibility and potential of HAC modified by ball milling on the practical application were developed. Besides, carrying out the Cr(VI) adsorption at near-neutral pH leads to the formation of $Cr(OH)_3(s)$ on HAC. $Cr(OH)_3(s)$ can be easily removed off by acid washing through which the HAC surface is regenerated and thereby regains its original adsorption capacity, and can be recycled to the Cr(VI) adsorption step. Once the adsorbent material has been regenerated, it can be used up to three stages without significantly losing its absorption capacity. The results obtained in this work showed that Cr(VI) adsorption of HAC at near-neutral pH proceeds through two mechanisms. One mechanism is the reduction of Cr(VI) to Cr(III) and hydrogen bonding of CrO_4^{2-} with COOH surface functional groups, and another is the Cr(III) precipitation to $Cr(OH)_3(s)$ in pores and surface of the HAC. This $Cr(OH)_3(s)$ could be removed by acid washing of the HAC, while the CrO_4^{2-} was removed by alkaline washing of the HAC. The studies of adsorption kinetic and isotherm show that the Pseudo-second order model and Freundlich fitted the adsorption data well, implying the chemisorption and multi-layer adsorption of Cr(VI) on HAC and AC. The intraparticle model study confirmed that the transfer rate of Cr(VI) from the bulk solution to the surface of AC was increased after ball milling. The thermodynamic study indicated that the adsorption of Cr(VI) by HAC and AC is endothermic and the spontaneity of Cr(VI) adsorption on HAC was higher. The work is yet needed to further improve the removal efficiency of the HAC for its recycling. This involved determining the performance of the HAC after a two-step treatment of the Cr-loaded HAC under acidic and alkaline conditions.

Credit author statement

Yi Fang, Investigation, Data curation, manuscript writing. Ke Yang, Formal analysis, Visualization. Yipeng Zhang, Visualization. Chang-sheng Peng, Supervision, Project administration, Formal analysis. Aurora Robledo-Cabrera, Formal analysis, Resources. Alejandro López-Valdivieso, Supervision, manuscript writing and reviewing, Project administration, financial responsible.

Declaration of competing interest

The authors declare that they have no known competing financial interests or personal relationships that could have appeared to influence the work reported in this paper.

Acknowledge

The authors gratefully acknowledge the financial support of the CONACYT (Consejo Nacional de Ciencia y Tecnología de Mexico) project (No.900339, 900347,900333) to carry out this research.

References

Acharya, J., Sahu, J.N., Sahoo, B.K., Mohanty, C.R., Meikap, B.C., 2009. Removal of chromium(VI) from wastewater by activated carbon developed from Tamarind wood activated with zinc chloride. Chem. Eng. J. 150, 25–39. https://doi.org/10.1016/j.cej.2008.11.035.

Acharya, R., Naik, B., Parida, K., 2018. Cr (VI) remediation from aqueous environment through modified-TiO2-mediated photocatalytic reduction. Beilstein J. Nanotechnol. 9, 1448–1470. https://doi.org/10.3762/bjnano.9.137.

Ahmadi, M., Foladivanda, M., Jaafarzadeh, N., Ramezani, Z., Ramavandi, B., Jorfi, S., Kakavandi, B., 2017. Synthesis of chitosan zero-valent iron nanoparticles-supported for cadmium removal: characterization, optimization and modeling approach. J. Water Supply Res. Technol. - Aqua 66, 116–130. https://doi.org/10.2166/aqua.2017.027.

Al-Othman, Z.A., Ali, R., Naushad, M., 2012. Hexavalent chromium removal from aqueous medium by activated carbon prepared from peanut shell: adsorption kinetics, equilibrium and thermodynamic studies. Chem. Eng. J. 184, 238–247. https://doi.org/10.1016/j.cej.2012.01.048.

Alvarado, L., Ramírez, A., Rodríguez-Torres, I., 2009. Cr(VI) removal by continuous electrodeionization: study of its basic technologies. Desalination 249, 423–428. https://doi.org/10.1016/j.desal.2009.06.051.

Anupam, K., Dutta, S., Bhattacharjee, C., Datta, S., 2011. Adsorptive removal of chromium (VI) from aqueous solution over powdered activated carbon: optimisation through response surface methodology. Chem. Eng. J. 173, 135–143. https://doi.org/10.1016/j.cej.2011.07.049.

Asimakopoulos, G., Baikousi, M., Salmas, C., Bourlinos, A.B., Zboril, R., Karakassides, M. A., 2020. Advanced Cr(VI) sorption properties of activated carbon produced via pyrolysis of the "Posidonia oceanica" seagrass. J. Hazard Mater. 124274 https://doi.org/10.1016/j.jhazmat.2020.124274.

Association, A.P.H., Association, A.W.W., Federation, W.P.C., Federation, W.E., 1915. Standard Methods for the Examination of Water and Wastewater. American Public Health Association.

Azari, A., Kakavandi, B., Kalantary, R.R., Ahmadi, E., Gholami, M., Torkshavand, Z., Azizi, M., 2015a. Rapid and efficient magnetically removal of heavy metals by magnetite-activated carbon composite: a statistical design approach. J. Porous Mater. 22, 1083–1096. https://doi.org/10.1007/s10934-015-9983-z.

Azari, A., Kalantary, R.R., Ghanizadeh, G., Kakavandi, B., Farzadkia, M., Ahmadi, E.J. R. a., 2015b. Iron–silver oxide nanoadsorbent synthesized by co-precipitation process for fluoride removal from aqueous solution and its adsorption mechanism. RSC Adv. 5, 87377–87391. https://doi.org/10.1039/C5RA17595J.

Babaei, A.A., Alavi, S.N., Akbarifar, M., Ahmadi, K., Ramazanpour Esfahani, A., Kakavandi, B., 2016. Experimental and modeling study on adsorption of cationic methylene blue dye onto mesoporous biochars prepared from agrowaste. Desalination and Water Treatment 57, 27199–27212. https://doi.org/10.1080/19443994.2016.1163736.

Baklanova, O., Knyazheva, O., Lavrenov, A., Drozdov, V., Trenikhin, M., Arbuzov, A., Kuznetsova, Y., Rempel, A., 2019. Mechanical treatment as highly effective method of physico-chemical properties control of carbon black. Microporous Mesoporous Mater. 279, 193–200. https://doi.org/10.1016/j.micromeso.2018.12.013.

Barrera-Diaz, C.E., Lugo-Lugo, V., Bilyeu, B., 2012. A review of chemical, electrochemical and biological methods for aqueous Cr(VI) reduction. J. Hazard Mater. 223–224, 1–12. https://doi.org/10.1016/j.jhazmat.2012.04.054.

Boehm, H.P., 2002. Surface oxides on carbon and their analysis: a critical assessment. Carbon 40, 145–149. https://doi.org/10.1016/S0008-6223(01)00165-8.

Butler, J.N., Butler, J.N., Cogley, D.R., 1998. Ionic Equilibrium: Solubility and pH Calculations. John Wiley & Sons.

Carasso, M.L., Rowlands, W.N., Kennedy, R.A., 1995. Electroacoustic determination of droplet size and zeta potential in concentrated intravenous fat emulsions. J. Colloid Interface Sci. 174, 405–413. https://doi.org/10.1006/jcis.1995.1408.

Chegrouche, S., Mellah, A., Barkat, M., 2009. Removal of strontium from aqueous solutions by adsorption onto activated carbon: kinetic and thermodynamic studies. Desalination 235, 306–318. https://doi.org/10.1016/j.desal.2008.01.018.

Chen, F., An, W., Liu, L., Liang, Y., Cui, W., 2017. Highly efficient removal of bisphenol A by a three-dimensional graphene hydrogel-AgBr@rGO exhibiting adsorption/photocatalysis synergy. Appl. Catal. B Environ. 217, 65–80. https://doi.org/10.1016/j.apcatb.2017.05.078.

Cho, K., An, B.M., So, S., Chae, A., Song, K.G., 2020. Simultaneous control of algal micropollutants based on ball-milled powdered activated carbon in combination with permanganate oxidation and coagulation. Water Res. 185, 116263. https://doi.org/10.1016/j.watres.2020.116263.

Cong, H.-P., Ren, X.-C., Wang, P., Yu, S.-H., 2012. Macroscopic multifunctional graphene-based hydrogels and aerogels by a metal ion induced self-assembly process. ACS Nano 6, 2693–2703. https://doi.org/10.1021/nn300082k.

Cruz-Espinoza, A., Ibarra-Galván, V., López-Valdivieso, A., González-González, J., 2012. Synthesis of microporous eskolaite from Cr(VI) using activated carbon as a reductant and template. J. Colloid Interface Sci. 374, 321–324. https://doi.org/10.1016/j.jcis.2012.01.059.

Cuesta, A., Dhamelincourt, P., Laureyns, J., Martínez-Alonso, A., Tascón, J.M.D., 1994. Raman microprobe studies on carbon materials. Carbon 32, 1523–1532. https://doi.org/10.1016/0008-6223(94)90148-1.

Dai, M., 1994. The effect of zeta potential of activated carbon on the adsorption of dyes from aqueous solution: I. The adsorption of cationic dyes: methyl green and methyl violet. J. Colloid Interface Sci. 164, 223–228. https://doi.org/10.1006/jcis.1994.1160.

Demiral, H., Demiral, I., Tümsek, F., Karabacakoğlu, B., 2008. Adsorption of chromium (VI) from aqueous solution by activated carbon derived from olive bagasse and applicability of different adsorption models. Chem. Eng. J. 144, 188–196. https://doi.org/10.1016/j.cej.2008.01.020.

Di Natale, F., Lancia, A., Molino, A., Musmarra, D., 2007. Removal of chromium ions form aqueous solutions by adsorption on activated carbon and char. J. Hazard Mater. 145, 381–390. https://doi.org/10.1016/j.jhazmat.2006.11.028.

Fahim, N., Barsoum, B., Eid, A., Khalil, M., 2006. Removal of chromium (III) from tannery wastewater using activated carbon from sugar industrial waste. J. Hazard Mater. 136, 303–309. https://doi.org/10.1016/j.jhazmat.2005.12.014.

Franz, M., Arafat, H.A., Pinto, N.G., 2000. Effect of chemical surface heterogeneity on the adsorption mechanism of dissolved aromatics on activated carbon. Carbon 38, 1807–1819. https://doi.org/10.1016/S0008-6223(00)00012-9.

Gherasim, C.-V., Bourceanu, G., Olariu, R.-I., Arsene, C., 2011. A novel polymer inclusion membrane applied in chromium (VI) separation from aqueous solutions. J. Hazard Mater. 197, 244–253. https://doi.org/10.1016/j.jhazmat.2011.09.082.

Ghosh, P.K., 2009. Hexavalent chromium [Cr(VI)] removal by acid modified waste activated carbons. J. Hazard Mater. 171, 116–122. https://doi.org/10.1016/j.jhazmat.2009.05.121.

Giri, A.K., Patel, R., Mandal, S., 2012. Removal of Cr (VI) from aqueous solution by Eichhornia crassipes root biomass-derived activated carbon. Chem. Eng. J. 185, 71–81. https://doi.org/10.1016/j.cej.2012.01.025.

Guedidi, H., Reinert, L., Lévêque, J.-M., Soneda, Y., Bellakhal, N., Duclaux, L., 2013. The effects of the surface oxidation of activated carbon, the solution pH and the temperature on adsorption of ibuprofen. Carbon 54, 432–443. https://doi.org/10.1016/j.carbon.2012.11.059.

Gürses, A., Doğar, Ç., Yalçın, M., Açıkyıldız, M., Bayrak, R., Karaca, S., 2006. The adsorption kinetics of the cationic dye, methylene blue, onto clay. J. Hazard Mater. 131, 217–228. https://doi.org/10.1016/j.jhazmat.2005.09.036.

Hanson, A.T., Dwyer, B., Samani, Z.A., York, D., 1993. Remediation of chromium-containing soils by heap leaching: column study. J. Environ. Eng. 119, 825–841. https://doi.org/10.1061/(ASCE)0733-9372, 1993)119:5(825.

Herrera-Gonzalez, A.M., Caldera-Villalobos, M., Pelaez-Cid, A.A., 2019. Adsorption of textile dyes using an activated carbon and crosslinked polyvinyl phosphonic acid composite. J. Environ. Manag. 234, 237–244. https://doi.org/10.1016/j.jenvman.2019.01.012.

Hu, C.Y., Lo, S.L., Liou, Y.H., Hsu, Y.W., Shih, K., Lin, C.J., 2010. Hexavalent chromium removal from near natural water by copper-iron bimetallic particles. Water Res. 44, 3101–3108. https://doi.org/10.1016/j.watres.2010.02.037.

Huang, C.P., Wu, M.H., 1977. The removal of chromium(VI) from dilute aqueous solution by activated carbon. Water Res. 11, 673–679. https://doi.org/10.1016/0043-1354(77)90106-3.

Huang, G., Shi, J.X., Langrish, T.A.G., 2009. Removal of Cr(VI) from aqueous solution using activated carbon modified with nitric acid. Chem. Eng. J. 152, 434–439. https://doi.org/10.1016/j.cej.2009.05.003.

Hunter, R.J., 2001. Foundations of Colloid Science. Oxford university press.

Ibarra-Galván, V., López-Valdivieso, A., Villavelazquez-Mendoza, C.I., Santoyo-Salazar, J., Song, S., 2014. Synthesis of eskolaite (α-Cr2O3) nanostructures by thermal processing of Cr2O3-loaded activated carbon. Part. Sci. Technol. 32, 451–455. https://doi.org/10.1080/02726351.2013.878774.

Jardine, P., Fendorf, S., Mayes, M., Larsen, I., Brooks, S., Bailey, W., 1999. Fate and transport of hexavalent chromium in undisturbed heterogeneous soil. Environ. Sci. Technol. 33, 2939–2944. https://doi.org/10.1021/es981211v.

Jiang, B., Wang, X., Liu, Y., Wang, Z., Zheng, J., Wu, M., 2016. The roles of polycarboxylates in Cr(VI)/sulfite reaction system: involvement of reactive oxygen species and intramolecular electron transfer. J. Hazard Mater. 304, 457–466. https://doi.org/10.1016/j.jhazmat.2015.11.011.

Julien, F., Baudu, M., Mazet, M., 1998. Relationship between chemical and physical surface properties of activated carbon. Water Res. 32, 3414–3424. https://doi.org/10.1016/S0043-1354(98)00109-2.

Kakavandi, B., Raofi, A., Peyghambarzadeh, S.M., Ramavandi, B., Niri, M.H., Ahmadi, M., 2018. Efficient adsorption of cobalt on chemical modified activated carbon: characterization, optimization and modeling studies. Desalination and Water Treatment 111, 310–321. https://doi.org/10.5004/dwt.2018.22238.

Kobya, M., 2004. Removal of Cr(VI) from aqueous solutions by adsorption onto hazelnut shell activated carbon: kinetic and equilibrium studies. Bioresour. Technol. 91, 317–321. https://doi.org/10.1016/j.biortech.2003.07.001.

Kocaoba, S., Akcin, G., 2002. Removal and recovery of chromium and chromium speciation with MINTEQA2. Talanta 57, 23–30. https://doi.org/10.1016/S0039-9140(01)00677-4.

Li, W., Gong, X., Li, X., Zhang, D., Gong, H., 2012. Removal of Cr(VI) from low-temperature micro-polluted surface water by tannic acid immobilized powdered activated carbon. Bioresour. Technol. 113, 106–113. https://doi.org/10.1016/j.biortech.2011.12.037.

Li, Y., Cui, W., Liu, L., Zong, R., Yao, W., Liang, Y., Zhu, Y., 2016. Removal of Cr(VI) by 3D TiO2-graphene hydrogel via adsorption enriched with photocatalytic reduction. Appl. Catal. B Environ. 199, 412–423. https://doi.org/10.1016/j.apcatb.2016.06.053.

Liu, W., Zhang, J., Zhang, C., Wang, Y., Li, Y., 2010. Adsorptive removal of Cr (VI) by Fe-modified activated carbon prepared from Trapa natans husk. Chem. Eng. J. 162, 677–684. https://doi.org/10.1016/j.cej.2010.06.020.

Lyu, H., Gao, B., He, F., Ding, C., Tang, J., Crittenden, J.C., 2017. Ball-milled carbon nanomaterials for energy and environmental applications. ACS Sustain. Chem. Eng. 5, 9568–9585. https://doi.org/10.1021/acssuschemeng.7b02170.

Lyu, H., Gao, B., He, F., Zimmerman, A.R., Ding, C., Huang, H., Tang, J., 2018a. Effects of ball milling on the physicochemical and sorptive properties of biochar: experimental observations and governing mechanisms. Environ. Pollut. 233, 54–63. https://doi.org/10.1016/j.envpol.2017.10.037.

Lyu, H., Gao, B., He, F., Zimmerman, A.R., Ding, C., Tang, J., Crittenden, J.C., 2018b. Experimental and modeling investigations of ball-milled biochar for the removal of aqueous methylene blue. Chem. Eng. J. 335, 110–119. https://doi.org/10.1016/j.cej.2017.10.130.

Lyubchik, S.I., Lyubchik, A.I., Galushko, O.L., Tikhonova, L.P., Vital, J., Fonseca, I.M., Lyubchik, S.B., 2004. Kinetics and thermodynamics of the Cr(III) adsorption on the activated carbon from co-mingled wastes. Colloid. Surface. Physicochem. Eng. Aspect. 242, 151–158. https://doi.org/10.1016/j.colsurfa.2004.04.066.

Massoudinejad, M., Asadi, A., Vosoughi, M., Gholami, M., kakavandi, B., Karami, M.A., 2015. A comprehensive study (kinetic, thermodynamic and equilibrium) of arsenic (V) adsorption using KMnO4 modified clinoptilolite. Kor. J. Chem. Eng. 32, 2078–2086. https://doi.org/10.1007/s11814-015-0018-x.

McKay, G., Otterburn, M.S., Sweeney, A.G., 1980. The removal of colour from effluent using various adsorbents—III. Silica: rate processes. Water Res. 14, 15–20. https://doi.org/10.1016/0043-1354(80)90037-8.

Miretzky, P., Cirelli, A.F., 2010. Cr(VI) and Cr(III) removal from aqueous solution by raw and modified lignocellulosic materials: a review. J. Hazard Mater. 180, 1–19. https://doi.org/10.1016/j.jhazmat.2010.04.060.

Mortazavian, S., Saber, A., Hong, J., Bae, J.-H., Chun, D., Wong, N., Gerrity, D., Batista, J., Kim, K.J., Moon, J., 2019. Synthesis, characterization, and kinetic study of activated carbon modified by polysulfide rubber coating for aqueous hexavalent chromium removal. J. Ind. Eng. Chem. 69, 196–210. https://doi.org/10.1016/j.jiec.2018.09.028.

Nemr, A.E., 2009. Potential of pomegranate husk carbon for Cr(VI) removal from wastewater: kinetic and isotherm studies. J. Hazard Mater. 161, 132–141. https://doi.org/10.1016/j.jhazmat.2008.03.093.

Niazi, L., Lashanizadegan, A., Sharififard, H., 2018. Chestnut oak shells activated carbon: preparation, characterization and application for Cr (VI) removal from dilute aqueous solutions. J. Clean. Prod. 185, 554–561. https://doi.org/10.1016/j.jclepro.2018.03.026.

Pamphile, N., Xuejiao, L., Guangwei, Y., Yin, W., 2019. Synthesis of a novel core-shell-structure activated carbon material and its application in sulfamethoxazole adsorption. J. Hazard Mater. 368, 602–612. https://doi.org/10.1016/j.jhazmat.2019.01.093.

Park, D., Lim, S.R., Yun, Y.S., Park, J.M., 2008. Development of a new Cr(VI)-biosorbent from agricultural biowaste. Bioresour. Technol. 99, 8810–8818. https://doi.org/10.1016/j.biortech.2008.04.042.

Park, D., Yun, Y.-S., Park, J.M., 2004. Reduction of hexavalent chromium with the brown seaweed Ecklonia biomass. Environmental science & technology, 38, 4860–4864.

Peng, C., Meng, H., Song, S., Lu, S., Lopez-Valdivieso, A., 2005. Elimination of Cr(VI) from electroplating wastewater by electrodialysis following chemical precipitation. Separ. Sci. Technol. 1501–1517. https://doi.org/10.1081/SS-120030788, 39.

Peng, C., Song, S., Lu, S., Lopez-Valdivieso, A.J.E.J., o, M.P., Protection, E., 2004. Electroplating Wastewater Treatment through Chemical Precipitation and Electrodialysis. 4.

Qin, H., Hu, T., Zhai, Y., Lu, N., Aliyeva, J., 2020. The improved methods of heavy metals removal by biosorbents: a review. Environ. Pollut. 258, 113777. https://doi.org/10.1016/j.envpol.2019.113777.

Ramos, R.L., Martinez, A.J., Coronado, R.G., 1994. Adsorption of chromium (VI) from aqueous solutions on activated carbon. Water Sci. Technol. 30, 191.

Rao, F., Song, S., Lopez-Valdivieso, A., 2009. Electrokinetic studies of minerals in aqueous solutions through electroacoustic measurement. Surf. Rev. Lett. 16, 65–71. https://doi.org/10.1142/S0218625X09012305.

Sangkarak, S., Phetrak, A., Kittipongvises, S., Kitkaew, D., Phihusut, D., Lohwacharin, J., 2020. Adsorptive performance of activated carbon reused from household drinking water filter for hexavalent chromium-contaminated water. J. Environ. Manag. 272, 111085. https://doi.org/10.1016/j.jenvman.2020.111085.

Sing, K.S.W., 1985. Reporting physisorption data for gas/solid systems with special reference to the determination of surface area and porosity (Recommendations 1984). Pure Appl. Chem. 57, 603–619. https://doi.org/10.1351/pac198557040603.

Smoluchowski, M.v.J.B. I., Barth-Verlag, Leipzig, 1921. Handbuch der Elektrizität und des Magnetismus, pp. 366–427.

Song, X., Liu, H., Cheng, L., Qu, Y., 2010. Surface modification of coconut-based activated carbon by liquid-phase oxidation and its effects on lead ion adsorption. Desalination 255, 78–83. https://doi.org/10.1016/j.desal.2010.01.011.

Sparks, D.L., 1998. Soil Physical Chemistry. CRC press.

Su, M., Fang, Y., Li, B., Yin, W., Gu, J., Liang, H., Li, P., Wu, J., 2019. Enhanced hexavalent chromium removal by activated carbon modified with micro-sized goethite using a facile impregnation method. Sci. Total Environ. 647, 47–56. https://doi.org/10.1016/j.scitotenv.2018.07.372.

Suzuki, I., 1999. Oxidation of inorganic sulfur compounds: chemical and enzymatic reactions. Can. J. Microbiol. 45, 97–105. https://doi.org/10.1139/w98-223.

Takaesu, H., Matsui, Y., Nishimura, Y., Matsushita, T., Shirasaki, N., 2019. Micro-milling super-fine powdered activated carbon decreases adsorption capacity by introducing oxygen/hydrogen-containing functional groups on carbon surface from water. Water Res. 155, 66–75. https://doi.org/10.1016/j.watres.2019.02.019.

Vainshtein, M., Kuschk, P., Mattusch, J., Vatsourina, A., Wiessner, A., 2003. Model experiments on the microbial removal of chromium from contaminated groundwater. Water Res. 37, 1401–1405. https://doi.org/10.1016/S0043-1354(02)00455-4.

Velasco, G., Gutiérrez-Granados, S., Ponce de León, C., Alatorre, A., Walsh, F.C., Rodríguez-Torres, I., 2016. The electrochemical reduction of Cr(VI) ions in acid solution at titanium and graphite electrodes. Journal of Environmental Chemical Engineering 4, 3610–3617. https://doi.org/10.1016/j.jece.2016.08.004.

Wang, Hu, B., Wang, C., Liang, Z., Cui, F., Zhao, Z., Yang, C., 2020a. Cr(VI) removal by micron-scale iron-carbon composite induced by ball milling: the role of activated carbon. Chem. Eng. J. 389, 122633. https://doi.org/10.1016/j.cej.2019.122633.

Wang, W., 2018. Chromium (VI) removal from aqueous solutions through powdered activated carbon countercurrent two-stage adsorption. Chemosphere 190, 97–102. https://doi.org/10.1016/j.chemosphere.2017.09.141.

Wang, X.S., Chen, L.F., Li, F.Y., Chen, K.L., Wan, W.Y., Tang, Y.J., 2010. Removal of Cr (VI) with wheat-residue derived black carbon: reaction mechanism and adsorption performance. J. Hazard Mater. 175, 816–822. https://doi.org/10.1016/j.jhazmat.2009.10.082.

Wang, Y., Peng, C., Padilla-Ortega, E., Robledo-Cabrera, A., López-Valdivieso, A., 2020b. Cr(VI) adsorption on activated carbon: mechanisms, modeling and limitations in water treatment. Journal of Environmental Chemical Engineering 8, 104031. https://doi.org/10.1016/j.jece.2020.104031.

Yang, C., Miao, G., Pi, Y., Xia, Q., Wu, J., Li, Z., Xiao, J., 2019. Abatement of various types of VOCs by adsorption/catalytic oxidation: a review. Chem. Eng. J. 370, 1128–1153. https://doi.org/10.1016/j.cej.2019.03.232.

Water Science & Technology

Water Science & Technology Vol 84 No 9, 2304 doi: 10.2166/wst.2021.449

A new insight into the restriction of Cr(VI) removal performance of activated carbon under neutral pH condition

Yi Fang[a,b], Ke Yang[a], Yipeng Zhang[a], Changsheng Peng[b,c], Aurora Robledo-Cabrera[a] and Alejandro López-Valdivieso[a,*]

[a] Instituto de metalurgia, Universidad Autónoma de San Luis Potosí, Av. Sierra Leona 550 C.P. 78210, San Luis Potosí, Mexico
[b] Guangdong Provincial Key Laboratory of Environmental Health and Land Resource, Zhaoqing University, Zhaoqing 526061, China
[c] The Key Lab of Marine Environmental Science and Ecology, Ministry of Education, Ocean University of China, Qingdao 266100, China
*Corresponding author. E-mail: alopez@uaslp.mx

YF, 0000-0003-4027-0323; KY, 0000-0002-8676-3097

ABSTRACT

Activated carbon has been widely used to remove hazardous Cr(VI); however, the impact of Cr_2O_3 precipitate on gradually declining removal ability as pH increases has received little attention. Herein, to investigate the effect of Cr_2O_3, SEM-EDX (scanning electron microscope-energy dispersive X-ray analysis) coupling elements mapping of chromium-loaded powdered activated carbon (PAC) revealed that a chromium layer was formed on the PAC exterior after being treated with Cr(VI) at pH 7. XPS (X-ray photoelectron spectroscopy) study confirmed that 69.93% and 39.91% Cr_2O_3 precipitated on the PAC surface at pH 7 and pH 3, respectively, corresponding to 17.77 mg/g and 20 mg/g removal capacity. Exhausted PAC had a removal efficiency of 92.43% after Cr_2O_3 being washed by H_2SO_4 solution, which was much higher than the removal efficiency of 51.27 % after NaOH washing. This further verified that the intrinsically developed Cr_2O_3 precipitate on PAC under neutral conditions limited the durability of PAC as an adsorbent. Consecutive elution assessments confirmed that adsorption and reduction ability both declined as pH increased. Raman spectroscopy and C 1s spectra of materials demonstrated two distinct Cr(VI) removal mechanisms under pH 3 and pH 7. In conclusion, the exhausted AC after Cr(VI) adsorption can be rejuvenated after the surface coated Cr_2O_3 is washed by the acid solution, which can expand the longevity of AC and recover Cr(III).

Key words: activated carbon, adsorption, chromium, neutral conditions, passivation, reduction

HIGHLIGHT

- In this work, we scrutinized the mechanism of poor removal capacity of commercial activated carbon on toxic heavy metal Cr(VI) under neutral pH conditions. Differing from the most accepted view that electrostatic repulsion is the main consideration, our study suggested that the relatively more Cr_2O_3 precipitate on the surface of activated carbon under higher pH led to the low Cr(VI) sequestration capability.

GRAPHICAL ABSTRACT

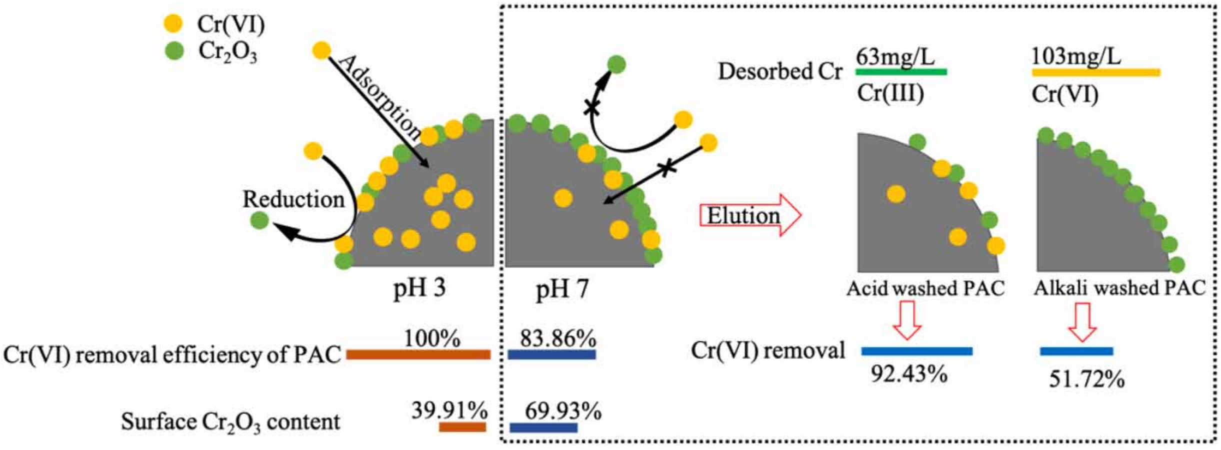

1. INTRODUCTION

Chromium abounds in nature and is highly toxic in the form of CrO_4^{2-} and $Cr_2O_7^{2-}$ through bioaccumulation (Li *et al.* 2018). The chromium pollution of water, land, and environment has attracted the interest of experts as electroplating plants, stainless steel manufacturing plants, leather manufacturing plants, and refractory plants have progressively appeared (Wang *et al.* 2019; Aparicio *et al.* 2021; Samuel *et al.* 2021). Cr(III) presents less mobility, toxicity, and solubility than Cr(VI) and generates sparingly soluble chromium hydroxides (Dognani *et al.* 2019). The reduction of Cr(VI) to Cr(III) is rapid at acidic conditions; meanwhile, the readily available electron is required for the reduction process (Deng *et al.* 2020; Fang *et al.* 2021b). It is well known that removing Cr(VI) from water by reduction and precipitation is a viable option (Barrera-Diaz *et al.* 2012; Qian *et al.* 2019; Wu *et al.* 2019; Zeng *et al.* 2019). Conventional reducing agents are sulfur and iron salts (Zhang *et al.* 2021a, 2021b); post-treated effluent that contained sulfate and iron salts would contaminate water and soil. Furthermore, the mandatory wastewater discharge would result in high costs.

The bulk of published studies on Cr(VI) removal by low-cost and readily accessible activated carbon (AC) demonstrated that removal capacity was greater in acidic conditions than alkaline conditions. This suggests that the Cr(VI) elimination is strongly pH dependent (Al-Othman *et al.* 2012; Zhou *et al.* 2016; Valentín-Reyes *et al.* 2019). The removal efficiency of Cr(VI) by activated carbon prepared from teakwood sawdust was 100% at pH 2, while it was below 20% at pH 10 (Ramirez *et al.* 2020). Table 1 shows the capacity of several ACs to remove Cr(VI) in acidic and alkaline environments. At low pH, the removal capacity was favored because the positively charged surface of Cr(VI) advanced the adsorption of anion Cr(VI) (Norouzi *et al.* 2018). It is worth noting that the pH-speciation of Cr(VI) reveals that $HCrO_4^-$ dominated below pH 6, whereas CrO_4^{2-} dominates above pH 7 (Rakhunde *et al.* 2012). Furthermore, prior studies have found that positively charged AC produced by protonation at a low pH value tends to attract chromate anions, which is thought to be the main mechanism for Cr(VI) adsorption (Mohan *et al.* 2005). It was discovered that as pH dropped, the reduction and adsorption process enhanced simultaneously.

To our understanding, there have been few investigations on systematic chromium adsorption and reduction study when pH rises over 7, to shed light on a substantial drop in AC performance. Most studies have only focused on the unfavorable effect of electrostatic repulsion between chromate anions and negatively charged AC surface at high pH values (Niazi *et al.* 2018; Ma *et al.* 2019; Liu *et al.* 2020). Besides, an earlier study failed to elucidate the removal paths at pH higher than 6 because the surface negatively charged bamboo bark-based AC that unfavored the adsorption of Cr(VI) anions, hence the reduction process of Cr(VI) to Cr(III) at high pH was omitted (Zhang *et al.* 2015). Cr(III) speciation as a function of pH was depicted clearly by Lopez-Valdivieso's study showing that $Cr(OH)_3$(s) predominates at pH over 6.4 (Fang *et al.* 2021a). The effect on the removal of Cr(VI) under alkaline conditions of the AC surface loaded Cr(III) precipitate was especially neglected. Early reported studies on the synthesis of eskolaite (α-Cr_2O_3) nanoparticles through AC following adsorption of Cr(VI) have shown that Cr_2O_3 was the reduced species of Cr(VI) on AC (Cruz-Espinoza *et al.* 2012; Ibarra-Galván *et al.* 2014). Recently study showed that the Cr_2O_3 reduced the adsorption rate of Cr(VI) significantly (Wang *et al.* 2020).

Table 1 | Comparison of Cr(VI) removal under different pH by various carbon materials

Carbon materials	Cr(VI) removal capacity (mg/g)		References
	Acid condition	Alkali condition	
AC derived from *Posidonia Oceanica* seagrass	30.5 (pH 3)	0 (pH > 4)	Asimakopoulos *et al.* (2021)
Biochar derived from corn straw	125 (pH 2)	50 (pH 6)	Qu *et al.* (2021)
Powdered AC	46 (pH 2)	8 (pH 7)	Sangkarak *et al.* (2020)
Biochar derived from waste glue residue	206.7 (pH 2)	90 (pH 6)	Shi *et al.* (2020)
AC prepared by calcination of wheat bran	22 (pH 2)	0 (pH 10)	Ogata *et al.* (2020)
Commercial AC	21 (pH 2.5)	13 (pH 5.5)	Wu *et al.* (2020)
KOH activated porous corn straw	98.3 (pH 3)	33.7 (pH 7)	Ma *et al.* (2019)
AC derived from an acrylonitrile-divinylbenzene copolymer	80 (pH 2)	9 (pH 8)	Duranoğlu *et al.* (2012)

Compared to the consensus that the electrostatic repulsion led to poor Cr(VI) removal efficiency of AC in alkaline conditions, the effect of AC surface-coated Cr_2O_3 precipitate on removal performance was not fully understood. This work aimed to study the effect of powdered AC (PAC) surface-formed Cr_2O_3 precipitate on Cr(VI) removal, SEM-EDX (scanning electron microscope-energy dispersive X-ray analysis), and XPS (X-ray photoelectron spectroscopy) were used to investigate the surface morphology and the chemical properties. Desorption and regeneration experiments were used to confirm the role of Cr_2O_3. The insight gained from this study would help to expand the longevity of AC and the recovery of Cr via AC.

2. MATERIALS AND METHODS

2.1. Characterization of PAC particle

To scrutinize the composition of loaded-chromium on PAC after Cr(VI) removal, three types of de-passivation agents were examined to desorb the adsorbed/reduced chromium on PAC. The formation process of the chromium layer on PAC at pH 3 and 7 was inspected by carrying out consecutive desorption tests following each Cr(VI) adsorption. SEM-EDX (JSM-6610LV, JEOL, Japan) and XPS (K-Alpha, Thermo Scientific, USA) were employed to characterize the distribution of chromium and the chemical species of Cr and C on PAC at pH 3 and 7, respectively. The difference of removal mechanisms under the two pH values was delineated by XPS and Raman spectroscopy (DXR, Thermo Scientific, USA).

2.2. Materials

All the chemicals were analytical grade and the aqueous solutions were prepared with deionized water through Barnstead pure II water purification system (Thermo Scientific, USA). Potassium dichromate ($K_2Cr_2O_7$) was purchased from J.T.Baker and used for preparing 1,000 mg/L Cr(VI) as a stock solution. 1.0 M H_2SO_4 and 1.0 M NaOH were used to adjust the pH of the aqueous solutions. H_2SO_4, NaOH, KCl, and 1,5–diphenylcarbazide were provided by J.T.Baker. Commercial available AC was provided by Calgon company, its chemical composition was 97% carbon and 3% inorganic residual. The AC was treated by ball milling and obtained a PAC with an average size of 4 m, a specific surface area of 929 m^2/g, and a pore radius of 15.9 Å, PAC used in this study was reported in our previous work (Fang *et al.* 2021b). Following the grinding step, the PAC was dried and stored in a desiccator.

2.3. Comparison of Cr(VI) removal at different pH

A comparison was conducted for the PAC removal efficiency at pH 3, 7, and 9 (Jiang *et al.* 2014). The desired mass of PAC (5 g) was mixed with deionized water (100 mL) for 1 h, then the pH was adjusted to 3, 7, and 9 using 1.0 M H_2SO_4 and NaOH aqueous solutions and monitoring the pH with an Orion 3 star pH meter (Thermo Scientific, USA). 0.2829 g $K_2Cr_2O_7$ reagent was added to the PAC suspension to prepare a 1,000 mg/L solution once the pH was stable. To follow the Cr(VI) uptake a 200 L aliquot was withdrawn from the aqueous solution at 3, 5, 9, 15, 30, 60, 360, and 1,440 min. The withdrawn aliquot was centrifuged in a centrifuge (Allegra^{TM} 21, Beckman Coulter, USA) for 15 min prior to analysis. The Cr(VI) removal capacity was calculated through Equation (1) (Krishna Kumar *et al.* 2019), wherein Γ(mg/g) is the removal capacity, C_0 (mg/L) is the initial concentrations and C_t is the concentration at time t, V (L) and M (g) are the volume of solution and dose of PAC, respectively.

$$G = (C_0 - C_t)V{=}M \tag{1}$$

2.4. Selection of desorption agents

Three kinds of desorption agents were evaluated to determine their effectiveness for desorbing the adsorbed chromium species on PAC. Analytical grade $K_2Cr_2O_7$ acted as a precursor of the chromium layer on PAC. To obtain adequate loaded chromium on PAC for assessment, consecutive uptake experiments were undertaken. 5.0 g PAC was mixed with 1,000 mg/L Cr(VI) aqueous solution at a fixed pH of 7 in a glass volumetric flask. This suspension was stirred magnetically (Thermo Scientific, USA) at 100 rpm to prevent deteriorating of the chromium layer formed on the PAC. A 200 L sample was withdrawn from the suspension at 0.25, 0.5, 1, 3, 5, 7, 9, 12, 15, 30, 60, 120, and 1,440 min to determine the concentration of Cr(VI), then the suspension was filtered to collect the PAC, which was rinsed with deionized water, and dried before the following removal experiments. Consecutive removal steps were performed with 1,000 mg/L Cr(VI). Dried chromium-loaded PAC after four repetitive adsorption runs was used for the desorption testing. All the batch experiments were conducted in duplicate under ambient conditions. The adsorption capacity at equilibrium for Cr on PAC was expressed as Equation (2)

$$q_p = \sum (1000 - Ce_i)V_i = M_i \tag{2}$$

where q_p (mg/g) is the content of chromium on PAC, Ce_i (mg/L),V_i (mL) and M_i (g) ($i = 1, 2, 3, 4$) are the equilibrium concentration, solution volume and mass of PAC of each removal cycle, respectively.

To desorb the loaded chromium from the PAC, 0.2M KCl, 0.2M H_2SO_4, and 0.1M NaOH were employed. 0.5 g chromium-loaded PAC was mixed with 50 ml of the desorption agent solution in a glass volumetric flask and stirred at 200 rpm, the concentration of desorbed chromium after 1, 3, 5, 7, 9, 24, 30, 48, 72, 96, and 148 h was determined, the efficiency of desorption was determined through Equation (3).

$$h = 100 \times (C_t V) = (q_p M) \tag{3}$$

where η (%) is desorption efficiency, C_t (mg/L) is the dissolved chromium concentration at t time, V (L) and M (g) are the volumes of desorption solution and dose of PAC correspondingly. In addition, the performance of PAC treated with Cr(VI) after desorption with different chemical agents was evaluated.

2.5. The formation process of chromium layer at pH 3 and 7

To ascertain the route of the chromium layer formed on PAC, the chromium speciation after consecutive adsorption runs was analyzed with selected desorption agents (0.2M H_2SO_4 and 0.1M NaOH solution). Four desorption tests followed four successive removal cycles were performed and the increment content of loaded chromium on PAC between two successive adsorption runs was determined by Equation (4).

$$Dq = (C_{ii} - C_i)V = M \tag{4}$$

where q (mg/g) is the increased content of chromium on PAC, C_{ii} and C_i (mg/L) are the equilibrium concentration of desorbed chromium after the two successive elution tests, V (ml) and M (g) are the volume of desorption solution and the dose of PAC after adsorption of Cr(VI).

The adsorption capacity of PAC loaded with chromium on Cr(VI) after the last elution assessment was examined, and all the adsorption experiments were conducted with 1,000 mg/L Cr(VI).

2.6. Analytical method

A colorimetric approach employing 1,5–diphenylcarbazide and a UV-Visible spectrophotometer (Thermo Scientific, USA) coupled with a 1 cm quartz cell was used to determine Cr(VI). 100 L filtered solution was diluted to 10 ml and mixed with 0.1 mL 49% H_2SO_4, 0.1 mL 42.5% H_3PO_4, and 0.4 mL 0.2% 1,5–diphenylcarbazide solution, sequentially. The mixed solution stood for 10 min and was then measured by a UV-Visible spectrophotometer under 540 nm. The absorbance of deionized water was used as a reference. With prepared 0, 0.02, 0.05, 0.1, 0.2, 0.4, 0.6, 0.8, and 1.0 mg/L Cr(VI), a standard curve of concentration versus absorbance was constructed; this standard curve was used to determine the Cr(VI) concentration of the sample. The total concentration of aqueous Cr was analyzed by atomic absorption spectrometry (AAS, Varian Spectra 220FS), a 50 L filtered solution was diluted to 10 mL and then sprayed into the flame of air-acetylene. The chromium ground state atoms formed under a high-temperature flame produce selective absorption of the 357.9 nm characteristic spectrum of chromium hollow cathode lamps, and the absorbance value is proportional to the concentration of Cr. The standard curve of total Cr was built in the same way as Cr(VI), and the concentration of total was determined by the standard curve as well. The presence of soluble Cr species in the solution was Cr(III) and Cr(VI), the concentration of aqueous Cr(III) was confirmed by the difference between total Cr and Cr(VI).

3. RESULTS AND DISCUSSION

3.1. Particle characterization

3.1.1. Surface morphology

The surface morphology of PAC after Cr(VI) adsorption under pH 7 was characterized by SEM-EDX and elements mapping. As seen in Figure 1, a chromium layer adsorbed mostly on the PAC surface. A similar observation was reported recently (Wang *et al.* 2020).

3.1.2. XPS spectra analysis

To further inspect the chemical species of Cr on the surface of PAC, XPS analysis was employed. Figure 2(a) and 2(b) show the XPS spectra, which were fitted and deconvoluted into multiple peaks by CasaXPS (version 2.3.23). The peak referenced as C 1 s at 284.8 eV, the Shirley type was designated as the background subtraction. As presented in Figure 2(a), the Cr 2p peak due to Cr(VI), denoted that the Cr(VI) was adsorbed onto PAC. The XPS spectrum of PAC after being treated with Cr(VI) at pH 3 (PAC-pH 3) and 7 (PAC-pH 7) was built as presented in Figure 2(b). The Cr 2p region of the photoelectron spectrum was both detected for PAC-pH 3 and PAC-pH 7, which was consistent with the EDX spectrum shown in Figure 1. Cr 2p involves two energy levels, 2p 1/2 and 2p 3/2. The XPS spectrum of PAC-pH 3 can be divided into the Cr1, Cr2, and Cr3 peaks, where the binding energies (BE) value of Cr1 peak of PAC-pH 3 was 587.5 eV, which was very close to that of Cr_2O_3 (587.4 eV $\pm$ 0.2) (Grohmann *et al.* 1995). The BE for Cr2 and Cr3 of PAC-pH 3 were 579.2 and 577.8 eV, respectively, which can be attributed to Cr(VI) (Murphy *et al.* 2009; Ren *et al.* 2016; Zhang *et al.* 2019). Two contributions of Cr1 and Cr2 for the Cr 2p region of PAC-pH 7 were 587.7 and 578.0 eV, matching well with the binding energy for Cr(VI) and Cr_2O_3 (Biesinger *et al.* 2004; Ren *et al.* 2016; Chen *et al.* 2019). Due to XPS detection depth being no more than 4 nm from the sample surface, it can be said that the chromium layers on the surface of PAC-pH 3 were mainly constituted by Cr(VI) and PAC-pH 7 was mainly constituted by Cr_2O_3(s) (Chowdhury *et al.* 2012). Consistent with the present results, previous studies have demonstrated that the reduction and adsorption participated principally in the Cr(VI) removal on biomass (Wu *et al.* 2010; Cui *et al.* 2011). Moreover, the peak area ratio (Cr1 versus total peaks) as determined by CasaXPS was 69.93% and

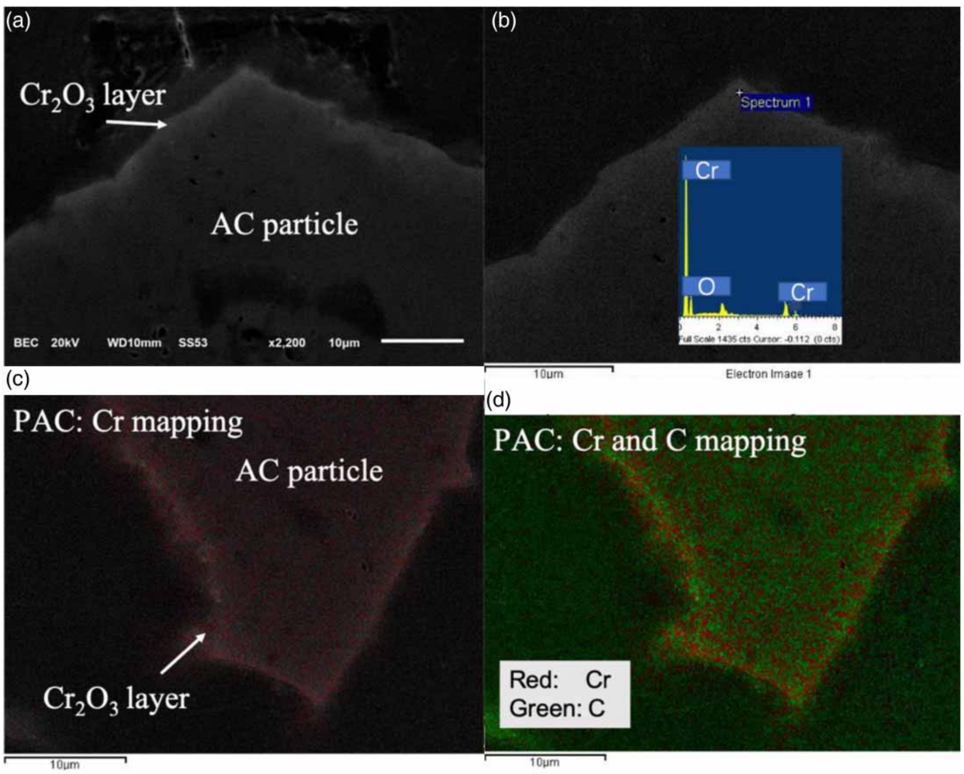

Figure 1 | SEM-EDX micrographs (a and b) and SEM coupling with elements mappings (c and d) of PAC after Cr(VI) adsorption at pH 7.

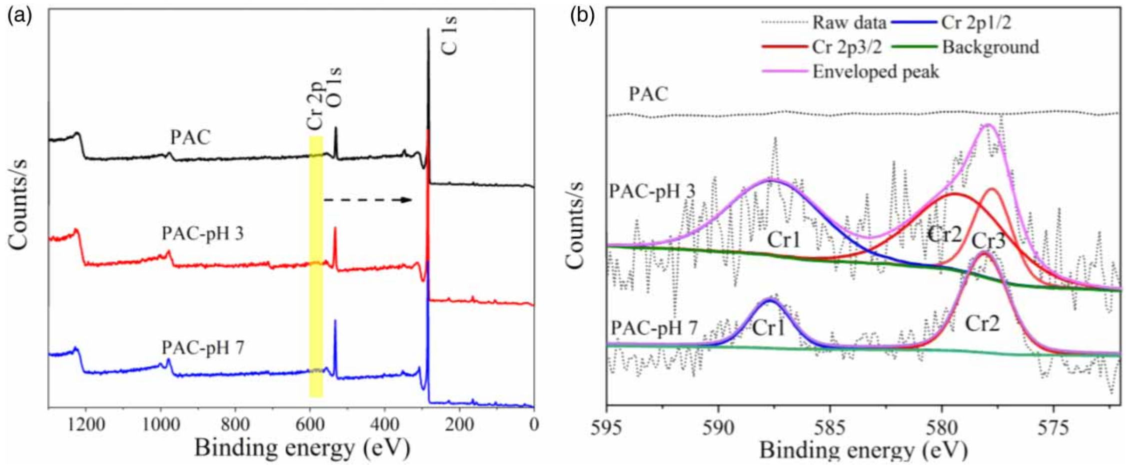

Figure 2 | The XPS spectra of PAC treated with Cr(VI) under pH 3 (PAC-pH 3), pH 7 (PAC-pH 7), and fresh PAC; (a) XPS survey, (b) scan of Cr 2p.

39.91% Cr_2O_3(s) on the surfaces of PAC-pH 7 and PAC-pH 3, respectively. This higher content of Cr_2O_3 on PAC-pH 7 clearly evidenced that more Cr_2O_3 formed on the PAC at pH 7 than at pH 3, impeding the diffusion of Cr(VI) into the PAC, leading to a lower level of Cr(VI) removal. Besides, the ratio of O/C on PAC, PAC-pH 3, and PAC-pH 7 were 0.075, 0.113, and 0.157, respectively (Table 2). This indicates more O on the PAC after adsorption at pH 7 than at pH 3, due to more Cr_2O_3 precipitate. As noted in Table 2, the ratio of Cr/C on PAC-pH 3 was higher than that on PAC-pH 7, which further substantiated that Cr(VI) removal efficiency under pH 3 was superior to that under pH 7 and indicated that not only was there Cr_2O_3 on the PAC surface but also Cr(VI).

The surface functional groups of PAC before and after Cr(VI) adsorption were investigated using high resolution C1 s spectra. The deconvolution of C 1 s produced four peaks, as shown in Figure 3. For PAC, there were four components: C = C (284.8 eV), C-O-C/C-OH (285.5 eV), C-O (286.7 eV), and COOR (286.7 eV) (290.0 eV) (Jieying *et al.* 2014). Similarly, the four peaks of PAC-pH 3 were assigned to the C = C (284.8 eV), C-OH (285.8 eV), C-O (286.5 eV), and COOR (288.7 eV) (Jia & Wang 2015; Ma *et al.* 2018). Meanwhile, the four peaks for PAC-pH 7 were allocated to C = C (284.8 eV), C-OH (285.8 eV), C-O (286.5 eV), and COOR (289.5 eV) (Chen *et al.* 2020). The relative percentages of C-OH for PAC, PAC-pH 3, and PAC-pH 7 were 23.62%, 6.77%, and 6.53%, respectively, which suggested that the group of C-OH contributed to the removal of Cr(VI). The oxidation of C-OH to C-O by Cr(VI) caused the increase of the C-O group (Su *et al.* 2019). Nonetheless, following Cr(VI) adsorption at pH 3, the relative percentage of COOR on PAC rose from 15.22% to 20.56% and dropped to 10.41% after Cr(VI) adsorption at pH 7. This inconsistency may be due to Cr(VI) oxidizing the surface of PAC at pH 3 and introducing more COOR groups (Yin *et al.* 2019), while the Cr(VI) exhibited weak oxidative capacity at higher pH (Gangadharan & Nambi 2014), and the removal of Cr(VI) under pH 7 consumed the COOR groups through the complex.

3.1.3. Raman spectra analysis

Raman spectroscopy investigation was carried out to evaluate the degree of structural order in carbonaceous PACs, as well as to investigate the difference in Cr(VI) removal mechanisms at pH 3 and pH 7. As depicted in Figure 4, the two sharp and strong bands are associated with the D-band (1,319 cm^{-1}. defect with sp^3 bonding) and G-band (1,563 cm^{-1}, graphitization with sp^2 bonding) (Cuesta *et al.* 1994). The intensity ratio of D-band (I_D) versus G-band (I_G) is often used to assess the degree

Table 2 | XPS analysis of PAC before and after treatment with Cr(VI)

Materials	O/C	Cr/C
PAC	0.075	0
PAC-pH 3	0.113	0.005
PAC-pH 7	0.157	0.004

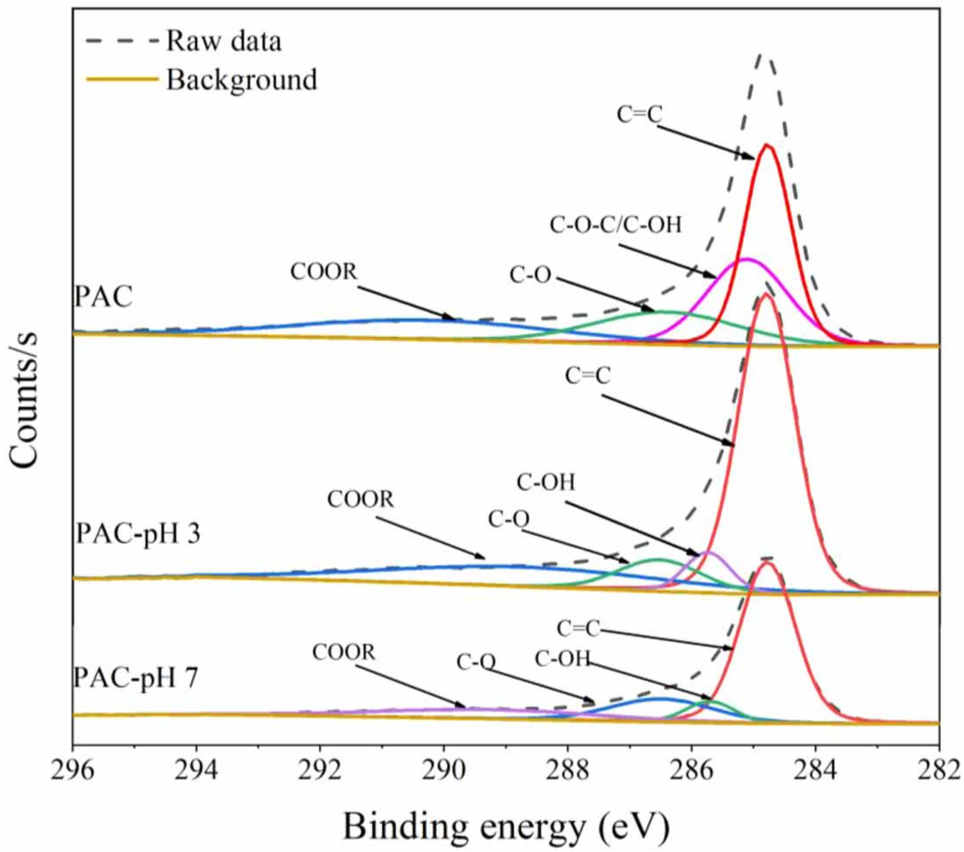

Figure 3 | High resolution C 1 s spectra of PAC, PAC-pH 3, and PAC-pH 7.

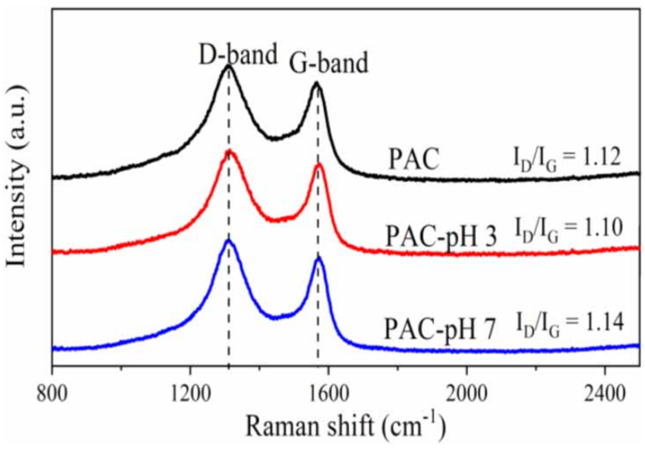

Figure 4 | Raman spectra investigation for pristine PAC, after removal of Cr(VI) at pH 3 and 7.

of disorder in graphite structure in carbon materials (Lespade *et al.* 1984). The value of I_D/I_G declined from 1.12 to 1.10 after treatment at pH 3 but increased from 1.12 to 1.14 after treatment at pH 7. As a result, the existence of defects in PAC was strengthened under pH 7, while at pH 3, a well-organized carbon structure formed. This divergence could be explained by the different Cr(VI) adsorption mechanisms at pH 3 and 7. In general, the reduction of surface oxygen-containing functional groups resulted in the increase of amorphous carbon at pH 7 (Cong *et al.* 2012; Yang *et al.* 2013; Li *et al.* 2016; Wang *et al.* 2017), while the oxidation of hybridized carbon atoms caused structural order to grow at pH 3 (Osswald *et al.* 2006).

3.2. Adsorption performance of PAC at pH 3 and 7

Figure 5 shows a comparison of adsorption performance at pH 3, 7, and 9 for 1,000 mg/L initial concentration of Cr(VI). Adsorption at those three pH values both reached pseudo-equilibrium immediately after 10 mins. Removal capacities for PAC at pH 7 and 3 were 16.8 mg/g and 20 mg/g, respectively, equivalent to 83.86% and nearly 100% removal efficiency. And adsorption capacity under pH 9 was 7.8 mg/g, which was much lower than that at pH 3 and 7. It indicated that the removal performance of PAC on Cr(VI) was higher at low pH, PAC is probably protonated and attracted more anionic Cr(VI).

3.3. Desorption performance of Cr-loaded PAC with chemical agents

The desorption of chromium from the Cr-loaded PAC was evaluated using various chemical agents including H_2SO_4, KCl, and NaOH. Abundant chromium-loaded PAC was prepared at pH 7. As shown in Figure 6, the Cr(VI) elimination experiment using PAC was repeated four times. The duration time for every removal cycle was 24 hours. The next removal cycle began once the previous cycle was completed. After four consecutive repetitive adsorption cycles, the content of chromium on PAC

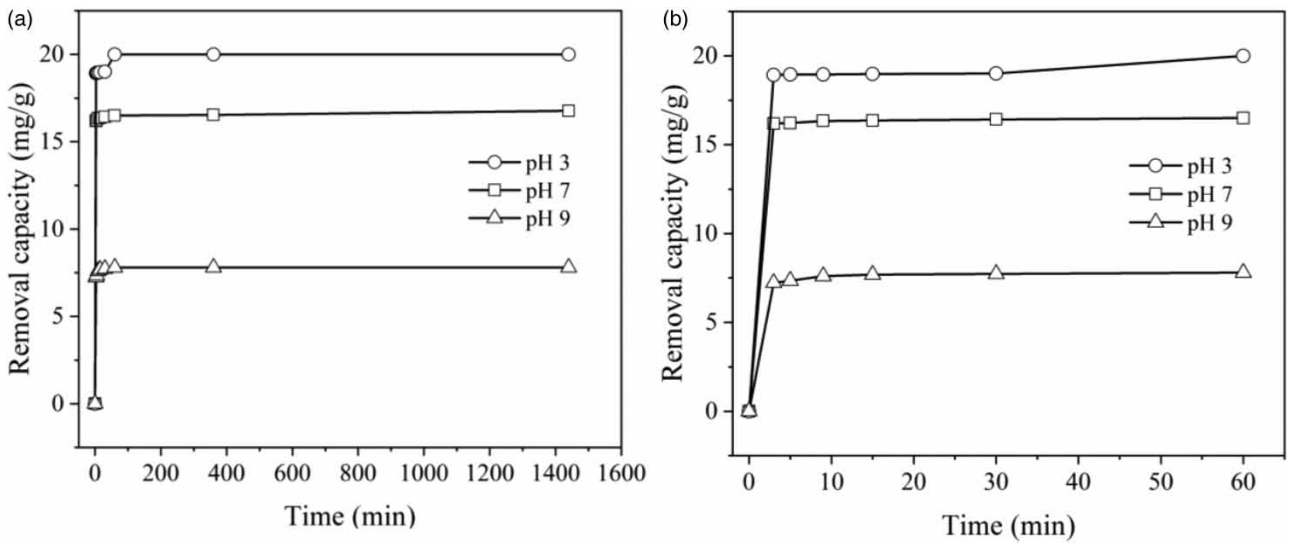

Figure 5 | The adsorption capacities comparison at pH 3, 7, and 9, (a) the full pro file of adsorption, (b) the first 60 min adsorption pro file (Initial concentration 1,000 mg/L, 50 g/L PAC, 295 K).

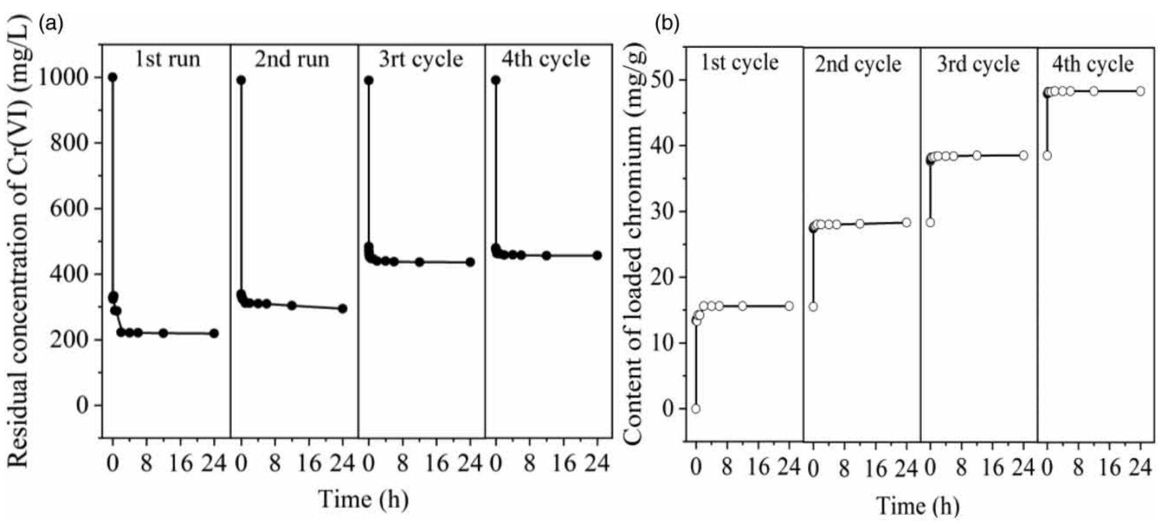

Figure 6 | The preparation of chromium-loaded PAC, (a) the residual concentration of Cr(VI) at each Cr(VI) adsorption cycle, (b) the content of loaded chromium as cycling (1,000 mg/L Cr(VI), 295 K, 50 g/L, pH 7).

reached 48.6 mg/g. The results of the desorption analysis using the three reagents are shown in Figure 7. It is noted that only Cr(III) was dissolved in H_2SO_4 aqueous solutions, whereas Cr(VI) was only desorbed in NaOH aqueous solutions. Negligible Cr(III) or Cr(VI) were detected in the KCl solution when compared to acidic and alkaline aqueous solutions. These findings agree well with Ouki & Neufeld's (1997) findings that 3 g/L Cr(III) and 8.4 g/L Cr(VI) were recovered when exhausted carbon was regenerated under acidic and alkaline conditions, respectively (Ouki & Neufeld 1997). Due to the great stability of the adsorbed chromium on the PAC, desorption of Cr(VI) and Cr(III) from the Cr-loaded PAC with deionized water was minimal. Our results are also in line with those of Jing *et al.* (2011), who found that the desorption rate of Cr-loaded AC was low with distilled water (Jing *et al.* 2011).

As shown in Figure 6(a), Cr(III) precipitate dissolved gradually in 0.2 M H_2SO_4, and 13.0% Cr(III) precipitate was removed under acidic conditions, this process was depicted by Equation (5).

$$Cr_2O_3 + 6H^+ \rightarrow 2Cr^{3+} + 3H_2O \quad (5)$$

With the NaOH aqueous solution (Figure 6(c)), 21.3% Cr(VI) was desorbed, which was higher than the dissolved Cr(III) by the H_2SO_4 aqueous solution. This seems to contradict the XPS conclusion that less Cr(VI) adsorbed on PAC-pH 7 surface. A possible explanation for this might be that more internally adsorbed Cr(VI) in PAC particles was desorbed by alkaline elution. Cr(VI) adsorbed on AC was previously shown to be bound to the surface functional groups (Singha *et al.* 2013). An ion-exchange mechanism could explain the desorption of adsorbed CrO_4^{2-} (the dominant chromium species under alkaline conditions) on surface functional groups by NaOH aqueous solutions, the OH^- ions substituting for CrO_4^{2-} anions, as demonstrated in Equation (6) (Daneshvar *et al.* 2019).

$$PAC - (COOH_2^+)_2 \cdots CrO_4^{2-}(s) + 2OH^- \rightarrow PAC - (COOH)(s) + CrO_4^{2-} + H_2O \quad (6)$$

These findings could be useful in the development of a selective recovery method of Cr(III) and Cr(VI) using acid and alkali aqueous solutions.

3.4. Formation process of chromium layer at pH 3 and 7

To clarify the influence of pH on the development process of the chromium layer on PAC, H_2SO_4, and NaOH desorption agents were used to determine the content of Cr(III) and Cr(VI) adsorbed on PAC-pH 3 and PAC-pH 7. Figure 8 compares

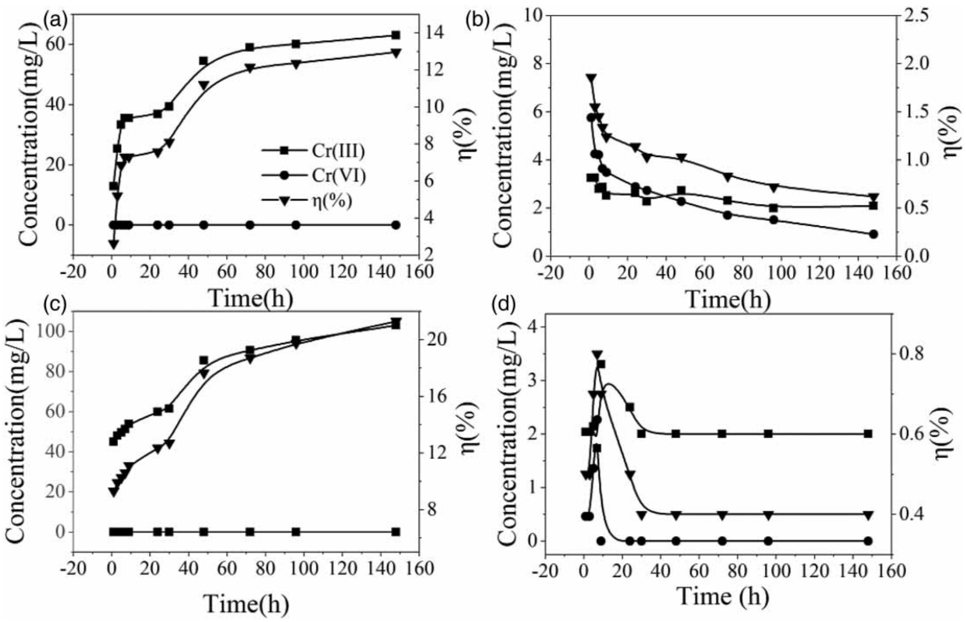

Figure 7 | The effect of chemical agents on desorption performance of Cr-loaded PAC (a) H_2SO_4 (b) KCl (c) NaOH (d) H_2O (0.2M KCl, 0.2M H_2SO_4, 0.1M NaOH, 1 g/100 mL Cr-loaded PAC, 298 K).

Figure 8 | The increment of chromium loaded on PAC as consecutive Cr(VI) removal cycles (295 K, 50 g/L).

the results obtained from elution tests of PAC-pH 3 and PAC-pH 7 after three consecutive adsorption cycles. It is apparent from the figure that the increment of adsorbed Cr(VI) is higher than reduced Cr(III) at each cycle for both PAC-pH 3 and PAC-pH 7. Hence, it is conceivable to suggest that the adsorption process prevailed for Cr(VI) elimination. This finding was also reported by Daneshvar *et al.* (2019). Another significant observation was that for PAC-pH 3 and PAC-pH 7, the adsorbed Cr(VI) and reduced Cr(III) decreased as the cycles progressed. PAC-pH 3 showed higher Cr(VI) adsorption and reduction capacity. This may be due to the more generated Cr(III) precipitate accumulating on the PAC surface over time at the neutral condition, sheltering the PAC active sites from Cr(VI adsorption.

3.5. Performance of Cr-loaded PAC after desorption

The performance of the PAC for Cr adsorption was assessed after chromium was desorbed from the PAC using the H_2SO_4 and NaOH. Re-adsorption experiments were conducted following the third cycle desorption step. As can be seen in Figure 9, 92.43% removal efficiency of Cr(VI) was achieved by PAC-pH 7 after washing with H_2SO_4, whereas only 51.72% removal was attained using NaOH aqueous. Therefore, it can be inferred that the Cr(III) precipitate is mainly responsible for the poor performance of PAC under neutral conditions. The removal performance after acid washing (92.43%) was higher than the preliminary removal efficiency (83.86%); this result indicated that the acid desorption procedure modified PAC

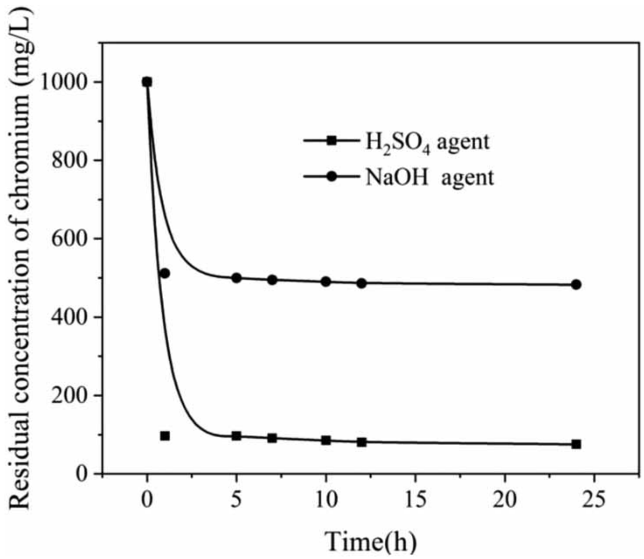

Figure 9 | The activity of chromium-loaded PAC-pH 7 after being treated with H_2SO_4 and NaOH (1,000 mg/L Cr(VI), pH 7).

properties and introduced surface functional groups. These results are consistent with those of Huang *et al.* (2009), who improved AC's Cr(VI) removal capacity by modifying it with nitric acid (Huang *et al.* 2009). As a result, it is proved that PAC's limited removal capability for Cr(VI) at pH 7 was mostly due to Cr(III) precipitate that formed on the surface of PAC. This finding backs the XPS results in that chromium oxide piled up mostly on PAC under neutral conditions. The sulfuric acid proved to be a potential chemical agent for the regeneration of Cr-loaded PAC after treating water contaminated with Cr(VI).

4. CONCLUSIONS

This study aimed to determine the mechanism of the limited sequestration capability of PAC on Cr(VI) under neutral conditions compared to acidic conditions. SEM-EDX substantiated that a chromium layer was formed on PAC, while XPS spectra corroborated the higher Cr_2O_3 content on PAC under alkaline conditions, resulting in poor Cr(VI) removal performance. Conversely, a lower Cr_2O_3 content on PAC under acid conditions is related to the higher Cr(VI) removal capacity. Desorption tests with H_2SO_4 and NaOH solution revealed that the precipitated Cr_2O_3 and adsorbed Cr(VI) can be selectively desorbed, proving that adsorption and reduction processes contributed significantly to the Cr(VI) removal. Consecutive desorption assays proved that the reduction and adsorption capability at 7 declined with time and were both lower than at pH 3. This is due to Cr(III) precipitate and adsorbed Cr(VI) blocking active sites. The superior performance on Cr(VI) removal of Cr-loaded PAC after desorption by H_2SO_4 further confirmed that the restricted removal performance under neutral conditions was ascribed to the formation of a Cr_2O_3 passivation layer on the surface of PAC particles. The insights gained from this work may be of assistance to the recycling of chromium from exhausted AC and extend the lifespan of AC.

ACKNOWLEDGEMENTS

Yi Fang acknowledges CONACYT (National Council of Science and Technology, Mexico) for the Fellowship (No. 900339) to pursue Ph.D. studies in Materials Science and Engineering at the Universidad Autónoma de San Luis Potosí, México. Authors acknowledge the partial financial support by the Guangdong College Students' Innovative Project (pdjh2021b0538, X201910580158), and the Zhaoqing Science and Technology Project (2018N005) to carry out this research.

DATA AVAILABILITY STATEMENT

All relevant data are included in the paper or its Supplementary Information.

REFERENCES

Al-Othman, Z. A., Ali, R. & Naushad, M. 2012 Hexavalent chromium removal from aqueous medium by activated carbon prepared from peanut shell: adsorption kinetics, equilibrium and thermodynamic studies. *Chemical Engineering Journal* **184**, 238–247. https://doi.org/10.1016/j.cej.2012.01.048.

Aparicio, J. D., Lacalle, R. G., Artetxe, U., Urionabarrenetxea, E., Becerril, J. M., Polti, M. A., Garbisu, C. & Soto, M. 2021 Successful remediation of soils with mixed contamination of chromium and lindane: integration of biological and physico-chemical strategies. *Environmental Research* **194**, 110666. https://doi.org/10.1016/j.envres.2020.110666.

Asimakopoulos, G., Baikousi, M., Salmas, C., Bourlinos, A. B., Zboril, R. & Karakassides, M. A. 2021 Advanced Cr(VI) sorption properties of activated carbon produced via pyrolysis of the 'Posidonia oceanica' seagrass. *Journal of Hazardous Materials* **405**, 124274. https://doi.org/10.1016/j.jhazmat.2020.124274.

Barrera-Diaz, C. E., Lugo-Lugo, V. & Bilyeu, B. 2012 A review of chemical, electrochemical and biological methods for aqueous Cr(VI) reduction. *Journal of Hazardous Materials* **223–224**, 1–12. https://doi.org/10.1016/j.jhazmat.2012.04.054.

Biesinger, M. C., Brown, C., Mycroft, J. R., Davidson, R. D. & McIntyre, N. S. 2004 X-ray photoelectron spectroscopy studies of chromium compounds. *Surface and Interface Analysis* **36**, 1550–1563. https://doi.org/10.1002/sia.1983.

Chen, Z., Wei, B., Yang, S., Li, Q., Liu, L., Yu, S., Wen, T., Hu, B., Chen, J. & Wang, X. 2019 Synthesis of PANI/AlOOH composite for Cr(VI) adsorption and reduction from aqueous solutions. *ChemistrySelect* **4**, 2352–2362. https://doi.org/10.1002/slct.201803898.

Chen, X., Wang, X. & Fang, D. 2020 A review on C1s XPS-spectra for some kinds of carbon materials. *Fullerenes, Nanotubes and Carbon Nanostructures* **28**, 1048–1058. https://doi.org/10.1080/1536383X.2020.1794851.

Chowdhury, S. R., Yanful, E. K. & Pratt, A. R. 2012 Chemical states in XPS and Raman analysis during removal of Cr(VI) from contaminated water by mixed maghemite–magnetite nanoparticles. *Journal of Hazardous Materials* 235–236. 246-256, https://doi.org/10.1016/j.jhazmat.2012.07.054.

Cong, H.-P., Ren, X.-C., Wang, P. & Yu, S.-H. 2012 Macroscopic multifunctional graphene-based hydrogels and aerogels by a metal ion induced self-assembly process. *ACS Nano.* **6**, 2693–2703. https://doi.org/10.1021/nn300082 k.

Cruz-Espinoza, A., Ibarra-Galván, V., López-Valdivieso, A. & González-González, J. 2012 Synthesis of microporous eskolaite from Cr(VI) using activated carbon as a reductant and template. *Journal of Colloid and Interface Science* **374**, 321–324. https://doi.org/10.1016/j.jcis.2012.01.059.

Cuesta, A., Dhamelincourt, P., Laureyns, J., Martínez-Alonso, A. & Tascón, J. M. D. 1994 Raman microprobe studies on carbon materials. *Carbon* **32**, 1523–1532. https://doi.org/10.1016/0008-6223(94)90148-1.

Cui, H., Fu, M., Yu, S. & Wang, M. K. 2011 Reduction and removal of Cr(VI) from aqueous solutions using modified byproducts of beer production. *Journal of Hazardous Materials* **186**, 1625–1631. https://doi.org/10.1016/j.jhazmat.2010.12.050.

Daneshvar, E., Zarrinmehr, M. J., Kousha, M., Hashtjin, A. M., Saratale, G. D., Maiti, A., Vithanage, M. & Bhatnagar, A. 2019 Hexavalent chromium removal from water by microalgal-based materials: adsorption, desorption and recovery studies. *Bioresource Technology* **293**, 122064. https://doi.org/10.1016/j.biortech.2019.122064.

Deng, M., Wang, X., Li, Y., Wang, F., Jiang, Z., Liu, Y., Gu, Z., Xia, S. & Zhao, J. 2020 Reduction and immobilization of Cr(VI) in aqueous solutions by blast furnace slag supported sulfidized nanoscale zerovalent iron. *Science of The Total Environment* **743**, 140722. https://doi.org/10.1016/j.scitotenv.2020.140722.

Dognani, G., Hadi, P., Ma, H., Cabrera, F. C., Job, A. E., Agostini, D. L. S. & Hsiao, B. S. 2019 Effective chromium removal from water by polyaniline-coated electrospun adsorbent membrane. *Chemical Engineering Journal* **372**, 341–351. https://doi.org/10.1016/j.cej.2019.04.154.

Duranoğlu, D., Trochimczuk, A. W. & Beker, U. 2012 Kinetics and thermodynamics of hexavalent chromium adsorption onto activated carbon derived from acrylonitrile-divinylbenzene copolymer. *Chemical Engineering Journal* **187**, 193–202. https://doi.org/10.1016/j.cej.2012.01.120.

Fang, Y., Wu, X., Dai, M., Lopez-Valdivieso, A., Raza, S., Ali, I., Peng, C., Li, J. & Naz, I. 2021a The sequestration of aqueous Cr(VI) by zero valent iron-based materials: from synthesis to practical application. *Journal of Cleaner Production* **312**, 127678. https://doi.org/10.1016/j.jclepro.2021.127678.

Fang, Y., Yang, K., Zhang, Y., Peng, C., Robledo-Cabrera, A. & López-Valdivieso, A. 2021b Highly surface activated carbon to remove Cr(VI) from aqueous solution with adsorbent recycling. *Environmental Research* **197**, 111151. https://doi.org/10.1016/j.envres.2021.111151.

Gangadharan, P. & Nambi, I. M. 2014 Hexavalent chromium reduction and energy recovery by using dual-chambered microbial fuel cell. *Water Science and Technology* **71**, 353–358. https://doi.org/10.2166/wst.2014.524.

Grohmann, I., Kemnitz, E., Lippitz, A. & Unger, W. E. S. 1995 Curve fitting of Cr 2p photoelectron spectra of cr2o3 and crf3. *Surface and Interface Analysis* **23**, 887–891. https://doi.org/10.1002/sia.740231306.

Huang, G., Shi, J. X. & Langrish, T. A. G. 2009 Removal of Cr(VI) from aqueous solution using activated carbon modified with nitric acid. *Chemical Engineering Journal* **152**, 434–439. https://doi.org/10.1016/j.cej.2009.05.003.

Ibarra-Galván, V., López-Valdivieso, A., Villavelazquez-Mendoza, C. I., Santoyo-Salazar, J. & Song, S. 2014 Synthesis of eskolaite (α-Cr_2O_3) nanostructures by thermal processing of Cr_2O_3-loaded activated carbon. *Part. Sci. Technol.* **32**, 451–455. https://doi.org/10.1080/02726351.2013.878774.

Jia, Z. & Wang, Y. 2015 Covalently crosslinked graphene oxide membranes by esterification reactions for ions separation. *Journal of Materials Chemistry A* **3**, 4405–4412. https://doi.org/10.1039/C4TA06193D.

Jiang, W., Cai, Q., Xu, W., Yang, M., Cai, Y., Dionysiou, D. D. & O'Shea, K. E. 2014 Cr(VI) adsorption and reduction by humic acid coated on magnetite. *Environmental Science & Technology* **48**, 8078–8085. https://doi.org/10.1021/es405804 m.

Jieying, Z., Zhao, Q. & Ye, Z. 2014 Preparation and characterization of activated carbon fiber (ACF) from cotton woven waste. *Applied Surface Science* **299**, 86–91. https://doi.org/10.1016/j.apsusc.2014.01.190.

Jing, G., Zhou, Z., Song, L. & Dong, M. 2011 Ultrasound enhanced adsorption and desorption of chromium (VI) on activated carbon and polymeric resin. *Desalination.* **279**, 423–427. https://doi.org/10.1016/j.desal.2011.06.001.

Krishna Kumar, A. S., You, J.-G., Tseng, W.-B., Dwivedi, G. D., Rajesh, N., Jiang, S.-J. & Tseng, W.-L. 2019 Magnetically separable nanospherical g-C3N4@Fe_3O_4 as a recyclable material for chromium adsorption and visible-light-driven catalytic reduction of aromatic nitro compounds. *ACS Sustainable Chemistry & Engineering* **7**, 6662–6671. doi:10.1021/acssuschemeng.8b05727.

Lespade, P., Marchand, A., Couzi, M. & Cruege, F. 1984 Caracterisation de materiaux carbones par microspectrometrie Raman. *Carbon* **22**, 375–385. https://doi.org/10.1016/0008-6223(84)90009-5.

Li, Y., Cui, W., Liu, L., Zong, R., Yao, W., Liang, Y. & Zhu, Y. 2016 Removal of Cr(VI) by 3D TiO_2-graphene hydrogel via adsorption enriched with photocatalytic reduction. *Applied Catalysis B: Environmental* **199**, 412–423. https://doi.org/10.1016/j.apcatb.2016.06.053.

Li, J., Zhang, X., Liu, M., Pan, B., Zhang, W., Shi, Z. & Guan, X. 2018 Enhanced reactivity and electron selectivity of sulfidated zerovalent iron toward chromate under aerobic conditions. *Environmental Science and Technology* **52**, 2988–2997. https://doi.org/10.1021/acs.est.7b06502.

Liu, N., Zhang, Y., Xu, C., Liu, P., Lv, J., Liu, Y. & Wang, Q. 2020 Removal mechanisms of aqueous Cr(VI) using apple wood biochar: a spectroscopic study. *Journal of Hazardous Materials* **384**, 121371. https://doi.org/10.1016/j.jhazmat.2019.121371.

Ma, J., Pan, J., Yue, J., Xu, Y. & Bao, J. 2018 High performance of poly(dopamine)-functionalized graphene oxide/poly(vinyl alcohol) nanocomposites. *Applied Surface Science* **427**, 428–436. https://doi.org/10.1016/j.apsusc.2017.07.040.

Ma, H., Yang, J., Gao, X., Liu, Z., Liu, X. & Xu, Z. 2019 Removal of chromium (VI) from water by porous carbon derived from corn straw: influencing factors, regeneration and mechanism. *Journal of Hazardous Materials* **369**, 550–560. https://doi.org/10.1016/j.jhazmat.2019.02.063.

Mohan, D., Singh, K. P. & Singh, V. K. 2005 Removal of hexavalent chromium from aqueous solution using low-cost activated carbons derived from agricultural waste materials and activated carbon fabric cloth. *Industrial and Engineering Chemistry Research* **44**, 1027–1042. https://doi.org/10.1021/ie0400898.

Murphy, V., Tofail, S. A. M., Hughes, H. & McLoughlin, P. 2009 A novel study of hexavalent chromium detoxification by selected seaweed species using SEM-EDX and XPS analysis. *Chemical Engineering Journal* **148**, 425–433. https://doi.org/10.1016/j.cej.2008.09.029.

Niazi, L., Lashanizadegan, A. & Sharififard, H. 2018 Chestnut oak shells activated carbon: preparation, characterization and application for Cr (VI) removal from dilute aqueous solutions. *Journal of Cleaner Production* **185**, 554–561. https://doi.org/10.1016/j.jclepro.2018.03.026.

Norouzi, S., Heidari, M., Alipour, V., Rahmanian, O., Fazlzadeh, M., Mohammadi-moghadam, F., Nourmoradi, H., Goudarzi, B. & Dindarloo, K. 2018 Preparation, characterization and Cr(VI) adsorption evaluation of NaOH-activated carbon produced from date press cake; an agro-industrial waste. *Bioresource Technology* **258**, 48–56. https://doi.org/10.1016/j.biortech.2018.02.106.

Ogata, F., Nagai, N., Itami, R., Nakamura, T. & Kawasaki, N. 2020 Potential of virgin and calcined wheat bran biomass for the removal of chromium(VI) ion from a synthetic aqueous solution. *Journal of Environmental Chemical Engineering* **8**, 103710. https://doi.org/10.1016/j.jece.2020.103710.

Osswald, S., Flahaut, E. & Gogotsi, Y. 2006 In situ Raman spectroscopy study of oxidation of double- and single-wall carbon nanotubes. *Chemistry of Materials* **18**, 1525–1533. https://doi.org/10.1021/cm052755 g.

Ouki, S. K. & Neufeld, R. D. 1997 Use of activated carbon for the recovery of chromium from industrial wastewaters. *Journal of Chemical Technology and Biotechnology* **70**, 3–8. https://doi.org/10.1002/(SICI)1097-4660(199709)70:1<3::AID-JCTB664>3.0.CO;2-5.

Qian, L., Liu, S., Zhang, W., Chen, Y., Ouyang, D., Han, L., Yan, J. & Chen, M. 2019 Enhanced reduction and adsorption of hexavalent chromium by palladium and silicon rich biochar supported nanoscale zero-valent iron. *Journal of Colloid and Interface Science* **533**, 428–436. https://doi.org/10.1016/j.jcis.2018.08.075.

Qu, J., Wang, Y., Tian, X., Jiang, Z., Deng, F., Tao, Y., Jiang, Q., Wang, L. & Zhang, Y. 2021 KOH-activated porous biochar with high specific surface area for adsorptive removal of chromium (VI) and naphthalene from water: affecting factors, mechanisms and reusability exploration. *Journal of Hazardous Materials* **401**, 123292. https://doi.org/10.1016/j.jhazmat.2020.123292.

Rakhunde, R., Deshpande, L. & Juneja, H. 2012 Chemical speciation of chromium in water: a review. *Critical Reviews in Environment Science and Technology* **42**, 776–810. https://doi.org/10.1080/10643389.2010.534029.

Ramirez, A., Ocampo, R., Giraldo, S., Padilla, E., Flórez, E. & Acelas, N. 2020 Removal of Cr (VI) from an aqueous solution using an activated carbon obtained from teakwood sawdust: kinetics, equilibrium, and density functional theory calculations. *Journal of Environmental Chemical Engineering* **8**, 103702. https://doi.org/10.1016/j.jece.2020.103702.

Ren, Z., Xu, X., Wang, X., Gao, B., Yue, Q., Song, W., Zhang, L. & Wang, H. 2016 FTIR, Raman, and XPS analysis during phosphate, nitrate and Cr(VI) removal by amine cross-linking biosorbent. *Journal of Colloid and Interface Science* **468**, 313–323. https://doi.org/10.1016/j.jcis.2016.01.079.

Samuel, M. S., Selvarajan, E., Chidambaram, R., Patel, H. & Brindhadevi, K. 2021 Clean approach for chromium removal in aqueous environments and role of nanomaterials in bioremediation: present research and future perspective. *Chemosphere* **284**, 131368. https://doi.org/10.1016/j.chemosphere.2021.131368.

Sangkarak, S., Phetrak, A., Kittipongvises, S., Kitkaew, D., Phihusut, D. & Lohwacharin, J. 2020 Adsorptive performance of activated carbon reused from household drinking water filter for hexavalent chromium-contaminated water. *Journal of Environmental Management* **272**, 111085. https://doi.org/10.1016/j.jenvman.2020.111085.

Shi, Y., Shan, R., Lu, L., Yuan, H., Jiang, H., Zhang, Y. & Chen, Y. 2020 High-efficiency removal of Cr(VI) by modified biochar derived from glue residue. *Journal of Cleaner Production* **254**, 119935. https://doi.org/10.1016/j.jclepro.2019.119935.

Singha, S., Sarkar, U. & Luharuka, P. 2013 Functionalized granular activated carbon and surface complexation with chromates and bi-chromates in wastewater. *Science of the Total Environment* **447**, 472–487. https://doi.org/10.1016/j.scitotenv.2013.01.006.

Su, M., Fang, Y., Li, B., Yin, W., Gu, J., Liang, H., Li, P. & Wu, J. 2019 Enhanced hexavalent chromium removal by activated carbon modified with micro-sized goethite using a facile impregnation method. *Sci Total Environ.* **647**, 47–56. https://doi.org/10.1016/j.scitotenv.2018.07.372.

Valentín-Reyes, J., García-Reyes, R., García-González, A., Soto-Regalado, E. & Cerino-Córdova, F. 2019 Adsorption mechanisms of hexavalent chromium from aqueous solutions on modified activated carbons. *Journal of Environmental Management* **236**, 815–822. https://doi.org/10.1016/j.jenvman.2019.02.014.

Wang, X., Liang, Y., An, W., Hu, J., Zhu, Y. & Cui, W. 2017 Removal of chromium (VI) by a self-regenerating and metal free g-c3n4/graphene hydrogel system via the synergy of adsorption and photo-catalysis under visible light. *Applied Catalysis B: Environmental* **219**, 53–62. https://doi.org/10.1016/j.apcatb.2017.07.008.

Wang, C., Wu, Y., Qu, T., Liu, S., Pi, Y. & Shen, J. 2019 Enhanced Cr (VI) removal in the synergy between the hydroxyl-functionalized ball-milled ZVI/Fe3O4 composite and Na2EDTA complexation. *Chemical Engineering Journal* **359**, 874–881. https://doi.org/10.1016/j.cej.2018.11.104.

Wang, Y., Peng, C., Padilla-Ortega, E., Robledo-Cabrera, A. & López-Valdivieso, A. 2020 Cr(VI) adsorption on activated carbon: mechanisms, modeling and limitations in water treatment. *Journal of Environmental Chemical Engineering* **8**, 104031. https://doi.org/10.1016/j.jece.2020.104031.

Wu, J., Zhang, H., He, P.-J., Yao, Q. & Shao, L.-M. 2010 Cr(VI) removal from aqueous solution by dried activated sludge biomass. *Journal of Hazardous Materials* **176**, 697–703. https://doi.org/10.1016/j.jhazmat.2009.11.088.

Wu, M., Li, Y., Li, J., Wang, Y., Xu, H. & Zhao, Y. 2019 Bioreduction of hexavalent chromium using a novel strain CRB-7 immobilized on multiple materials. *Journal of Hazardous Materials* **368**, 412–420.

Wu, F., Zhao, T., Yao, Y., Jiang, T., Wang, B. & Wang, M. 2020 Recycling supercapacitor activated carbons for adsorption of silver (I) and chromium (VI) ions from aqueous solutions. *Chemosphere* **238**, 124638. https://doi.org/10.1016/j.chemosphere.2019.124638.

Yang, X., Cui, H., Li, Y., Qin, J., Zhang, R. & Tang, H. 2013 Fabrication of Ag_3PO_4-Graphene composites with highly efficient and stable visible light photocatalytic performance. *ACS Catalysis* **3**, 363–369. 10.1021/cs3008126.

Yin, W., Guo, Z., Zhao, C. & Xu, J. 2019 Removal of Cr(VI) from aqueous media by biochar derived from mixture biomass precursors of *Acorus calamus* Linn. and feather waste. *Journal of Analytical and Applied Pyrolysis* **140**, 86–92. https://doi.org/10.1016/j.jaap.2019.04.024.

Zeng, Q., Hu, Y., Yang, Y., Hu, L., Zhong, H. & He, Z. 2019 Cell envelope is the key site for Cr (VI) reduction by *Oceanobacillus oncorhynchi* W4, a newly isolated Cr (VI) reducing bacterium. *Journal of Hazardous Materials* **368**, 149–155. https://doi.org/10.1016/j.jhazmat.2019.01.031.

Zhang, Y.-J., Ou, J.-L., Duan, Z.-K., Xing, Z.-J. & Wang, Y. 2015 Adsorption of Cr(VI) on bamboo bark-based activated carbon in the absence and presence of humic acid. *Colloids and Surfaces A: Physicochemical and Engineering Aspects* **481**, 108–116. https://doi.org/10.1016/j.colsurfa.2015.04.050.

Zhang, L., Fu, F. & Tang, B. 2019 Adsorption and redox conversion behaviors of Cr(VI) on goethite/carbon microspheres and akaganeite/carbon microspheres composites. *Chemical Engineering Journal* **356**, 151–160. https://doi.org/10.1016/j.cej.2018.08.224.

Zhang, L., Qiu, Y.-Y., Zhou, Y., Chen, G.-H., van Loosdrecht, M. C. M. & Jiang, F. 2021a Elemental sulfur as electron donor and/or acceptor: mechanisms, applications and perspectives for biological water and wastewater treatment. *Water Research* **202**, 117373. https://doi.org/10.1016/j.watres.2021.117373.

Zhang, W., Qian, L., Chen, Y., Ouyang, D., Han, L., Shang, X., Li, J., Gu, M. & Chen, M. 2021b Nanoscale zero-valent iron supported by attapulgite produced at different acid modification: synthesis mechanism and the role of silicon on Cr(VI) removal. *Chemosphere* **267**, 129183. https://doi.org/10.1016/j.chemosphere.2020.129183.

Zhou, L., Liu, Y., Liu, S., Yin, Y., Zeng, G., Tan, X., Hu, X., Hu, X., Jiang, L., Ding, Y., Liu, S. & Huang, X. 2016 Investigation of the adsorption-reduction mechanisms of hexavalent chromium by ramie biochars of different pyrolytic temperatures. *Bioresource Technology* **218**, 351–359. https://doi.org/10.1016/j.biortech.2016.06.102.

First received 11 August 2021; accepted in revised form 29 September 2021. Available online 12 October 2021

© by PSP Volume 29 – No. 07A/2020 pages 6072-6081 Fresenius Environmental Bulletin

ADSORPTIVE REMOVAL OF CATIONIC TOXIC DYES FROM AQUEOUS SOLUTION: ADSORBENTS DEVELOPMENT AND PERFORMANCE INVESTIGATION

Yi Fang[1,2], Changshang Peng[1,3], Ke Yang[2], Yipeng Zhang[2], A Lopez-Valdivieso[2], Min Dai[1], Imran Ali[4], Muhammad Sultan[5,*], Iffat Naz[6], Naila Asghar[7], Muhammad H Mahmood[5], Hafiz MU Raza[5]

[1]School of Environmental and Chemical Engineering, Zhaoqing University, Zhaoqing 526061, China
[2]Instituto de Metalurgia, Universidad Autónoma de San Luis Potosí, San Luis Potosí, C. P. 78210, Mexico
[3]The Key Lab of Marine Environmental Science and Ecology, Ministry of Education, College of Environmental Science and Engineering, Ocean University of China, Qingdao 266100, China
[4]Department of Environmental Science and Engineering, College of Chemistry and Environmental Engineering, Shenzhen University, Shenzhen, Guangdong, 518060, China
[5]Department of Agricultural Engineering, Bahauddin Zakariya University, Bosan Road, Multan 60800, Pakistan
[6]Department of Biology, Scientific Unit, Deanship of Educational Services, Qassim University, Buraidah 51452, Qassim, Saudi Arabia
[7]Department of Botany, University of Agriculture, Faisalabad 38000, Pakistan

ABSTRACT

Co-effect of pore size and specific surface area of the two different kinds of synthetic adsorbents on the adsorptive performance/ removal against cationic toxic dyes *i.e.,* methylene blue (MB) and crystal violet (CV) was observed. Two different kinds of synthetic adsorbents were prepared using waste coal fly-ash and bentonite mixed with paper fiber (AP) and enteromorpha powder (AE). The findings depicted that an equilibrium adsorptive capacity for AE and AP against MB were 167.0 and 157.0 mg/g, respectively. On the other hand, equilibrium adsorptive capacities of AE and AP against CV were 130.0 and 150.0 mg/g, respectively. The adsorptive performance of AP and AE against MB showed positive correlation with specific surface area which was 21.94 and 34.23 m^2/g, respectively. In contrast, adsorptive performance of CV indicated positive correlation with pore size not with the specific surface area of the adsorbents, which were 4.28 and 1.52 nm, respectively. The findings hinted that the specific surface area controlled the adsorption capacity, if the contamination molecules could pass through the pores of adsorbents. In contrast, the pores size of the adsorbents governed the adsorption capacity, if contamination molecules could not reach the active/ vacant sites of the adsorbents. Overall, it can be assumed that the pore size has a promising effect on the removal efficiency of dye molecules by these adsorbents. Moreover, the adsorption kinetics of AP and AE against MB and CV hinted that the contaminant molecules diffused within adsorbents and played a significant role to control adsorptive rate.

KEYWORDS:
Adsorbent, pore size, specific surface area, cationic dye, adsorptive capacity

INTRODUCTION

Pollutants found in wastewater *i.e.,* toxic metal ions, dyes, sulfamethazine, phosphorous, refectory organic & inorganic chemicals, etc. (which normally have a density less than 5g/cm^3 and their atomic mass ranging from 63.5 to 200.6) are deteriorating aquatic and biotic environment/ life [1-3]. These pollutants are being released from various chemical industries such as mining, battery manufacturing, textile, metal plating, dyes stuffs, paper making, fertilizer, tannery, pesticides, etc. Among them, synthetic organic dyes have been extensively utilized in various industrial practices i.e., printing, cosmetics, textiles, leather, food and paper making [4]. Moreover, the discharge of toxic dyes-containing wastewater into the natural environment has caused serious environmental concern globally. Meanwhile, the level of water quality is also swayed by the manifestation of toxic dyes owing to having their visible color and carcinogenic nature [5]. Therefore, the removal and degradation of these toxic dyes from wastewater is imperative to minimize the threats to the environment. In this regard, various technologies (including membrane filtration, adsorption, coagulation, chemical precipitation, electrochemical treatment, etc.) have been developed and utilized to treat dyes containing wastewaters/ effluents. Among them, adsorption technology has been assumed to be the most reliable and attractive option to remove dyes-bearing wastewater owing to its miscellaneous merits including cost-effective, simple, fast and environmentally friendly process [6].

Hence, experts are using their strengths to fabricate novel adsorbents, which should possess highest adsorptive capability by using minimum cost and energy. In this regard, various kinds of adsorbents have been developed and used (including carbon nanotubes, clay, zeolites, polysaccharides, functionalized, activated carbon, sawdust, fly-ash, rice husk ash, metal organic frameworks, peanut hull carbon, graphene oxide, biochar, coal fly ash, coir pith carbon, etc.) to remove and adsorb toxic dyes from domestic wastewater and industrial effluents [7-8]. In addition, comprehensive detail is given in authors previously published reports [1-9]. In this regard, in the present research work, novel adsorbents were fabricated by using coal fly ash, bentonite, paper fiber (AP) and enteromorpha powder (AE) for possible adsorption of cationic toxic dyes such as methylene blue (MB) and crystal violet (CV) from aqueous solution.

Coal fly ash (CFA) is produced due to the combustion of pulverized from coal-fired power stations. Presently, China is producing about 100-200 million tons of CFA annually from different coal-fired power stations [10-14]. Basically, CFA is a by-product that partially developed porous solid waste consisting of Al_2O_3, Fe_2O_3, SiO_2 and CaO as its main components, along-with varying quantity of unburned carbon. It is also recognized as an environmental pollutant. Moreover, CFA has been already used as a cost-effective adsorbent to remove organic and inorganic substances from wastewaters/ effluents. Though, CFA had substandard adsorptive capacity compared to activated carbon, however, its cheap costs and easy availability make it an economically viable alternative and attractive candidate to remove pollutants from wastewaters/ industrial effluents [15]. On the other hand, it is also suffering some drawbacks such as solid-liquid separation and disposal of the metal or poisonous organic sludges [16].

Therefore, to overcome these disadvantages, the present research work was designed to fabricate novel materials/ adsorbents based on CFA and bentonite clay as the binder, and pore forming agents. Three forms of pore forming agents were employed including powder starch, paper fiber and enteromorpha powder, because the pore forming agents may develop various structures of pores after sintering at high temperature. The main objective of this work was to compare the effect of different pore size and surface area on the adsorptive performance of three adsorbents in removing cationic toxic dyes i.e., CV and MB under optimum experiment conditions, and also to find out low-cost and high performance adsorbent for the removal of these dyes.

MATERIALS AND METHODS

Materials and Instrumentation. The Methylene blue (MB) and Crystal violet (CV) dyes were purchased from Sinopharm Chemical Reagent Beijing, China. Bentonite was provided by the Mingxi Mineral factory, Anhui, China. CFA was obtained from Shenhua group of ningxia, China. Enteromorpha was collected from the offshore of Qingdao, China. The paper fiber (AP) was provided by a paper mill in Gaotang, China. UV-visible light photometer (UV 2600, Unic) was purchased from Unic, Shanghai, China. Electric blast drying oven (DHG-9023A), atmosphere sintering furnace (HMX-1400-30A), particle forming machine (LG-120A) were used for the preparation of the adsorbents.

Preparation of synthetic adsorbents. The detail composition of CFA is listed in the Table 1. Firstly, CFA was dried overnight in an oven at 60ºC and screened through 200 meshes. The main components of CFA were SiO_2 (50.2%) and Al_2O_3 (27.1%), which comprised the major weight, and rest of the minor components were Fe_2O_3 (2.8%), CaO (7.1%) and MgO (1.2%), (as detail given in Table 1). Enteromorpha was rinsed several times, and then dried overnight at 105ºC. A fixed amount of 200 grams took and grinded for 10 min, and then the obtained powder (named herein as AE) was preserved for further applications. The ratio of CFA and bentonite was 2:1 and 1:1 for the fabrication of AP and AE, respectively. Pore forming agent's addition ratio for the preparation of adsorbents was 3% and 3%, respectively. The following heating rates i.e., 0.2ºC/min, 0.5ºC/min and 630ºC were regulated to make these adsorbents. Various conditions (i.e., CFA/ bentonite composition, addition proportion of pore-forming agents and sintering temperature) were first employed to figure out optimal conditions.

Characterization of Synthetic Adsorbents (as-prepared). The surface of the as-prepared adsorbents (i.e., AP and AE) depicted abundant holes and showing better mechanical performance. The loss rate is an index for checking material's mechanical performance. Regarding this, 1.00 g sample was introduced into 50mL deionized water and stirred at 200rpm for 0.5 h, and then it was dried prior to noting its weight. The weight after dried was m (g). Thereafter, the loss rate was equal to (1-m) %, and the loss rates of these two adsorbents were all lower than 0.5%, and it can be ignored. For a further observation of the inner structure, surface area and pore diameter of AP and AE, SEM (scan electron microscope) and N2 adsorption BET instrument were performed. The UV-visible light photometer was used to investigate the concentration of dyes before and after the interaction with adsorbents.

Experiments and Adsorptive Performance Investigation. For elucidating the effect of pore size and surface area on the adsorptive performance of the prepared adsorbents, the toxic dyes such as crystal violent (CV) and methylene blue (MB) were selected as target adsorbate/ pollutant. CV and MB dyes hold various molecular structures, in which the CV molecular presents fork style and MB presents chain style. Detail information about

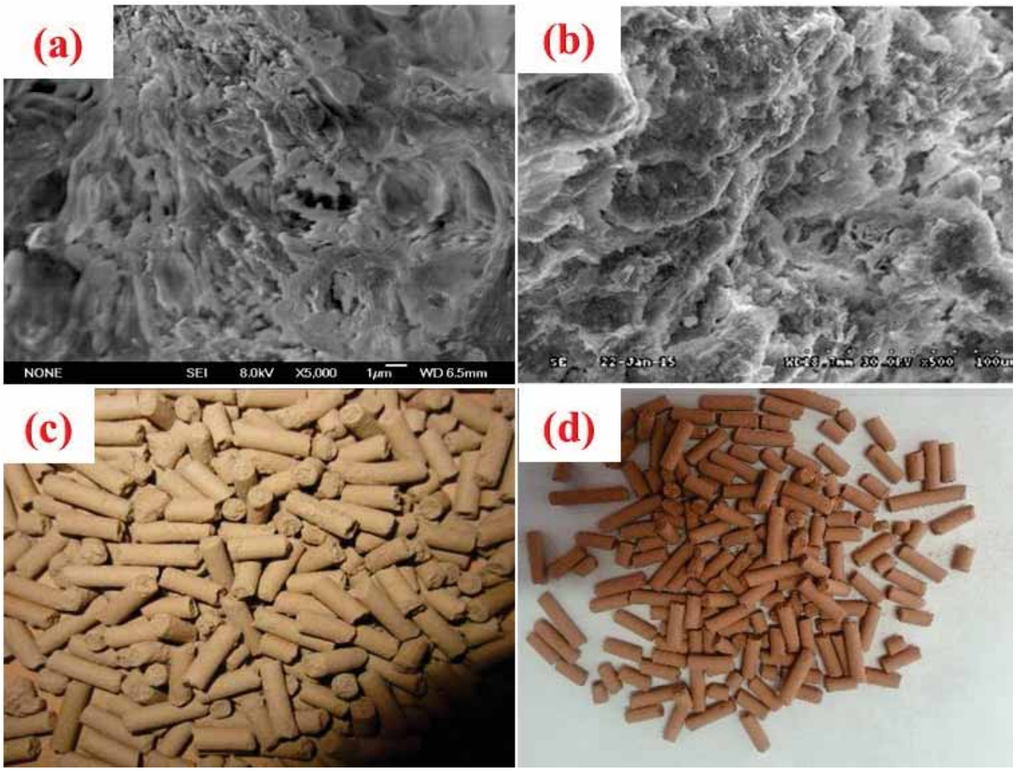

FIGURE 1
SEM images of the developed adsorbents (as-prepared): (a) AP, (b)AE; and pictorial images of adsorbents (as-prepared): (c) AP, and (d) AE.

CV and MB dyes is given in Table 2. The stock solutions were made by using distilled water. The desired concentration solutions were made by using equation $C_1V_1=C_2V_2$. All the chemicals and reagents (employed in the current work) were pure and analytical grade. To investigate the adsorptive performance of the prepared adsorbents against cationic toxic dyes, initially a fixed amount of 0.5g adsorbents was added in 250 mL dye solution (100mg/L), and these bottles were stirred at 120rmp and heated at 40ºC until to approach equilibrium. After reaching equilibrium, the final solution was filtered via using 0.45μm filter paper, and then the final concentrations of the dyes/ adsorbates/ pollutants were estimated by UV-vis spectrophotometer (Unico UV 2600) at its maximum absorbance (λ_{max}=584nm for CV and λ_{max}=665nm for MB). Finally, the adsorptive capacities were estimated by using equations as:

$$q_e = \frac{V\,(C_o - C_e)}{m} \tag{1}$$

Where, C_o(mg/L) and C_e(mg/L) are the initial and the final or equilibrium concentrations of the cationic toxic dyes in the solutions, V(L) is the volume of dyes solution, and m(g) is the adsorbents dosage.

TABLE 1
The chemical composition of CFA (wt%)

Composition	SiO_2	Al_2O_3	CaO	MgO	Fe_2O_3	K_2O	Na_2O	SO_3	Residue on ignition
Average Value	50.2	27.1	7.1	1.2	2.8	1.3	0.5	0.3	8.2

TABLE 2
The characteristics of MB and CV cationic dyes.

Property	MB	CV
Molar mass(g/mol)	319.85	407.98
Molecular size(nm)	1.43×0.61×0.40	1.45×1.28×0.35
Schematic diagram	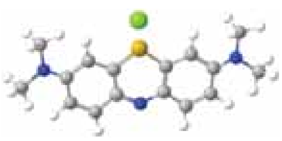	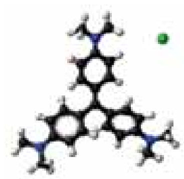

RESULT AND DISCUSSION

Physical Characterization of Synthetic Adsorbents (as-prepared). Normally, it is assumed that physical and chemical interaction (between adsorbent and adsorbate) is mainly responsible to determine the adsorptive performance/ capacity of the as-prepared adsorbent. The shape/ structure and diameter of the pores is mainly determined the attachment/ adsorption of pollutants/ adsorbates on the vacant/ active sites of the adsorbent. In this regard, SEM images of the as-prepared adsorbents were studied (Figure 1). The results depicted that AP had higher develop pore structure and its pores are unified/ interconnected. The networks in the AP and AE structure were left with the burning out of paper fiber and enteromorpha, and the structure of these channels was described to the sharp of pore former, so the fibrous paper fiber behaved relatively developed pore channel compare to particle entermorpha.

For elucidating physical characteristic of the as-prepared adsorbents, nitrogen adsorption-desorption test was carried out at 77.3K (Quantachrome Autosorb 1) [17]. Moreover, BJH method was employed to find out corresponding specific surface area and pore size of the as-prepared adsorbents [18]. Figure 2 is depicting adsorption-desorption isotherms of the as prepared adsorbents. Adsorption isotherms of AP and AE can be attributed to Type IV, as classified by the IUPAC [19]. The display of isotherms hinted a rough assessment of the porous structure

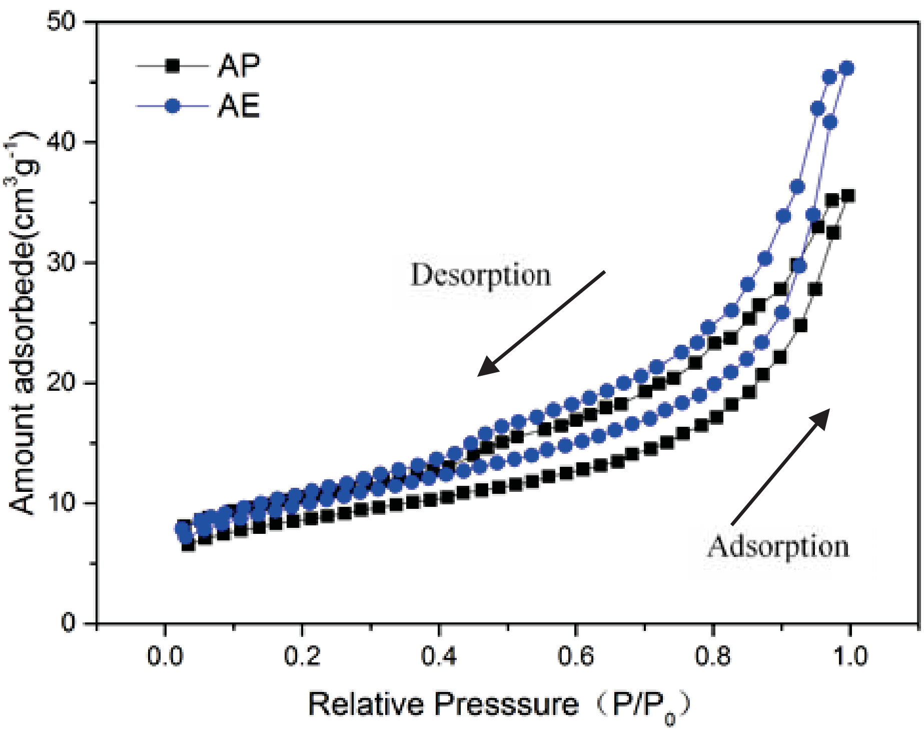

FIGURE 2
N_2-adsorption-desorption hysteresis loops of AP and AE at liquid nitrogen (77.3K) temperature.

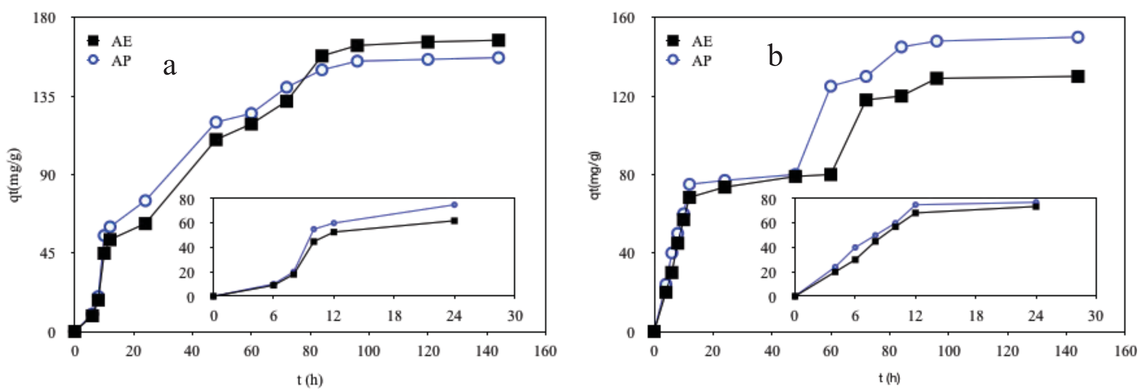

FIGURE 3
The comparison of the adsorptive performance of the AE and AP against cationic toxic dyes using dosage 0.5g; (a) MB (1000mg/l, 100ml) (b) CV (1000mg/l, 100ml)

of the as-prepared adsorbents. Figure 1 depicted that hysteresis loops of APF and AEP were H3 type, and this type of loops indicated that both APF and AEP had dominantly macroporous and absence of micro-mesoporous structure in the prepared adsorbents. On the other hand, ASP indicated a noteworthy hysteresis pattern including a sharp isotherm, which hinted that the prepared adsorbent had both mesopores and silt-like pores structure [20]. Importantly, Type H2 hysteresis loop had been found previously with mesocellular silica foams and some mesoporous ordered silicas after hydrothermal treatment [21-23]. In contrast, Type H3 hysteresis loop was observed in certain clays [20]. Table 3 is depicting that the surface area and pore diameter of the as-prepared adsorbents were different, and interestingly, AEP (34.23 m^2/g) showed greater specific surface area than APF (21.94 m^2/g).

Adsorptive Performance of Synthetic Adsorbents (as-prepared). The adsorptive performance/ uptake rate of the adsorbent/ material is mainly depended on the adsorbent dosage, diffusion coefficient of the pollutants in the bulk phase, structure/ pore size distribution of the adsorbent, mass of the pollutants/ adsorbate molecules and affinity of the pollutants/ adsorbate to the adsorbent [24, 25]. Figure 3 depicted that the uptake rate of the AE and AP was greater in the first stage, and the plots were not liner over the complete adsorption process, hinting that the

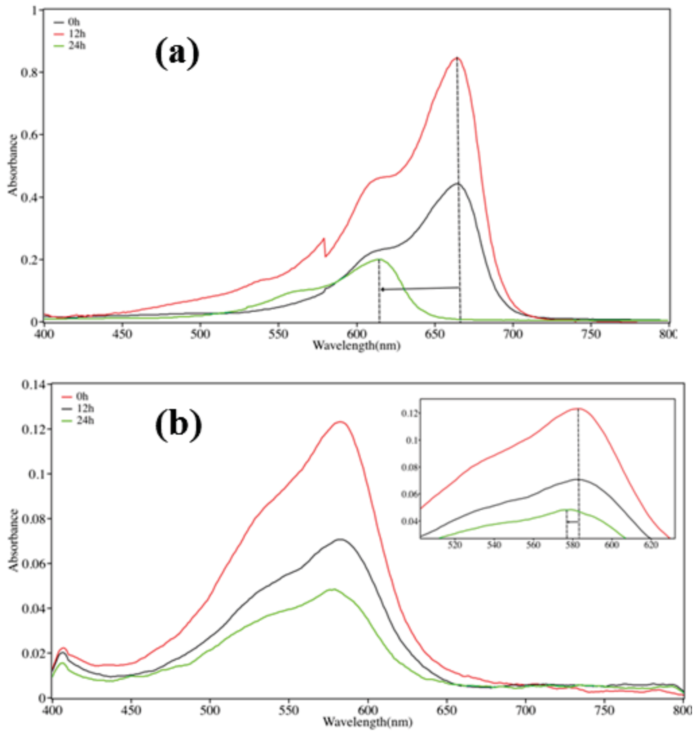

FIGURE 4
The Maximum absorption peak shift of (a) MB; and (b) CV as time elapsed while used AE adsorbent.

TABLE 3
Specific surface are and pore size of the as-prepared adsorbents

Adsorbents	$S_{BJH}(m^2/g)$	$D_{aver}(nm)$
AP	21.94	4.28
AE	34.23	1.52

TABLE 4
The values of intraparticle diffusion parameters

Adsorbent/adsorbate	$k_{id}(mg/g\ h^{1/2})$	D_1 ($\times10^{-3}mm^2/h$)	D_2 ($\times10^{-3}mm^2/h$)
AE/MB	16.688	$0.87a^2$	$4.02a^2$
AP/MB	15.456	$0.27a^2$	$4.19a^2$
AE/CV	11.207	$0.65a^2$	$3.63a^2$
AP/CV	13.372	$0.70a^2$	$3.75a^2$

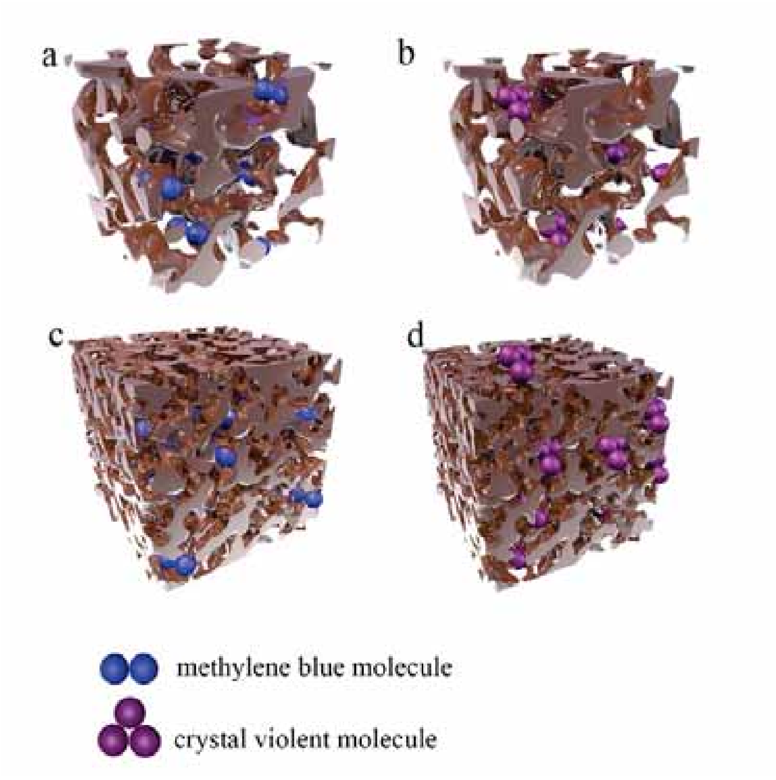

FIGURE 5
The schematic diagram of the adsorption removal mechanism of (a) MB; and (b) CV while used AP adsorbent and (c) MB, (d) CV while used AE adsorbent.

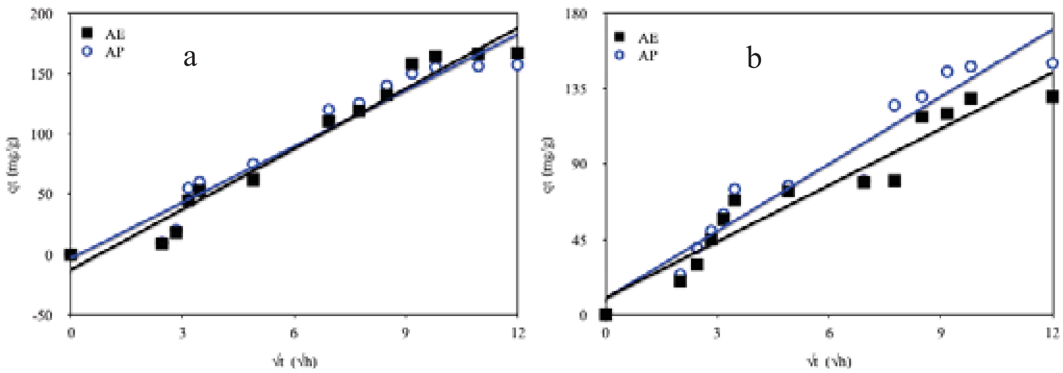

FIGURE 6
The linear fit of intraparticle diffusion model of (a) MB and (b) CV during adsorption by AE and AP

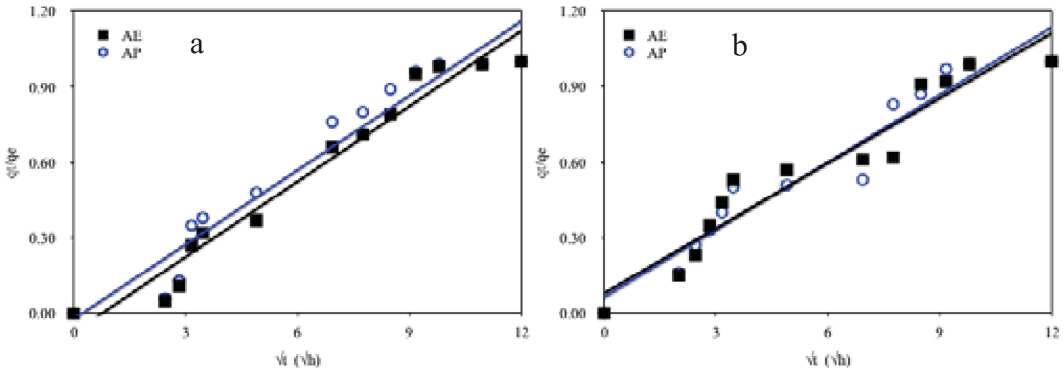

FIGURE 7
Determination of film diffusion coefficient D1 of (a) MB and (b) CV during adsorption by AE and AP

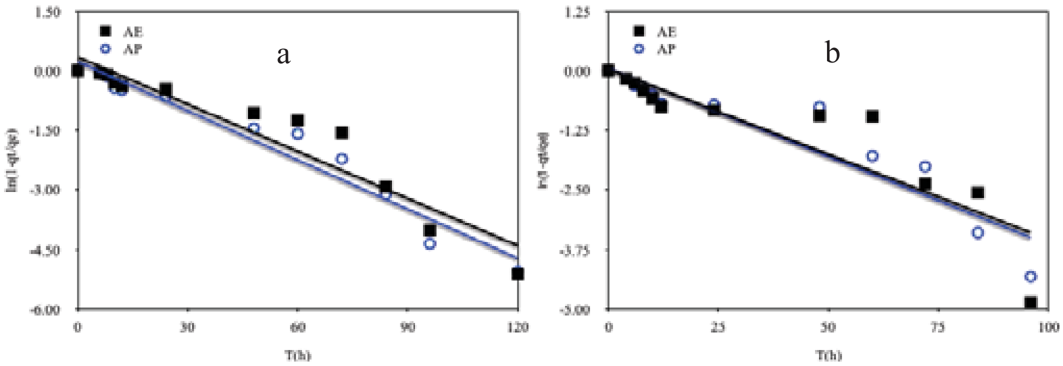

FIGURE 8
Determination of inner diffusion coefficient D2 of (a) MB and (b) CV during adsorption by AE and AP.

adsorption process affected by more than one routes. The deviation of straight lines might be owing to the difference in the electrostatic attraction between adsorbate molecule and adsorbent in initial stage of adsorption. Moreover, the initial pH values (of MB and CV dyes) were 6.00 and 4.64, respectively. The point of zero charge (pH_{PZC}) of the as-prepared adsorbents was determined by the pH drift method as explained by Ali et al. [1,2]. The point of zero charge is an important trait which can influence on the surface charges/ functional groups present on the adsorbents and can alter chemical nature of the solution. The values of pH_{PZC} of the as-prepared adsorbents (i.e. AP, and AE) were 1.50 and 1.93, respectively. Considering the pH_{pzc} values of AP and AE, which were lower than compared to pH of the reactive solution, and as a consequence, it presents negative charge on the surface of the as-prepared adsorbents. AP and AE showed more intensity net charge by the means of its considerable surface functional groups. The MB and CV dyes molecules appeared positive charge in the solution. The electrostatic attraction rank was in the following order with respect to their pH_{pzc} of AP>AE, which corresponded with the sequence of uptake rate at the initial step.

The MB molecules could penetrate through the pore channels of AP and AE to the adsorption sites because its molecule size was smaller than the pore diameter of adsorbents, so the adsorption performance was mainly controlled by the special surface area and followed the order of AE>AP, and the equilibrium adsorption amount of

AE and AP against MB were 167.0 and 157.0 mg/g, respectively. On the other hand, equilibrium adsorptive capacities of AE and AP against CV were 130.0 and 150.0 mg/g, respectively. In Figure 3b, during the initial step of adsorption, CV dye performed the same reaction rate sequence as it can be seen in Figure 3a, but as for AE and AP at the time range from 24h to 48h, the adsorption rate sharply decreased. It might be ascribed to the aggregated MB and CV molecules blocked the minor pore channel and restricted the adsorption effectiveness [26]. Comparing with the molecular structure of CV dye, the aggregated MB molecules barely attributed to the adsorption retard [27]. As shown in Figure 4(b), the maximum absorbance of CV solution contacted with AE shifted from 584nm to 578nm at 0h to 24h, these results were in good agreement with those of the uptake rate variety [28]. The MB aggregates observed in the solution for the maximum absorbance off-set from 665 nm to 610 nm, as shown in Figure 4(a). The Figure 5 is the schematic diagram of adsorption process of MB and CV dyes onto and/or in the AEP and ASP adsorbents.

TABLE 5
Specific surface are and pore size of the as-prepared adsorbents

Adsorbents	S_{BJH}(m^2/g)	D_{aver}(nm)
AP	21.94	4.28
AE	34.23	1.52

TABLE 6
The values of intraparticle diffusion parameters

Adsorbent/adsorbate	k_{id}(mg/g $h^{1/2}$)	D_1 (×$10^{-3}$$mm^2$/h)	D_2 (×$10^{-3}$$mm^2$/h)
AE/MB	16.688	0.87a^2	4.02a^2
AP/MB	15.456	0.27a^2	4.19a^2
AE/CV	11.207	0.65a^2	3.63a^2
AP/CV	13.372	0.70a^2	3.75a^2

Adsorption/Removal Mechanism. Intraparticle diffusion model is the first concern related to the rate-determining stage [28, 29,30,31]. The intraparticle diffusion model presented as:

$$q_t = k_{id} t^{1/2} \quad (2)$$

Where, q_t is the adsorption amount at time t (mg/g), t is the reaction time (h), k_{id} is the rate constant of intraparticle diffusion model (mg/g $h^{1/2}$), and the linear fit of intraparticle diffusion, as shown in Figure 6. The whole scale intraparticle diffusion could be divided into two portions, firstly, the initial portion is related to the film diffusion (D_1), and secondly, the second portion will relate to ion diffusion (D_2) within adsorbent, and a is the radius. The equation of weight uptake verse time is given below as [28]:

$$\frac{q_t}{q_e} = 6\left(\frac{D_t}{a^2}\right)^{1/2}\left\{\pi^{-1/2} + 2\sum_{n=1}^{\infty} \mathrm{ierfc}\frac{na}{\sqrt{Dt}}\right\} - 3\frac{D_t}{a^2} \quad (3)$$

For short time scale, the D is replaced by D_1 and the equation simplified as:

$$\frac{q_t}{q_e} = 6\left(\frac{D_1}{\pi a^2}\right)^{1/2} t^{1/2} \quad (4)$$

For long time scale, the relationship between weight uptake and time is as:

$$\frac{q_t}{q_e} = 1 - \frac{6}{\pi^2}\sum_{n=1}^{\infty}\frac{1}{n^2}\exp\left(\frac{-Dn^2\pi^2 t}{a^2}\right) \quad (5)$$

If time (t) tends to large, the Eq. (5) can be written as:

$$\ln\left(1 - \frac{q_t}{q_e}\right) = \ln\frac{6}{\pi^2} - \left(\frac{D_2\pi^2}{a^2}t\right) \quad (6)$$

D_1 and D_2 can be calculated from the slope of q_t/q_e verse $t^{1/2}$ and ln(1- q_t/q_e) verse t, as shown in Figure 7 and Figure 8.

Intraparticle diffusion coefficient D_1 and D_2 and rate constant k_{id} were presented in the Table 4. During the adsorption of MB, the rate constant of AE (16.688 mg/g $h^{1/2}$) was higher than AP (15.456 mg/g $h^{1/2}$) and it validated that the adsorption capacity of AE was higher than AP. During the adsorption of CV, the adsorption performance of AP was higher than AE, and it was proven by the rate constant magnitude, which were 13.372 mg/g $h^{1/2}$ and 11.207 mg/g $h^{1/2}$, respectively. On the other side, the value of D_2 was higher than D_1 in all the adsorption groups, indicted that the ion diffusion within adsorbent determine the adsorption rate, probably.

CONCLUSIONS

Altogether, the pore size and specific surface area is normally governed adsorptive performance/ uptake rate of the adsorbent and it is also correlated to the dimension of the molecular structure of the pollutant/ contaminant. Moreover, the adsorption capacity is also positively correlated with specific surface area of the adsorbent only if contaminant molecule could diffuse to/ on or in the effective adsorption sites of the adsorbent. The results showed that the pore size of the as-prepared adsorbents depicted significant meaning if we compared with specific surface area. Adsorption rate mainly depended on the diffusion of dyes molecules within adsorbents principally, which verified by the intraparticle diffusion constant such as K_{id} and D_2 values. The formation of MB and CV dimers after 24h impeded the adsorption rate, evidently. Overall, our findings recommended that the selection of adsorbent should be according to the nature/ property of the targeted pollutant/ contaminant, which should match with the pore size and reasonable specific surface area of the adsorbent. In addition, the influence of aggregation/ accumulation of pollutants/ contaminants on the removal/ uptake rate should be imagined, absolutely.

ACKNOWLEDGEMENTS

The authors acknowledge the support of the Key Project of the Joint Fund Between the State Fund Committee and Shandong Province (U1806210) and the State Key Laboratory of Environmental Criteria and Risk Assessment (SKLECRA2013FP12).

Conflict of interest. The authors have declared no conflict of interest.

REFERENCES

[1] Ali, I., Peng, C., Lin, D., Saroj, D.P., Naz, I., Khan, Z.M., Sultan, M., Ali, M. (2019) Encapsulated green magnetic nanoparticles for the removal of toxic Pb^{2+} and Cd^{2+} from water: Development, characterization and application. Journal of Environmental Management. 234, 273-289.

[2] Ali, I., Peng, C., Naz, I., Lin, D., Saroj, D.P., Ali, M. (2019) Development and application of novel bio-magnetic membrane capsules for the removal of the cationic dye malachite green in wastewater treatment. RSC Advances. 9(7), 3625-3646.

[3] Ali, I., Peng, C., Khan, Z.M., Naz, I., Sultan, M., Ali, M., Abbasi, I.A., Islam, T., Ye, T. (2019) Overview of microbes based fabricated biogenic nanoparticles for water and wastewater treatment. Journal of Environmental Management. 230, 128-150.

[4] Ali, I., Peng, C., Lin, D., Naz, I. (2019) Green synthesis of the innovative super paramagnetic nanoparticles from the leaves extract of Fraxinus chinensis Roxb and their application for the decolourisation of toxic dyes. Green Processing and Synthesis. 8(1), 256-271.

[5] Ali, I., Peng, C., Khan, Z.M., Sultan, M., Naz, I., Ali, M., Farid, H.U., Mahmood, M.H., Ahsen, R. (2019) Removal of Crystal Violet and Eriochrome Black T Dyes from Aqueous Solutions by Magnetic Nanoparticles Biosynthesized from Leaf Extract of Fraxinus Chinensis Roxb. Polish Journal of Environmental Studies. 28(4), 2027-2040.

[6] Ali, I., Peng, C., Khan, Z.M., Naz, I., Sultan, M. (2018) An overview of heavy metal removal from wastewater using magnetotactic bacteria. Journal of Chemical Technology & Biotechnology. 93(10), 2817-2832.

[7] Ali, I., Peng, C., Khan, Z.M., Sultan, M., Naz, I. (2018) Green synthesis of phytogenic magnetic nanoparticles and their applications in the adsorptive removal of crystal violet from aqueous solution. Arabian Journal for Science and Engineering. 43(11), 6245-6259.

[8] Ali, I., Peng, C., Ye, T., Naz, I. (2018) Sorption of cationic malachite green dye on phytogenic magnetic nanoparticles functionalized by 3-marcaptopropanic acid. RSC Advances. 8(16), 8878-8897.

[9] Ali, I., Peng, C., Naz, I., Khan, Z.M., Sultan, M., Islam, T., Abbasi, I.A. (2017) Phytogenic magnetic nanoparticles for wastewater treatment: a review. RSC Advances. 7(64), 40158-40178.

[10] Wang, S., Wu, H. (2006) Environmental-benign utilisation of fly ash as low-cost adsorbents. Journal of Hazardous Materials. 136(3), 482-501.

[11] Wei, L., Wang, K., Zhao, Q., Xie, C., Qiu, W., Jia, T. (2011) Kinetics and equilibrium of adsorption of dissolved organic matter fractions from secondary effluent by fly ash. Journal of Environmental Sciences. 23(7), 1057-1065.

[12] Birol, F. (2008) World energy outlook. Paris: International Energy Agency, 23(4), p.329.

[13] Brandt, L., Rawski, T.G., Sutton, J. (2008) China's industrial development. China's Great Economic Transformation. 569-632.

[14] Banat, I.M., Nigam, P., Singh, D., Marchant, R. (1996) Microbial decolorization of textile-dye-containing effluents: a review. Bioresource Technology. 58(3), 217-227.

[15] Visa, M., Bogatu, C., Duta, A. (2010) Simultaneous adsorption of dyes and heavy metals from multicomponent solutions using fly ash. Applied Surface Science. 256(17), 5486-5491.

[16] Ho, Y.S., McKay, G. (1999) Comparative sorption kinetic studies of dye and aromatic compounds onto fly ash. Journal of Environmental Science & Health Part A. 34(5), 1179-1204.

[17] Nelsen, F.M., Eggertsen, F.T. (1958) Determination of surface area. adsorption measurements by continuous flow method. Analytical Chemistry. 30(8), 1387-1390.

[18] Pierce, C. (1953) Computation of pore sizes from physical adsorption data. The Journal of Physical Chemistry. 57(2), 149-152.

[19] Thommes, M., Kaneko, K., Neimark, A.V., Olivier, J.P., Rodriguez-Reinoso, F., Rouquerol, J., Sing, K.S. (2015) Physisorption of gases, with special reference to the evaluation of surface area and pore size distribution (IUPAC Technical Report). Pure and Applied Chemistry. 87(9-10), 1051-1069.

[20] Kuila, U., Prasad, M. (2013) Specific surface area and pore-size distribution in clays and shales. Geophysical Prospecting. 61(2), 341-362.

[21] Suzuki, K., Ikari, K., Imai, H. (2003) Synthesis of mesoporous silica foams with hierarchical trimodal pore structures. Journal of Materials Chemistry. 13(7), 1812-1816.

[22] Zhao, D., Feng, J., Huo, Q., Melosh, N., Fredrickson, G.H., Chmelka, B.F., Stucky, G.D. (1998) Triblock copolymer syntheses of mesoporous silica with periodic 50 to 300 angstrom pores. Science. 279(5350), 548-552.

[23] Babić, B.M., Milonjić, S.K., Polovina, M.J., Kaludierović, B.V. (1999) Point of zero charge and intrinsic equilibrium constants of activated carbon cloth. Carbon. 37(3), 477-481.

[24] Turan, N.G., Ergun, O.N. (2009) Removal of Cu (II) from leachate using natural zeolite as a landfill liner material. Journal of Hazardous Materials. 167(1-3), 696-700.

[25] Stork, W.H.J., Lippits, G.J.M., Mandel, M. (1972) Association of crystal violet in aqueous solutions. The Journal of Physical Chemistry. 76(12), 1772-1775.

[26] Li, D., Li, J., Gu, Q., Song, S., Peng, C. (2016) Co-influence of the pore size of adsorbents and the structure of adsorbates on adsorption of dyes. Desalination and Water Treatment. 57(31), 14686-14695.

[27] Yariv, S., Nasser, A., Bar-on, P. (1990) Metachromasy in clay minerals. Spectroscopic study of the adsorption of crystal violet by laponite. Journal of the Chemical Society, Faraday Transactions. 86(9), 1593-1598.

[28] Song, Q., Liang, J., Fang, Y., Cao, C., Liu, Z., Li, L., Huang, Y., Lin, J., Tang, C. (2019) Selective adsorption behavior/mechanism of antibiotic contaminants on novel boron nitride bundles. Journal of Hazardous Materials. 364, 654-662.

[29] Crank, J. (1979). The mathematics of diffusion. Oxford University Press.

[30] Bhatnagar, A., Minocha, A.K., Jeon, B., Park, J.M., Lee, G. (2007) Adsorption of orange G dye on paper mill sludge: equilibrium and kinetic modeling. Fresen. Environ. Bull. 16(9), 1049-1055.

[31] Marahel, F., Ghaedi, M., Kokhdan, S.N. (2012) Silver nanoparticle loaded on activated carbon as an adsorbent for the removal of Sudan Red 7B from aqueous solution. Fresen. Environ. Bull. 21(1A), 163-170.

Received: 01.01.2020
Accepted: 23.02.2020

CORRESPONDING AUTHORS

Muhammad Sultan
Department of Agricultural Engineering,
Bahauddin Zakariya University,
Multan 60800 – Pakistan

e-mail: muhammadsultan@bzu.edu.pk

References

1. Li, Z.; Jones, H. K.; Bowman, R. S.; Helferich, R., Enhanced Reduction of Chromate and PCE by Pelletized Surfactant-Modified Zeolite/Zerovalent Iron. *Environmental Science & Technology* **1999,** *33*, (23), 4326-4330.
2. Devlin, J. F.; Klausen, J.; Schwarzenbach, R. P., Kinetics of Nitroaromatic Reduction on Granular Iron in Recirculating Batch Experiments. *Environmental Science & Technology* **1998,** *32*, (13), 1941-1947.
3. Zhang, P.; Tao, X.; Li, Z.; Bowman, R. S., Enhanced Perchloroethylene Reduction in Column Systems Using Surfactant-Modified Zeolite/Zero-Valent Iron Pellets. *Environmental Science & Technology* **2002,** *36*, (16), 3597-3603.
4. Cho, H.-H.; Lee, T.; Hwang, S.-J.; Park, J.-W., Iron and organo-bentonite for the reduction and sorption of trichloroethylene. *Chemosphere* **2005,** *58*, (1), 103-108.
5. Mak, M. S. H.; Lo, I. M. C.; Liu, T., Synergistic effect of coupling zero-valent iron with iron oxide-coated sand in columns for chromate and arsenate removal from groundwater: Influences of humic acid and the reactive media configuration. *Water Res.* **2011,** *45*, (19), 6575-6584.
6. Du, J.; Bao, J.; Fu, X.; Lu, C.; Kim, S. H., Mesoporous sulfur-modified iron oxide as an effective Fenton-like catalyst for degradation of bisphenol A. *Applied Catalysis B: Environmental* **2016,** *184*, 132-141.
7. Fennelly, J. P.; Roberts, A. L., Reaction of 1,1,1-Trichloroethane with Zero-Valent Metals and Bimetallic Reductants. *Environmental Science & Technology* **1998,** *32*, (13), 1980-1988.
8. Tao, N. R.; Sui, M. L.; Lu, J.; Lua, K., Surface nanocrystallization of iron induced by ultrasonic shot peening. *Nanostructured Materials* **1999,** *11*, (4), 433-440.
9. Decyk, P.; Trejda, M.; Ziolek, M.; Kujawa, J.; Głaszczka, K.; Bettahar, M.; Monteverdi, S.; Mercy, M., Physicochemical and catalytic properties of iron-doped silica—the effect of preparation and pretreatment methods. *Journal of Catalysis* **2003,** *219*, (1), 146-155.
10. Li, Y.; Zimmerman, A. R.; He, F.; Chen, J.; Han, L.; Chen, H.; Hu, X.; Gao, B. J. S. o. T. T. E., Solvent-free synthesis of magnetic biochar and activated carbon through ball-mill extrusion with Fe3O4 nanoparticles for enhancing adsorption of methylene blue. **2020,** *722*, 137972.
11. Meng, P.; Fang, X.; Maimaiti, A.; Yu, G.; Deng, S. J. C., Efficient removal of perfluorinated compounds from water using a regenerable magnetic activated carbon. **2019,** *224*, 187-194.
12. Mu, Y.; Jia, F.; Ai, Z.; Zhang, L. J. E. S. N., Iron oxide shell mediated environmental remediation properties of nano zero-valent iron. **2017,** *4*, (1), 27-45.
13. Lyu, H.; Gao, B.; He, F.; Ding, C.; Tang, J.; Crittenden, J. C., Ball-Milled Carbon Nanomaterials for Energy and Environmental Applications. *ACS Sustain. Chem. Eng.* **2017,** *5*, (11), 9568-9585.
14. Shan, D.; Deng, S.; Zhao, T.; Wang, B.; Wang, Y.; Huang, J.; Yu, G.; Winglee, J.; Wiesner, M. R. J. J. o. h. m., Preparation of ultrafine magnetic biochar and activated carbon for pharmaceutical adsorption and subsequent degradation by ball milling. **2016,** *305*, 156-163.
15. Li, S.; Yan, W.; Zhang, W.-x. J. G. C., Solvent-free production of nanoscale zero-valent iron (nZVI) with precision milling. **2009,** *11*, (10), 1618-1626.
16. Takaesu, H.; Matsui, Y.; Nishimura, Y.; Matsushita, T.; Shirasaki, N., Micro-milling super-fine powdered activated carbon decreases adsorption capacity by introducing oxygen/hydrogen-

containing functional groups on carbon surface from water. *Water research* **2019,** *155*, 66-75.
17. Baklanova, O.; Knyazheva, O.; Lavrenov, A.; Drozdov, V.; Trenikhin, M.; Arbuzov, A.; Kuznetsova, Y.; Rempel, A., Mechanical treatment as highly effective method of physico-chemical properties control of carbon black. *Microporous and Mesoporous Materials* **2019,** *279*, 193-200.
18. Tran, T.; Gray, S.; Naughton, R.; Bolto, B., Polysilicato-iron for improved NOM removal and membrane performance. *Journal of Membrane Science* **2006,** *280*, (1), 560-571.
19. Ambika, S.; Devasena, M.; Nambi, I. M., Synthesis, characterization and performance of high energy ball milled meso-scale zero valent iron in Fenton reaction. *J Environ Manage* **2016,** *181*, 847-855.
20. Wu, P.; Wu, W.; Li, S.; Xing, N.; Zhu, N.; Li, P.; Wu, J.; Yang, C.; Dang, Z., Removal of Cd2+ from aqueous solution by adsorption using Fe-montmorillonite. *Journal of Hazardous Materials* **2009,** *169*, (1), 824-830.
21. Song, S.; Su, Y.; Adeleye, A. S.; Zhang, Y.; Zhou, X., Optimal design and characterization of sulfide-modified nanoscale zerovalent iron for diclofenac removal. *Applied Catalysis B: Environmental* **2017,** *201*, 211-220.
22. Sheng, G.; Alsaedi, A.; Shammakh, W.; Monaquel, S.; Sheng, J.; Wang, X.; Li, H.; Huang, Y., Enhanced sequestration of selenite in water by nanoscale zero valent iron immobilization on carbon nanotubes by a combined batch, XPS and XAFS investigation. *Carbon* **2016,** *99*, 123-130.
23. Luo, S.; Yang, S.; Sun, C.; Gu, J.-D., Improved debromination of polybrominated diphenyl ethers by bimetallic iron–silver nanoparticles coupled with microwave energy. *Science of The Total Environment* **2012,** *429*, 300-308.
24. Tang, H.; Cheng, W.; Yi, Y.; Ding, C.; Nie, X., Nano zero valent iron encapsulated in graphene oxide for reducing uranium. *Chemosphere* **2021,** *278*, 130229.
25. Zheng, Y.; Wan, Y.; Chen, J.; Chen, H.; Gao, B., MgO modified biochar produced through ball milling: A dual-functional adsorbent for removal of different contaminants. *Chemosphere* **2020,** *243*, 125344.
26. Kumar, M.; Xiong, X.; Wan, Z.; Sun, Y.; Tsang, D. C. W.; Gupta, J.; Gao, B.; Cao, X.; Tang, J.; Ok, Y. S., Ball milling as a mechanochemical technology for fabrication of novel biochar nanomaterials. *Bioresource Technology* **2020,** *312*, 123613.
27. Al-Othman, Z. A.; Ali, R.; Naushad, M., Hexavalent chromium removal from aqueous medium by activated carbon prepared from peanut shell: Adsorption kinetics, equilibrium and thermodynamic studies. *Chemical Engineering Journal* **2012,** *184*, 238-247.
28. Fazlzadeh, M.; Rahmani, K.; Zarei, A.; Abdoallahzadeh, H.; Nasiri, F.; Khosravi, R., A novel green synthesis of zero valent iron nanoparticles (NZVI) using three plant extracts and their efficient application for removal of Cr(VI) from aqueous solutions. *Advanced Powder Technology* **2017,** *28*, (1), 122-130.
29. Norouzi, S.; Heidari, M.; Alipour, V.; Rahmanian, O.; Fazlzadeh, M.; Mohammadi-Moghadam, F.; Nourmoradi, H.; Goudarzi, B.; Dindarloo, K., Preparation, characterization and Cr(VI) adsorption evaluation of NaOH-activated carbon produced from Date Press Cake; an agro-industrial waste. *Bioresour Technol* **2018,** *258*, 48-56.
30. Zhou, L.; Zhang, G.; Wang, M.; Wang, D.; Cai, D.; Wu, Z., Efficient removal of hexavalent chromium from water and soil using magnetic ceramsite coated by functionalized nano carbon spheres. *Chemical Engineering Journal* **2018,** *334*, 400-409.
31. Chingombe, P.; Saha, B.; Wakeman, R. J., Surface modification and characterisation of a coal-

based activated carbon. *Carbon* **2005,** *43*, (15), 3132-3143.
32. Cimino, G.; Passerini, A.; Toscano, G., Removal of toxic cations and Cr (VI) from aqueous solution by hazelnut shell. *Water research* **2000,** *34*, (11), 2955-2962.
33. Kobya, M., Adsorption, kinetic and equilibrium studies of Cr (VI) by hazelnut shell activated carbon. *Adsorption Science & Technology* **2004,** *22*, (1), 51-64.
34. Mohanty, K.; Jha, M.; Meikap, B.; Biswas, M., Removal of chromium (VI) from dilute aqueous solutions by activated carbon developed from Terminalia arjuna nuts activated with zinc chloride. *Chemical Engineering Science* **2005,** *60*, (11), 3049-3059.
35. Owlad, M.; Aroua, M. K.; Daud, W. A. W.; Baroutian, S., Removal of Hexavalent Chromium-Contaminated Water and Wastewater: A Review. *Water, Air, and Soil Pollution* **2008,** *200*, (1-4), 59-77.
36. Yang, J.; Yu, M.; Chen, W., Adsorption of hexavalent chromium from aqueous solution by activated carbon prepared from longan seed: Kinetics, equilibrium and thermodynamics. *Journal of Industrial and Engineering Chemistry* **2015,** *21*, 414-422.
37. Ghosh, P. K., Hexavalent chromium [Cr(VI)] removal by acid modified waste activated carbons. *J Hazard Mater* **2009,** *171*, (1-3), 116-22.
38. Cronje, K. J.; Chetty, K.; Carsky, M.; Sahu, J. N.; Meikap, B. C., Optimization of chromium(VI) sorption potential using developed activated carbon from sugarcane bagasse with chemical activation by zinc chloride. *Desalination* **2011,** *275*, (1-3), 276-284.
39. Rodriguez-Reinoso, F.; Molina-Sabio, M., Activated carbons from lignocellulosic materials by chemical and/or physical activation: an overview. *Carbon* **1992,** *30*, (7), 1111-1118.
40. Bouchelta, C.; Medjram, M. S.; Bertrand, O.; Bellat, J.-P., Preparation and characterization of activated carbon from date stones by physical activation with steam. *Journal of Analytical and Applied Pyrolysis* **2008,** *82*, (1), 70-77.
41. Bajpai, J.; Shrivastava, R.; Bajpai, A. K., Dynamic and equilibrium studies on adsorption of Cr(VI) ions onto binary bio-polymeric beads of cross linked alginate and gelatin. *Colloids and Surfaces A: Physicochemical and Engineering Aspects* **2004,** *236*, (1-3), 81-90.
42. Benhammou, A.; Yaacoubi, A.; Nibou, L.; Tanouti, B., Study of the removal of mercury(II) and chromium(VI) from aqueous solutions by Moroccan stevensite. *J Hazard Mater* **2005,** *117*, (2-3), 243-9.
43. Karthikeyan, T.; Rajgopal, S.; Miranda, L. R., Chromium(VI) adsorption from aqueous solution by Hevea Brasilinesis sawdust activated carbon. *J Hazard Mater* **2005,** *124*, (1-3), 192-9.
44. Ewais, H. A.; Obaid, A. Y., Adsorption characteristics of toxic chromium (VI) from aqueous media onto nanosized silver nanoparticles-treated activated carbon. *Separation Science and Technology* **2019,** *54*, (4), 494-506.
45. Ma, H.; Yang, J.; Gao, X.; Liu, Z.; Liu, X.; Xu, Z., Removal of chromium (VI) from water by porous carbon derived from corn straw: Influencing factors, regeneration and mechanism. *Journal of hazardous materials* **2019,** *369*, 550-560.
46. Samani, M. R.; Toghraie, D., Removal of hexavalent chromium from water using polyaniline/wood sawdust/poly ethylene glycol composite: an experimental study. *Journal of Environmental Health Science and Engineering* **2019**, 1-10.
47. Su, M.; Fang, Y.; Li, B.; Yin, W.; Gu, J.; Liang, H.; Li, P.; Wu, J., Enhanced hexavalent chromium removal by activated carbon modified with micro-sized goethite using a facile impregnation method. *Science of the total environment* **2019,** *647*, 47-56.

48. Valentín-Reyes, J.; García-Reyes, R.; García-González, A.; Soto-Regalado, E.; Cerino-Córdova, F., Adsorption mechanisms of hexavalent chromium from aqueous solutions on modified activated carbons. *J. Environ. Manage.* **2019,** *236*, 815-822.
49. Wu, J.; Zheng, H.; Zhang, F.; Zeng, R. J.; Xing, B., Iron-carbon composite from carbonization of iron-crosslinked sodium alginate for Cr (VI) removal. *Chemical Engineering Journal* **2019,** *362*, 21-29.
50. Vilardi, G.; Ochando-Pulido, J. M.; Verdone, N.; Stoller, M.; Di Palma, L., On the removal of hexavalent chromium by olive stones coated by iron-based nanoparticles: Equilibrium study and chromium recovery. *Journal of Cleaner Production* **2018,** *190*, 200-210.
51. Bavasso, I.; Verdone, N.; Di Palma, L., Cr (VI) Removal by Green-Synthetized Iron-Based Nanoparticles: Effect of Cr (VI) Concentration and pH Condition on Adsorption Process. *Chemical Engineering Transactions* **2018,** *70*, 469-474.
52. Bencheikh-Latmani, R.; Obraztsova, A.; Mackey, M. R.; Ellisman, M. H.; Tebo, B. M., Toxicity of Cr(III) to Shewanella sp. Strain MR-4 during Cr(VI) Reduction. *Environmental Science & Technology* **2007,** *41*, (1), 214-220.
53. Zhao, F.; Yang, Z.; Wei, Z.; Spinney, R.; Sillanpää, M.; Tang, J.; Tam, M.; Xiao, R., Polyethylenimine-modified chitosan materials for the recovery of La(III) from leachates of bauxite residue. *Chemical Engineering Journal* **2020,** *388*, 124307.
54. Muthukrishnan, M.; Guha, B. K., Effect of pH on rejection of hexavalent chromium by nanofiltration. *Desalination* **2008,** *219*, (1), 171-178.
55. Peng, H.; Guo, J., Removal of chromium from wastewater by membrane filtration, chemical precipitation, ion exchange, adsorption electrocoagulation, electrochemical reduction, electrodialysis, electrodeionization, photocatalysis and nanotechnology: a review. *Environmental Chemistry Letters* **2020,** *18*, (6), 2055-2068.
56. Zhang, Y.; Jiao, X.; Liu, N.; Lv, J.; Yang, Y., Enhanced removal of aqueous Cr (VI) by a green synthesized nanoscale zero-valent iron supported on oak wood biochar. *Chemosphere* **2020,** *245*, 125542.
57. Chatterjee, S.; Mahanty, S.; Das, P.; Chaudhuri, P.; Das, S., Biofabrication of iron oxide nanoparticles using manglicolous fungus Aspergillus niger BSC-1 and removal of Cr (VI) from aqueous solution. *Chemical Engineering Journal* **2020,** *385*, 123790.
58. Zhao, F.; Liu, Y.; Hammouda, S. B.; Doshi, B.; Guijarro, N.; Min, X.; Tang, C.-J.; Sillanpää, M.; Sivula, K.; Wang, S., MIL-101(Fe)/g-C3N4 for enhanced visible-light-driven photocatalysis toward simultaneous reduction of Cr(VI) and oxidation of bisphenol A in aqueous media. *Applied Catalysis B: Environmental* **2020,** *272*, 119033.
59. Gheju, M., Hexavalent Chromium Reduction with Zero-Valent Iron (ZVI) in Aquatic Systems. *Water, Air, & Soil Pollution* **2011,** *222*, (1), 103-148.
60. Vilardi, G.; Di Palma, L.; Verdone, N., On the critical use of zero valent iron nanoparticles and Fenton processes for the treatment of tannery wastewater. *Journal of Water Process Engineering* **2018,** *22*, 109-122.
61. Puls, R. W.; Blowes, D. W.; Gillham, R. W., Long-term performance monitoring for a permeable reactive barrier at the U.S. Coast Guard Support Center, Elizabeth City, North Carolina. *J. Hazard. Mater.* **1999,** *68*, (1), 109-124.
62. El Asmar, R.; Baalbaki, A.; Abou Khalil, Z.; Naim, S.; Bejjani, A.; Ghauch, A., Iron-based metal organic framework MIL-88-A for the degradation of naproxen in water through persulfate

activation. *Chemical Engineering Journal* **2021,** *405*, 126701.
63. Pascu, O.; Carenza, E.; Gich, M.; Estradé, S.; Peiró, F.; Herranz, G.; Roig, A., Surface Reactivity of Iron Oxide Nanoparticles by Microwave-Assisted Synthesis; Comparison with the Thermal Decomposition Route. *The Journal of Physical Chemistry C* **2012,** *116*, (28), 15108-15116.
64. Lv, X.; Hu, Y.; Tang, J.; Sheng, T.; Jiang, G.; Xu, X., Effects of co-existing ions and natural organic matter on removal of chromium (VI) from aqueous solution by nanoscale zero valent iron (nZVI)-Fe3O4 nanocomposites. *Chemical Engineering Journal* **2013,** *218*, 55-64.
65. Mamindy-Pajany, Y.; Hurel, C.; Marmier, N.; Roméo, M., Arsenic (V) adsorption from aqueous solution onto goethite, hematite, magnetite and zero-valent iron: effects of pH, concentration and reversibility. *Desalination* **2011,** *281*, 93-99.
66. Katsoyiannis, I. A.; Ruettimann, T.; Hug, S. J., pH dependence of Fenton reagent generation and As (III) oxidation and removal by corrosion of zero valent iron in aerated water. *Environmental Science & Technology* **2008,** *42*, (19), 7424-7430.
67. Vilardi, G.; Di Palma, L.; Verdone, N., Competitive reaction modelling in aqueous systems: the case of contemporary reduction of dichromates and nitrates by nZVI. *Chemical Engineering Transactions* **2017,** *60*, 175-180.
68. Vilardi, G.; Verdone, N.; Di Palma, L., The influence of nitrate on the reduction of hexavalent chromium by zero-valent iron nanoparticles in polluted wastewater. *Desalination Water Treatment* **2017,** *86*, 252-258.
69. Vilardi, G.; Stoller, M.; Di Palma, L.; Verdone, N., CFD Model of Agitated Vessel for the Removal of Cr (vi) by Nano-hematite Particles. *Chemical Engineering Transactions* **2019,** *73*, 157-162.
70. Shi, L.-n.; Zhang, X.; Chen, Z.-l., Removal of chromium (VI) from wastewater using bentonite-supported nanoscale zero-valent iron. *Water Research* **2011,** *45*, (2), 886-892.
71. He, Y. T.; Traina, S. J., Cr(VI) Reduction and Immobilization by Magnetite under Alkaline pH Conditions: The Role of Passivation. *Environmental Science & Technology* **2005,** *39*, (12), 4499-4504.
72. Fu; Cheng, Z.; Dionysiou, D. D.; Tang, B., Fe/Al bimetallic particles for the fast and highly efficient removal of Cr(VI) over a wide pH range: Performance and mechanism. *Journal of Hazardous Materials* **2015,** *298*, 261-269.
73. Dai, Y.; Hu, Y.; Jiang, B.; Zou, J.; Tian, G.; Fu, H., Carbothermal synthesis of ordered mesoporous carbon-supported nano zero-valent iron with enhanced stability and activity for hexavalent chromium reduction. *Journal of hazardous materials* **2016,** *309*, 249-258.
74. Petala, E.; Dimos, K.; Douvalis, A.; Bakas, T.; Tucek, J.; Zbořil, R.; Karakassides, M. A., Nanoscale zero-valent iron supported on mesoporous silica: characterization and reactivity for Cr (VI) removal from aqueous solution. *Journal of Hazardous Materials* **2013,** *261*, 295-306.
75. Zhu, F.; Li, L.; Ren, W.; Deng, X.; Liu, T., Effect of pH, temperature, humic acid and coexisting anions on reduction of Cr(VI) in the soil leachate by nZVI/Ni bimetal material. *Environmental Pollution* **2017,** *227*, 444-450.
76. Koutsospyros, A.; Pavlov, J.; Fawcett, J.; Strickland, D.; Smolinski, B.; Braida, W., Degradation of high energetic and insensitive munitions compounds by Fe/Cu bimetal reduction. *Journal of hazardous materials* **2012,** *219*, 75-81.
77. Hoch, L. B.; Mack, E. J.; Hydutsky, B. W.; Hershman, J. M.; Skluzacek, J. M.; Mallouk, T. E., Carbothermal synthesis of carbon-supported nanoscale zero-valent iron particles for the remediation of hexavalent chromium. *Environmental Science & Technology* **2008,** *42*, (7), 2600-

2605.
78. Patterson, R. R.; Fendorf, S.; Fendorf, M., Reduction of hexavalent chromium by amorphous iron sulfide. *Environmental Science & Technology* **1997,** *31*, (7), 2039-2044.
79. Lv, X.; Xu, J.; Jiang, G.; Xu, X., Removal of chromium (VI) from wastewater by nanoscale zero-valent iron particles supported on multiwalled carbon nanotubes. *Chemosphere* **2011,** *85*, (7), 1204-1209.
80. Sun, H.; Zhou, G.; Liu, S.; Ang, H. M.; Tadé, M. O.; Wang, S., Nano-Fe0 Encapsulated in Microcarbon Spheres: Synthesis, Characterization, and Environmental Applications. *ACS Applied Materials & Interfaces* **2012,** *4*, (11), 6235-6241.
81. Crane, R. A.; Scott, T. B., Nanoscale zero-valent iron: Future prospects for an emerging water treatment technology. *Journal of Hazardous Materials* **2012,** *211-212*, 112-125.
82. Zou, Y.; Wang, X.; Khan, A.; Wang, P.; Liu, Y.; Alsaedi, A.; Hayat, T.; Wang, X., Environmental Remediation and Application of Nanoscale Zero-Valent Iron and Its Composites for the Removal of Heavy Metal Ions: A Review. *Environmental Science & Technology* **2016,** *50*, (14), 7290-7304.
83. Sun, Y.; Li, J.; Huang, T.; Guan, X., The influences of iron characteristics, operating conditions and solution chemistry on contaminants removal by zero-valent iron: A review. *Water Research* **2016,** *100*, 277-295.
84. Flury, B.; Frommer, J.; Eggenberger, U.; Mäder, U.; Nachtegaal, M.; Kretzschmar, R., Assessment of Long-Term Performance and Chromate Reduction Mechanisms in a Field Scale Permeable Reactive Barrier. *Environmental Science & Technology* **2009,** *43*, (17), 6786-6792.
85. Yoon, I.-H.; Bang, S.; Chang, J.-S.; Gyu Kim, M.; Kim, K.-W., Effects of pH and dissolved oxygen on Cr(VI) removal in Fe(0)/H2O systems. *Journal of Hazardous Materials* **2011,** *186*, (1), 855-862.
86. Tavakoli, A.; Sohrabi, M.; Kargari, A., A review of methods for synthesis of nanostructured metals with emphasis on iron compounds. *Chemical Papers* **2007,** *61*, (3), 151-170.
87. Wang; Zhao, M.; Zhou, M.; Li, Y. C.; Wang, J.; Gao, B.; Sato, S.; Feng, K.; Yin, W.; Igalavithana, A. D.; Oleszczuk, P.; Wang, X.; Ok, Y. S., Biochar-supported nZVI (nZVI/BC) for contaminant removal from soil and water: A critical review. *Journal of Hazardous Materials* **2019,** *373*, 820-834.
88. Xu; Deng, S.; Xu, J.; Zhang, W.; Wu, M.; Wang, B.; Huang, J.; Yu, G., Highly Active and Stable Ni–Fe Bimetal Prepared by Ball Milling for Catalytic Hydrodechlorination of 4-Chlorophenol. *Environ. Sci. Technol.* **2012,** *46*, (8), 4576-4582.
89. He; Min, X.; Peng, T.; Zhao, F.; Ke, Y.; Wang, Y.; Jiang, G.; Xu, Q.; Wang, J., Mechanochemically Activated Microsized Zero-Valent Iron/Pyrite Composite for Effective Hexavalent Chromium Sequestration in Aqueous Solution. *J. Chem. Eng. Data* **2020,** *65*, (4), 1936-1945.
90. Glavee, G. N.; Klabunde, K. J.; Sorensen, C. M.; Hadjipanayis, G. C., Chemistry of Borohydride Reduction of Iron(II) and Iron(III) Ions in Aqueous and Nonaqueous Media. Formation of Nanoscale Fe, FeB, and Fe2B Powders. *Inorganic Chemistry* **1995,** *34*, (1), 28-35.
91. Nurmi, J. T.; Tratnyek, P. G.; Sarathy, V.; Baer, D. R.; Amonette, J. E.; Pecher, K.; Wang, C.; Linehan, J. C.; Matson, D. W.; Penn, R. L.; Driessen, M. D., Characterization and Properties of Metallic Iron Nanoparticles: Spectroscopy, Electrochemistry, and Kinetics. *Environmental Science & Technology* **2005,** *39*, (5), 1221-1230.
92. Wang, C.-B.; Zhang, W.-x., Synthesizing Nanoscale Iron Particles for Rapid and Complete Dechlorination of TCE and PCBs. *Environmental Science & Technology* **1997,** *31*, (7), 2154-2156.
93. Yang, G. C. C.; Lee, H.-L., Chemical reduction of nitrate by nanosized iron: kinetics and pathways. *Water Research* **2005,** *39*, (5), 884-894.

94. Hwang, Y.-H.; Kim, D.-G.; Shin, H.-S., Mechanism study of nitrate reduction by nano zero valent iron. *Journal of Hazardous Materials* **2011,** *185*, (2), 1513-1521.

95. Wang; Chen, G.; Wang, X.; Li, S.; Liu, Y.; Yang, G., Removal of hexavalent chromium by bentonite supported organosolv lignin-stabilized zero-valent iron nanoparticles from wastewater. *Journal of Cleaner Production* **2020,** *267*, 122009.

96. Mortazavian, S.; An, H.; Chun, D.; Moon, J., Activated carbon impregnated by zero-valent iron nanoparticles (AC/nZVI) optimized for simultaneous adsorption and reduction of aqueous hexavalent chromium: Material characterizations and kinetic studies. *Chemical Engineering Journal* **2018,** *353*, 781-795.

97. Lyu, H.; Tang, J.; Huang, Y.; Gai, L.; Zeng, E. Y.; Liber, K.; Gong, Y., Removal of hexavalent chromium from aqueous solutions by a novel biochar supported nanoscale iron sulfide composite. *Chemical Engineering Journal* **2017,** *322*, 516-524.

98. Xu, C.; Yang, W.; Liu, W.; Sun, H.; Jiao, C.; Lin, A.-j., Performance and mechanism of Cr(VI) removal by zero-valent iron loaded onto expanded graphite. *Journal of Environmental Sciences* **2018,** *67*, 14-22.

99. Liu, T.; Zhao, L.; Sun, D.; Tan, X., Entrapment of nanoscale zero-valent iron in chitosan beads for hexavalent chromium removal from wastewater. *Journal of Hazardous Materials* **2010,** *184*, (1), 724-730.

100. Qian, L.; Zhang, W.; Yan, J.; Han, L.; Chen, Y.; Ouyang, D.; Chen, M., Nanoscale zero-valent iron supported by biochars produced at different temperatures: Synthesis mechanism and effect on Cr(VI) removal. *Environmental Pollution* **2017,** *223*, 153-160.

101. Zhang; Qian, L.; Ouyang, D.; Chen, Y.; Han, L.; Chen, M., Effective removal of Cr(VI) by attapulgite-supported nanoscale zero-valent iron from aqueous solution: Enhanced adsorption and crystallization. *Chemosphere* **2019,** *221*, 683-692.

102. Kerekes, L.; Hakl, J.; Meszaros, S.; Vad, K.; Gurin, P.; Kis-Varga, M.; Uzonyi, I.; Szabo, S.; Beke, D. J. C. j. o. p., Study of magnetic relaxation in partially oxidized nanocrystalline iron. *Czechoslovak Journal of Physics* **2002,** *52*, (1), A89-A92.

103. Ambika, S.; Devasena, M.; Nambi, I. M., Synthesis, characterization and performance of high energy ball milled meso-scale zero valent iron in Fenton reaction. *J. Environ. Manage.* **2016,** *181*, 847-855.

104. Huber, D., Synthesis, Properties, and Applications of Iron Nanoparticles. *Small* **2005,** *1*, 482-501.

105. Ambika, S.; Devasena, M.; Nambi, I. M., Single-step removal of Hexavalent chromium and phenol using meso zerovalent iron. *Chemosphere* **2020,** *248*, 125912.

106. Wang; Hu, B.; Wang, C.; Liang, Z.; Cui, F.; Zhao, Z.; Yang, C., Cr(VI) removal by micron-scale iron-carbon composite induced by ball milling: The role of activated carbon. *Chemical Engineering Journal* **2020,** *389*, 122633.

107. Wang; Sun, Y.; Tang, J.; He, J.; Sun, H., Aqueous Cr(VI) removal by a novel ball milled Fe0-biochar composite: Role of biochar electron transfer capacity under high pyrolysis temperature. *Chemosphere* **2020,** *241*, 125044.

108. Pardavi-Horvath, M.; Takacs, L., Magnetic nanocomposites by reaction milling. *Scripta Metallurgica et Materialia* **1995,** *33*, (10), 1731-1740.

109. Takacs, L., Reduction of magnetite by aluminum: a displacement reaction induced by mechanical alloying. *Materials Letters* **1992,** *13*, (2), 119-124.

110. Matteazzi, P.; Le Caër, G., Mechanochemical reduction of hematite by room temperature ball milling. *Hyperfine Interact.* **1992,** *68*, (1), 177-180.
111. Liu, G.-s.; Strezov, V.; Lucas, J. A.; Wibberley, L. J., Thermal investigations of direct iron ore reduction with coal. *Thermochimica Acta* **2004,** *410*, (1), 133-140.
112. Choi, C. J.; Tolochko, O.; Kim, B. K., Preparation of iron nanoparticles by chemical vapor condensation. *Materials Letters* **2002,** *56*, (3), 289-294.
113. Liu, J.; Liu, H.; Wang, C.; Li, X.; Tong, Y.; Xuan, X.; Cui, G., Synthesis, characterization and re-activation of a Fe0/Ti system for the reduction of aqueous Cr(VI). *Journal of Hazardous Materials* **2008,** *151*, (2), 761-769.
114. Natter, H.; Schmelzer, M.; Löffler, M. S.; Krill, C. E.; Fitch, A.; Hempelmann, R., Grain-Growth Kinetics of Nanocrystalline Iron Studied In Situ by Synchrotron Real-Time X-ray Diffraction. *The Journal of Physical Chemistry B* **2000,** *104*, (11), 2467-2476.
115. Vilardi, G.; Stoller, M.; Di Palma, L.; Boodhoo, K.; Verdone, N., Metallic iron nanoparticles intensified production by spinning disk reactor: Optimization and fluid dynamics modelling. *Chemical Engineering and Processing - Process Intensification* **2019,** *146*, 107683.
116. Ponder, S. M.; Darab, J. G.; Mallouk, T. E., Remediation of Cr(VI) and Pb(II) Aqueous Solutions Using Supported, Nanoscale Zero-valent Iron. *Environ. Sci. Technol.* **2000,** *34*, (12), 2564-2569.
117. Ribas, D.; Pešková, K.; Jubany, I.; Parma, P.; Černik, M.; Benito, J. A.; Martí, V., High reactive nano zero-valent iron produced via wet milling through abrasion by alumina. *Chemical Engineering Journal* **2019,** *366*, 235-245.
118. Man, Y.; Feng, J. X.; Li, F. J.; Ge, Q.; Chen, Y. M.; Zhou, J. Z., Influence of temperature and time on reduction behavior in iron ore–coal composite pellets. *Powder Technology* **2014,** *256*, 361-366.
119. Choi, C. J.; Dong, X. L.; Kim, B. K., Characterization of Fe and Co nanoparticles synthesized by chemical vapor condensation. *Scripta Materialia* **2001,** *44*, (8), 2225-2229.
120. Yanez, J. E.; Wang, Z.; Lege, S.; Obst, M.; Roehler, S.; Burkhardt, C. J.; Zwiener, C., Application and characterization of electroactive membranes based on carbon nanotubes and zerovalent iron nanoparticles. *Water Research* **2017,** *108*, 78-85.
121. Vilardi, G.; Stoller, M.; Verdone, N.; Di Palma, L., Production of nano Zero Valent Iron particles by means of a spinning disk reactor. *Chemical Engineering Transactions* **2017,** *57*, 751-756.
122. Zhou; Gao, B.; Zimmerman, A. R.; Chen, H.; Zhang, M.; Cao, X., Biochar-supported zerovalent iron for removal of various contaminants from aqueous solutions. *Bioresource Technology* **2014,** *152*, 538-542.
123. Oliveira, L. C. A.; Rios, R. V. R. A.; Fabris, J. D.; Garg, V.; Sapag, K.; Lago, R. M., Activated carbon/iron oxide magnetic composites for the adsorption of contaminants in water. *Carbon* **2002,** *40*, (12), 2177-2183.
124. Karthikeyan, T.; Rajgopal, S.; Miranda, L. R., Chromium (VI) adsorption from aqueous solution by Hevea Brasilinesis sawdust activated carbon. *Journal of hazardous materials* **2005,** *124*, (1-3), 192-199.
125. Cronje, K.; Chetty, K.; Carsky, M.; Sahu, J.; Meikap, B., Optimization of chromium (VI) sorption potential using developed activated carbon from sugarcane bagasse with chemical activation by zinc chloride. *Desalination* **2011,** *275*, (1-3), 276-284.
126. Huang, L.; Zhou, S.; Jin, F.; Huang, J.; Bao, N., Characterization and mechanism analysis of activated carbon fiber felt-stabilized nanoscale zero-valent iron for the removal of Cr (VI) from

aqueous solution. *Colloids and Surfaces A: Physicochemical and Engineering Aspects* **2014,** *447*, 59-66.

127. Wu, L.; Liao, L.; Lv, G.; Qin, F.; He, Y.; Wang, X., Micro-electrolysis of Cr (VI) in the nanoscale zero-valent iron loaded activated carbon. *Journal of hazardous materials* **2013,** *254*, 277-283.

128. Dong, H.; Deng, J.; Xie, Y.; Zhang, C.; Jiang, Z.; Cheng, Y.; Hou, K.; Zeng, G., Stabilization of nanoscale zero-valent iron (nZVI) with modified biochar for Cr (VI) removal from aqueous solution. *Journal of hazardous materials* **2017,** *332*, 79-86.

129. Qian, L.; Shang, X.; Zhang, B.; Zhang, W.; Su, A.; Chen, Y.; Ouyang, D.; Han, L.; Yan, J.; Chen, M., Enhanced removal of Cr (VI) by silicon rich biochar-supported nanoscale zero-valent iron. *Chemosphere* **2019,** *215*, 739-745.

130. Qiu, B.; Wang, Y.; Sun, D.; Wang, Q.; Zhang, X.; Weeks, B. L.; O'Connor, R.; Huang, X.; Wei, S.; Guo, Z., Cr(vi) removal by magnetic carbon nanocomposites derived from cellulose at different carbonization temperatures. *Journal of Materials Chemistry A* **2015,** *3*, (18), 9817-9825.

131. Salam, M. A., Preparation and characterization of chitin/magnetite/multiwalled carbon nanotubes magnetic nanocomposite for toxic hexavalent chromium removal from solution. *Journal of Molecular Liquids* **2017,** *233*, 197-202.

132. Rajput, S.; Pittman Jr, C. U.; Mohan, D., Magnetic magnetite (Fe3O4) nanoparticle synthesis and applications for lead (Pb2+) and chromium (Cr6+) removal from water. *Journal of colloid and interface science* **2016,** *468*, 334-346.

133. Nethaji, S.; Sivasamy, A.; Mandal, A., Preparation and characterization of corn cob activated carbon coated with nano-sized magnetite particles for the removal of Cr (VI). *Bioresource Technology* **2013,** *134*, 94-100.

134. Gupta, V.; Agarwal, S.; Saleh, T. A., Chromium removal by combining the magnetic properties of iron oxide with adsorption properties of carbon nanotubes. *Water Research* **2011,** *45*, (6), 2207-2212.

135. Huang, Z.-n.; Wang, X.-l.; Yang, D.-s., Adsorption of Cr(VI) in wastewater using magnetic multi-wall carbon nanotubes. *Water Science and Engineering* **2015,** *8*, (3), 226-232.

136. Rebodos, R. L.; Vikesland, P. J., Effects of oxidation on the magnetization of nanoparticulate magnetite. *Langmuir* **2010,** *26*, (22), 16745-16753.

137. Lu; Li, J.; Sheng, Y.; Zhang, X.; You, J.; Chen, L., One-pot synthesis of magnetic iron oxide nanoparticle-multiwalled carbon nanotube composites for enhanced removal of Cr(VI) from aqueous solution. *Journal of Colloid and Interface Science* **2017,** *505*, 1134-1146.

138. Baikousi, M.; Bourlinos, A. B.; Douvalis, A.; Bakas, T.; Anagnostopoulos, D. F.; Tuček, J.; Šafářová, K.; Zboril, R.; Karakassides, M. A., Synthesis and Characterization of γ-Fe2O3/Carbon Hybrids and Their Application in Removal of Hexavalent Chromium Ions from Aqueous Solutions. *Langmuir* **2012,** *28*, (8), 3918-3930.

139. Han, Y.; Yan, W., Reductive dechlorination of trichloroethene by zero-valent iron nanoparticles: reactivity enhancement through sulfidation treatment. *Environmental science & technology* **2016,** *50*, (23), 12992-13001.

140. Fan, D.; Lan, Y.; Tratnyek, P. G.; Johnson, R. L.; Filip, J.; O' Carroll, D. M.; Nunez Garcia, A.; Agrawal, A., Sulfidation of Iron-Based Materials: A Review of Processes and Implications for Water Treatment and Remediation. *Environ. Sci. Technol.* **2017,** *51*, (22), 13070-13085.

141. Fan, D.; O'Brien Johnson, G.; Tratnyek, P. G.; Johnson, R. L., Sulfidation of Nano Zerovalent Iron (nZVI) for Improved Selectivity During In-Situ Chemical Reduction (ISCR). *Environ Sci Technol*

2016, *50*, (17), 9558-65.
142. Li, J.; Zhang, X.; Sun, Y.; Liang, L.; Pan, B.; Zhang, W.; Guan, X., Advances in Sulfidation of Zerovalent Iron for Water Decontamination. *Environ. Sci. Technol.* **2017,** *51*, (23), 13533-13544.
143. Gu, Y.; Wang, B.; He, F.; Bradley, M. J.; Tratnyek, P. G., Mechanochemically sulfidated microscale zero valent iron: pathways, kinetics, mechanism, and efficiency of trichloroethylene dechlorination. *Environ. Sci. Technol.* **2017,** *51*, (21), 12653-12662.
144. Cao, Z.; Liu, X.; Xu, J.; Zhang, J.; Yang, Y.; Zhou, J.; Xu, X.; Lowry, G. V., Removal of antibiotic florfenicol by sulfide-modified nanoscale zero-valent iron. *Environmental Science & Technology* **2017,** *51*, (19), 11269-11277.
145. Xiao, R.; He, L.; Luo, Z.; Spinney, R.; Wei, Z.; Dionysiou, D. D.; Zhao, F., An experimental and theoretical study on the degradation of clonidine by hydroxyl and sulfate radicals. *Science of The Total Environment* **2020,** *710*, 136333.
146. Li, J.; Zhang, X.; Liu, M.; Pan, B.; Zhang, W.; Shi, Z.; Guan, X., Enhanced Reactivity and Electron Selectivity of Sulfidated Zerovalent Iron toward Chromate under Aerobic Conditions. *Environmental Science & Technology* **2018,** *52*, (5), 2988-2997.
147. Lv, D.; Zhou, J.; Cao, Z.; Xu, J.; Liu, Y.; Li, Y.; Yang, K.; Lou, Z.; Lou, L.; Xu, X., Mechanism and influence factors of chromium (VI) removal by sulfide-modified nanoscale zerovalent iron. *Chemosphere* **2019,** *224*, 306-315.
148. Liu, Y.; Lowry, G., Effect of Particle Age (Fe 0 Content) and Solution pH On NZVI Reactivity: H 2 Evolution and TCE Dechlorination. *Environmental Science & Technology* **2006,** *40*, 6085-6090.
149. Paar, H.; Ruhl, A. S.; Jekel, M., Influences of nanoscale zero valent iron loadings and bicarbonate and calcium concentrations on hydrogen evolution in anaerobic column experiments. *Water Research* **2015,** *68*, 731-739.
150. Reardon, E., Anaerobic Corrosion of Granular Iron: Measurement and Interpretation of Hydrogen Evolution Rates. *Environmental Science & Technology* **1995,** *29*, 2936-45.
151. Reardon, E., Zerovalent Irons: Styles of Corrosion and Inorganic Control on Hydrogen Pressure Buildup. *Environmental Science & Technology* **2005,** *39*, 7311-7.
152. Rajajayavel, S.; Ghoshal, S., Enhanced reductive dechlorination of trichloroethylene by sulfidated nanoscale zero valent iron. *Water Research* **2015,** *78*, 144-153.
153. Xu, J.; Wang, Y.; Weng, C.; Bai, W.; Jiao, Y.; Kaegi, R.; Lowry, G. V., Reactivity, Selectivity, and Long-Term Performance of Sulfidized Nanoscale Zerovalent Iron with Different Properties. *Environmental Science & Technology* **2019,** *53*, (10), 5936-5945.
154. Gu, Y.; Gong, L.; Qi, J.; Cai, S.; Tu, W.; He, F., Sulfidation mitigates the passivation of zero valent iron at alkaline pHs: Experimental evidences and mechanism. *Water Research* **2019,** *159*, 233-241.
155. Nunez Garcia, A.; Boparai, H. K.; de Boer, C. V.; Chowdhury, A. I. A.; Kocur, C. M. D.; Austrins, L. M.; Herrera, J.; O' Carroll, D. M., Fate and transport of sulfidated nano zerovalent iron (S-nZVI): A field study. *Water Research* **2020,** *170*, 115319.
156. Liu, W.-J.; Qian, T.-T.; Jiang, H., Bimetallic Fe nanoparticles: Recent advances in synthesis and application in catalytic elimination of environmental pollutants. *Chemical Engineering Journal* **2014,** *236*, 448-463.
157. Dong, T.; Luo, H.; Wang, Y.; Hu, B.; Chen, H., Stabilization of Fe–Pd bimetallic nanoparticles with sodium carboxymethyl cellulose for catalytic reduction of para-nitrochlorobenzene in water. *Desalination* **2011,** *271*, 11-19.
158. Hu, C. Y.; Lo, S. L.; Liou, Y. H.; Hsu, Y. W.; Shih, K.; Lin, C. J., Hexavalent chromium removal

from near natural water by copper-iron bimetallic particles. *Water Research* **2010,** *44*, (10), 3101-8.
159. Gunawardana, B.; Singhal, N.; Swedlund, P., Degradation of Chlorinated Phenols by Zero Valent Iron and Bimetals of Iron: A Review. *Environmental Engineering Research* **2011,** *16*, (4), 187-203.
160. Jiang, B.; Xin, S.; Gao, L.; Luo, S.; Xue, J.; Wu, M., Dramatically enhanced aerobic Cr(VI) reduction with scrap zero-valent aluminum induced by oxalate. *Chem. Eng. J.* **2017,** *308*, 588-596.
161. Yang, S.; Zheng, D.; Ren, T.; Zhang, Y., Zero-valent aluminum for reductive removal of aqueous pollutants over a wide pH range: Performance and mechanism especially at near-neutral pH. *Water Research* **2017,** *123*.
162.Yang, Y.; Gai, W.-Z.; Zhou, J.-G.; Deng, Z.-Y., Surface modified zero-valent aluminum for Cr(VI) removal at neutral pH. *Chemical Engineering Journal* **2020,** *395*, 125140.
163. Zhang; Yang, S.; Ren, T.; Zhang, Y.; Jiang, Y.; Xue, Y.; Wang, M.; Chen, H.; Chen, Y., Enhancing surface gully erosion of micron-sized zero-valent aluminum (mZVAl) for Cr(VI) removal: Performance and mechanism in the presence of carbonate buffer. *Journal of Cleaner Production* **2019,** *238*, 117943.
164. Lin, K.-Y.; Lin, C.-H.; Yang, H., Enhanced Bromate Reduction using Zero-Valent Aluminum mediated by Oxalic Acid. *Journal of Environmental Chemical Engineering* **2017,** *5*, 5085-5090.
165. Ren, T.; Yang, S.; Jiang, Y.; Sun, X.; Zhang, Y., Enhancing surface corrosion of zero-valent aluminum (ZVAl) and electron transfer process for the degradation of trichloroethylene with the presence of persulfate. *Chemical Engineering Journal* **2018,** *348*.
166. Wu, S.; Yang, S.; Liu, S.; Zhang, Y.; Ren, T.; Zhang, Y., Enhanced reactivity of zero-valent aluminum with ball milling for phenol oxidative degradation. *Journal of Colloid and Interface Science* **2020,** *560*, 260-272.
167. He, Y.; Sun, H.; Liu, W.; Yang, W.; Lin, A., Study on removal effect of Cr(VI) and surface reaction mechanisms by bimetallic system in aqueous solution. *Environmental Technology* **2018**, 1-23.
168. Ou, J.-H.; Sheu, Y.-T.; Tsang, D. C. W.; Sun, Y.-J.; Kao, C.-M., Application of iron/aluminum bimetallic nanoparticle system for chromium-contaminated groundwater remediation. *Chemosphere* **2020,** *256*, 127158.
169. Qin; Zhang, Y.; Zhou, H.; Geng, Z.; Liu, G.; Zhang, Y.; Zhao, H.; Wang, G., Enhanced removal of trace Cr(VI) from neutral and alkaline aqueous solution by FeCo bimetallic nanoparticles. *Journal of Colloid and Interface Science* **2016,** *472*, 8-15.
170. Xu, F.; Deng, S.; Xu, J.; Zhang, W.; Wu, M.; Wang, B.; Huang, J.; Yu, G., Highly Active and Stable Ni-Fe Bimetal Prepared by Ball Milling for Catalytic Hydrodechlorination of 4-Chlorophenol. *Environ. Sci. Technol.* **2012,** *46*, 4576-82.
171. Zhao, W.; Zhu, X.; Wang, Y.; Ai, Z.; Zhao, D., Catalytic reduction of aqueous nitrates by metal supported catalysts on Al particles. *Chemical Engineering Journal* **2014,** *254*, 410–417.
172. Xu, J.; Pu, Y.; Yang, X.; Wan, P.; Wang, R.; Song, P.; Fisher, A., Rapid removal of chloroform, carbon tetrachloride and trichloroethylene in water by aluminum-iron alloy particles. *Environmental technology* **2017,** *39*, 1-23.
173. Xu, J.; Pu, Y.; Qi, W.-K.; Yang, X.; Tang, Y.; Wan, P.; Fisher, A., Chemical removal of nitrate from water by aluminum-iron alloys. *Chemosphere* **2017,** *166*, 197-202.
174. Zhang; Wu, J.; Chao, J.; Shi, N.; Li, H.; Hu, Q.; Yang, X. J., Simultaneous removal of nitrate, copper and hexavalent chromium from water by aluminum-iron alloy particles. *Journal of*

Contaminant Hydrology **2019,** *227*, 103541.

175. Kumar, V.; Talreja, N.; Deva, D.; Sankararamakrishnan, N.; Sharma, A.; Verma, N., Development of bi-metal doped micro- and nano multi-functional polymeric adsorbents for the removal of fluoride and arsenic(V) from wastewater. *Desalination* **2011,** *282*, 27-38.

176. Sui, H.; Rong, Y.; Song, J.; Zhang, D.; Li, H.; Wu, P.; Shen, Y.; Huang, Y., Mechanochemical destruction of DDTs with Fe-Zn bimetal in a high-energy planetary ball mill. *Journal of hazardous materials* **2017,** *342*, 201-209.

177. Yang, B.; Zhang, J.; Zhang, Y.; Deng, S.; Yu, G.; Wu, J.; Zhang, H.; Liu, J., Promoting effect of EDTA on catalytic activity of highly stable Al–Ni bimetal alloy for dechlorination of 2-chlorophenol. *Chemical Engineering Journal* **2014,** *250*, 222-229.

178. Wang; Wu, Y.; Qu, T.; Liu, S.; Pi, Y.; Shen, J., Enhanced Cr(VI) removal in the synergy between the hydroxyl-functionalized ball-milled ZVI/Fe3O4 composite and Na2EDTA complexation. *Chemical Engineering Journal* **2019,** *359*, 874-881.

179. Zhou; Li, Y.; Chen, J.; Liu, Z.; Wang, Z.; Na, P., Enhanced Cr(VI) removal from aqueous solutions using Ni/Fe bimetallic nanoparticles: characterization, kinetics and mechanism. *RSC Advances* **2014,** *4*, 50699-50707.

180. Kadu, B. S.; Sathe, Y. D.; Ingle, A. B.; Chikate, R. C.; Patil, K. R.; Rode, C. V., Efficiency and recycling capability of montmorillonite supported Fe–Ni bimetallic nanocomposites towards hexavalent chromium remediation. *Applied Catalysis B: Environmental* **2011,** *104*, (3), 407-414.

181. Lu; Xu, Y.; Zhou, S., High saturation magnetization superparamagnetic Fe/Ni core/shell microparticles for chromium removal. *RSC Adv.* **2017,** *7*, 42363-42369.

182. Shao, F.; Zhou, S.; Xu, J.; Du, Q.; Chen, J.; Shang, J., Detoxification of Cr(VI) using biochar supported Cu/Fe bimetallic nanoparticles. *Desalination and Water Treatment* **2019,** *158*, 121-129.

183. He; Lin, H.; Luo, M.; Liu, J.; Dong, Y.; Li, B., Highly efficient remediation of groundwater co-contaminated with Cr(VI) and nitrate by using nano-Fe/Pd bimetal-loaded zeolite: Process product and interaction mechanism. *Environ. Pollut.* **2020,** *263*, 114479.

184. Zhu, F.; Ma, S.; Liu, T.; Deng, X., Green synthesis of nano zero-valent iron/Cu by green tea to remove hexavalent chromium from groundwater. *Journal of Cleaner Production* **2018,** *174*, 184-190.

185. Jia, T.; Zhang, B.; Huang, L.; Wang, S.; Xu, C., Enhanced sequestration of Cr(VI) by copper doped sulfidated zerovalent iron (SZVI-Cu): Characterization, performance, and mechanisms. *Chemical Engineering Journal* **2019,** *366*, 200-207.

186. Su, C., Environmental implications and applications of engineered nanoscale magnetite and its hybrid nanocomposites: A review of recent literature. *Journal of Hazardous Materials* **2017,** *322*, 48-84.

187. Petrova, T.; Fachikov, L.; Hristov, J., The magnetite as adsorbent for some hazardous species from aqueous solutions: A review. *International Review of Chemical Engineering* **2011,** *3*, 134-152.

188. Gorski, C. A.; Nurmi, J. T.; Tratnyek, P. G.; Hofstetter, T. B.; Scherer, M. M., Redox Behavior of Magnetite: Implications for Contaminant Reduction. *Environmental Science & Technology* **2010,** *44*, (1), 55-60.

189. Wiatrowski, H. A.; Das, S.; Kukkadapu, R.; Ilton, E. S.; Barkay, T.; Yee, N., Reduction of Hg(II) to Hg(0) by Magnetite. *Environ. Sci. Technol.* **2009,** *43*, (14), 5307-5313.

190. Crean, D. E.; Coker, V. S.; van der Laan, G.; Lloyd, J. R., Engineering Biogenic Magnetite for Sustained Cr(VI) Remediation in Flow-through Systems. *Environmental Science & Technology*

2012, *46*, (6), 3352-3359.
191. Yuan, P.; Liu, D.; Fan, M.; Yang, D.; Zhu, R.; Ge, F.; Zhu, J.; He, H., Removal of hexavalent chromium [Cr(VI)] from aqueous solutions by the diatomite-supported/unsupported magnetite nanoparticles. *Journal of Hazardous Materials* **2010,** *173*, (1), 614-621.
192. Yuan, P.; Fan, M.; Yang, D.; He, H.; Liu, D.; Yuan, A.; Zhu, J.; Chen, T., Montmorillonite-supported magnetite nanoparticles for the removal of hexavalent chromium [Cr(VI)] from aqueous solutions. *Journal of Hazardous Materials* **2009,** *166*, (2), 821-829.
193. Peterson, M. L.; Brown, G. E.; Parks, G. A., Direct XAFS evidence for heterogeneous redox reaction at the aqueous chromium/magnetite interface. *Colloids and Surfaces A: Physicochemical and Engineering Aspects* **1996,** *107*, 77-88.
194. Villacís-García, M.; Villalobos, M.; Gutiérrez-Ruiz, M., Optimizing the use of natural and synthetic magnetites with very small amounts of coarse Fe(0) particles for reduction of aqueous Cr(VI). *Journal of Hazardous Materials* **2015,** *281*, 77-86.
195. Qu, G.; Zeng, D.; Chu, R.; Wang, T.; Liang, D.; Qiang, H., Magnetic Fe3O4 assembled on nZVI supported on activated carbon fiber for Cr(VI) and Cu(II) removal from aqueous solution through a permeable reactive column. *Environmental Science and Pollution Research* **2019,** *26*, (5), 5176-5188.
196. Rao, A.; Bankar, A.; Kumar, A. R.; Zinjarde, S.; Gosavi, S., Phytofabrication of Fe0/Fe3O4 Composites for the Removal of Hexavalent Chromium. *Journal of Nanoengineering and Nanomanufacturing* **2013,** *3*, (2), 114-120.
197. Jonoush, Z. A.; Rezaee, A.; Ghaffarinejad, A., Electrocatalytic nitrate reduction using Fe0/Fe3O4 nanoparticles immobilized on nickel foam: Selectivity and energy consumption studies. *Journal of Cleaner Production* **2020,** *242*, 118569.
198. Moura, F. C. C.; Oliveira, G. C.; Araujo, M. H.; Ardisson, J. D.; Macedo, W. A. A.; Lago, R. M., Highly reactive species formed by interface reaction between Fe0–iron oxides particles: An efficient electron transfer system for environmental applications. *Applied Catalysis A: General* **2006,** *307*, (2), 195-204.
199. Moura, F. C. C.; Oliveira, G. C.; Araujo, M. H.; Ardisson, J. D.; Macedo, W. A. d. A.; Lago, R. M., Formation of Highly Reactive Species at the Interface Fe°–Iron Oxides Particles by Mechanical Alloying and Thermal Treatment: Potential Application in Environmental Remediation Processes. *Chemistry Letters* **2005,** *34*, (8), 1172-1173.
200. Rao, A.; Bankar, A.; Kumar, A. R.; Gosavi, S.; Zinjarde, S., Removal of hexavalent chromium ions by Yarrowia lipolytica cells modified with phyto-inspired Fe0/Fe3O4 nanoparticles. *Journal of Contaminant Hydrology* **2013,** *146*, 63-73.
201. Coelho, F. d. S.; Ardisson, J. D.; Moura, F. C. C.; Lago, R. M.; Murad, E.; Fabris, J. D., Potential application of highly reactive Fe(0)/Fe3O4 composites for the reduction of Cr(VI) environmental contaminants. *Chemosphere* **2008,** *71*, (1), 90-96.
202. Lv, X.; Xu, J.; Jiang, G.; Tang, J.; Xu, X., Highly active nanoscale zero-valent iron (nZVI)–Fe3O4 nanocomposites for the removal of chromium(VI) from aqueous solutions. *Journal of Colloid and Interface Science* **2012,** *369*, (1), 460-469.
203. Peterson, M. L.; White, A. F.; Brown, G. E.; Parks, G. A., Surface Passivation of Magnetite by Reaction with Aqueous Cr(VI): XAFS and TEM Results. *Environmental Science & Technology* **1997,** *31*, (5), 1573-1576.
204. Zhou, H.; He, Y.; Lan, Y.; Mao, J.; Chen, S., Influence of complex reagents on removal of

chromium(VI) by zero-valent iron. *Chemosphere* **2008,** *72*, (6), 870-4.
205. Fu, F.; Han, W.; Tang, B.; Hu, M.; Cheng, Z., Insights into environmental remediation of heavy metal and organic pollutants: Simultaneous removal of hexavalent chromium and dye from wastewater by zero-valent iron with ligand-enhanced reactivity. *Chemical Engineering Journal* **2013,** *232*, 534-540.
206. Wang, M.; Wang, N.; Tang, H.; Cao, M.; She, Y.; Zhu, L., Surface modification of nano-Fe3O4 with EDTA and its use in H2O2 activation for removing organic pollutants. *Catalysis Science & Technology* **2012,** *2*, (1), 187-194.
207. Luo, W.; Zhu, L.; Wang, N.; Tang, H.; Cao, M.; She, Y., Efficient Removal of Organic Pollutants with Magnetic Nanoscaled BiFeO3 as a Reusable Heterogeneous Fenton-Like Catalyst. *Environmental Science & Technology* **2010,** *44*, (5), 1786-1791.
208. López, M. L.; Peralta-Videa, J. R.; Benitez, T.; Gardea-Torresdey, J. L., Enhancement of lead uptake by alfalfa (Medicago sativa) using EDTA and a plant growth promoter. *Chemosphere* **2005,** *61*, (4), 595-598.
209. Zhang, Y.; Li, Y.; Yang, L.-q.; Ma, X.-j.; Wang, L.-y.; Ye, Z.-F., Characterization and adsorption mechanism of Zn2+ removal by PVA/EDTA resin in polluted water. *Journal of Hazardous Materials* **2010,** *178*, (1), 1046-1054.
210. Englehardt, J. D.; Meeroff, D. E.; Echegoyen, L.; Deng, Y.; Raymo, F. M.; Shibata, T., Oxidation of Aqueous EDTA and Associated Organics and Coprecipitation of Inorganics by Ambient Iron-Mediated Aeration. *Environmental Science & Technology* **2007,** *41*, (1), 270-276.
211. Vilardi, G.; Di Palma, L.; Verdone, N., A physical-based interpretation of mechanism and kinetics of Cr(VI) reduction in aqueous solution by zero-valent iron nanoparticles. *Chemosphere* **2019,** *220*, 590-599.
212. Huang, D.; Wang, G.; Shi, Z.; Li, Z.; Kang, F.; Liu, F., Removal of hexavalent chromium in natural groundwater using activated carbon and cast iron combined system. *Journal of Cleaner Production* **2017,** *165*, 667-676.
213. Lugo-Lugo, V.; Bernal-Martínez, L. A.; Ureña-Núñez, F.; Linares-Hernández, I.; Almazán-Sánchez, P. T.; Vázquez-Santillán, P. d. J. B., Treatment of Cr(VI) present in plating wastewater using a Cu/Fe galvanic reactor. *Fuel* **2014,** *138*, 203-214.
214. Lugo-Lugo, V.; Barrera-Díaz, C.; Bilyeu, B.; Balderas-Hernández, P.; Ureña-Nuñez, F.; Sánchez-Mendieta, V., Cr(VI) reduction in wastewater using a bimetallic galvanic reactor. *Journal of Hazardous Materials* **2010,** *176*, (1), 418-425.
215. Jiang, D.; Huang, D.; Lai, C.; Xu, P.; Zeng, G.; Wan, J.; Tang, L.; Dong, H.; Huang, B.; Hu, T., Difunctional chitosan-stabilized Fe/Cu bimetallic nanoparticles for removal of hexavalent chromium wastewater. *Science of The Total Environment* **2018,** *644*, 1181-1189.
216. Zhang; Zhao, D.; Ding, Y.; Chen, Y.; Li, F.; Alsaedi, A.; Hayat, T.; Chen, C., Synthesis of Fe–Ni/graphene oxide composite and its highly efficient removal of uranium(VI) from aqueous solution. *Journal of Cleaner Production* **2019,** *230*, 1305-1315.
217. Zhou, X.; Jing, G.; Lv, B.; Zhou, Z.; Zhu, R., Highly efficient removal of chromium(VI) by Fe/Ni bimetallic nanoparticles in an ultrasound-assisted system. *Chemosphere* **2016,** *160*, 332-341.
218. Lai, B.; Zhang, Y.; Chen, Z.; Yang, P.; Zhou, Y.; Wang, J., Removal of p-nitrophenol (PNP) in aqueous solution by the micron-scale iron–copper (Fe/Cu) bimetallic particles. *Applied Catalysis B: Environmental* **2014,** *144*, 816-830.
219. Cheng, Z.; Fu, F.; Dionysiou, D. D.; Tang, B., Adsorption, oxidation, and reduction behavior of

arsenic in the removal of aqueous As(III) by mesoporous Fe/Al bimetallic particles. *Water Res.* **2016,** *96*, 22-31.
220. Shao, Q.; Xu, C.; Wang, Y.; Huang, S.; Zhang, B.; Huang, L.; Fan, D.; Tratnyek, P. G., Dynamic interactions between sulfidated zerovalent iron and dissolved oxygen: Mechanistic insights for enhanced chromate removal. *Water Research* **2018,** *135*, 322-330.
221. Zhang; Zhang, Y.; Gao, X.; Xu, C., Insights on the effects of pH and Fe(II) regeneration during the chromate sequestration by sulfidated zero-valent iron. *Chemical Engineering Journal* **2019,** *378*, 122115.
222. Zou, H.; Hu, E.; Yang, S.; Gong, L.; He, F., Chromium(VI) removal by mechanochemically sulfidated zero valent iron and its effect on dechlorination of trichloroethene as a co-contaminant. *Science of The Total Environment* **2019,** *650*, 419-426.
223. Wu; Zhang, J.; Tong, Y.; Xu, X., Chromium (VI) reduction in aqueous solutions by Fe3O4-stabilized Fe0 nanoparticles. *Journal of Hazardous Materials* **2009,** *172*, (2), 1640-1645.
224. Lian, J.; Wang, H.; He, H.; Huang, W.; Yang, M.; Zhong, Y.; Peng, P. a., The reaction of amorphous iron sulfide with Mo(VI) under different pH conditions. *Chemosphere* **2021,** *266*, 128946.
225. Si, Z.; Song, X.; Wang, Y.; Cao, X.; Wang, Y.; Zhao, Y.; Ge, X., Natural pyrite improves nitrate removal in constructed wetlands and makes wetland a sink for phosphorus in cold climates. *Journal of Cleaner Production* **2021,** *280*, 124304.
226. Perez, J. P. H.; Schiefler, A. A.; Rubio, S. N.; Reischer, M.; Overheu, N. D.; Benning, L. G.; Tobler, D. J., Arsenic removal from natural groundwater using 'green rust': Solid phase stability and contaminant fate. *Journal of Hazardous Materials* **2021,** *401*, 123327.
227. Zhao, J.; Xiong, S.; Ai, J.; Wu, J.; Huang, L.-Z.; Yin, W., Stabilized green rusts for aqueous Cr(VI) removal: Fast kinetics, high iron utilization rate and anti-acidification. *Chemosphere* **2021,** *262*, 127853.
228. Bae, S.; Yoon, S.; Kaplan, U.; Kim, H.; Han, S.; Lee, W., Effect of groundwater ions (Ca2+, Na+, and HCO3−) on removal of hexavalent chromium by Fe(II)-phosphate mineral. *Journal of Hazardous Materials* **2020,** *398*, 122948.
229. Wang; Qian, T.; Huo, L.; Li, Y.; Zhao, D., Immobilization of hexavalent chromium in soil and groundwater using synthetic pyrite particles. *Environmental Pollution* **2019,** *255*, 112992.
230. Li, K.; Hanpei, Y.; Lina, W.; Siqi, C.; Ruichen, Z.; Junming, W.; Xiaona, L., Facile integration of FeS and titanate nanotubes for efficient removal of total Cr from aqueous solution: Synergy in simultaneous reduction of Cr(VI) and adsorption of Cr(III). *Journal of Hazardous Materials* **2020,** *398*, 122834.
231. Ramos, R. L.; Martinez, A. J.; Coronado, R. G., Adsorption of chromium (VI) from aqueous solutions on activated carbon. *Water Science and Technology* **1994,** *30*, (9), 191.
232. White, A. F.; Peterson, M. L., Reduction of aqueous transition metal species on the surfaces of Fe (II)-containing oxides. *Geochimica et Cosmochimica Acta* **1996,** *60*, (20), 3799-3814.
233. Alowitz, M. J.; Scherer, M. M., Kinetics of Nitrate, Nitrite, and Cr(VI) Reduction by Iron Metal. *Environmental Science & Technology* **2002,** *36*, (3), 299-306.
234. Cissoko, N.; Zhang, Z.; Zhang, J.; Xu, X., Removal of Cr(VI) from simulative contaminated groundwater by iron metal. *Process Safety and Environmental Protection* **2009,** *87*, (6), 395-400.
235. Yoon, R. H.; Salman, T.; Donnay, G., Predicting points of zero charge of oxides and hydroxides. *Journal of Colloid and Interface Science* **1979,** *70*, (3), 483-493.

236. Sun, Y.-P.; Li, X.-q.; Cao, J.; Zhang, W.-x.; Wang, H. P., Characterization of zero-valent iron nanoparticles. *Adv. Colloid Interface Sci.* **2006,** *120*, (1), 47-56.
237. Choi, K.; Lee, W., Enhanced degradation of trichloroethylene in nano-scale zero-valent iron Fenton system with Cu(II). *Journal of Hazardous Materials* **2012,** *211-212*, 146-153.
238. Giasuddin, A. B. M.; Kanel, S. R.; Choi, H., Adsorption of Humic Acid onto Nanoscale Zerovalent Iron and Its Effect on Arsenic Removal. *Environmental Science & Technology* **2007,** *41*, (6), 2022-2027.
239. Kanel, S. R.; Manning, B.; Charlet, L.; Choi, H., Removal of Arsenic(III) from Groundwater by Nanoscale Zero-Valent Iron. *Environmental Science & Technology* **2005,** *39*, (5), 1291-1298.
240. Zhang, S.-H.; Wu, M.-F.; Tang, T.-T.; Xing, Q.-J.; Peng, C.-Q.; Li, F.; Liu, H.; Luo, X.-B.; Zou, J.-P.; Min, X.-B.; Luo, J.-M., Mechanism investigation of anoxic Cr(VI) removal by nano zero-valent iron based on XPS analysis in time scale. *Chemical Engineering Journal* **2018,** *335*, 945-953.
241. Alidokht, L.; Khataee, A. R.; Reyhanitabar, A.; Oustan, S., Reductive removal of Cr(VI) by starch-stabilized Fe0 nanoparticles in aqueous solution. *Desalination* **2011,** *270*, (1), 105-110.
242. Nahuel Montesinos, V.; Quici, N.; Beatriz Halac, E.; Leyva, A. G.; Custo, G.; Bengio, S.; Zampieri, G.; Litter, M. I., Highly efficient removal of Cr(VI) from water with nanoparticulated zerovalent iron: Understanding the Fe(III)–Cr(III) passive outer layer structure. *Chemical Engineering Journal* **2014,** *244*, 569-575.
243. Zhang, Y.-Y.; Jiang, H.; Zhang, Y.; Xie, J.-F., The dispersity-dependent interaction between montmorillonite supported nZVI and Cr(VI) in aqueous solution. *Chemical Engineering Journal* **2013,** *229*, 412-419.
244. Fang, Z.; Qiu, X.; Huang, R.; Qiu, X.; Li, M., Removal of chromium in electroplating wastewater by nanoscale zero-valent metal with synergistic effect of reduction and immobilization. *Desalination* **2011,** *280*, (1), 224-231.
245. Fan, H.; Ren, H.; Ma, X.; Zhou, S.; Huang, J.; Jiao, W.; Qi, G.; Liu, Y., High-gravity continuous preparation of chitosan-stabilized nanoscale zero-valent iron towards Cr(VI) removal. *Chemical Engineering Journal* **2020,** *390*, 124639.
246. Rivero-Huguet, M.; Marshall, W. D., Impact of various inorganic oxyanions on the removal rates of hexavalent chromium mediated by zero-valent iron. *Environmental Chemistry* **2010,** *7*, (3), 250-258.
247. Guan, X.; Dong, H.; Ma, J.; Lo, I. M. C.; Dou, X., Performance and mechanism of simultaneous removal of chromium and arsenate by Fe(II) from contaminated groundwater. *Separation and Purification Technology* **2011,** *80*, (1), 179-185.
248. Wang, Y.; Shao, Q.; Huang, S.; Zhang, B.; Xu, C., High performance and simultaneous sequestration of Cr (VI) and Sb (III) by sulfidated zerovalent iron. *Journal of Cleaner Production* **2018,** *191*, 436-444.
249. Noubactep, C., An analysis of the evolution of reactive species in Fe0/H2O systems. *Journal of Hazardous Materials* **2009,** *168*, (2), 1626-1631.
250. Qin; Li, J.; Bao, Q.; Li, L.; Guan, X., Role of dissolved oxygen in metal(loid) removal by zerovalent iron at different pH: its dependence on the removal mechanisms. *RSC Advances* **2016,** *6*, (55), 50144-50152.
251. Lewis, D. G., Factors influencing the stability and properties of green rusts. In Catena Verlag: 1997.
252. Fendorf, S. E.; Li, G., Kinetics of Chromate Reduction by Ferrous Iron. *Environmental Science*

& Technology **1996,** *30*, (5), 1614-1617.
253. Lan, Y.-Q.; Yang, J.-X.; Deng, B., Catalysis of Dissolved and Adsorbed Iron in Soil Suspension for Chromium(VI) Reduction by Sulfide. *Pedosphere* **2006,** *16*, (5), 572-578.
254. Mu, Y.; Wu, H.; Ai, Z., Negative impact of oxygen molecular activation on Cr(VI) removal with core–shell Fe@Fe2O3 nanowires. *Journal of Hazardous Materials* **2015,** *298*, 1-10.
255. Manning, B. A.; Kiser, J. R.; Kwon, H.; Kanel, S. R., Spectroscopic Investigation of Cr(III)- and Cr(VI)-Treated Nanoscale Zerovalent Iron. *Environmental Science & Technology* **2007,** *41*, (2), 586-592.
256. Pratt, A. R.; Blowes, D. W.; Ptacek, C. J., Products of Chromate Reduction on Proposed Subsurface Remediation Material. *Environmental Science & Technology* **1997,** *31*, (9), 2492-2498.
257. Astrup, T.; Stipp, S. L. S.; Christensen, T. H., Immobilization of Chromate from Coal Fly Ash Leachate Using an Attenuating Barrier Containing Zero-valent Iron. *Environmental Science & Technology* **2000,** *34*, (19), 4163-4168.
258. Komárek, M.; Vaněk, A.; Ettler, V., Chemical stabilization of metals and arsenic in contaminated soils using oxides – A review. *Environmental Pollution* **2013,** *172*, 9-22.
259. Mu, Y.; Ai, Z.; Zhang, L.; Song, F., Insight into core–shell dependent anoxic Cr (VI) removal with Fe@ Fe2O3 nanowires: indispensable role of surface bound Fe (II). *ACS applied materials & interfaces* **2015,** *7*, (3), 1997-2005.
260. Li, X.-q.; Cao, J.; Zhang, W.-x., Stoichiometry of Cr(VI) Immobilization Using Nanoscale Zerovalent Iron (nZVI): A Study with High-Resolution X-Ray Photoelectron Spectroscopy (HR-XPS). *Ind. Eng. Chem. Res.* **2008,** *47*, (7), 2131-2139.
261. Gheju, M.; Balcu, I., Removal of chromium from Cr(VI) polluted wastewaters by reduction with scrap iron and subsequent precipitation of resulted cations. *Journal of Hazardous Materials* **2011,** *196*, 131-138.
262. Liu, Q.; Xu, M.; Li, F.; Wu, T.; Li, Y., Rapid and effective removal of Cr(VI) from aqueous solutions using the FeCl3/NaBH4 system. *Chemical Engineering Journal* **2016,** *296*, 340-348.
263. He, Y. T.; Chen; Traina, S. J., Inhibited Cr(VI) Reduction by Aqueous Fe(II) under Hyperalkaline Conditions. *Environmental Science & Technology* **2004,** *38*, (21), 5535-5539.
264. Ai, Z.; Gao, Z.; Zhang, L.; He, W.; Yin, J. J., Core–shell structure dependent reactivity of Fe@ Fe2O3 nanowires on aerobic degradation of 4-chlorophenol. *Environmental Science & Technology* **2013,** *47*, (10), 5344-5352.
265. Diao, Z.-H.; Xu, X.-R.; Chen, H.; Jiang, D.; Yang, Y.-X.; Kong, L.-J.; Sun, Y.-X.; Hu, Y.-X.; Hao, Q.-W.; Liu, L., Simultaneous removal of Cr(VI) and phenol by persulfate activated with bentonite-supported nanoscale zero-valent iron: Reactivity and mechanism. *Journal of Hazardous Materials* **2016,** *316*, 186-193.
266. Jeen, S.-W.; Blowes, D. W.; Gillham, R. W., Performance evaluation of granular iron for removing hexavalent chromium under different geochemical conditions. *Journal of Contaminant Hydrology* **2008,** *95*, (1), 76-91.
267. Rhodes, F.; Carty, J., The Corrosion of Certain Metals by Carbon Tetrachloride. *Industrial & Engineering Chemistry* **1925,** *17*, (9), 909-911.
268. Blowes, D. W.; Ptacek, C. J.; Benner, S. G.; McRae, C. W.; Bennett, T. A.; Puls, R. W., Treatment of inorganic contaminants using permeable reactive barriers. *Journal of contaminant hydrology* **2000,** *45*, (1-2), 123-137.
269. ITRC, Permeable reactive barrier: Technology update. In Interstate Technology & Regulatory

Council: 2011.
270. Obiri-Nyarko, F.; Grajales-Mesa, S. J.; Malina, G., An overview of permeable reactive barriers for in situ sustainable groundwater remediation. *Chemosphere* **2014,** *111*, 243-259.
271. Cundy, A. B.; Hopkinson, L.; Whitby, R. L. D., Use of iron-based technologies in contaminated land and groundwater remediation: A review. *Science of The Total Environment* **2008,** *400*, (1), 42-51.
272. Blowes, D. W.; Ptacek, C. J.; Jambor, J. L., In-situ remediation of Cr (VI)-contaminated groundwater using permeable reactive walls: laboratory studies. *Environmental Science & Technology* **1997,** *31*, (12), 3348-3357.
273. Wilkin, R. T.; Puls, R. W.; Sewell, G. W., Long-Term Performance of Permeable Reactive Barriers Using Zero-Valent Iron: Geochemical and Microbiological Effects. *Groundwater* **2003,** *41*, (4), 493-503.
274. Phillips, D.; Watson, D.; Roh, Y.; Gu, B., Mineralogical Characteristics and Transformations during Long-Term Operation of a Zerovalent Iron Reactive Barrier. *Journal of environmental quality* **2003,** *32*, 2033-45.
275. Lai, K.; Lo, I.; Birkelund, V.; Kjeldsen, P., Field Monitoring of Permeable Reactive Barrier for Removal of Chlorinated Organics. *Journal of Environmental Engineering* **2006,** *132*.
276. Lo, I. M. C.; Lam, C. S. C.; Lai, K. C. K., Hardness and carbonate effects on the reactivity of zero-valent iron for Cr(VI) removal. *Water Research* **2006,** *40*, (3), 595-605.
277. Lai, K. C.; Lo, I. M., Removal of chromium (VI) by acid-washed zero-valent iron under various groundwater geochemistry conditions. *Environmental Science & Technology* **2008,** *42*, (4), 1238-1244.
278. Roh, Y.; Lee, S.; Elless, M. J. E. G., Characterization of corrosion products in the permeable reactive barriers. *Environmental Geology* **2000,** *40*, (1-2), 184-194.
279. Ritter, K.; Odziemkowski, M. S.; Gillham, R. W., An in situ study of the role of surface films on granular iron in the permeable iron wall technology. *Journal of Contaminant Hydrology* **2002,** *55*, (1), 87-111.
280. Carniato, L.; Schoups, G.; Seuntjens, P.; Van Nooten, T.; Simons, Q.; Bastiaens, L., Predicting longevity of iron permeable reactive barriers using multiple iron deactivation models. *Journal of Contaminant Hydrology* **2012,** *142-143*, 93-108.
281. Mak; Lo, I. M., Environmental life cycle assessment of permeable reactive barriers: effects of construction methods, reactive materials and groundwater constituents. *Environmental science & technology* **2011,** *45*, (23), 10148-10154.
282. Wilkin, R. T.; Su, C.; Ford, R. G.; Paul, C. J., Chromium-Removal Processes during Groundwater Remediation by a Zerovalent Iron Permeable Reactive Barrier. *Environmental Science & Technology* **2005,** *39*, (12), 4599-4605.
283. Bronstein, K. J. N. N. o. E. M. S. F., Permeable reactive barriers for inorganic and radionuclide contamination. **2005**.
284. Henderson, A. D.; Demond, A. H. J. E. E. S., Long-term performance of zero-valent iron permeable reactive barriers: a critical review. *Environmental Engineering Science* **2007,** *24*, (4), 401-423.
285. Sun, X.; Yan, Y.; Li, J.; Han, W.; Wang, L., SBA-15-incorporated nanoscale zero-valent iron particles for chromium(VI) removal from groundwater: Mechanism, effect of pH, humic acid and sustained reactivity. *Journal of Hazardous Materials* **2014,** *266*, 26-33.

286. Fu; Yang, Y.; Xu, Z.; Zhang, X.; Guo, X.; Bi, D., The removal of chromium (VI) and lead (II) from groundwater using sepiolite-supported nanoscale zero-valent iron (S-NZVI). *Chemosphere* **2015,** *138*, 726-734.
287. Qu, G.; Kou, L.; Wang, T.; Liang, D.; Hu, S., Evaluation of activated carbon fiber supported nanoscale zero-valent iron for chromium (VI) removal from groundwater in a permeable reactive column. *Journal of Environmental Management* **2017,** *201*, 378-387.
288. Mueller, N. C.; Braun, J.; Bruns, J.; Černík, M.; Rissing, P.; Rickerby, D.; Nowack, B., Application of nanoscale zero valent iron (NZVI) for groundwater remediation in Europe. *Environmental Science and Pollution Research* **2012,** *19*, (2), 550-558.
289. Ludwig, R. D.; Su, C.; Lee, T. R.; Wilkin, R. T.; Acree, S. D.; Ross, R. R.; Keeley, A., In Situ Chemical Reduction of Cr(VI) in Groundwater Using a Combination of Ferrous Sulfate and Sodium Dithionite: A Field Investigation. *Environmental Science & Technology* **2007,** *41*, (15), 5299-5305.
290. Elliott, D. W.; Zhang, W.-x., Field Assessment of Nanoscale Bimetallic Particles for Groundwater Treatment. *Environmental Science & Technology* **2001,** *35*, (24), 4922-4926.
291. He, F.; Zhao, D.; Paul, C., Field assessment of carboxymethyl cellulose stabilized iron nanoparticles for in situ destruction of chlorinated solvents in source zones. *Water Research* **2010,** *44*, (7), 2360-2370.
292. He, F.; Zhao, D., Manipulating the Size and Dispersibility of Zerovalent Iron Nanoparticles by Use of Carboxymethyl Cellulose Stabilizers. *Environmental Science & Technology* **2007,** *41*, (17), 6216-6221.
293. Yang; Cai, J.; Wang, X.; Li, Y.; Wu, Z.; Wu, W. D.; Chen, X. D.; Sun, J.; Sun, S.-P.; Wang, Z., A Bimetallic Fe–Mn Oxide-Activated Oxone for In Situ Chemical Oxidation (ISCO) of Trichloroethylene in Groundwater: Efficiency, Sustained Activity, and Mechanism Investigation. *Environmental Science & Technology* **2020,** *54*, (6), 3714-3724.
294. Kocur, C. M. D.; Lomheim, L.; Molenda, O.; Weber, K. P.; Austrins, L. M.; Sleep, B. E.; Boparai, H. K.; Edwards, E. A.; O' Carroll, D. M., Long-Term Field Study of Microbial Community and Dechlorinating Activity Following Carboxymethyl Cellulose-Stabilized Nanoscale Zero-Valent Iron Injection. *Environmental Science & Technology* **2016,** *50*, (14), 7658-7670.
295. Němeček, J.; Lhotský, O.; Cajthaml, T., Nanoscale zero-valent iron application for in situ reduction of hexavalent chromium and its effects on indigenous microorganism populations. *Science of The Total Environment* **2014,** *485-486*, 739-747.
296. Dong, H.; Deng, J.; Xie, Y.; Zhang, C.; Jiang, Z.; Cheng, Y.; Hou, K.; Zeng, G., Stabilization of nanoscale zero-valent iron (nZVI) with modified biochar for Cr(VI) removal from aqueous solution. *Journal of Hazardous Materials* **2017,** *332*, 79-86.
297. Hu, Y.-b.; Zhang, M.; Li, X.-y., Improved longevity of nanoscale zero-valent iron with a magnesium hydroxide coating shell for the removal of Cr(VI) in sand columns. *Environment International* **2019,** *133*, 105249.
298. Xue, W.; Huang, D.; Zeng, G.; Wan, J.; Cheng, M.; Zhang, C.; Hu, C.; Li, J., Performance and toxicity assessment of nanoscale zero valent iron particles in the remediation of contaminated soil: A review. *Chemosphere* **2018,** *210*, 1145-1156.
299. Lefevre, E.; Bossa, N.; Wiesner, M. R.; Gunsch, C. K., A review of the environmental implications of in situ remediation by nanoscale zero valent iron (nZVI): Behavior, transport and impacts on microbial communities. *Sci Total Environ* **2016,** *565*, 889-901.
300. El-Temsah, Y. S.; Joner, E. J., Ecotoxicological effects on earthworms of fresh and aged nano-

sized zero-valent iron (nZVI) in soil. *Chemosphere* **2012,** *89*, (1), 76-82.
301. Brasili, E.; Bavasso, I.; Petruccelli, V.; Vilardi, G.; Valletta, A.; Bosco, C. D.; Gentili, A.; Pasqua, G.; Di Palma, L., Remediation of hexavalent chromium contaminated water through zero-valent iron nanoparticles and effects on tomato plant growth performance. *Scientific Reports* **2020,** *10*, (1), 1920.
302. Dong, H.; He, Q.; Zeng, G.; Tang, L.; Zhang, C.; Xie, Y.; Zeng, Y.; Zhao, F.; Wu, Y., Chromate removal by surface-modified nanoscale zero-valent iron: Effect of different surface coatings and water chemistry. *Journal of Colloid and Interface Science* **2016,** *471*, 7-13.
303. Fang, Y.; Wu, X.; Dai, M.; Lopez-Valdivieso, A.; Raza, S.; Ali, I.; Peng, C.; Li, J.; Naz, I., The sequestration of aqueous Cr(VI) by zero valent iron-based materials: From synthesis to practical application. *J. Clean. Prod.* **2021,** *312*, 127678.
304. Guan, X.; Sun, Y.; Qin, H.; Li, J.; Lo, I. M. C.; He, D.; Dong, H., The limitations of applying zero-valent iron technology in contaminants sequestration and the corresponding countermeasures: The development in zero-valent iron technology in the last two decades (1994–2014). *Water Res.* **2015,** *75*, 224-248.
305. Dou, X.; Li, R.; Zhao, B.; Liang, W., Arsenate removal from water by zero-valent iron/activated carbon galvanic couples. *J. Hazard. Mater.* **2010,** *182*, (1), 108-114.
306. Luo, J.; Song, G.; Liu, J.; Qian, G.; Xu, Z. P., Mechanism of enhanced nitrate reduction via micro-electrolysis at the powdered zero-valent iron/activated carbon interface. *J. Colloid Interface Sci.* **2014,** *435*, 21-25.
307. Chang, Q.; Lin, W.; Ying, W.-c., Preparation of iron-impregnated granular activated carbon for arsenic removal from drinking water. *J. Hazard. Mater.* **2010,** *184*, (1), 515-522.
308. Lee, Y.-C.; Li, Y.-f.; Chen, M.-J.; Chen, Y.-C.; Kuo, J.; Lo, S.-L., Efficient decomposition of perfluorooctanic acid by persulfate with iron-modified activated carbon. *Water Res.* **2020,** *174*, 115618.
309. Rey, A.; Faraldos, M.; Casas, J. A.; Zazo, J. A.; Bahamonde, A.; Rodríguez, J. J., Catalytic wet peroxide oxidation of phenol over Fe/AC catalysts: Influence of iron precursor and activated carbon surface. *Appl. Catal., B: Environ* **2009,** *86*, (1), 69-77.
310. Shimada, H.; Akazawa, T.; Ikenaga, N.-o.; Suzuki, T., Dehydrogenation of isobutane to isobutene with iron-loaded activated carbon catalyst. *Applied Catalysis A: General* **1998,** *168*, (2), 243-250.
311. Ratso, S.; Sougrati, M. T.; Käärik, M.; Merisalu, M.; Rähn, M.; Kisand, V.; Kikas, A.; Paiste, P.; Leis, J.; Sammelselg, V.; Jaouen, F.; Tammeveski, K., Effect of Ball-Milling on the Oxygen Reduction Reaction Activity of Iron and Nitrogen Co-doped Carbide-Derived Carbon Catalysts in Acid Media. *ACS Applied Energy Materials* **2019,** *2*, (11), 7952-7962.
312. Zou, H.; Zhao, J.; He, F.; Zhong, Z.; Huang, J.; Zheng, Y.; Zhang, Y.; Yang, Y.; Yu, F.; Bashir, M. A.; Gao, B., Ball milling biochar iron oxide composites for the removal of chromium (Cr(VI)) from water: Performance and mechanisms. *J. Hazard. Mater.* **2021,** *413*, 125252.
313. Lyu, H.; Tang, J.; Cui, M.; Gao, B.; Shen, B., Biochar/iron (BC/Fe) composites for soil and groundwater remediation: Synthesis, applications, and mechanisms. *Chemosphere* **2020,** *246*, 125609.
314. Shan, D.; Deng, S.; Zhao, T.; Wang, B.; Wang, Y.; Huang, J.; Yu, G.; Winglee, J.; Wiesner, M. R., Preparation of ultrafine magnetic biochar and activated carbon for pharmaceutical adsorption and subsequent degradation by ball milling. *J. Hazard. Mater.* **2016,** *305*, 156-163.

315. Lyu, H.; Gao, B.; He, F.; Zimmerman, A. R.; Ding, C.; Huang, H.; Tang, J., Effects of ball milling on the physicochemical and sorptive properties of biochar: Experimental observations and governing mechanisms. *Environ. Pollut.* **2018,** *233*, 54-63.
316. Xu, X.; Xu, Z.; Huang, J.; Gao, B.; Zhao, L.; Qiu, H.; Cao, X., Sorption of reactive red by biochars ball milled in different atmospheres: Co-effect of surface morphology and functional groups. *Chem. Eng. J.* **2020**, 127468.
317. Takacs, L., Quicksilver from cinnabar: The first documented mechanochemical reaction? *JOM* **2000,** *52*, (1), 12-13.
318. Peters, K.; Pajakoff, S., Mechanochemische Farbreaktionen. *Microchimica Acta* **1962,** *50*, (1), 314-320.
319. Feng, K.; Xu, Z.; Gao, B.; Xu, X.; Zhao, L.; Qiu, H.; Cao, X., Mesoporous ball-milling iron-loaded biochar for enhanced sorption of reactive red: Performance and mechanisms. *Environ. Pollut.* **2021,** *290*, 117992.
320. Su, Y.; Jassby, D.; Song, S.; Zhou, X.; Zhao, H.; Filip, J.; Petala, E.; Zhang, Y., Enhanced Oxidative and Adsorptive Removal of Diclofenac in Heterogeneous Fenton-like Reaction with Sulfide Modified Nanoscale Zerovalent Iron. *Environ. Sci. Technol.* **2018,** *52*, (11), 6466-6475.
321. Zhang, W.; Huang, J.; Xu, F.; Deng, S.; Zhu, W.; Yu, G., Mechanochemical destruction of pentachloronitrobenzene with reactive iron powder. *J. Hazard. Mater.* **2011,** *198*, 275-281.
322. Zhang, K.; Huang, J.; Yu, G.; Zhang, Q.; Deng, S.; Wang, B., Destruction of Perfluorooctane Sulfonate (PFOS) and Perfluorooctanoic Acid (PFOA) by Ball Milling. *Environ. Sci. Technol.* **2013,** *47*, (12), 6471-6477.
323. Zhang, W.; Wang, H.; Jun, H.; Yu, M.; Wang, F.; Zhou, L.; Yu, G., Acceleration and mechanistic studies of the mechanochemical dechlorination of HCB with iron powder and quartz sand. *Chem. Eng. J.* **2014,** *239*, 185-191.
324. Gao, J.; Wang, W.; Rondinone, A. J.; He, F.; Liang, L., Degradation of Trichloroethene with a Novel Ball Milled Fe–C Nanocomposite. *J. Hazard. Mater.* **2015,** *300*, 443-450.
325. Kang, S.; Liu, S.; Wang, H.; Cai, W., Enhanced degradation performances of plate-like micro/nanostructured zero valent iron to DDT. *J. Hazard. Mater.* **2016,** *307*, 145-153.
326. Cagnetta, G.; Huang, J.; Lomovskiy, I. O.; Yu, G., Tailoring the properties of a zero-valent iron-based composite by mechanochemistry for nitrophenols degradation in wastewaters. *Environ. Technol.* **2017,** *38*, (22), 2916-2927.
327. Wang, S.; Song, Y.; Sun, Y., Enhanced dyes removal by sulfidated zerovalent iron: Kinetics and influencing factors. *Environ. Technol. Innov.* **2018,** *11*, 339-347.
328. Wang, K.; Liu, X.; Tang, J.; Wang, L.; Sun, H., Ball milled Fe0@FeS hybrids coupled with peroxydisulfate for Cr(VI) and phenol removal: Novel surface reduction and activation mechanisms. *Sci. Total Environ.* **2020,** *739*, 139748.
329. He, J.; Tang, J.; Zhang, Z.; Wang, L.; Liu, Q.; Liu, X., Magnetic ball-milled FeS@biochar as persulfate activator for degradation of tetracycline. *Chem. Eng. J.* **2021,** *404*, 126997.
330. Chen, Y.; Halstead, T.; Williams, J. S., Influence of milling temperature and atmosphere on the synthesis of iron nitrides by ball milling. *Mater. Sci. Eng., A* **1996,** *206*, (1), 24-29.
331. Baláž, P., *Extractive metallurgy of activated minerals*. Elsevier: 2000.
332. Tan, Y.; Sha, L.; Qu, J.; Jiang, J.; Ren, J.; Wu, C.; Xu, Z., Oleic acid as grinding aid and surface antioxidant for ultrafine zirconium hydride particle preparation. *Appl. Surf. Sci.* **2021,** *535*, 147688.
333. Yang, Z.; Ma, X.; Shan, C.; Guan, X.; Zhang, W.; Lv, L.; Pan, B., Activation of zero-valent iron

through ball-milling synthesis of hybrid Fe0/Fe3O4/FeCl2 microcomposite for enhanced nitrobenzene reduction. *J. Hazard. Mater.* **2019,** *368*, 698-704.

334. Guan, X.; Yang, H.; Sun, Y.; Qiao, J., Enhanced immobilization of chromium(VI) in soil using sulfidated zero-valent iron. *Chemosphere* **2019,** *228*, 370-376.

335. Du, M.; Zhang, Y.; Zeng, X.; Kuang, H.; Huang, S., Enhancement of ball-miling on pyrite/zero-valent iron for arsenic removal in water: A mechanistic study. *Chemosphere* **2020,** *249*, 126130.

336. Shen, W.; Zhang, J.; Xiao, M.; Zhang, X.; Li, J.; Jiang, W.; Yan, J.; qin, Z.; Zhang, S.; He, W.; He, Y., Ethylenediaminetetraacetic acid induces surface erosion of zero-valent iron for enhanced hexavalent chromium removal. *Appl. Surf. Sci.* **2020,** *525*, 146593.

337. Qiao, J.; Liu, Y.; Yang, H.; Guan, X.; Sun, Y., Remediation of arsenic contaminated soil by sulfidated zero-valent iron. *Front. Environ. Sci. Eng.* **2020,** *15*, (5), 83.

338. Kang, S.; Wang, G.; Zhao, H.; Cai, W., Ball Milling-Induced Plate-like Sub-microstructured Iron for Enhancing Degradation of DDT in a Real Soil Environment. *ACS Omega* **2018,** *3*, (6), 6955-6961.

339. Liu, X.; Lai, D.; Wang, Y., Performance of Pb(II) removal by an activated carbon supported nanoscale zero-valent iron composite at ultralow iron content. *J. Hazard. Mater.* **2019,** *361*, 37-48.

340. Vaughan, R. L.; Reed, B. E., Modeling As(V) removal by a iron oxide impregnated activated carbon using the surface complexation approach. *Water Res.* **2005,** *39*, (6), 1005-1014.

341. Liu, C.; Liu, L.; Tian, X.; Wang, Y.; Li, R.; Zhang, Y.; Song, Z.; Xu, B.; Chu, W.; Qi, F.; Ikhlaq, A., Coupling metal–organic frameworks and g-C3N4 to derive Fe@N-doped graphene-like carbon for peroxymonosulfate activation: Upgrading framework stability and performance. *Appl. Catal., B: Environ* **2019,** *255*, 117763.

342. Peng, L.; Duan, X.; Shang, Y.; Gao, B.; Xu, X., Engineered carbon supported single iron atom sites and iron clusters from Fe-rich Enteromorpha for Fenton-like reactions via nonradical pathways. *Appl. Catal., B: Environ* **2021,** *287*, 119963.

343. Li, Y.; Zimmerman, A. R.; He, F.; Chen, J.; Han, L.; Chen, H.; Hu, X.; Gao, B. J. S. o. T. T. E., Solvent-free synthesis of magnetic biochar and activated carbon through ball-mill extrusion with Fe3O4 nanoparticles for enhancing adsorption of methylene blue. *Sci. Total Environ.* **2020,** *722*, 137972.

344. He, D.; Niu, H.; He, S.; Mao, L.; Cai, Y.; Liang, Y., Strengthened Fenton degradation of phenol catalyzed by core/shell Fe–Pd@C nanocomposites derived from mechanochemically synthesized Fe-Metal organic frameworks. *Water Res.* **2019,** *162*, 151-160.

345. Lv, H.; Niu, H.; Zhao, X.; Cai, Y.; Wu, F., Carbon zero-valent iron materials possessing high-content fine Fe0 nanoparticles with enhanced microelectrolysis-Fenton-like catalytic performance for water purification. *Appl. Catal., B: Environ* **2021,** *286*, 119940.

346. Meng, P.; Fang, X.; Maimaiti, A.; Yu, G.; Deng, S. J. C., Efficient removal of perfluorinated compounds from water using a regenerable magnetic activated carbon. *Chemosphere* **2019,** *224*, 187-194.

347. Li, R.; Zhang, Y.; Deng, H.; Zhang, Z.; Wang, J. J.; Shaheen, S. M.; Xiao, R.; Rinklebe, J.; Xi, B.; He, X.; Du, J., Removing tetracycline and Hg(II) with ball-milled magnetic nanobiochar and its potential on polluted irrigation water reclamation. *J. Hazard. Mater.* **2020,** *384*, 121095.

348. Huang, X.-y.; Ling, L.; Zhang, W.-x., Nanoencapsulation of hexavalent chromium with nanoscale zero-valent iron: High resolution chemical mapping of the passivation layer. *J Environ*

Sci **2018,** *67*, 4-13.
349. Xin, J.; Tang, F.; Zheng, X.; Shao, H.; Kolditz, O.; Lu, X., Distinct kinetics and mechanisms of mZVI particles aging in saline and fresh groundwater: H2 evolution and surface passivation. *Water Res.* **2016,** *100*, 80-87.
350. Mitra, P.; Sarkar, D.; Chakrabarti, S.; Dutta, B. K., Reduction of hexa-valent chromium with zero-valent iron: Batch kinetic studies and rate model. *Chem. Eng. J.* **2011,** *171*, (1), 54-60.
351. Dong, H.; Zhang, C.; Deng, J.; Jiang, Z.; Zhang, L.; Cheng, Y.; Hou, K.; Tang, L.; Zeng, G., Factors influencing degradation of trichloroethylene by sulfide-modified nanoscale zero-valent iron in aqueous solution. *Water Res.* **2018,** *135*, 1-10.
352. Lü, Y.; Li, Z.; Li, J.; Chen, K.; Dong, H.; Shou, J.; Li, Y., Synergetic effect of pyrite on Cr(VI) removal by zero valent iron in column experiments: An investigation of mechanisms. *Chem. Eng. J.* **2018,** *349*, 522-529.
353. Du, M.; Zhang, Y.; Hussain, I.; Du, X.; Huang, S.; Wen, W., Effect of pyrite on enhancement of zero-valent iron corrosion for arsenic removal in water: A mechanistic study. *Chemosphere* **2019,** *233*, 744-753.
354. Kim, E.-J.; Kim, J.-H.; Azad, A.-M.; Chang, Y.-S., Facile Synthesis and Characterization of Fe/FeS Nanoparticles for Environmental Applications. *ACS Appl. Mater. Interfaces* **2011,** *3*, (5), 1457-1462.
355. Cai, S.; Chen, B.; Qiu, X.; Li, J.; Tratnyek, P. G.; He, F., Sulfidation of Zero-Valent Iron by Direct Reaction with Elemental Sulfur in Water: Efficiencies, Mechanism, and Dechlorination of Trichloroethylene. *Environ. Sci. Technol.* **2021,** *55*, (1), 645-654.
356. Min, X.; Li, Y.; Ke, Y.; Shi, M.; Chai, L.; Xue, K., Fe-FeS2 adsorbent prepared with iron powder and pyrite by facile ball milling and its application for arsenic removal. *Water Sci. Technol.* **2017,** *76*, (1), 192-200.
357. He, X.; Min, X.; Peng, T.; Ke, Y.; Zhao, F.; Sillanpää, M.; Wang, Y., Enhanced adsorption of antimonate by ball-milled microscale zero valent iron/pyrite composite: adsorption properties and mechanism insight. *Environ. Sci. Pollut. Res.* **2020,** *27*, (14), 16484-16495.
358. Brumovský, M.; Filip, J.; Malina, O.; Oborná, J.; Sracek, O.; Reichenauer, T. G.; Andrýsková, P.; Zbořil, R., Core–Shell Fe/FeS Nanoparticles with Controlled Shell Thickness for Enhanced Trichloroethylene Removal. *ACS Appl. Mater. Interfaces* **2020,** *12*, (31), 35424-35434.
359. Mangayayam, M.; Dideriksen, K.; Ceccato, M.; Tobler, D. J., The Structure of Sulfidized Zero-Valent Iron by One-Pot Synthesis: Impact on Contaminant Selectivity and Long-Term Performance. *Environ. Sci. Technol.* **2019,** *53*, (8), 4389-4396.
360. Garcia, A. N.; Zhang, Y.; Ghoshal, S.; He, F.; O' Carroll, D. M., Recent Advances in Sulfidated Zerovalent Iron for Contaminant Transformation. *Environ. Sci. Technol.* **2021,** *55*, (13), 8464-8483.
361. Xu, J.; Avellan, A.; Li, H.; Clark, E. A.; Henkelman, G.; Kaegi, R.; Lowry, G. V., Iron and Sulfur Precursors Affect Crystalline Structure, Speciation, and Reactivity of Sulfidized Nanoscale Zerovalent Iron. *Environ. Sci. Technol.* **2020,** *54*, (20), 13294-13303.
362. Wen, J.; Liu, X.; Liu, L.; Ma, X.; Fakhri, A.; Gupta, V. K., Bimetal cobalt-Iron based organic frameworks with coordinated sites as synergistic catalyst for fenton catalysis study and antibacterial efficiency. *Colloids Surf, A Physicochem Eng Asp* **2021,** *610*, 125683.
363. Li, X.; Dou, X.; Li, J., Antimony(V) removal from water by iron-zirconium bimetal oxide: Performance and mechanism. *J Environ Sci* **2012,** *24*, (7), 1197-1203.
364. Fang, L.; Liu, K.; Li, F.; Zeng, W.; Hong, Z.; Xu, L.; Shi, Q.; Ma, Y., New insights into stoichiometric

efficiency and synergistic mechanism of persulfate activation by zero-valent bimetal (Iron/Copper) for organic pollutant degradation. *J. Hazard. Mater.* **2021,** *403*, 123669.

365. Huang, Q.; Liu, W.; Peng, P. a.; Huang, W., Reductive debromination of tetrabromobisphenol A by Pd/Fe bimetallic catalysts. *Chemosphere* **2013,** *92*, (10), 1321-1327.

366. Liu, J.; Luo, K.; Li, X.; Yang, Q.; Wang, D.; Wu, Y.; Chen, Z.; Huang, X.; Pi, Z.; Du, W.; Guan, Z., The biochar-supported iron-copper bimetallic composite activating oxygen system for simultaneous adsorption and degradation of tetracycline. *Chem. Eng. J.* **2020,** *402*, 126039.

367. Li, T.; Chen, Y.; Wan, P.; Fan, M.; Yang, X. J., Chemical Degradation of Drinking Water Disinfection Byproducts by Millimeter-Sized Particles of Iron−Silicon and Magnesium−Aluminum Alloys. *JACS* **2010,** *132*, (8), 2500-2501.

368. Zhu, H.; Xu, F.; Zhao, J.; Jia, L.; Wu, K., Catalytic hydrodechlorination of monochloroacetic acid in wastewater using Ni-Fe bimetal prepared by ball milling. *Environ. Sci. Pollut. Res.* **2015,** *22*, (18), 14299-14306.

369. Fan, J.; Qin, H.; Zhang, Y.; Jiang, S., Degradation of 4-chlorophenol by BM Fe/Cu-O2 system: The symbiosis of and ·OH radicals. *Water Environ. Res* **2019,** *91*, (8), 770-779.

370. Li, H.; Qiu, Y.-f.; Wang, X.-l.; Yang, J.; Yu, Y.-j.; Chen, Y.-q.; Liu, Y.-d., Biochar supported Ni/Fe bimetallic nanoparticles to remove 1,1,1-trichloroethane under various reaction conditions. *Chemosphere* **2017,** *169*, 534-541.

371. Wen, Z.; Lu, J.; Zhang, Y.; Cheng, G.; Guo, S.; Wei, P.; Ming, Y.-a.; Wang, Y.; Chen, R., Simultaneous oxidation and immobilization of arsenite from water by nanosized magnetic mesoporous iron manganese bimetal oxides (Nanosized-MMIM): Synergistic effect and interface catalysis. *Chem. Eng. J.* **2020,** *391*, 123578.

372. Simeonidis, K.; Gkinis, T.; Tresintsi, S.; Martinez-Boubeta, C.; Vourlias, G.; Tsiaoussis, I.; Stavropoulos, G.; Mitrakas, M.; Angelakeris, M., Magnetic separation of hematite-coated Fe3O4 particles used as arsenic adsorbents. *Chem. Eng. J.* **2011,** *168*, (3), 1008-1015.

373. Bujňáková, Z.; Baláž, P.; Zorkovská, A.; Sayagués, M. J.; Kováč, J.; Timko, M., Arsenic sorption by nanocrystalline magnetite: An example of environmentally promising interface with geosphere. *J. Hazard. Mater.* **2013,** *262*, 1204-1212.

374. Li, Y.; Li, J.; Zhang, Y., Mechanism insights into enhanced Cr(VI) removal using nanoscale zerovalent iron supported on the pillared bentonite by macroscopic and spectroscopic studies. *J. Hazard. Mater.* **2012,** *227-228*, 211-218.

375. Lin, Y.; Chen, Z.; Chen, Z.; Megharaj, M.; Naidu, R., Decoloration of acid violet red B by bentonite-supported nanoscale zero-valent iron: Reactivity, characterization, kinetics and reaction pathway. *Appl. Clay Sci.* **2014,** *93-94*, 56-61.

376. Wei, G.; Li, Y.; Zhang, L.; Cai, S.; Zhu, T.; Li, Z.; Mo, J., Synthesis of bentonite-supported Fe(II) and heteropolyacid (HPW) composite through a mechanochemical processing. *Appl. Clay Sci.* **2018,** *152*, 342-351.

377. Neumann, A.; Hofstetter, T. B.; Skarpeli-Liati, M.; Schwarzenbach, R. P., Reduction of Polychlorinated Ethanes and Carbon Tetrachloride by Structural Fe(II) in Smectites. *Environ. Sci. Technol.* **2009,** *43*, (11), 4082-4089.

378. Williams, A. G. B.; Scherer, M. M., Kinetics of Cr(VI) Reduction by Carbonate Green Rust. *Environ. Sci. Technol.* **2001,** *35*, (17), 3488-3494.

379. Demoisson, F.; Mullet, M.; Humbert, B., Pyrite Oxidation by Hexavalent Chromium: Investigation of the Chemical Processes by Monitoring of Aqueous Metal Species. *Environ. Sci.*

Technol. **2005,** *39*, (22), 8747-8752.
380. Jeong, H. Y.; Kim, H.; Hayes, K. F., Reductive Dechlorination Pathways of Tetrachloroethylene and Trichloroethylene and Subsequent Transformation of Their Dechlorination Products by Mackinawite (FeS) in the Presence of Metals. *Environ. Sci. Technol.* **2007,** *41*, (22), 7736-7743.
381. Du, M.; Kuang, H.; Zhang, Y.; Zeng, X.; Yi, C.; Hussain, I.; Huang, S.; Zhao, S., Enhancement of ball-milling on pyrite/zero-valent iron for persulfate activation on imidacloprid removal in aqueous solution: A mechanistic study. *J. Environ. Chem. Eng.* **2021,** *9*, (4), 105647.
382. Tang, J.; Zhao, B.; Lyu, H.; Li, D., Development of a novel pyrite/biochar composite (BM-FeS2@BC) by ball milling for aqueous Cr(VI) removal and its mechanisms. *J. Hazard. Mater.* **2021,** *413*, 125415.
383. Furukawa, H.; Cordova, K. E.; O' Keeffe, M.; Yaghi, O. M., The Chemistry and Applications of Metal-Organic Frameworks. *Science* **2013,** *341*, (6149), 1230444.
384. Mueller, U.; Schubert, M.; Teich, F.; Puetter, H.; Schierle-Arndt, K.; Pastré, J., Metal–organic frameworks—prospective industrial applications. *J. Mater. Chem.* **2006,** *16*, (7), 626-636.
385. Głowniak, S.; Szczęśniak, B.; Choma, J.; Jaroniec, M., Mechanochemistry: Toward green synthesis of metal–organic frameworks. *Mater. Today* **2021,** *46*, 109-124.
386. Hou, S.; Wu, Y.-n.; Feng, L.; Chen, W.; Wang, Y.; Morlay, C.; Li, F., Green synthesis and evaluation of an iron-based metal–organic framework MIL-88B for efficient decontamination of arsenate from water. *Dalton Trans.* **2018,** *47*, (7), 2222-2231.
387. Chen, D.-D.; Yi, X.-H.; Zhao, C.; Fu, H.; Wang, P.; Wang, C.-C., Polyaniline modified MIL-100(Fe) for enhanced photocatalytic Cr(VI) reduction and tetracycline degradation under white light. *Chemosphere* **2020,** *245*, 125659.
388. Lee, H. K.; Lee, J. H.; Moon, H. R., Mechanochemistry as a Reconstruction Tool of Decomposed Metal–Organic Frameworks. *Inorg. Chem.* **2021,** *60*, (16), 11825-11829.
389. Xu, J.; Pu, Y.; Yang, X. J.; Wan, P.; Wang, R.; Song, P.; Fisher, A., Rapid removal of chloroform, carbon tetrachloride and trichloroethylene in water by aluminum–iron alloy particles. *Environ. Technol.* **2018,** *39*, (22), 2882-2890.
390. Zhuang, Y.; Han, B.; Chen, R.; Shi, B., Structural transformation and potential toxicity of iron-based deposits in drinking water distribution systems. *Water Res.* **2019,** *165*, 114999.
391. Cadmus, P.; Brinkman, S. F.; May, M. K., Chronic Toxicity of Ferric Iron for North American Aquatic Organisms: Derivation of a Chronic Water Quality Criterion Using Single Species and Mesocosm Data. *Arch. Environ. Contam. Toxicol.* **2018,** *74*, (4), 605-615.
392. Biesinger, K. E.; Christensen, G. M., Effects of Various Metals on Survival, Growth, Reproduction, and Metabolism of Daphnia magna. *J. Fish. Res. Board Can.* **1972,** *29*, (12), 1691-1700.
393. Gong, L.; Qi, J.; Lv, N.; Qiu, X.; Gu, Y.; Zhao, J.; He, F., Mechanistic role of nitrate anion in TCE dechlorination by ball milled ZVI and sulfidated ZVI: Experimental investigation and theoretical analysis. *J. Hazard. Mater.* **2021,** *403*, 123844.
394. Mokete, R.; Eljamal, O. In *Analogy of iron-copper and iron-silver bimetals during the corrosion process*, Proceedings of International Exchange and Innovation Conference on Engineering & Sciences (IEICES), 2019; Interdisciplinary Graduate School of Engineering Sciences, Kyushu University: 2019; pp 16-18.
395. Nie, X.; Liu, J.; Zeng, X.; Yue, D., Rapid degradation of hexachlorobenzene by micron Ag/Fe bimetal particles. *J Environ Sci* **2013,** *25*, (3), 473-478.

396. Wang, S.; Gao, B.; Li, Y.; Creamer, A. E.; He, F., Adsorptive removal of arsenate from aqueous solutions by biochar supported zero-valent iron nanocomposite: Batch and continuous flow tests. *J. Hazard. Mater.* **2017,** *322*, 172-181.
397. Zhu, S.; Huang, X.; Wang, D.; Wang, L.; Ma, F., Enhanced hexavalent chromium removal performance and stabilization by magnetic iron nanoparticles assisted biochar in aqueous solution: Mechanisms and application potential. *Chemosphere* **2018,** *207*, 50-59.
398. Zhou, L.; Thanh, T. L.; Gong, J.; Kim, J.-H.; Kim, E.-J.; Chang, Y.-S., Carboxymethyl cellulose coating decreases toxicity and oxidizing capacity of nanoscale zerovalent iron. *Chemosphere* **2014,** *104*, 155-161.
399. Dong, H.; Xie, Y.; Zeng, G.; Tang, L.; Liang, J.; He, Q.; Zhao, F.; Zeng, Y.; Wu, Y., The dual effects of carboxymethyl cellulose on the colloidal stability and toxicity of nanoscale zero-valent iron. *Chemosphere* **2016,** *144*, 1682-1689.
400. Jung Lin, C.; Lo, S.-L., Effects of iron surface pretreatment on sorption and reduction kinetics of trichloroethylene in a closed batch system. *Water Res.* **2005,** *39*, (6), 1037-1046.
401. Liou, Y. H.; Lo, S.-L.; Lin, C.-J.; Kuan, W. H.; Weng, S. C., Effects of iron surface pretreatment on kinetics of aqueous nitrate reduction. *J. Hazard. Mater.* **2005,** *126*, (1), 189-194.
402. Su, C.; Puls, R. W., Kinetics of Trichloroethene Reduction by Zerovalent Iron and Tin: Pretreatment Effect, Apparent Activation Energy, and Intermediate Products. *Environ. Sci. Technol.* **1999,** *33*, (1), 163-168.
403. Bui, T. T.; Le, X. Q.; To, D. P.; Nguyen, V. T., Investigation of typical properties of nanocrystalline iron powders prepared by ball milling techniques. *Advances in Natural Sciences: Nanoscience and Nanotechnology* **2013,** *4*, (4), 045003.
404. Tang, W. M.; Zheng, Z. X.; Tang, H. J.; Ren, R.; Wu, Y. C., Structural evolution and grain growth kinetics of the Fe–28Al elemental powder during mechanical alloying and annealing. *Intermetallics* **2007,** *15*, (8), 1020-1026.
405. Wu, L.; Liao, L.; Lv, G.; Qin, F.; He, Y.; Wang, X., Micro-electrolysis of Cr (VI) in the nanoscale zero-valent iron loaded activated carbon. *J. Hazard. Mater.* **2013,** *254-255*, 277-283.
406. Li, Z.; Sun, Y.; Yang, Y.; Han, Y.; Wang, T.; Chen, J.; Tsang, D. C. W., Biochar-supported nanoscale zero-valent iron as an efficient catalyst for organic degradation in groundwater. *J. Hazard. Mater.* **2020,** *383*, 121240.
407. Ravikumar, K. V. G.; Kumar, D.; Kumar, G.; Mrudula, P.; Natarajan, C.; Mukherjee, A., Enhanced Cr(VI) Removal by Nanozerovalent Iron-Immobilized Alginate Beads in the Presence of a Biofilm in a Continuous-Flow Reactor. *Ind. Eng. Chem. Res.* **2016,** *55*, (20), 5973-5982.
408. Liu, H.; Ruan, X.; Zhao, D.; Fan, X.; Feng, T., Enhanced Adsorption of 2,4-Dichlorophenol by Nanoscale Zero-Valent Iron Loaded on Bentonite and Modified with a Cationic Surfactant. *Ind. Eng. Chem. Res.* **2017,** *56*, (1), 191-197.
409. Jin, X.; Zhuang, Z.; Yu, B.; Chen, Z.; Chen, Z., Functional chitosan-stabilized nanoscale zero-valent iron used to remove acid fuchsine with the assistance of ultrasound. *Carbohydr. Polym.* **2016,** *136*, 1085-1090.
410. Gu, W.; Zhang, Q.; Qu, J.; Li, Z.; Hu, H.; Liu, Y.; Li, Y.; Ai, Z., Formation of active zero-valent iron by simple co-grinding with CaCO3 to protect fresh active surface for efficient removal of hexavalent chromium. *Appl. Surf. Sci.* **2019,** *490*, 81-88.
411. Reardon, E. J., Anaerobic Corrosion of Granular Iron: Measurement and Interpretation of Hydrogen Evolution Rates. *Environ. Sci. Technol.* **1995,** *29*, (12), 2936-2945.

412. Qin, H.; Guan, X.; Bandstra, J. Z.; Johnson, R. L.; Tratnyek, P. G., Modeling the Kinetics of Hydrogen Formation by Zerovalent Iron: Effects of Sulfidation on Micro- and Nano-Scale Particles. *Environ. Sci. Technol.* **2018,** *52*, (23), 13887-13896.

413. Mohammed, O.; Mumford, K. G.; Sleep, B. E., Effects of hydrogen gas production, trapping and bubble-facilitated transport during nanoscale zero-valent iron (nZVI) injection in porous media. *J. Contam. Hydrol.* **2020,** *234*, 103677.

414. Kocur, C. M. D.; Lomheim, L.; Boparai, H. K.; Chowdhury, A. I. A.; Weber, K. P.; Austrins, L. M.; Edwards, E. A.; Sleep, B. E.; O' Carroll, D. M., Contributions of Abiotic and Biotic Dechlorination Following Carboxymethyl Cellulose Stabilized Nanoscale Zero Valent Iron Injection. *Environ. Sci. Technol.* **2015,** *49*, (14), 8648-8656.

415. Schöftner, P.; Waldner, G.; Lottermoser, W.; Stöger-Pollach, M.; Freitag, P.; Reichenauer, T. G., Electron efficiency of nZVI does not change with variation of environmental parameters. *Sci. Total Environ.* **2015,** *535*, 69-78.

416. Liu, Y.; Lowry, G. V., Effect of Particle Age (Fe0 Content) and Solution pH On NZVI Reactivity: H2 Evolution and TCE Dechlorination. *Environ. Sci. Technol.* **2006,** *40*, (19), 6085-6090.

417. Wang, C.; Wu, Y.; Qu, T.; Liu, S.; Pi, Y.; Shen, J., Enhanced Cr (VI) removal in the synergy between the hydroxyl-functionalized ball-milled ZVI/Fe3O4 composite and Na2EDTA complexation. *Chem. Eng. J.* **2019,** *359*, 874-881.

418. Wu, S.; Deng, S.; Ma, Z.; Liu, Y.; Yang, Y.; Jiang, Y., Ferrous oxalate covered ZVI through ball-milling for enhanced catalytic oxidation of organic contaminants with persulfate. *Chemosphere* **2022,** *287*, 132421.

419. Hu, Y.; Zhan, G.; Peng, X.; Liu, X.; Ai, Z.; Jia, F.; Cao, S.; Quan, F.; Shen, W.; Zhang, L., Enhanced Cr(VI) removal of zero-valent iron with high proton conductive FeC2O4·2H2O shell. *Chem. Eng. J.* **2020,** *389*, 124414.

420. Chen, K.-F.; Li, S.; Zhang, W.-x., Renewable hydrogen generation by bimetallic zero valent iron nanoparticles. *Chem. Eng. J.* **2011,** *170*, (2), 562-567.

421. Yan, W.; Herzing, A. A.; Li, X.-q.; Kiely, C. J.; Zhang, W.-x., Structural Evolution of Pd-Doped Nanoscale Zero-Valent Iron (nZVI) in Aqueous Media and Implications for Particle Aging and Reactivity. *Environ. Sci. Technol.* **2010,** *44*, (11), 4288-4294.

422. Xu, J.; Li, H.; Lowry, G. V., Sulfidized Nanoscale Zero-Valent Iron: Tuning the Properties of This Complex Material for Efficient Groundwater Remediation. *Acct. Mater. Res.* **2021,** *2*, (6), 420-431.

423. Xu, J.; Cao, Z.; Zhou, H.; Lou, Z.; Wang, Y.; Xu, X.; Lowry, G. V., Sulfur Dose and Sulfidation Time Affect Reactivity and Selectivity of Post-Sulfidized Nanoscale Zerovalent Iron. *Environ. Sci. Technol.* **2019,** *53*, (22), 13344-13352.

424. Rajajayavel, S. R. C.; Ghoshal, S., Enhanced reductive dechlorination of trichloroethylene by sulfidated nanoscale zerovalent iron. *Water Res.* **2015,** *78*, 144-153.

425. He, F.; Li, Z.; Shi, S.; Xu, W.; Sheng, H.; Gu, Y.; Jiang, Y.; Xi, B., Dechlorination of Excess Trichloroethene by Bimetallic and Sulfidated Nanoscale Zero-Valent Iron. *Environ. Sci. Technol.* **2018,** *52*, (15), 8627-8637.

426. Deng, S.; Liu, L.; Cagnetta, G.; Huang, J.; Yu, G., Mechanochemically synthesized S-ZVIbm composites for the activation of persulfate in the pH-independent degradation of atrazine: Effects of sulfur dose and ball-milling conditions. *Chem. Eng. J.* **2021,** *423*, 129789.

427. Kim, E.-J.; Kim, J.-H.; Chang, Y.-S.; Turcio-Ortega, D.; Tratnyek, P. G., Effects of Metal Ions on the Reactivity and Corrosion Electrochemistry of Fe/FeS Nanoparticles. *Environ. Sci. Technol.* **2014,**

48, (7), 4002-4011.
428. Li, D.; Zhu, X.; Zhong, Y.; Huang, W.; Peng, P. a., Abiotic transformation of hexabromocyclododecane by sulfidated nanoscale zerovalent iron: Kinetics, mechanism and influencing factors. *Water Res.* **2017,** *121*, 140-149.
429. Ling, J.; Qiao, J.; Song, Y.; Sun, Y., Influence of coexisting ions on the electron efficiency of sulfidated zerovalent iron toward Se(VI) removal. *Chem. Eng. J.* **2019,** *378*, 122124.
430. Gong, L.; Lv, N.; Qi, J.; Qiu, X.; Gu, Y.; He, F., Effects of non-reducible dissolved solutes on reductive dechlorination of trichloroethylene by ball milled zero valent irons. *J. Hazard. Mater.* **2020,** *396*, 122620.
431. Fan, P.; Sun, Y.; Zhou, B.; Guan, X., Coupled Effect of Sulfidation and Ferrous Dosing on Selenate Removal by Zerovalent Iron Under Aerobic Conditions. *Environ. Sci. Technol.* **2019,** *53*, (24), 14577-14585.
432. Nunez Garcia, A.; Boparai, H. K.; Chowdhury, A. I. A.; de Boer, C. V.; Kocur, C. M. D.; Passeport, E.; Sherwood Lollar, B.; Austrins, L. M.; Herrera, J.; O' Carroll, D. M., Sulfidated nano zerovalent iron (S-nZVI) for in situ treatment of chlorinated solvents: A field study. *Water Res.* **2020,** *174*, 115594.
433. Wu, D.; Peng, S.; Yan, K.; Shao, B.; Feng, Y.; Zhang, Y., Enhanced As(III) Sequestration Using Sulfide-Modified Nano-Scale Zero-Valent Iron with a Characteristic Core–Shell Structure: Sulfidation and As Distribution. *ACS Sustain. Chem. Eng.* **2018,** *6*, (3), 3039-3048.
434. Shi, D.; Zhang, X.; Wang, J.; Fan, J., Highly reactive and stable nanoscale zero-valent iron prepared within vesicles and its high-performance removal of water pollutants. *Appl. Catal., B: Environ* **2018,** *221*, 610-617.
435. Yabusaki, S.; Cantrell, K.; Sass, B.; Steefel, C., Multicomponent Reactive Transport in an In Situ Zero-Valent Iron Cell. *Environ. Sci. Technol.* **2001,** *35*, (7), 1493-1503.
436. Gavaskar, A.; Yoon, W.; Sminchak, J.; Sass, B.; Gupta, N.; Hicks, J.; Lal, V. *Long Term Performance Assessment of a Permeable Reactive Barrier at Former Naval AITR Station Moffett Field*; NAVAL FACILITIES ENGINEERING SERVICE CENTER PORT HUENEME CA: 2005.
437. Son, A.; Lee, J.; Chiu, P. C.; Kim, B. J.; Cha, D. K., Microbial reduction of perchlorate with zero-valent iron. *Water Res.* **2006,** *40*, (10), 2027-2032.
438. Oh, S.-Y.; Chiu, P. C.; Kim, B. J.; Cha, D. K., Zero-valent iron pretreatment for enhancing the biodegradability of RDX. *Water Res.* **2005,** *39*, (20), 5027-5032.
439. Sun, H.; Wang, L.; Zhang, R.; Sui, J.; Xu, G., Treatment of groundwater polluted by arsenic compounds by zero valent iron. *J. Hazard. Mater.* **2006,** *129*, (1), 297-303.
440. Yin, W.; Wu, J.; Huang, W.; Li, Y.; Jiang, G., The effects of flow rate and concentration on nitrobenzene removal in abiotic and biotic zero-valent iron columns. *Sci. Total Environ.* **2016,** *560-561*, 12-18.
441. Tyrovola, K.; Nikolaidis, N. P.; Veranis, N.; Kallithrakas-Kontos, N.; Koulouridakis, P. E., Arsenic removal from geothermal waters with zero-valent iron—Effect of temperature, phosphate and nitrate. *Water Res.* **2006,** *40*, (12), 2375-2386.
442. Zhang, Y.; Li, Y.; Li, J.; Sheng, G.; Zhang, Y.; Zheng, X., Enhanced Cr(VI) removal by using the mixture of pillared bentonite and zero-valent iron. *Chem. Eng. J.* **2012,** *185-186*, 243-249.
443. Li, Z.; Kirk Jones, H.; Zhang, P.; Bowman, R. S., Chromate transport through columns packed with surfactant-modified zeolite/zero valent iron pellets. *Chemosphere* **2007,** *68*, (10), 1861-1866.
444. Ambika, S.; Devasena, M.; Manivannan Nambi, I., Assessment of meso scale zero valent iron

catalyzed Fenton reaction in continuous-flow porous media for sustainable groundwater remediation. *Chem. Eng. J.* **2018,** *334*, 264-272.
445. Han, W.; Fu, F.; Cheng, Z.; Tang, B.; Wu, S., Studies on the optimum conditions using acid-washed zero-valent iron/aluminum mixtures in permeable reactive barriers for the removal of different heavy metal ions from wastewater. *J. Hazard. Mater.* **2016,** *302*, 437-446.
446. Chen, L.-H.; Huang, C.-C.; Lien, H.-L., Bimetallic iron–aluminum particles for dechlorination of carbon tetrachloride. *Chemosphere* **2008,** *73*, (5), 692-697.
447. Barrera-Diaz, C. E.; Lugo-Lugo, V.; Bilyeu, B., A review of chemical, electrochemical and biological methods for aqueous Cr(VI) reduction. *J Hazard Mater* **2012,** *223-224*, 1-12.
448. Hu, C. Y.; Lo, S. L.; Liou, Y. H.; Hsu, Y. W.; Shih, K.; Lin, C. J., Hexavalent chromium removal from near natural water by copper-iron bimetallic particles. *Water Res* **2010,** *44*, (10), 3101-8.
449. Acharya, R.; Naik, B.; Parida, K., Cr (VI) remediation from aqueous environment through modified-TiO2-mediated photocatalytic reduction. *Beilstein Journal of Nanotechnology* **2018,** *9*, (1), 1448-1470.
450. Jiang, B.; Wang, X.; Liu, Y.; Wang, Z.; Zheng, J.; Wu, M., The roles of polycarboxylates in Cr(VI)/sulfite reaction system: Involvement of reactive oxygen species and intramolecular electron transfer. *J Hazard Mater* **2016,** *304*, 457-66.
451. Suzuki, I., Oxidation of inorganic sulfur compounds: chemical and enzymatic reactions. *Canadian Journal of Microbiology* **1999,** *45*, (2), 97-105.
452. Jardine, P.; Fendorf, S.; Mayes, M.; Larsen, I.; Brooks, S.; Bailey, W., Fate and transport of hexavalent chromium in undisturbed heterogeneous soil. *Environmental Science & Technology* **1999,** *33*, (17), 2939-2944.
453. Peng, C.; Meng, H.; Song, S.; Lu, S.; Lopez-Valdivieso, A., Elimination of Cr(VI) from Electroplating Wastewater by Electrodialysis Following Chemical Precipitation. *Separation Science and Technology* **2005,** *39*, (7), 1501-1517.
454. Peng, C.; Song, S.; Lu, S.; Lopez-Valdivieso, A. J. E. J. o. M. P.; Protection, E., Electroplating wastewater treatment through chemical precipitation and electrodialysis. **2004,** *4*, (3).
455. Velasco, G.; Gutiérrez-Granados, S.; Ponce de León, C.; Alatorre, A.; Walsh, F. C.; Rodríguez-Torres, I., The electrochemical reduction of Cr(VI) ions in acid solution at titanium and graphite electrodes. *Journal of Environmental Chemical Engineering* **2016,** *4*, (3), 3610-3617.
456. Alvarado, L.; Ramírez, A.; Rodríguez-Torres, I., Cr(VI) removal by continuous electrodeionization: Study of its basic technologies. *Desalination* **2009,** *249*, (1), 423-428.
457. Qin, H.; Hu, T.; Zhai, Y.; Lu, N.; Aliyeva, J., The improved methods of heavy metals removal by biosorbents: A review. *Environmental Pollution* **2020,** *258*, 113777.
458. Massoudinejad, M.; Asadi, A.; Vosoughi, M.; Gholami, M.; kakavandi, B.; Karami, M. A., A comprehensive study (kinetic, thermodynamic and equilibrium) of arsenic (V) adsorption using KMnO4 modified clinoptilolite. *Korean Journal of Chemical Engineering* **2015,** *32*, (10), 2078-2086.
459. Ahmadi, M.; Foladivanda, M.; Jaafarzadeh, N.; Ramezani, Z.; Ramavandi, B.; Jorfi, S.; Kakavandi, B., Synthesis of chitosan zero-valent iron nanoparticles-supported for cadmium removal: characterization, optimization and modeling approach. *Journal of Water Supply: Research and Technology-Aqua* **2017,** *66*, (2), 116-130.
460. Su, M.; Fang, Y.; Li, B.; Yin, W.; Gu, J.; Liang, H.; Li, P.; Wu, J., Enhanced hexavalent chromium removal by activated carbon modified with micro-sized goethite using a facile impregnation method. *Sci Total Environ* **2019,** *647*, 47-56.

461. Kakavandi, B.; Raofi, A.; Peyghambarzadeh, S. M.; Ramavandi, B.; Niri, M. H.; Ahmadi, M., Efficient adsorption of cobalt on chemical modified activated carbon: characterization, optimization and modeling studies. *Desalination and Water Treatment* **2018,** *111*, 310-321.

462. Park, D.; Lim, S. R.; Yun, Y. S.; Park, J. M., Development of a new Cr(VI)-biosorbent from agricultural biowaste. *Bioresour Technol* **2008,** *99*, (18), 8810-8.

463. Huang, G.; Shi, J. X.; Langrish, T. A. G., Removal of Cr(VI) from aqueous solution using activated carbon modified with nitric acid. *Chemical Engineering Journal* **2009,** *152*, (2-3), 434-439.

464. Wang, X. S.; Chen, L. F.; Li, F. Y.; Chen, K. L.; Wan, W. Y.; Tang, Y. J., Removal of Cr (VI) with wheat-residue derived black carbon: reaction mechanism and adsorption performance. *J Hazard Mater* **2010,** *175*, (1-3), 816-22.

465. Herrera-Gonzalez, A. M.; Caldera-Villalobos, M.; Pelaez-Cid, A. A., Adsorption of textile dyes using an activated carbon and crosslinked polyvinyl phosphonic acid composite. *J Environ Manage* **2019,** *234*, 237-244.

466. Pamphile, N.; Xuejiao, L.; Guangwei, Y.; Yin, W., Synthesis of a novel core-shell-structure activated carbon material and its application in sulfamethoxazole adsorption. *J Hazard Mater* **2019,** *368*, 602-612.

467. Anupam, K.; Dutta, S.; Bhattacharjee, C.; Datta, S., Adsorptive removal of chromium (VI) from aqueous solution over powdered activated carbon: Optimisation through response surface methodology. *Chemical Engineering Journal* **2011,** *173*, (1), 135-143.

468. Wang, Y.; Peng, C.; Padilla-Ortega, E.; Robledo-Cabrera, A.; López-Valdivieso, A., Cr(VI) adsorption on activated carbon: Mechanisms, modeling and limitations in water treatment. *J. Environ. Chem. Eng.* **2020,** *8*, (4), 104031.

469. Cruz-Espinoza, A.; Ibarra-Galván, V.; López-Valdivieso, A.; González-González, J., Synthesis of microporous eskolaite from Cr(VI) using activated carbon as a reductant and template. *Journal of Colloid and Interface Science* **2012,** *374*, (1), 321-324.

470. Ibarra-Galván, V.; López-Valdivieso, A.; Villavelazquez-Mendoza, C. I.; Santoyo-Salazar, J.; Song, S., Synthesis of Eskolaite (α-Cr2O3) Nanostructures by Thermal Processing of Cr2O3-Loaded Activated Carbon. *Particulate Science and Technology* **2014,** *32*, (5), 451-455.

471. Park, D.; Yun, Y.-S.; Park, J. M., Reduction of hexavalent chromium with the brown seaweed Ecklonia biomass. *Environmental science & technology* **2004,** *38*, (18), 4860-4864.

472. Hanson, A. T.; Dwyer, B.; Samani, Z. A.; York, D., Remediation of chromium-containing soils by heap leaching: Column study. *Journal of Environmental Engineering* **1993,** *119*, (5), 825-841.

473. Vainshtein, M.; Kuschk, P.; Mattusch, J.; Vatsourina, A.; Wiessner, A., Model experiments on the microbial removal of chromium from contaminated groundwater. *Water Research* **2003,** *37*, (6), 1401-1405.

474. Cho, K.; An, B. M.; So, S.; Chae, A.; Song, K. G., Simultaneous control of algal micropollutants based on ball-milled powdered activated carbon in combination with permanganate oxidation and coagulation. *Water Research* **2020,** *185*, 116263.

475. Boehm, H. P., Surface oxides on carbon and their analysis: a critical assessment. *Carbon* **2002,** *40*, (2), 145-149.

476. Carasso, M. L.; Rowlands, W. N.; Kennedy, R. A., Electroacoustic Determination of Droplet Size and Zeta Potential in Concentrated Intravenous Fat Emulsions. *Journal of Colloid and Interface Science* **1995,** *174*, (2), 405-413.

477. Rao, F.; Song, S.; Lopez-Valdivieso, A., Electrokinetic studies of minerals in aqueous solutions through electroacoustic measurement. *Surface Review and Letters* **2009,** *16*, (01), 65-71.
478. Hunter, R. J., *Foundations of colloid science*. Oxford university press: 2001.
479. Smoluchowski, M. v. J. B. I., Barth-Verlag, Leipzig, Handbuch der Elektrizität und des Magnetismus. **1921**, 366-427.
480. Association, A. P. H.; Association, A. W. W.; Federation, W. P. C.; Federation, W. E., *Standard methods for the examination of water and wastewater*. American Public Health Association.: 1915; Vol. 2.
481. Giri, A. K.; Patel, R.; Mandal, S., Removal of Cr (VI) from aqueous solution by Eichhornia crassipes root biomass-derived activated carbon. *Chemical Engineering Journal* **2012,** *185*, 71-81.
482. Dai, M., The Effect of Zeta Potential of Activated Carbon on the Adsorption of Dyes from Aqueous Solution: I. The Adsorption of Cationic Dyes: Methyl Green and Methyl Violet. *Journal of Colloid and Interface Science* **1994,** *164*, (1), 223-228.
483. Julien, F.; Baudu, M.; Mazet, M., Relationship between chemical and physical surface properties of activated carbon. *Water Research* **1998,** *32*, (11), 3414-3424.
484. Song, X.; Liu, H.; Cheng, L.; Qu, Y., Surface modification of coconut-based activated carbon by liquid-phase oxidation and its effects on lead ion adsorption. *Desalination* **2010,** *255*, (1), 78-83.
485. Lyu, H.; Gao, B.; He, F.; Zimmerman, A. R.; Ding, C.; Tang, J.; Crittenden, J. C., Experimental and modeling investigations of ball-milled biochar for the removal of aqueous methylene blue. *Chemical Engineering Journal* **2018,** *335*, 110-119.
486. Sing, K. S. W., Reporting physisorption data for gas/solid systems with special reference to the determination of surface area and porosity (Recommendations 1984). *Pure and Applied Chemistry* **1985,** *57*, (4), 603-619.
487. Guedidi, H.; Reinert, L.; Lévêque, J.-M.; Soneda, Y.; Bellakhal, N.; Duclaux, L., The effects of the surface oxidation of activated carbon, the solution pH and the temperature on adsorption of ibuprofen. *Carbon* **2013,** *54*, 432-443.
488. Cuesta, A.; Dhamelincourt, P.; Laureyns, J.; Martínez-Alonso, A.; Tascón, J. M. D., Raman microprobe studies on carbon materials. *Carbon* **1994,** *32*, (8), 1523-1532.
489. Chen, F.; An, W.; Liu, L.; Liang, Y.; Cui, W., Highly efficient removal of bisphenol A by a three-dimensional graphene hydrogel-AgBr@rGO exhibiting adsorption/photocatalysis synergy. *Applied Catalysis B: Environmental* **2017,** *217*, 65-80.
490. Cong, H.-P.; Ren, X.-C.; Wang, P.; Yu, S.-H., Macroscopic Multifunctional Graphene-Based Hydrogels and Aerogels by a Metal Ion Induced Self-Assembly Process. *ACS Nano* **2012,** *6*, (3), 2693-2703.
491. Sangkarak, S.; Phetrak, A.; Kittipongvises, S.; Kitkaew, D.; Phihusut, D.; Lohwacharin, J., Adsorptive performance of activated carbon reused from household drinking water filter for hexavalent chromium-contaminated water. *Journal of Environmental Management* **2020,** *272*, 111085.
492. Li, Y.; Cui, W.; Liu, L.; Zong, R.; Yao, W.; Liang, Y.; Zhu, Y., Removal of Cr(VI) by 3D TiO2-graphene hydrogel via adsorption enriched with photocatalytic reduction. *Applied Catalysis B: Environmental* **2016,** *199*, 412-423.
493. Azari, A.; Kakavandi, B.; Kalantary, R. R.; Ahmadi, E.; Gholami, M.; Torkshavand, Z.; Azizi, M., Rapid and efficient magnetically removal of heavy metals by magnetite-activated carbon

composite: a statistical design approach. *Journal of Porous Materials* **2015,** *22*, (4), 1083-1096.
494. Sparks, D. L., *Soil physical chemistry*. CRC press: 1998.
495. Demiral, H.; Demiral, I.; Tümsek, F.; Karabacakoğlu, B., Adsorption of chromium (VI) from aqueous solution by activated carbon derived from olive bagasse and applicability of different adsorption models. *Chemical Engineering Journal* **2008,** *144*, (2), 188-196.
496. Wang, W., Chromium (VI) removal from aqueous solutions through powdered activated carbon countercurrent two-stage adsorption. *Chemosphere* **2018,** *190*, 97-102.
497. Acharya, J.; Sahu, J. N.; Sahoo, B. K.; Mohanty, C. R.; Meikap, B. C., Removal of chromium(VI) from wastewater by activated carbon developed from Tamarind wood activated with zinc chloride. *Chemical Engineering Journal* **2009,** *150*, (1), 25-39.
498. Gürses, A.; Doğar, Ç.; Yalçın, M.; Açıkyıldız, M.; Bayrak, R.; Karaca, S., The adsorption kinetics of the cationic dye, methylene blue, onto clay. *Journal of Hazardous Materials* **2006,** *131*, (1), 217-228.
499. **!!! INVALID CITATION !!! (Azari et al., 2015b; Babaei et al., 2016)**.
500. McKay, G.; Otterburn, M. S.; Sweeney, A. G., The removal of colour from effluent using various adsorbents—III. Silica: Rate processes. *Water Research* **1980,** *14*, (1), 15-20.
501. Huang, C. P.; Wu, M. H., The removal of chromium(VI) from dilute aqueous solution by activated carbon. *Water Research* **1977,** *11*, (8), 673-679.
502. Mortazavian, S.; Saber, A.; Hong, J.; Bae, J.-H.; Chun, D.; Wong, N.; Gerrity, D.; Batista, J.; Kim, K. J.; Moon, J., Synthesis, characterization, and kinetic study of activated carbon modified by polysulfide rubber coating for aqueous hexavalent chromium removal. *Journal of Industrial and Engineering Chemistry* **2019,** *69*, 196-210.
503. Nemr, A. E., Potential of pomegranate husk carbon for Cr(VI) removal from wastewater: Kinetic and isotherm studies. *Journal of Hazardous Materials* **2009,** *161*, (1), 132-141.
504. Niazi, L.; Lashanizadegan, A.; Sharififard, H., Chestnut oak shells activated carbon: Preparation, characterization and application for Cr (VI) removal from dilute aqueous solutions. *J. Clean. Prod.* **2018,** *185*, 554-561.
505. Li, W.; Gong, X.; Li, X.; Zhang, D.; Gong, H., Removal of Cr(VI) from low-temperature micro-polluted surface water by tannic acid immobilized powdered activated carbon. *Bioresource Technology* **2012,** *113*, 106-113.
506. Kobya, M., Removal of Cr(VI) from aqueous solutions by adsorption onto hazelnut shell activated carbon: kinetic and equilibrium studies. *Bioresource Technology* **2004,** *91*, (3), 317-321.
507. Di Natale, F.; Lancia, A.; Molino, A.; Musmarra, D., Removal of chromium ions form aqueous solutions by adsorption on activated carbon and char. *Journal of Hazardous Materials* **2007,** *145*, (3), 381-390.
508. Liu, W.; Zhang, J.; Zhang, C.; Wang, Y.; Li, Y., Adsorptive removal of Cr (VI) by Fe-modified activated carbon prepared from Trapa natans husk. *Chemical Engineering Journal* **2010,** *162*, (2), 677-684.
509. Asimakopoulos, G.; Baikousi, M.; Salmas, C.; Bourlinos, A. B.; Zboril, R.; Karakassides, M. A., Advanced Cr(VI) sorption properties of activated carbon produced via pyrolysis of the "Posidonia oceanica" seagrass. *Journal of Hazardous Materials* **2020**, 124274.
510. Lyubchik, S. I.; Lyubchik, A. I.; Galushko, O. L.; Tikhonova, L. P.; Vital, J.; Fonseca, I. M.; Lyubchik, S. B., Kinetics and thermodynamics of the Cr(III) adsorption on the activated carbon from co-mingled wastes. *Colloids and Surfaces A: Physicochemical and Engineering Aspects* **2004,** *242*, (1),

151-158.
511. Chegrouche, S.; Mellah, A.; Barkat, M., Removal of strontium from aqueous solutions by adsorption onto activated carbon: kinetic and thermodynamic studies. *Desalination* **2009,** *235*, (1), 306-318.
512. Kocaoba, S.; Akcin, G., Removal and recovery of chromium and chromium speciation with MINTEQA2. *Talanta* **2002,** *57*, (1), 23-30.
513. Fahim, N.; Barsoum, B.; Eid, A.; Khalil, M., Removal of chromium (III) from tannery wastewater using activated carbon from sugar industrial waste. *Journal of Hazardous Materials* **2006,** *136*, (2), 303-309.
514. Gherasim, C.-V.; Bourceanu, G.; Olariu, R.-I.; Arsene, C., A novel polymer inclusion membrane applied in chromium (VI) separation from aqueous solutions. *Journal of Hazardous Materials* **2011,** *197*, 244-253.
515. Butler, J. N.; Butler, J. N.; Cogley, D. R., *Ionic equilibrium: solubility and pH calculations*. John Wiley & Sons: 1998.
516. Franz, M.; Arafat, H. A.; Pinto, N. G., Effect of chemical surface heterogeneity on the adsorption mechanism of dissolved aromatics on activated carbon. *Carbon* **2000,** *38*, (13), 1807-1819.
517. Yang, C.; Miao, G.; Pi, Y.; Xia, Q.; Wu, J.; Li, Z.; Xiao, J., Abatement of various types of VOCs by adsorption/catalytic oxidation: A review. *Chemical Engineering Journal* **2019**.
518. Miretzky, P.; Cirelli, A. F., Cr(VI) and Cr(III) removal from aqueous solution by raw and modified lignocellulosic materials: a review. *J Hazard Mater* **2010,** *180*, (1-3), 1-19.
519. Li, J.; Zhang, X.; Liu, M.; Pan, B.; Zhang, W.; Shi, Z.; Guan, X., Enhanced Reactivity and Electron Selectivity of Sulfidated Zerovalent Iron toward Chromate under Aerobic Conditions. *Environmental Science and Technology* **2018,** *52*, (5), 2988-2997.
520. Aparicio, J. D.; Lacalle, R. G.; Artetxe, U.; Urionabarrenetxea, E.; Becerril, J. M.; Polti, M. A.; Garbisu, C.; Soto, M., Successful remediation of soils with mixed contamination of chromium and lindane: Integration of biological and physico-chemical strategies. *Environ. Res.* **2021,** *194*, 110666.
521. Samuel, M. S.; Selvarajan, E.; Chidambaram, R.; Patel, H.; Brindhadevi, K., Clean approach for chromium removal in aqueous environments and role of nanomaterials in bioremediation: Present research and future perspective. *Chemosphere* **2021,** *284*, 131368.
522. Dognani, G.; Hadi, P.; Ma, H.; Cabrera, F. C.; Job, A. E.; Agostini, D. L. S.; Hsiao, B. S., Effective chromium removal from water by polyaniline-coated electrospun adsorbent membrane. *Chem. Eng. J.* **2019,** *372*, 341-351.
523. Fang, Y.; Yang, K.; Zhang, Y.; Peng, C.; Robledo-Cabrera, A.; López-Valdivieso, A., Highly surface activated carbon to remove Cr(VI) from aqueous solution with adsorbent recycling. *Environ. Res.* **2021,** *197*, 111151.
524. Deng, M.; Wang, X.; Li, Y.; Wang, F.; Jiang, Z.; Liu, Y.; Gu, Z.; Xia, S.; Zhao, J., Reduction and immobilization of Cr(VI) in aqueous solutions by blast furnace slag supported sulfidized nanoscale zerovalent iron. *Sci. Total Environ.* **2020,** *743*, 140722.
525. Wu, M.; Li, Y.; Li, J.; Wang, Y.; Xu, H.; Zhao, Y., Bioreduction of hexavalent chromium using a novel strain CRB-7 immobilized on multiple materials. *J. Hazard. Mater.* **2019,** *368*, 412-420.
526. Zeng, Q.; Hu, Y.; Yang, Y.; Hu, L.; Zhong, H.; He, Z., Cell envelop is the key site for Cr (VI) reduction by Oceanobacillus oncorhynchi W4, a newly isolated Cr (VI) reducing bacterium. *J. Hazard. Mater.* **2019,** *368*, 149-155.
527. Qian, L.; Liu, S.; Zhang, W.; Chen, Y.; Ouyang, D.; Han, L.; Yan, J.; Chen, M., Enhanced reduction

and adsorption of hexavalent chromium by palladium and silicon rich biochar supported nanoscale zero-valent iron. *J. Colloid Interface Sci.* **2019,** *533*, 428-436.
528. Zhang, L.; Qiu, Y.-Y.; Zhou, Y.; Chen, G.-H.; van Loosdrecht, M. C. M.; Jiang, F., Elemental sulfur as electron donor and/or acceptor: Mechanisms, applications and perspectives for biological water and wastewater treatment. *Water Res.* **2021,** *202*, 117373.
529. Zhang, W.; Qian, L.; Chen, Y.; Ouyang, D.; Han, L.; Shang, X.; Li, J.; Gu, M.; Chen, M., Nanoscale zero-valent iron supported by attapulgite produced at different acid modification: Synthesis mechanism and the role of silicon on Cr(VI) removal. *Chemosphere* **2021,** *267*, 129183.
530. Zhou, L.; Liu, Y.; Liu, S.; Yin, Y.; Zeng, G.; Tan, X.; Hu, X.; Hu, X.; Jiang, L.; Ding, Y.; Liu, S.; Huang, X., Investigation of the adsorption-reduction mechanisms of hexavalent chromium by ramie biochars of different pyrolytic temperatures. *Bioresour. Technol.* **2016,** *218*, 351-359.
531. Ramirez, A.; Ocampo, R.; Giraldo, S.; Padilla, E.; Flórez, E.; Acelas, N., Removal of Cr (VI) from an aqueous solution using an activated carbon obtained from teakwood sawdust: Kinetics, equilibrium, and density functional theory calculations. *J. Environ. Chem. Eng.* **2020,** *8*, (2), 103702.
532. Norouzi, S.; Heidari, M.; Alipour, V.; Rahmanian, O.; Fazlzadeh, M.; Mohammadi-moghadam, F.; Nourmoradi, H.; Goudarzi, B.; Dindarloo, K., Preparation, characterization and Cr(VI) adsorption evaluation of NaOH-activated carbon produced from Date Press Cake; an agro-industrial waste. *Bioresour. Technol.* **2018,** *258*, 48-56.
533. Rakhunde, R.; Deshpande, L.; Juneja, H., Chemical speciation of chromium in water: a review. *Crit. Rev. Env. Sci. Technol.* **2012,** *42*, (7), 776-810.
534. Mohan, D.; Singh, K. P.; Singh, V. K., Removal of Hexavalent Chromium from Aqueous Solution Using Low-Cost Activated Carbons Derived from Agricultural Waste Materials and Activated Carbon Fabric Cloth. *Industrial and Engineering Chemistry Research* **2005,** *44*, (4), 1027-1042.
535. Asimakopoulos, G.; Baikousi, M.; Salmas, C.; Bourlinos, A. B.; Zboril, R.; Karakassides, M. A., Advanced Cr(VI) sorption properties of activated carbon produced via pyrolysis of the "Posidonia oceanica" seagrass. *J. Hazard. Mater.* **2021,** *405*, 124274.
536. Qu, J.; Wang, Y.; Tian, X.; Jiang, Z.; Deng, F.; Tao, Y.; Jiang, Q.; Wang, L.; Zhang, Y., KOH-activated porous biochar with high specific surface area for adsorptive removal of chromium (VI) and naphthalene from water: Affecting factors, mechanisms and reusability exploration. *J. Hazard. Mater.* **2021,** *401*, 123292.
537. Shi, Y.; Shan, R.; Lu, L.; Yuan, H.; Jiang, H.; Zhang, Y.; Chen, Y., High-efficiency removal of Cr(VI) by modified biochar derived from glue residue. *J. Clean. Prod.* **2020,** *254*, 119935.
538. Ogata, F.; Nagai, N.; Itami, R.; Nakamura, T.; Kawasaki, N., Potential of virgin and calcined wheat bran biomass for the removal of chromium(VI) ion from a synthetic aqueous solution. *J. Environ. Chem. Eng.* **2020,** *8*, (2), 103710.
539. Wu, F.; Zhao, T.; Yao, Y.; Jiang, T.; Wang, B.; Wang, M., Recycling supercapacitor activated carbons for adsorption of silver (I) and chromium (VI) ions from aqueous solutions. *Chemosphere* **2020,** *238*, 124638.
540. Duranoğlu, D.; Trochimczuk, A. W.; Beker, U., Kinetics and thermodynamics of hexavalent chromium adsorption onto activated carbon derived from acrylonitrile-divinylbenzene copolymer. *Chem. Eng. J.* **2012,** *187*, 193-202.
541. Liu, N.; Zhang, Y.; Xu, C.; Liu, P.; Lv, J.; Liu, Y.; Wang, Q., Removal mechanisms of aqueous Cr(VI) using apple wood biochar: a spectroscopic study. *J. Hazard. Mater.* **2020,** *384*, 121371.
542. Zhang, Y.-J.; Ou, J.-L.; Duan, Z.-K.; Xing, Z.-J.; Wang, Y., Adsorption of Cr(VI) on bamboo

bark-based activated carbon in the absence and presence of humic acid. *Colloids Surf, A Physicochem Eng Asp* **2015,** *481*, 108-116.

543. Ibarra-Galván, V.; López-Valdivieso, A.; Villavelazquez-Mendoza, C. I.; Santoyo-Salazar, J.; Song, S., Synthesis of Eskolaite (α-Cr2O3) Nanostructures by Thermal Processing of Cr2O3-Loaded Activated Carbon. *Part. Sci. Technol.* **2014,** *32*, (5), 451-455.

544. Jiang, W.; Cai, Q.; Xu, W.; Yang, M.; Cai, Y.; Dionysiou, D. D.; O' Shea, K. E., Cr(VI) Adsorption and Reduction by Humic Acid Coated on Magnetite. *Environ. Sci. Technol.* **2014,** *48*, (14), 8078-8085.

545. Krishna Kumar, A. S.; You, J.-G.; Tseng, W.-B.; Dwivedi, G. D.; Rajesh, N.; Jiang, S.-J.; Tseng, W.-L., Magnetically Separable Nanospherical g-C3N4@Fe3O4 as a Recyclable Material for Chromium Adsorption and Visible-Light-Driven Catalytic Reduction of Aromatic Nitro Compounds. *ACS Sustain. Chem. Eng.* **2019,** *7*, (7), 6662-6671.

546. Grohmann, I.; Kemnitz, E.; Lippitz, A.; Unger, W. E. S., Curve fitting of Cr 2p photoelectron spectra of Cr2O3 and CrF3. *Surf. Interface Anal.* **1995,** *23*, (13), 887-891.

547. Murphy, V.; Tofail, S. A. M.; Hughes, H.; McLoughlin, P., A novel study of hexavalent chromium detoxification by selected seaweed species using SEM-EDX and XPS analysis. *Chem. Eng. J.* **2009,** *148*, (2), 425-433.

548. Zhang, L.; Fu, F.; Tang, B., Adsorption and redox conversion behaviors of Cr(VI) on goethite/carbon microspheres and akaganeite/carbon microspheres composites. *Chem. Eng. J.* **2019,** *356*, 151-160.

549. Ren, Z.; Xu, X.; Wang, X.; Gao, B.; Yue, Q.; Song, W.; Zhang, L.; Wang, H., FTIR, Raman, and XPS analysis during phosphate, nitrate and Cr(VI) removal by amine cross-linking biosorbent. *J. Colloid Interface Sci.* **2016,** *468*, 313-323.

550. Biesinger, M. C.; Brown, C.; Mycroft, J. R.; Davidson, R. D.; McIntyre, N. S., X-ray photoelectron spectroscopy studies of chromium compounds. *Surf. Interface Anal.* **2004,** *36*, (12), 1550-1563.

551. Chen, Z.; Wei, B.; Yang, S.; Li, Q.; Liu, L.; Yu, S.; Wen, T.; Hu, B.; Chen, J.; Wang, X., Synthesis of PANI/AlOOH composite for Cr(VI) adsorption and reduction from aqueous solutions. *ChemistrySelect* **2019,** *4*, (8), 2352-2362.

552. Chowdhury, S. R.; Yanful, E. K.; Pratt, A. R., Chemical states in XPS and Raman analysis during removal of Cr(VI) from contaminated water by mixed maghemite–magnetite nanoparticles. *J. Hazard. Mater.* **2012,** *235-236*, 246-256.

553. Wu, J.; Zhang, H.; He, P.-J.; Yao, Q.; Shao, L.-M., Cr(VI) removal from aqueous solution by dried activated sludge biomass. *J. Hazard. Mater.* **2010,** *176*, (1), 697-703.

554. Cui, H.; Fu, M.; Yu, S.; Wang, M. K., Reduction and removal of Cr(VI) from aqueous solutions using modified byproducts of beer production. *J. Hazard. Mater.* **2011,** *186*, (2), 1625-1631.

555. Jieying, Z.; Zhao, Q.; Ye, Z., Preparation and characterization of activated carbon fiber (ACF) from cotton woven waste. *Appl. Surf. Sci.* **2014,** *299*, 86-91.

556. Jia, Z.; Wang, Y., Covalently crosslinked graphene oxide membranes by esterification reactions for ions separation. *Journal of Materials Chemistry A* **2015,** *3*, (8), 4405-4412.

557. Ma, J.; Pan, J.; Yue, J.; Xu, Y.; Bao, J., High performance of poly(dopamine)-functionalized graphene oxide/poly(vinyl alcohol) nanocomposites. *Appl. Surf. Sci.* **2018,** *427*, 428-436.

558. Chen, X.; Wang, X.; Fang, D., A review on C1s XPS-spectra for some kinds of carbon materials. *Fullerenes, Nanotubes and Carbon Nanostructures* **2020,** *28*, (12), 1048-1058.

559. Yin, W.; Guo, Z.; Zhao, C.; Xu, J., Removal of Cr(VI) from aqueous media by biochar derived

from mixture biomass precursors of Acorus calamus Linn. and feather waste. *J. Anal. Appl. Pyrolysis* **2019,** *140*, 86-92.
560. Gangadharan, P.; Nambi, I. M., Hexavalent chromium reduction and energy recovery by using dual-chambered microbial fuel cell. *Water Sci. Technol.* **2014,** *71*, (3), 353-358.
561. Lespade, P.; Marchand, A.; Couzi, M.; Cruege, F., Caracterisation de materiaux carbones par microspectrometrie Raman. *Carbon* **1984,** *22*, (4), 375-385.
562. Wang, X.; Liang, Y.; An, W.; Hu, J.; Zhu, Y.; Cui, W., Removal of chromium (VI) by a self-regenerating and metal free g-C3N4/graphene hydrogel system via the synergy of adsorption and photo-catalysis under visible light. *Appl. Catal., B: Environ* **2017,** *219*, 53-62.
563. Yang, X.; Cui, H.; Li, Y.; Qin, J.; Zhang, R.; Tang, H., Fabrication of Ag3PO4-Graphene Composites with Highly Efficient and Stable Visible Light Photocatalytic Performance. *ACS Catalysis* **2013,** *3*, (3), 363-369.
564. Osswald, S.; Flahaut, E.; Gogotsi, Y., In Situ Raman Spectroscopy Study of Oxidation of Double- and Single-Wall Carbon Nanotubes. *Chem. Mater.* **2006,** *18*, (6), 1525-1533.
565. Ouki, S. K.; Neufeld, R. D., Use of activated carbon for the recovery of chromium from industrial wastewaters. *J. Chem. Technol. Biotechnol.* **1997,** *70*, (1), 3-8.
566. Jing, G.; Zhou, Z.; Song, L.; Dong, M., Ultrasound enhanced adsorption and desorption of chromium (VI) on activated carbon and polymeric resin. *Desalination* **2011,** *279*, (1), 423-427.
567. Singha, S.; Sarkar, U.; Luharuka, P., Functionalized granular activated carbon and surface complexation with chromates and bi-chromates in wastewater. *Sci. Total Environ.* **2013,** *447*, 472-487.
568. Daneshvar, E.; Zarrinmehr, M. J.; Kousha, M.; Hashtjin, A. M.; Saratale, G. D.; Maiti, A.; Vithanage, M.; Bhatnagar, A., Hexavalent chromium removal from water by microalgal-based materials: Adsorption, desorption and recovery studies. *Bioresour. Technol.* **2019,** *293*, 122064.
569. Nriagu, J. O.; Nieboer, E., *Chromium in the natural and human environments*. John Wiley & Sons: 1988; Vol. 20.
570. Anderson, R. A., Essentiality of chromium in humans. *Sci. Total Environ.* **1989,** *86*, (1-2), 75-81.
571. Ellis, A. S.; Johnson, T. M.; Bullen, T. D., Chromium isotopes and the fate of hexavalent chromium in the environment. *Science* **2002,** *295*, (5562), 2060-2062.
572. Shi, Z.; Shen, W.; Yang, K.; Zheng, N.; Jiang, X.; Liu, L.; Yang, D.; Zhang, L.; Ai, Z.; Xie, B., Hexavalent chromium removal by a new composite system of dissimilatory iron reduction bacteria Aeromonas hydrophila and nanoscale zero-valent iron. *Chem. Eng. J.* **2019,** *362*, 63-70.
573. Chirwa, E. M.; Wang, Y.-T., Hexavalent chromium reduction by Bacillus sp. in a packed-bed bioreactor. *Environ. Sci. Technol.* **1997,** *31*, (5), 1446-1451.
574. Mukherjee, R.; Kumar, R.; Sinha, A.; Lama, Y.; Saha, A. K., A review on synthesis, characterization, and applications of nano zero valent iron (nZVI) for environmental remediation. *Critical Reviews in Environmental Science and Technology* **2016,** *46*, (5), 443-466.
575. Bae, S.; Collins, R. N.; Waite, T. D.; Hanna, K., Advances in Surface Passivation of Nanoscale Zerovalent Iron: A Critical Review. *Environ. Sci. Technol.* **2018,** *52*, (21), 12010-12025.
576. Lv, X.; Qin, X.; Wang, K.; Peng, Y.; Wang, P.; Jiang, G., Nanoscale zero valent iron supported on MgAl-LDH-decorated reduced graphene oxide: enhanced performance in Cr (VI) removal, mechanism and regeneration. *J. Hazard. Mater.* **2019,** *373*, 176-186.
577. Park, M. H.; Lee, J.; Kim, J. Y., Oxidation resistance of nanoscale zero-valent iron supported

on exhausted coffee grounds. *Chemosphere* **2019**.
578. Fu, F.; Cheng, Z.; Dionysiou, D. D.; Tang, B., Fe/Al bimetallic particles for the fast and highly efficient removal of Cr(VI) over a wide pH range: Performance and mechanism. *J Hazard Mater* **2015,** *298*, 261-9.
579. Wu, J.; Yan, M.; Lv, S.; Yin, W.; Bu, H.; Liu, L.; Li, P.; Deng, H.; Zheng, X., Preparation of highly dispersive and antioxidative nano zero-valent iron for the removal of hexavalent chromium. *Chemosphere* **2021,** *262*, 127733.
580. Zhang, Y.; Jiao, X.; Liu, N.; Lv, J.; Yang, Y., Enhanced removal of aqueous Cr(VI) by a green synthesized nanoscale zero-valent iron supported on oak wood biochar. *Chemosphere* **2020,** *245*, 125542.
581. Ma, L.; Du, Y.; Chen, S.; Du, D.; Ye, H.; Zhang, T. C., Highly efficient removal of Cr(VI) from aqueous solution by pinecone biochar supported nanoscale zero-valent iron coupling with Shewanella oneidensis MR-1. *Chemosphere* **2022,** *287*, 132184.
582. Zou, H.; Hu, E.; Yang, S.; Gong, L.; He, F., Chromium (VI) removal by mechanochemically sulfidated zero valent iron and its effect on dechlorination of trichloroethene as a co-contaminant. *Sci. Total Environ.* **2019,** *650*, 419-426.
583. Fecht, H.; Hellstern, E.; Fu, Z.; Johnson, W., Nanocrystalline metals prepared by high-energy ball milling. *Metall. Trans. A* **1990,** *21*, (9), 2333.
584. Wang, W.; Hu, B.; Wang, C.; Liang, Z.; Cui, F.; Zhao, Z.; Yang, C., Cr(VI) removal by micron-scale iron-carbon composite induced by ball milling: The role of activated carbon. *Chem. Eng. J.* **2020,** *389*, 122633.
585. Prasad, P. V. V. V.; Das, C.; Golder, A. K., Reduction of Cr(VI) to Cr(III) and removal of total chromium from wastewater using scrap iron in the form of zerovalent iron(ZVI): Batch and column studies. *The Canadian Journal of Chemical Engineering* **2011,** *89*, (6), 1575-1582.
586. Gao, X.; Zhang, Y.; Li, F.; Tian, B.; Wang, X.; Wang, Z.; Carozza, J. C.; Zhou, Z.; Han, H.; Xu, C., Surface Modulation and Chromium Complexation: All-in-One Solution for the Cr(VI) Sequestration with Bifunctional Molecules. *Environ. Sci. Technol.* **2020,** *54*, (13), 8373-8379.
587. Onari, S.; Arai, T.; Kudo, K., Infrared lattice vibrations and dielectric dispersion in α—Fe2O3. *Physical Review B* **1977,** *16*, (4), 1717-1721.
588. El Mendili, Y.; Bardeau, J.-F.; Randrianantoandro, N.; Gourbil, A.; Greneche, J.-M.; Mercier, A.-M.; Grasset, F., New evidences of in situ laser irradiation effects on γ-Fe2O3 nanoparticles: a Raman spectroscopic study. *Journal of Raman Spectroscopy* **2011,** *42*, (2), 239-242.
589. El Mendili, Y.; Bardeau, J.-F.; Randrianantoandro, N.; Grasset, F.; Greneche, J.-M., Insights into the Mechanism Related to the Phase Transition from γ-Fe2O3 to α-Fe2O3 Nanoparticles Induced by Thermal Treatment and Laser Irradiation. *The Journal of Physical Chemistry C* **2012,** *116*, (44), 23785-23792.
590. Heyns, J. B. B.; Cruywagen, J. J.; Carron, K. T., Raman spectroscopic investigation of chromium(VI) equilibria — another look. *Journal of Raman Spectroscopy* **1999,** *30*, (4), 335-338.
591. Chastain, J.; King Jr, R. C., Handbook of X-ray photoelectron spectroscopy. **1992**, 261.
592. Mills, P.; Sullivan, J. L., A study of the core level electrons in iron and its three oxides by means of X-ray photoelectron spectroscopy. *J. Phys. D: Appl. Phys.* **1983,** *16*, (5), 723-732.
593. Zhangda, L.; Yun-qi, C.; Xiao-lin, W., Studies of α-Fe2O3 electrode surface of wet cells for the photodecomposition of water. *Surf. Sci.* **1984,** *147*, (2), 377-384.
594. Ai, Z.; Cheng, Y.; Zhang, L.; Qiu, J., Efficient Removal of Cr(VI) from Aqueous Solution with

Fe@Fe2O3 Core−Shell Nanowires. *Environ. Sci. Technol.* **2008,** *42*, (18), 6955-6960.
595. Yamashita, T.; Hayes, P., Analysis of XPS spectra of Fe2+ and Fe3+ ions in oxide materials. *Appl. Surf. Sci.* **2008,** *254*, (8), 2441-2449.
596. Oscarson, D. W.; Huang, P. M.; Defosse, C.; Herbillon, A., Oxidative power of Mn(IV) and Fe(III) oxides with respect to As(III) in terrestrial and aquatic environments. *Nature* **1981,** *291*, (5810), 50-51.
597. McIntyre, N. S.; Zetaruk, D. G., X-ray photoelectron spectroscopic studies of iron oxides. *Anal. Chem.* **1977,** *49*, (11), 1521-1529.
598. Hawn, D. D.; DeKoven, B. M., Deconvolution as a correction for photoelectron inelastic energy losses in the core level XPS spectra of iron oxides. **1987,** *10*, (2-3), 63-74.
599. Melitas, N.; Chuffe-Moscoso, O.; Farrell, J., Kinetics of soluble chromium removal from contaminated water by zerovalent iron media: corrosion inhibition and passive oxide effects. *Environ. Sci. Technol.* **2001,** *35*, (19), 3948-3953.
600. Powell, R. M.; Puls, R. W.; Hightower, S. K.; Sabatini, D. A., Coupled iron corrosion and chromate reduction: mechanisms for subsurface remediation. *Environ. Sci. Technol.* **1995,** *29*, (8), 1913-1922.
601. Wang, C.; Wu, Y.; Qu, T.; Liu, S.; Pi, Y.; Shen, J., Enhanced Cr(VI) removal in the synergy between the hydroxyl-functionalized ball-milled ZVI/Fe3O4 composite and Na2EDTA complexation. *Chemical Engineering Journal* **2018,** *359*.
602. Lee, J.-Y.; Hozalski, R. M.; Arnold, W. A., Effects of dissolved oxygen and iron aging on the reduction of trichloronitromethane, trichloracetonitrile, and trichloropropanone. *Chemosphere* **2007,** *66*, (11), 2127-2135.
603. Pettine, M.; D' ottone, L.; Campanella, L.; Millero, F. J.; Passino, R., The reduction of chromium (VI) by iron (II) in aqueous solutions. *Geochim. Cosmochim. Acta* **1998,** *62*, (9), 1509-1519.